UNIVERSITÀ
DEGLI STUDI
DI UDINE
hic sunt futura

www.uniud.it

DIPARTIMENTO DI INGEGNERIA E ARCHITETTURA

Corso di Dottorato di ricerca in
Ingegneria Industriale e dell'Informazione
in convenzione con The Research Hub by Electrolux Professional

Ciclo XXXII

Identification and control of vibration transmission in a professional washing machine

Dottorando
Ing. Nicola Battistella

Supervisor
Chiar.mo Prof. Paolo Gardonio

Company Scientific Referee
Ing. Riccardo Furlanetto

Company Technical Coordinator
Ing. Michele Simonato

Anno 2019

“Un uomo è vecchio
solo quando i rimpianti,
in lui,
superano i sogni.”

Albert Einstein

Acknowledgments

My utmost gratitude to my supervisor Prof. Paolo Gardonio for his kindness, guidance and encouragement during this challenging project.

I express my sincerest thanks to Electrolux Professional S.p.A. for establishing and funding this PhD project. I thank my scientific tutor Riccardo Furlanetto and technical coordinator Michele Simonato, and all the members of The research Hub and Advance Development & Technology for their help with this work.

Very special thanks to all the Research & Development department at Electrolux Professional Laundry System Sweden AB in Ljungby for their aid during my period aboard.

A special thank to C.R.M. di Battistella B.&C. to help me to take on and solve many challenges.

I would also like to thank my colleagues and friends at the University of Udine, Loris dal Bo, Emanuele Turco, Aleksander Kras and Roberto Del Sal for their suggestions and help.

Many thanks to Federico Furlan, Giulia Diamante, Lorenzo Manera, Alessia Cazzato, Emma Michelle Manera, Andrea De Bernardo, Filippo Paggiarin, and Lorenzo Del Frari for their insightful comments, their encouragement to my PhD and for all the time spent together.

Many thanks go to my friends with whom I shared the best moments during these three years.

I am extremely thankful to my parents and to my large family who, through their support have helped me to get here. I have appreciated a lot their hints and suggestions. Also, I would like to express a great thank you to my grandparents and to the friends past away for have gone with me in my journey.

On a personal level, my deepest gratitude goes to Sara, for her patience, comprehension and support she gave me throughout the course of PhD studies.

Abstract

This thesis presents theoretical and experimental works on the identification and the control of vibrations in professional washing machines equipped with semi-active dampers and with semi-active Tunable Vibration Absorbers (TVAs). The study is focused on tub-drum oscillations and ground force transmission during the spinning, which is the most critical phase of the whole washing cycle.

The in-house built semi-active dampers are designed and manufactured in such a way as to vary from low to high friction damping levels. Each of the four semi-active dampers are composed by three components: the brake shoe assembly, the piston and the brackets to support linear solenoid transducers. The damping ratio is tuned by varying the clamping force at the brake shoes. The tuned vibration absorbers are made by thin cantilever beams with annular cross section and tip masses at the free ends. The four devices are manually tuned by sliding the tip masses along the beams in such a way as to modify their fundamental natural frequencies. The prototypes are built in such a way as to be installed in the frame structure of the tub-drum assembly of a professional washing machine.

The study is based on a lumped parameter model for the oscillations of the tub-drum assembly in the vertical and horizontal directions and for the normal force transmitted to the floor via the suspension system formed by four springs and friction dampers connected in parallel. This standard model is expanded to take into account the dynamic effects produced by semi-active friction dampers in the suspension system and to take into account the dynamic effects generated by Tunable Vibration Absorbers connected to the tub-drum assembly. The oscillations of the tub-drum assembly and the normal force transmitted to the floor are derived in terms of Frequency Response Functions (FRFs) with respect to the components in horizontal and vertical directions of the centrifugal force produced by the unbalanced load in the drum. The simulation results are validated experimentally for all configurations studied, using an off-the-shelf Electrolux W565H washing machine, which has been equipped with the prototyped semi-active friction dampers and with the prototyped Tunable Vibration Absorbers specifically built for this study.

The thesis is structured in three parts. The first part is focused on the derivation of the standard lumped parameter model and the derivation of

the equations of motion for the oscillations of the tub-drum assembly in the vertical and horizontal directions and for the normal force transmitted to the floor via the suspension system formed by four springs and friction dampers connected in parallel. The validity of the proposed model and formulations is assessed experimentally by comparing the FRFs of the displacements of the tub-drum assembly per unit centrifugal force in horizontal and vertical directions with measured FRFs taken with accelerometers placed on top and on the side of the tub of the washing machine. Also, the FRF of the normal force transmitted to the floor per unit centrifugal force in vertical direction is compared with the FRF measured using four load cells placed on the feet of the washing machine. The experimental validations consider two configurations of the suspension system: the first is formed only by lightly damped springs whereas the second is formed by the lightly damped springs with in parallel heavily damped passive friction dampers. The latter configuration replicates the standard operative conditions of the tested washing machine. The study shows that the model reproduces the principal features of the dynamic response of the washing machine in the entire frequency range covered by the drum spinning velocity. The spectra of the FRFs for the amplitude of the drum oscillations in horizontal and vertical directions are characterized by two resonance peaks at low frequencies whose amplitude is dictated by the resonant responses of the fundamental modes in horizontal and vertical directions of the tub-drum assembly mounted on the four elastic mounts and dampers. At higher frequencies, the amplitude of the oscillations in the horizontal and vertical directions levels to a constant value, which is proportional to the unbalance factor produced by the load in the drum. The normal force transmitted to the floor is also characterized by two resonance peaks at low frequencies. However, at higher frequencies, the transmitted force rises proportionally with frequency and with the damping factor of the dampers in the suspension system. Therefore, the general conclusion of this introductory study was that, to lower the oscillations of the tub-drum assembly and the force transmission at the low frequency resonances, high damping levels should be implemented in the suspension system. However, this would also tend to magnify the force transmission to the floor at high spinning velocities. For this reason, normally designers select the dampers in such a way as to guarantee a compromise where the low frequency resonance effects are mitigated as well as the high frequencies force transmission. In this way the two principal problems that affects the dynamic response of washing machines are somehow tackled: first, the amount of space

needed to avoid the tub-drum assembly hits the chassis of the machine at low spinning speeds and second, the walking phenomenon at higher spinning speeds.

Furthermore, the first part of the thesis provides an empirical model of the time and frequency dependent residual moisture content in clothes, which can be used to predict the variation of the amount of unbalance during the spinning cycle. Constant garments composition, constant temperature, constant filling coefficient and no use of detergent are assumed. A scaling analysis showed there is no significant influence of the drum shape and washing capacity on water retention for the shape factors and G-acceleration range of professional washing machines.

The second part of the thesis is focused on the modelling, theoretical analysis and experimental implementation of semi-active dampers in a professional washing machine, specifically designed to reduce the tub-drum assembly oscillations and the normal force transmission to ground. Based on the findings in the first part of the study, the semi-active damper has been designed in such a way as it can switch from a very high to a very low damping level. The four semi-active dampers connected in parallel with the elastic suspension are therefore set to work with high damping levels at low spinning frequencies where the tub-drum oscillations and normal force transmission are characterized by the resonant responses of the fundamental natural modes of the tub-drum assembly and elastic suspension system. At higher spinning frequencies, the four semi-active dampers are instead switched to very low damping values such that the normal force transmitted to the floor is minimized without affecting the amplitude of the tub-drum oscillations, which, in this frequency range, only depend on the unbalance factor. Also in this part of the work, the validity of the model and formulations developed for the tub-drum assembly mounted on elastic mounts equipped with the proposed semi-active dampers has been assessed experimentally by comparing the FRFs of the displacements of the tub-drum assembly in horizontal and vertical directions with measured FRFs taken with accelerometers placed on top and on the side of the tub of the tested washing machine. Moreover, the FRF of the normal force transmitted to the floor in vertical direction has been compared with the FRF measured using four load cells placed on the feet of the tested washing machine. Also in this case the model has been found to accurately reproduce the principal features of the dynamic response of the washing machine equipped with the semi-active dampers in the entire frequency range covered by the drum spinning velocity. The amplitudes of the two resonance peaks that

characterize the spectra of the FRFs for the amplitude of the tub-drum oscillations in horizontal and vertical directions and the FRF for the normal force transmitted to the floor at low frequencies are greatly reduced by the high level of damping generated at low frequencies. Moreover, the low levels of damping produced at higher frequencies effectively reduce the normal force transmitted to the floor without affecting the amplitudes of the tub-drum oscillations, which are mitigated by the ballast masses.

The third part of the thesis is focused on the modelling, formulation and experimental implementation of semi-active Tunable Vibration Absorbers in a professional washing machine, which replace the classical ballast masses used to mitigate the dynamic response of the machine at higher frequencies than the fundamental resonance frequencies. These devices are designed to reduce the drum oscillations and normal force transmission to ground specifically at the excitation frequency, by tuning their characteristic resonance frequency to the excitation frequency, that is the drum spinning velocity. Therefore, to operate in the entire spinning range of the washing machine, they require a continuous tracking of the drum spinning velocity to adapt the tuning of the TVAs to the excitation frequency. Also in this case the validity of the model and formulations developed for the tub-drum mounted on classical spring-damper mounts and equipped with the proposed tunable vibration absorbers, which replace the ballast masses, has been assessed experimentally by comparing the FRFs of the displacements of the tub-drum assembly per unit centrifugal force in horizontal and vertical directions with measured FRFs taken with accelerometers placed on top and on the side of the tub of the tested washing machine. Moreover, the FRF of the normal force transmitted to the floor per unit centrifugal force in vertical direction has been contrasted with the FRF measured using four load cells placed on the feet of the washing machine. In this case the model has been found to partially reproduce the principal features of the dynamic response of the washing machine. This was due to the design chosen for the tunable vibration absorbers, which resulted being characterised by side effects not taken into account during the design stage. In particular, the cantilever beam-tip mass construction resulted difficult to install and balance. Nevertheless, initial tests were implemented, which showed that the spectra of the FRFs for the amplitude of the drum oscillations in horizontal and vertical directions and the FRF for the normal force transmission to the floor would be characterized by an antiresonance peak at the tuning frequency of the TVA, that is a significant reduction of the tub-drum oscillations and normal force transmission to ground.

Although the results produced in this third part of the study refer to a limited set of tuning frequencies, they clearly indicate the potential advantages of this solution, which could in fact require a fraction of the ballast mass with clear practical advantages in terms of transportation and production costs of the washing machine.

The thesis is enriched with three appendixes that provide the technical drawings of the semi-active damper, of the cantilever beam with tip mass and of the base-framework used to performed the tests.

Contents

List of Figures

List of Tables

Nomenclature

List of Acronyms

DOF	Degree Of Freedom
DVA	Dynamic Vibration Absorber
FF	Fill Factor
FRF	Frequency Response Function
MRF	Magnetorheological Fluid
RMC	Residual Moisture Content
SOR	Sistem Of Reference
TMD	Tunable Mass Damper
TVA	Tunable Vibration Absorber
TVN	Tunable Vibration Neutraliser
WM	Washing Machine

List of Symbols - *Latin letters*

Parameter	**Description**	**Unit**
A	Area	m^2
a	Coefficient	
c_v	Viscous damping	Ns/m
c_f	Coulomb damping	Ns/m
D	Diameter of the drum	m
d	Depth of the drum	m
E	Young's modulus	N/m^2
F	Centrifugal force	N
f	Distributed force	N/m
F_{c_f}	Coulomb friction force	N
F_{c_v}	Viscous damping force	N
F_k	Spring force	N
F_{m_t}	Lumped inertial force of the tip mass	N
G	Dimensionless acceleration	
g	Gravitational acceleration	m/s^2
I	Second moment of area	m^4
k	Stiffness	N/m
L	Length	m
M	Internal bending moment	Nm
M_b	Mass of ballast	kg

m_{bd}	Bonedry mass of the textile	kg
m_{cd}	Conditioned mass of the textile	kg
m_{H2O}	Residual mass of water in the textile	kg
M_{m_t}	Lumped inertial moment of the tip mass	Nm
m_u	Unbalance mass	kg
m_t	Tip mass	kg
M_{tot}	Mass of the tub-drum-ballast assembly	kg
M_w	Mass of water	kg
m_{wet}	Mass of the wet textiles	kg
$m_{w,exr}$	Mass of water extracted	kg
R	Force transmitted to ground	N
r	Radius	m
R_t	Water retention	
s	Average thickness of the textile layer	m
S_f	Shape factor	
T	Shear stress	N
t	Time	s
u	Horizontal displacement (non-inertial SOR)	m
V	Volume	m^3
v	Vertical displacement (non-inertial SOR)	m
x	Horizontal displacement (inertial SOR)	m
y	Vertical displacement with (inertial SOR)	m

LIST OF SYMBOLS - *Greek letters*

Parameter	**Description**	**Unit**
δ	Delta Dirac function	
ξ	Damping ratio	
λ	Eigenvalues	
μ	Mass ratio	
ρ	Density	kg/m^3
Φ	Modal amplitude	
Ψ	Modal amplitude	
ω	Frequency	Hz

FREQUENCY RESPONSE FUNCTION

Parameter	**Description**	**Unit**
G	FRF of the harmonic drum oscillations	m/N
T	FRF of the harmonic force transmitted	N/N

X	Spectra of the amplitude of the drum oscillations in horizontal direction	m
Y	Spectra of the amplitude of the drum oscillations in vertical direction	m
R	Spectra of the amplitude of the force transmitted	N

1

Introduction

This thesis studies the dynamic response of professional washing machines in order to reduce vibration transmission and to improve mechanical design. More specifically, this work aims to diminish the oscillations of the tub-drum assembly generated by non uniform mass distribution of washed garments and, furthermore, to enhance the ground vibration isolation in such a way as to mitigate the undesired vibrations transferred to the floor. In particular it considers both semi-active dampers composed by disengaging system and Tunable Vibration Absorbers (TVA) based on cantilever beam with a movable tip mass construction. The thesis presents a detailed model of the dynamic response of the washing machine and introduces a new experimental load characterisation by predicting the amount of water contained in the cloths during an extraction cycle. This affects the "dewatering performance" of the washing machine, and this has a direct impact on the drum oscillations and vibration transmission to the floor.

This section introduces the use and development of professional appliances in history with special attention on cloth washers, and the effects of laundry system on electricity and water consumption. It then points out the main constrains for the mechanical design of professional washing machines, with respect to the dynamic response of the tub-drum assembly. The principal phases of a washing cycle are described with a particular focus on the spinning phase where the water retention phenomena on the washed load are particularly relevant. Successively, vibrational effects of the appliances are introduced in details and associated to the distribution of garments inside the drum. Moreover the different typology of suspension system and TVAs devices is revised in detail and a comparison between passive and semi-active vibration control solutions is thoroughly examined. A summary of the objectives, contributes and structure of the thesis concludes the chapter.

Figure 1.1: Picture of the first sketch of a mechanism to wash textile done by Ottavio Strada in 15th century [1].

1.1 Professional washing machine

The invention of washing machines goes back to the 15th century, when Ottavio Strada sketched his first idea about a mechanism probably intended for use in textile manufacturing as showed in Figure 1.1.

A century later John Hoskins put some dirty garments in a sort of bag which could be immersed in water and squeezed by using a gear with wheels and cylinders. Later, on 1691, an English patent was described as a kind of "engine" for variety of usages, like oiling and dressing leather and cloth, raising water, washing clothes, milling sugar canes, pounding minerals, pounding and brushing seeds, pounding charcoal and pounding rags to make paper [2]. Several designs were patented before 1800, but the most famous was done by Edward Beetham hooked up with Thomas Todd in 1790's in London where the first portable washing mill was described as showed in Figure 1.2. The machine was composed by a large wooden tub where the clothes were inserted to be washed. A manual rotating lever was used to set some blades into rotation, in such a way as to create the mechanical action that simulate the rubbing of

Figure 1.2: Picture of the original Beetham's royal patent washing mill No. 27 Fleet Street, London / Miss Beetham delt. Published in January. 1st, 1791 by Crouch & Stevenson [3].

laundresses. The development of washing machines, and more in general laundry machineries, collided with the fear of laundrywomen to lose their job, even though this invention was developed to help them and facilitate their working conditions. These concerns were mitigated thanks to the persuasive advertising campaigns of Schäffer in Germany and Beetham in London and the development of laundry machinery grew in the later years.

Several patents came in succession among which it is relevant to mention the first washing machine equipped with a rotating drum invented by Henry Sidgier, which started the electromechanical integration by installing an electrical motor to rotate the drum. Soon after the concept

The new THOR-32 is ready. We believe it to be the simplest, handsomest and most perfect washing machine ever produced.

It is the result of 14 years' cumulative experience, the loyal effort of old and skilled workmen, and was inspired by a vision of what people demand in new and better things.

The new THOR-32 is made entirely of metal and has a capacity 60% greater than previous models occupying the same floor space.

In the THOR-32, as in all previous Thor models, quick thorough washing, without wear on clothes, is accomplished by the revolving, reversing cylinder which gently lifts and dips the clothes through active, soapy water.

There is a self-draining cover, never attempted in any washing machine before, and a wonderful metal swinging wringer.

Proud Thor dealers, more proud than ever now, will be happy to show the new THOR-32 and explain the liberal terms.

Write to us for our new book, "You and Your Laundry," Mrs. Christine Frederick's late work. It will be sent free and prepaid.

Other Products of the Hurley Machine Company are the Thor Electric Ironer and the Thor Electric Vacuum Cleaner

HURLEY MACHINE COMPANY

General Offices and Factories, Chicago

147 W. 42nd St., New York
817 Walnut St., Kansas City
209 Tremont St., Boston
413 Yonge St., Toronto
319 N. 10th St., St. Louis
822 S. Broadway, Los Angeles
124 Post St., San Francisco
Durant Bldg., Flint, Mich.
British Distributors
Chas. E. Beck & Co., Ltd., 70 New Bond St., London

Figure 1.3: Picture of the Thor washing machine, the first washing machine that provided an electrical engine directly coupled to the rotating drum (1910).

of automation was introduced in laundry by Alva J.Fisher as reported in the patent registered at United States Patent Office. He first designed a drive mechanism for the rotating drum in 1910 [4] and then improved the concept using shaft coupling systems to directly connect the electric engine to the rotating drum of the appliance [5]. This solution was implemented on "Thor washing machine" (showed in Figure 1.3) and manufactured by the Hurley Machine Company of Chicago.

Over the years, the technological development has greatly improved the mechanical design of washing machines, making them more reliable and cheap, which has led to widespread use in the laundry automation. The economic development, which brought to the development of new commercial activities, introduced professional machines in the market in order to satisfy the new habits of people. The Electrolux AB public annual report 2018 documents the increase of net sales from 7723 to 8666 million SEK during the last year in professional market [6] with the great contribute of laundry market. Professional laundry machines are specifically designed and manufactured for industrial applications or when longer life, robustness, high load capacity and fast cleaning cycle become relevant. Indeed, these products have not only to preserve the features and the usability of home appliances but also improve both their durability and washing performances. In fact, they must handle the high extraction force of the spin cycles which results from the high washing load capacity that can reach up to 400 kg with consequent effects on the final cost. This makes professional washing machines suitable for use in commercial laundry shops, hotels and apartment buildings. In fact, self service laundries are characterised by many typology of professional machines like cloth washers, tumble dryers, ironers, etc. in order to cover all the different types of use and requirements. Business working hours of these companies typically run from 6 a.m. to 10 p.m. and the stores usually occupy from 1000 to 5000 square feet of retail space. There are about 29500 coin laundries in the United States, generating nearly $5 billion dollars in gross revenue annually that grows proportionally to the increase in population [7]. These data make possible to understand how professional machines, unlike domestic machines, have to guarantee a daily operation continuity in diverse environmental conditions. Indeed, wide range of temperature, humidity, amount of detergent, hardness of water, plant layout, etc. vary considerably throughout the world. Even more, the final user typically do not pay much attention on the use of professional appliance and this increases the damage or break down risk. For these reasons professional appliances have a comparatively much more robust structure as showed in Figure 1.4 where the panels, the frame and the structure of the machine are made in stainless steel instead of plastic as happens in the domestic cloth washers.

Laundry activities have an important impact on world energy and water consumption. Therefore the new regulations impose limits in order to lower their environmental impacts. As described in the “Final report: Preparatory Studies for Eco-design Requirements of Energy-using Products” written by Öko-Institute e.V. and BIO Intelligence Service, the relative energy consumption of professional washing machines can be divided in sub-categories based on three needs: energy used for water heating, energy for the motor action and the energy supply for all the electronic components [8]. Considering the classification of professional washing machines based on washing capacity, Table 1.1 provides a summary of the energy, water and detergent consumption.

Energy, water and detergent consumption are real and relevant problems also thanks to the wide global diffusion of professional laundries and in particular washing machines. So the attempt to improve the whole cleaning cycle is an important aspect in order to increase the efficiency

Figure 1.4: Picture of a professional washing machine WH6-20 by Electrolux Professional S.p.A. with 20 kg of dry load washing capacity (2019).

Table 1.1: Annual energy, water and detergent consumption per professional washing machine by Öko-Institute e.V. and BIO Intelligence Service.

Washing capacity [kg]	**Cleaned laundry [kg/year]**	**Energy [kWh/year]**	**Water [litres/year]**	**Detergent [kg/year]**
< 15	14400	3026	233280	330
$15 \div 40$	42200	10973	740610	798
> 40	194400	81648	3265920	4199
barrier washer	56300	26461	1080960	1216
washing tunnel	3825000	1606500	27540000	41310

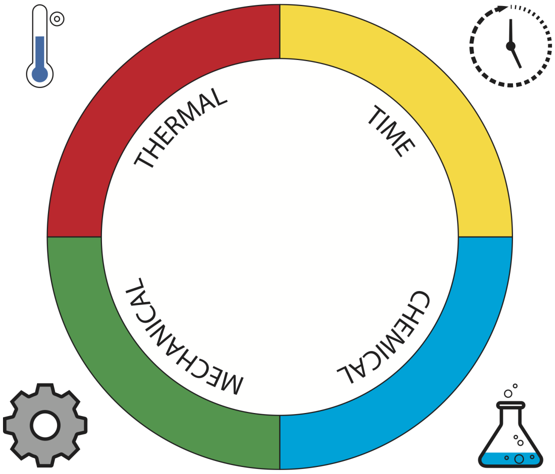

Figure 1.5: Sinner's circle for cleaning operations.

of the system. The main influences on resources need and cleaning performance are described in the Sinner's circle of Figure 1.5. This diagram defines the relations and quantify the energy needs of the washing phases that affect the final washing result, which are: time, thermal, chemical and mechanical action. The idea behind the scheme is that, different sections of the circle can be changed in their size by privileging one action in respect to the others, but the total area remains preserved in order to guarantee the energy necessary to perform the cleaning. For instance if the temperature is reduced to save energy, the washing time gets longer or more detergent has to be used [9] to balance the cleaning operation. However the Sinner's circle does not take into account the type of textile and consumer behaviour in laundry care. In recent years there is greater attention on reducing the environmental impact of laundry machines, therefore the mechanical action is advantaged in order to lower water consumption in the washing cycle. For this reason the mechanical design of the machine is becoming more and more relevant to guarantee the required performance and limit the use of other forms of energy.

1.2 Operation phases of washing machines

A professional washing machine provides different washing cycles which are specifically design based on the type of cloth and its level of dirty. The cleaning program most known and used is the "60°C cotton cycle" which is composed by a combination of main-wash, drain, extraction and rise phases and it is normally provided by all the suppliers of appliances. Throughout the main-wash, the tub is filled of water previously warmed up to the desired temperature and mixed with detergent and softener. The drum rotates clockwise and counter clockwise at low speed to blend the laundry in such a way as to enhance the rubbing of the clothes. This improves the mechanical action that removes the stains of dirt. The main-wash is followed by the drain phase where the residual water not absorbed by the textile is drained through the plumbing of the machine in few seconds. Often an intermediate short and weak extraction phase is required in order to lower the water content of the textile before a successive rising phase starts. This allows to remove any detergent and dirty particles dissolved in the water and to refresh washed clothes. A series of drain, extraction and rinse cycles can be planned in succession after the main-wash, depending on the type, amount and quality of washed load. Any cloth washer ends its operations with the extraction cycle, also defined spinning cycle, in which the revolution speed of the drum normally increases up to the maximum limit. Thus the clothes are exposed to the centrifugal force that drains out the water in the so called dewatering process, which is relevant to short the post drying operations in tumble dryers and thus to save energy and time in the entire laundry process. The spinning phase is critical both for dewatering and for the vibration transmission to floor. The not uniform mass distribution of the clothes inside the rotating drum produces an unbalance effect in the rotor, which generates a centrifugal force that excites the structure of the appliance as well as the base floor. This force grows with the square of the angular speed of the rotating drum. Therefore the spinning phase produces the maximum mechanical excitation of the structure and floor. Hence the features of the spinning cycle, i.e. both in terms of time and speed, plays a fundamental role to avoid overloading the appliance and to maintain an acceptable duration of the washing process. To guarantee the final drying specifications it is relevant the washing machine can detect and predict the amount of moisture content in the clothes during the extraction cycle based on the type of load and on the dimension of the washing tub.

1.2.1 Water retention

The mechanical design of the principal components of the washing machine is strongly related to the extraction performances since the centrifugal force, which is responsible of the water removal from wet textiles, increases with the diameter and spinning velocity of the drum. The amount of residual water content in the garments, greatly influences the successive dry process, which normally has a significant impact on the time and cost of the washing process. Indeed, as discussed by Carter & Shah [10], the energy necessary for drying fabrics strongly depends on the textile residual moisture. For this reason, it is important to predict and control the water content during the extraction phase. Many parameters may influence this process, such as the type of textile, the appliance capacity, the amount of load and its aging, the quantity and chemical composition of detergents, the principal fluid parameters (water temperature and hardness), the spinning speed and washing programs [11]. In general, literature lacks data on textiles water retention, in particular in relation to washing machines operations. In contrast, studies can be found on soil and generic porous media. These works are typically based on empirical models derived from numerical approaches, which are usually implemented with Computational Fluid Dynamics (CFD) and thus are limited to special cases and configurations where the CFD model can provide reliable results. The laundry dewatering process considered in this study is a rather complex process, and thus, this study presents an empirical model for the dewatering based on measurements taken on typical washing machines used for professional laundry. Although literature lacks studies on the dewatering process in washing machines, several water retention models are used in hydrology to predict fluid flow through soil. Normally these models are based on either analytical formulations, numerical simulations or experimental measurements. Nevertheless, the complexity of the water retention phenomenon makes it necessary that all these approaches are based on important hypothesis that simplify the problem at hand while yet preserving the most relevant aspects. Therefore the construction of these models is strongly related to the practical application at hand, as in fact this thesis does by referring to the specific problem of water retention in washing machines.

Analytical models of water retention

Brooks [12] and Cheng & Gulliksson [13] described analytically the flow of fluids on porous media considering bi-phasic fluid composed by water and air. They presented some analytical solutions to model the effective permeability, like for example Corey's approximated formulation [14], which includes also the capillarity pressure profile across the fluid interface. The use of Richard's equation [15] was suggested to simplify the calculation considering the air-phase pressure constant. Brooks & Corey [12] also proposed a test rig to characterise the average features when air and water flow through fabrics is in steady-state conditions. Nevertheless, these models cannot be satisfactorily implemented to study the water retention of fabrics in spinning washing machines since the hypothesis of constant pore size distribution made in the models is not satisfied in practice due to the stretching and compressing phenomena that occur in the fabrics during the spinning. Moreover, the effective permeability estimation cannot be considered under steady-state conditions. An experimental setup was built by Brasquet et al. [16] to study pressure drops of air and water through several different textile fabrics. The collected data were used into Belkacemi and Broadbent's model and the outcomes were employed to train a Neural Network (NN) model for successive statistical analysis. The study confirmed the influence of operating conditions and swelling phenomena on pressure drops effects.

Loeb [17] used Gurnham and Masson's soil hypothesis to describe water retention of cotton fabric. A step-by-step compressional load was used to reduce water content. However, the model resulted reliable only for low pressure ranges. Salehi Rad et al. [18] analysed water retention in hollow fibres compared to solid assemblies with equal linear density. They highlighted a simple law for the water retention with respect to the hollow-fibre weight fractions.

Several analytical models for the prediction of water flow in porous media is available in hydrology. Darcy's law is commonly implemented to predict steady-state laminar water flow. Mongan [19] used a centrifugal technique to vary the gradient of pressure and extend the validity of the Darcy's equation also to transient conditions, whereas Ghane et al. [20] introduced Forchheimer's coefficient to consider non-Darcy inertial effects. Beckett & Augarde [21] presented a pore-size distribution analysis incorporating porosity and particles of different dimensions, shapes and separation distances to predict water retention properties. This geometry approach is time consuming and needs knowledge of micro and macro structure of every media. Other techniques were discussed by Castellini et al. [22] using three different Beerkan Estimation of Soil Transfer (BEST) procedures in such a way as to obtain a complete hydraulic characterization which was compared to the reference evaporation method. Here, two constants of the soil must be determined: β, related to the shape of the grains and ν, which is a geometric correction factor. Nevertheless the results obtained with these procedures were found to underestimate the flow unless a fine tuning of the input data is provided.

The mathematical models described above used many parameters connected to the physical characteristics of soil and textiles. Maggi [23] proposed an algorithm to reliably derive these parameters, which is based on a heuristic global optimization method (well suited to solve multidimensional problems involving continuous variables), and achieved significant results. Furthermore Neural Networks (NN) can be exploited to derive the key coefficients of the models. Ebrahimi et al. [24] applied a NN on ten soil water retention curve models with fitting accuracy that depends on the functions used in the hidden layer. Moosavizadeh-Mojarrad et al. [25] implemented two NNs to estimate volumetric water content of soil and matrix head as input for Van Genuchten model with an accuracy strongly dependent on the equation used.

Numerical models

Multi-phase fluid flow on porous media must be considered to properly reconstruct the permeability and retention properties of fabrics. This is a rather challenging numerical task, which, however, can nowadays be implemented even for the fabrics with complex structure thanks to the increasing computational power of computers [26]. Rief et al. [27] did numerical simulations with virtual models including the macro, meso and microstructures to generate permeability data of fabrics with complex structures. The models were derived following two approaches: the first was based on realistic input parameters of woven textiles whereas the second reconstructed the 3D geometry from sequences of 2D cross section images. The 3D geometry was then used to predict the mechanical flow properties of the fabric by solving the equations of motion of the equivalent porous medium. Despite the complexity of the proposed model, the results obtained from the simulations were not entirely satisfactory, primarily because the model was not able to correctly predict the stresses (mechanical, thermal and chemical) occurring in real fabrics.

CFD techniques cannot be easily employed to predict the fluid flow properties of fabrics in washing machines because the gradient of pressure generated during the spinning phase is unknown. To predict the transient state both the water and airflow conditions should be taken into consideration in the model of the equivalent loaded porous medium. Moreover, the equations of motion should also describe the textile elastic behaviour and the absorption limit due to capillary effects [28]. During the cycle, the physical and geometrical parameters of the textiles change in relation with the relative stretching produced by the spinning. This further complicates the model and makes the computing time unacceptable for laundry applications.

Water retention numerical analysis has been successfully applied to study soil drainage. Narasimhan & Witherspoon [29] presented an Integrated Finite Difference Method (IFDM) to solve ground water flow problems. The proposed approach is easier and faster to implement with respect to a Finite Element Method (FEM) of similar accuracy. Nevertheless this approach also cannot be easily implemented to predict fluid flow on textiles, particularly on textiles contained on a spinning drum.

In conclusion, the fluid flow models available in the literature cannot be successfully employed to predict and generate water retention data for textiles in spinning washing machines.

Experimental models

Water retention phenomena can also be successfully described with empirical laws based on experimental data. For instance, a number of experimental techniques can be found in the literature to estimate the water retained by different porous media under controlled conditions. One of these is the spinning technique, which is similar to what happens to cloths in the drum of a washing machine. Carter & Shah [10] studied the water surface tension on cotton, which is related to the residual water content in fabrics, using a centrifugal system. The setup was made by a centrifuge tube with a drilled copper insert on it, in such a way as water can flow out of it. The relationship between the Residual Moisture Content (RMC) and the water surface tension was demonstrated. They showed that the RMC tends to lower exponentially by increasing the ejection force. Similar techniques are also used for soil, clay and cellulose as proved by Reatto et al. [30] who obtained encouraging results and compared the centrifuged method with respect to the standard one. Saboya et al. [31] exploited a small centrifuge system to confirm the Van Genuchten model. Caputo & Nimmo [32] compared Steady-State Centrifuge (SSC) and Quasi Steady-State (QSC) methods to establish water flow in unsaturated porous rock samples. Spinning tests increase driving force, yielding more accurate values of water retention and hydraulic conductivity. They reported that, in the most favourable condition, the SSC approach has an uncertainty of about ±8% for compressible media. Cheng et al. [33] demonstrated that for cellulosic material, the main parameters affecting water retention under centrifugal force are time, speed, and the type of filter used in the machine.

The water absorption of terry towels was investigated by Petrulyte & Baltakyte [34] using stereoscopic zoom microscope and a digital camera.

They studied the impact of water, heat, mechanical action and industrial washing on absorption performance. The wetting process was faster in fabrics affected by laundry and the experimental results were best described by polynomial and exponential empirical equations. Furthermore it was found that adding detergent at the washing of terry woven fabrics increases water absorption up to 1.8 – 2.2 times compared to grey samples [35].

1.3 Vibration in washing machines

The spinning process in a washing machine is a source of undesired vibrations and noise, which can cause distress on people as well as reduce system lifetime, reliability and washing capacity [36]. As previously described in Section 1.2 the extraction cycle is the most relevant operation from the mechanical point of view because the mechanical forces produced by the drum increase proportionally with the square of the angular speed. In order to lower the residual water content, an even greater extraction speed is desired in such a way as to guarantee high performances and fast drying process. This need clashes with the mechanical requirements and thus the design of the machine requires a proper optimisation study to improve the durability of the entire system. Random distribution of the cloths inside the tub, resulting from the previous washing cycle, tend to imbalance the rotating drum and thus to generate high levels of vibrations. Indeed serious vibrational problems can occur when the cylinder spins up to high speed bringing the machine even to failure. The amount of unbalance mass depends on both the weight of the laundry, its position and the conditions of the washing mode [37].

To mitigate vibrations and noise emission, the isolation system used to suspend the drum must be carefully designed in the first instance. Despite the appliance has to pass certification tests before being released into the market, nowadays, in Europe, the only official vibration output in terms of performance classifications concerns noise sound pressure measurements. The sound levels are not necessarily related to drum vibrations since also the motor and other components can also generate significant levels of noise. Few attempts have been made to classify the amount of vibration due to contacts: for example the method developed for Consumers Union (USA) [38] and the one used by Swedish Consumer Agency. These tests measure the accelerations of the mechanical components at specific points when the appliance is placed in a standardised floor. In practice, the measures are influenced by the external environments, i.e. structure and material of the floor, and by the mechanical configurations of the tested machines. This makes the tests unreliable and difficult to compare. In fact, these type of tests have caused problems in ensuring repeatability and are perhaps one of the reasons why a standard international measurement method has not been not established yet [36].

Vibrations in washing machine are also responsible of the “walking” phenomenon, which is an unstable behaviour of the appliance that occurs during the spinning and is characterised by a sliding oscillation of the feet, which progressively moves away from the set position of the machine. As shown in Figure 1.6, the walking phenomenon has three primary vibrational modes [39]

- translational slip
- rotational slip
- tip

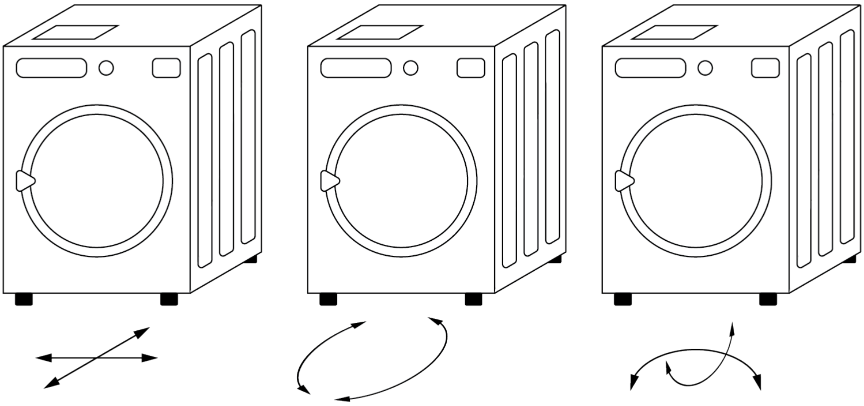

Figure 1.6: Representation of the three waking vibrational modes of washing machine: translational slip (left), rotational slip (center), tip (right).

The tip mode is typically negligible in modern washing machines, thanks to the unbalance control system and to the suspension system used to hold the tub-drum assembly. The prevalent effects are therefore the translational and rotational slips. To limit these effects the feet are designed to guarantee the maximum friction coefficient with a wider rage of floors. The torque effects, produced by the unbalance load on the tub-drum assembly, are typically low, thus the walking phenomenon is mainly generated by the two components of the centrifugal force, which harmonically affects the force components transferred to the ground through the feet. In particular the normal component harmonically varies the friction force between the floor and connection points which is alternatively reduced and increased, while the tangential component opposes the static friction and moves the appliance. In case of professional washing machines, the washing capacities, and consequently the unbalance loads, are comparatively much higher than in domestic machine, therefore standard supports do not ensure the adherence. Clamping system are commonly provided in order to fix the chassis of the machine to the floor through four or more screws of different strength. Figure 1.7 shows an example of the anchorage system for one foot of the W565H professional washing machine by Electrolux Professional.

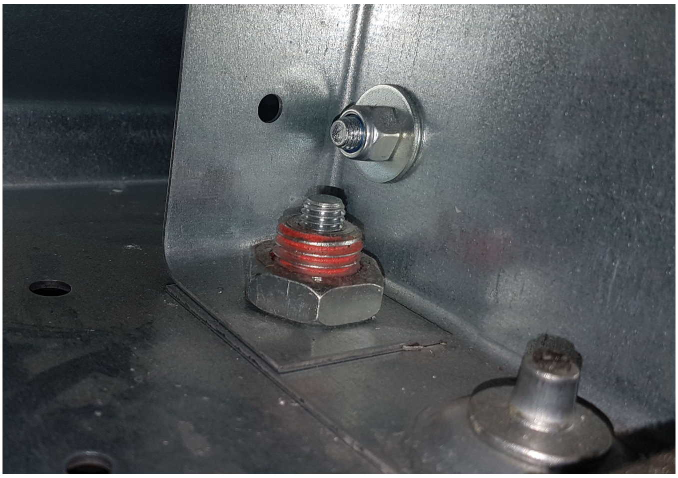

Figure 1.7: Detail view of the anchorage system for the W565H professional washing machine.

To minimise the walking phenomenon, the suspension system for the tub-drum assembly must be properly designed. Indeed, it should be designed to effectively dissipate vibrations, to guarantee a low static deflection of the tub-drum assembly and to minimise the energy transfer from the machine to the floor.

The washing capacity is a key parameter both in terms of customer satisfaction and business market positioning. For this reason the main suppliers aim to manufacture appliances equipped with larger and larger drum capacity. This generally amplifies the centrifugal force, due to the scale of the radial dimension of the inner drum, whit the consequent increase of the mechanical stress and oscillations of the tub-drum assembly. The size of the of the tub-drum assembly must be kept inside a safety range to avoid the drum impacting the external frame of the cloth washer. In fact, when the motor spins the drum from low speed to the centrifugal speed, the system harmonic oscillations pass by the fundamental resonance frequency of the tub-drum-mounts assembly, where the oscillations are greatly magnified so that the tub-drum assembly could collide with the external framework of the machine and panels. In order to lower the ground force transmission, the suspensions are normally chosen as soft as possible compatibly with the static deflection requirement. Therefore it is not possible to avoid the oscillation produced by the drum spinning and so avoid the fundamental resonance frequency of the machine.

1.3.1 Design constrains

As shown in Figure 1.8, the oscillations of the tub-drum assembly are characterised by 6 Degrees Of Freedom (DOFs) in the frequency range of interest.

The non-uniform mass distribution of the clothes inside the rotating drum generates the unbalance of the rotor and thus additional and not uniform centrifugal forces and torques act on the structure once the machine is set to spin. Figure 1.9 shows a sketch of the oscillation mode of a rotor with lumped imbalance masses m_u on it. When the mass is placed in the rotating cylinder in such a way as to only shift its ellipsoid of inertia also the center of mass of the entire system is shifted in turn as shown in Figure 1.9 (a). This leads to translations of the system along the two axes. On the contrary when the lumped masses provide a torque into the rotating drum, the ellipsoid of inertia rotates around its center as shown in Figure 1.9 (b). This configuration does not shift the center of revolution of the system, but generates rotary oscillations of the drum [40].

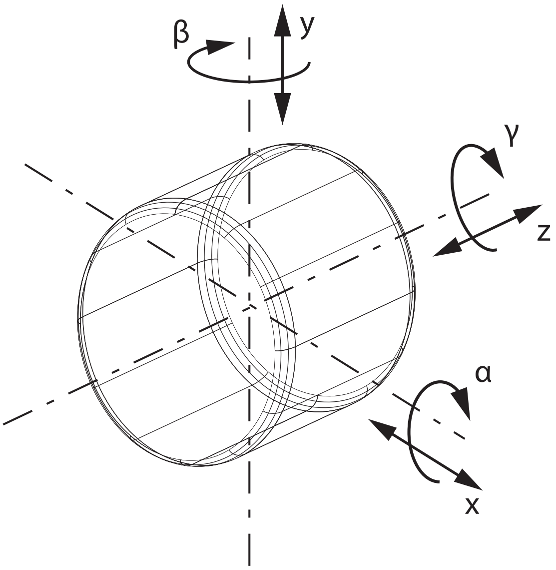

Figure 1.8: Degrees of freedom of the tub-drum assembly in a washing machines.

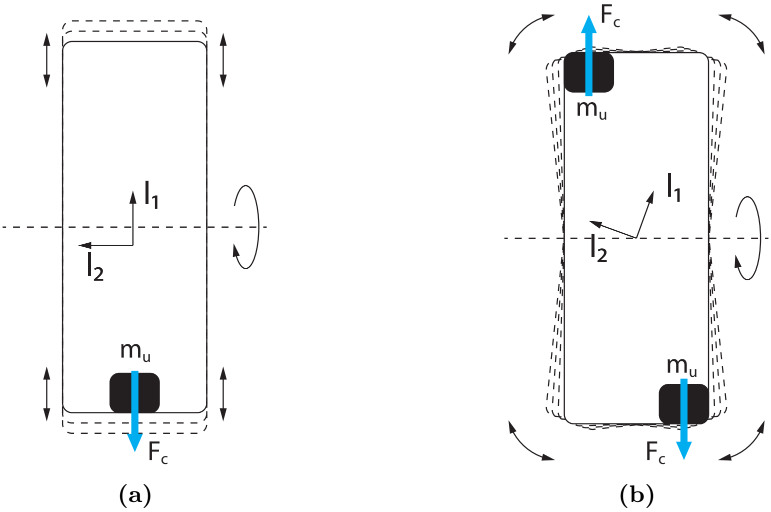

Figure 1.9: Static (a) and dynamic (b) unbalance behaviour of a rotating drum [41].

To mitigate these effects, precise design constraints are needed to avoid possible collisions of the tub with the chassis of the machine and to weaken the force transferred to the floor. First of all the diameter of the rotating drum is normally chosen slightly smaller than that of the initial design stage, thus at the expense of the washing capacity, but in such a way as to ensure safety gaps with the lateral panels of the chassis of the machine. This solution helps to avoid undesired collisions when the frequency of excitation is close to the resonance frequency of the elastic suspension and tub-drum assembly.

To lower large oscillations, the suspended components are connected to the framework by a suspension system which is typically composed of four passive dampers and helical springs connected in parallel, as shown in Figure 1.10. Since the static unbalance is typically more relevant with respect to the dynamic unbalance, the dampers are installed in such a way as to primarily dissipate drum vibration energy in vertical (y) and horizontal (x) directions, whereas the energy due to the rotating modes is mitigated by the silent block bushings of the mounts. The translations along the longitudinal axis of the cylinder (z) are commonly low and weakened by a gummy seal placed between the cylinder and the front or back panels of the case. Since the ground force transmission is a critical problem in washing machines, the springs are chosen to be as soft as possible, compatible with the allowed static deflection of the suspended mass. This solution lowers the vibration of the elastic mounts and tub-drum assembly at the resonance frequency and also lowers the ground force transmissibility at higher speeds [42].

In addition, as shown in Figure 1.10 to reduce the resonance frequency of the elastic suspension and tub assembly, ballast masses are installed in the suspended frame. This solution is commonly implemented in professional washing machines because it lowers the amplitude of the drum oscillations for a given unbalance, thus higher loads can be used without excessive oscillations of the tub-drum assembly. Ballast masses can commonly reach 60% of the total suspended mass. This obviously increases the final cost of the appliance.

1.4 Suspensions: passive and semi-active

In general vibration reduction can be achieved in many different ways; the most commons are based on *stiffening*, *damping*, and *isolation* solutions. Stiffening consists of shifting the resonance frequency of the structure beyond the frequency band of excitation. Damping con-

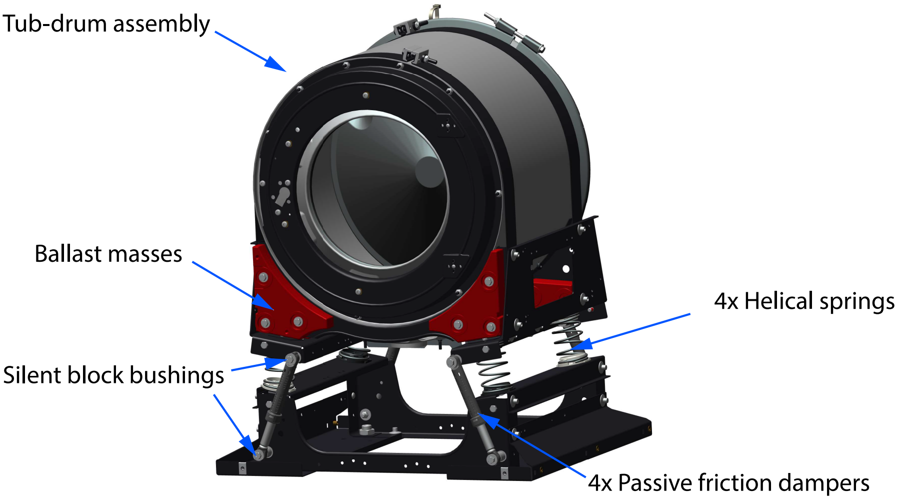

Figure 1.10: CAD view of the tub-drum assembly mounted on the suspension system composed by four passive dampers and four helical springs connected in parallel.

sists of reducing the amplitude of the response at resonance frequencies by energy dissipation. Isolation consists of preventing the propagation of disturbances to sensitive parts of the systems via a damped elastic element [43]. Stiffening techniques are not suitable for washing machine because they would excessively stiffen the elastic suspension and thus increase the force transmitted to the ground, which is the vibration of the floor and consequent noise radiation. Damping treatments are normally effective for the reduction of vibrations of large distributed flexible structures, such as the lateral panels of machine chassis. Vibration isolation with damped elastic mounts is instead a very convenient option to lower the vibration and force transmission produced by an unbalanced rotating drum. The mounts are typically composed by springs and dampers specifically designed to support and minimise the amplitude of oscillation of the tub-drum assembly and the force transmissibility to the ground. They normally act by changing the dynamic response of the suspended element, which is by lowering the stiffness of the joint, thus lowering the fundamental resonance frequency of the suspension-tub-drum assembly and by optimally damping the resonant response. Isolators can be passive, semi-active or active devices, even though the latter are never used in laundry applications due to their initial and maintenance costs and energy consumptions. Passive devices have mechanical features that can not be modified during the operations of the hosting structures. In contrast, semi-active devices present the possibility to vary their damping or elastic properties during operations. In any case both passive and semi-active elements can not provide a mechanical actuation which is instead an intrinsic feature of the active devices.

In washing machines the tub-drum-ballast masses assembly is normally supported by four helical springs connected in parallel with friction dampers. The helical springs are made of steel for reliability, cost and life cycle reasons. Therefore the elastic element of the mount is always passive. The dampers can be either passive or semi-active devices elements. In literature there are many examples of passive and semi-active shock absorbers. Figure 1.11 shows a sketch of the operative principle for the two best known passive shock absorbers: the hydraulic damper on left hand side and the friction damper on right hand side. Hydraulic damper, or viscous dampers, use the viscous loss mechanism of fluid flow through small orifices to dissipate energy by converting mechanical energy into thermal energy. The damping performance is proportional to the relative velocity of the piston cylinder components of the damper and can be modified by acting on the type of fluid and on the geometry of the orifices. For this reason, the external hermetic case is normally filled with highly viscous fluid, as for example oil, in order to provide high damping. The main disadvantage of this setup concerns the wearing of the piston-cylinder components and the consequent leakage of fluid that bring to performance degradation. Instead friction dampers are characterised by a simpler mechanism in which the friction effect, produced by the relative motion between the piston and cylinder, tends to vary a lot depending on temperature and ageing effects. The friction force F_a opposes the relative movement between the piston and the cylinder, so the mechanical energy is converted into thermal through the rubbing of the surfaces. This solution is cheaper compared to hydraulic damper, but the friction damper is more subject to wear and introduce hysteresis into the system.

Passive devices can not be optimised to properly work in all operation conditions since they are normally designed to work at frequencies close to the principal resonance frequency of the system, where the oscillations of the tub-drum assembly are rather large. Therefore undesired effects may occur at other frequencies where other solutions should be

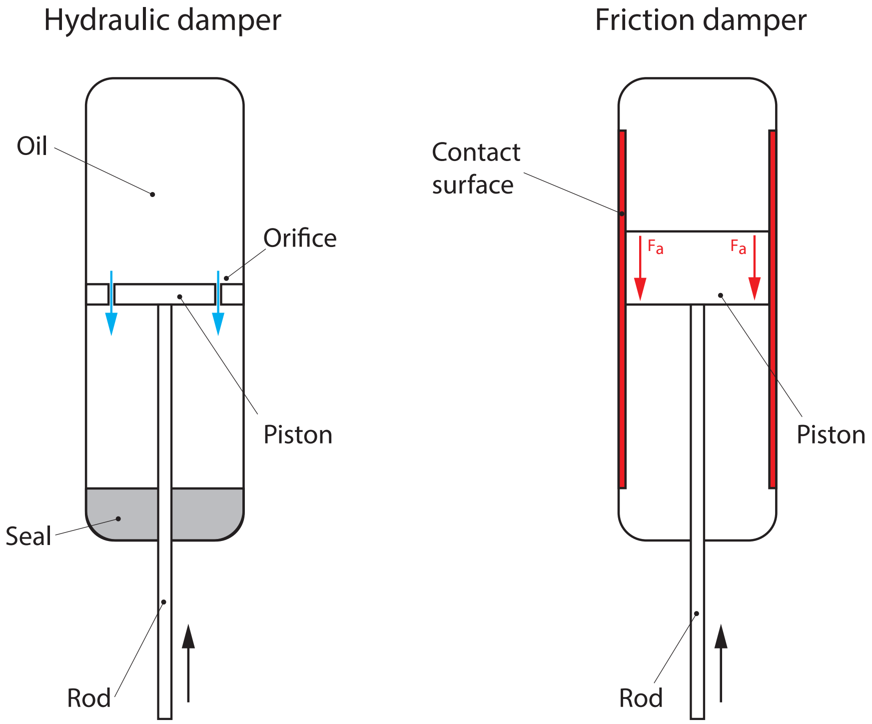

Figure 1.11: Sketch of common passive shock absorbers: hydraulic damper (left hand side) and friction damper (right hand side).

applied to improve the global dynamic response of the system. In order to keep production costs low but extend the operative damping range, passive friction dampers with two damping levels based on the amplitude of oscillation have been developed; which are called *Free-stroke dampers* and are showed in Figure 1.12. Free-stroke dampers are commonly employed in commercial washing machines to reduce the damping contribution during the extraction cycle in order to lower the ground force transmission as suggested by Suspa Inc. [44] and Sanhua Aweco Appliance System [45] manufacturers. When small amplitude of oscillations occur, the piston rod moves alternately and rubs against the low friction contact surface generating low damping effects. For large oscillations the rod applies a force on the spring, which is compressed between the piston and the limit switch. When the potential force exerted by the elastic helical spring evinces the static friction between the high friction

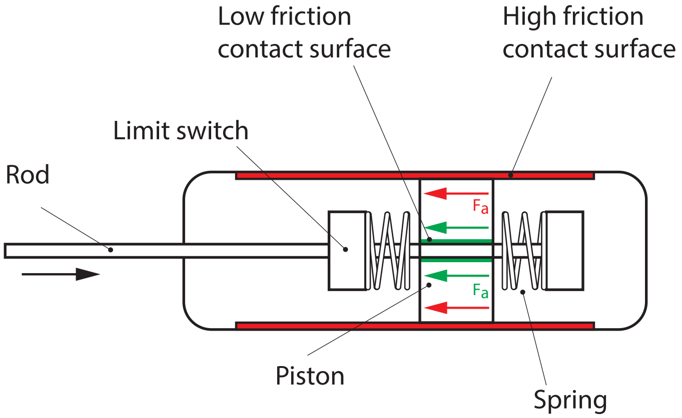

Figure 1.12: Sketch of the passive free-stroke damper.

surface and the piston, the latter moves and dissipates the kinetic energy of the structure. This solution brings benefits in terms of force transmission to the ground when is installed on a small professional washing machine that is running extraction operations, as will be described in the next chapters. In fact, during those phases, low damping levels are preferable. The energy loss of the Free-stroke damper is related to the amplitude of oscillation of the suspended load and is not directly dependent on the frequency of excitation, therefore it is not the optimal solution for laundry applications. This is because the oscillations of the drum are also related to the amount of unbalanced mass on it, which can not be controlled in front. Therefore the free-stroke shock absorber can provide good performance only in a small range of loads.

In order to optimise the vibration isolation effect of the damper at different frequencies, semi-active devices have been introduced, which can adjust the damping level using a control unit system. Thus in semi-active suspensions the damping is tuned in such a way as to guarantee, as discussed in References [46,47], low drum vibrations and force transmission both at low angular speeds, in correspondence of the system fundamental natural frequency, and also at higher frequencies where the drum is set to spin. Semi-active dampers often use magnetorheological fluids (MRFs), which are suspensions of magnetically responsive particles in a liquid carrier. The MR effect is primarily observed as a significant change of the yielding shear stress, which can be continuously controlled by the intensity of the applied magnetic fields [48,49]. In free-flowing liquid state (off-state), MRFs exhibit magnetic field-independent behaviour with only viscosity of the liquid contributing to damping. In the semi-solid state (on-state), MRFs exhibit magnetic field-dependent behaviour characterized by a variable yield stress produced by fluid flow through the skeleton of magnetised particles and thus a damping effect [48, 50, 51]. For these reasons MRFs are increasingly used to develop and manufacture semi-active dampers in which the damping effect produced by the fluid is controlled by varying a magnetic field on the fluid [52]. An example of semi-active magnetorheological damper design is reported in Figure 1.13 from the US5277281A patent [53] assigned to LORD Corporation. It is based on a piston rod cylinder assembly, where the cylinder is divided into extension and compression chambers. The piston has some orifices, in order to allow the flow of the fluid through it. Also it is equipped with coils used to generate a local magnetic field. During operation the piston is immersed in the fluid, which, due to the action of the magnetic field, undergoes a variation in viscosity in the proximity of the orifice and thus a change of damping effect produced by the device. The damper includes an accumulator with compressed gas (usually nitrogen) to compensate the volume change of the fluid due to the piston movements. This introduces an additional spring effect [54, 55], which considerably increases the total stiffness of the hosting structure. Therefore this device tends to raise the resonance frequency of the isolator-machine, which in the case of washing machines should be as low as possible. However, the MR absorbers have been successfully implemented in problems of vibration isolation.

In this respect, considering the washing machine suspension system, Chen & Zhang [56] proposed several control strategies for enhancing the resistance to walking effects. They found that the total mass of the drum, the control law of the semi-active damper and the orientation of the dampers and springs significantly influence the oscillations of the drum and thus the required clearance. Also Spelta et al. [57] analysed the benefit of using a MR damper on a cloths washer. They proposed two adaptive control strategies and tested the system in an anechoic chamber to assess noise radiation from the machine. The mechanical behaviour of MR fluid sponge damping devices was investigated by Michael and David [58], who analysed the damper durability simulating an equivalent of 2 million washing cycles on a fatigue machine. The device showed only a small decrement of performances with such a large number of cycles. Nevertheless, a professional washing machine should work for higher number of washing cycles compared to a home appliance and

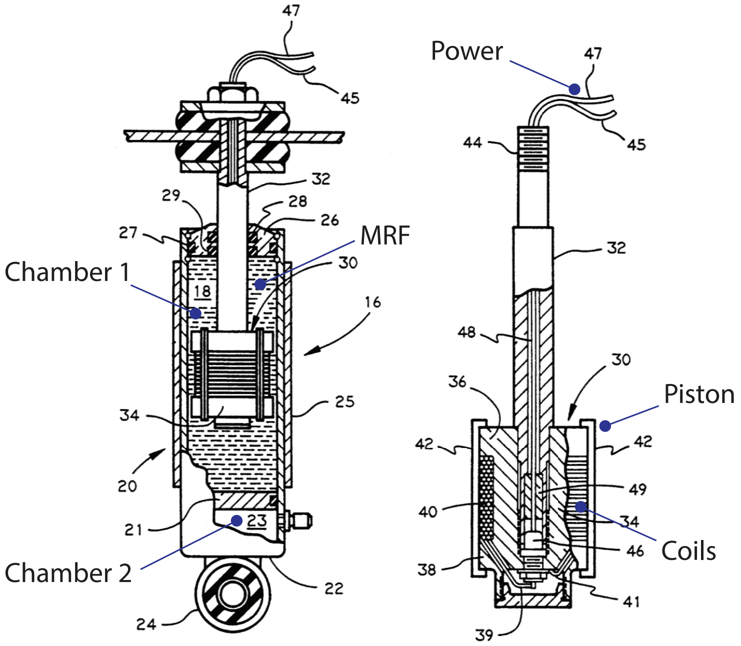

Figure 1.13: Sketch of the magnetorheological fluid damper from the US5277281A patent assigned to LORD Corporation [53].

it has bigger forces acting on it. For these reason MR dampers present some limitations, in terms of reliability and cost that must be considered during design phase. A different solution was proposed by Buškiewicz & Pittner [59]. They studied the implementation of a new semi-active technique for reducing the vibration of a washing machine frame during spinning cycle. A disengaging damper and a control unit for tuning the state were presented. With this device, the average value of accelerations of the chassis decreased by about 80% at higher speed compare to classical configuration. The patent US20050188472A1 assigned to LG Electronics Inc. [60] proposes a disengaging friction damper with coil magnet control.

Several works are present in literature about active vibration as for example the work done by Gardonio & Elliott, where different control strategies and cost functions are presented and compared both in terms of structure vibration [61, 62] and transmissibility [63].

1.5 TVA: passive and semi-active

There are different approaches to design vibration control systems. One of these involves the use of localised devices placed in strategic locations of the hosting system in order to attenuate its resonant response to a broad band excitation or to a tonal excitation [64]. A typical example of such a passive device consists in a single degree of freedom mass-spring-damper system, either tuned to a resonance frequency of the structure (Tuned Vibration Absorber - TVA) or to the disturbance frequency (Tuned Vibration Neutraliser - TVN) [65]. Tuned Mass Damper (TMD) and Dynamic Vibration Absorber (DVA) are acronyms often used in literature. These systems can efficiently reduce the vibration level only at frequencies close to those they are tuned. The idea was patented by Frahm in 1911 [66] and has been used in many industrial fields like automotive, marine, aerospace and civil engineering. The early theoretical work on its effectiveness and optimization was conduced by Den Hartog and Ormondroyd in 1928 [40, 67]. Later on, many studies were carried out on this topic, focusing on practical implementations using springs [68, 69], beam-like [70, 71] and plate-like systems [72]. A survey about the tuning criteria has been presented by Asami [73], which collects six optimization results. In many applications passive vibration control can offer satisfactory attenuation of a machine-structure vibration response, with low cost and maintenance. Tuned Vibration Neutraliser are suitable also to control tonal excitations since they can be tuned to generate an antiresonance effect at the frequency of the tonal excitation. However to control time varying tonal excitations, semi-active vibration neutralisers should be adopted, which can track and adapt to the frequency of the tonal excitation. Semi-active vibration absorbers behave like passive devices, but with the possibility to change over time the main mechanical parameters like stiffness, damping and mass in order to tune the absorbers in such a way as to lower the vibrations of the hosting system over a wider range of frequencies. The literature presents several solutions to vary the mechanical properties of vibration absorbers. Most solutions are focussed on stiffness tunable devices, which can be effectively used to change the resonance frequency of the absorber and thus adapt to the frequency of the tonal excitation. For this purpose an example of variable stiffness springs is provided by Brennan [68] who considered pneumatic springs, whose stiffness can be varied by changing air pressure inside. Rustighi et al. [74] used shape memory alloys to set the stiffness of the TVA, by varying the Young's module of the material and thus the elasticity of the spring element. Also specific geometrical configurations have been designed to modify the elastic properties of the absorber. For example configurations encompassing a leverage spring mechanisms have been investigated in References [75, 76]. In general, adaptive TVA design involves several mechanical and electrical components that define the tuning range and tuning speed of the absorber [77]. Therefore smart materials and system have been investigated to provide a fast stiffness change with very compact, light-weight and reliable solutions like those in the work reported by Blaŝzkiewicz et al. [78] and Dimarogonas-Andrew and Kollias [79]. Gardonio & Zilletti [80] presented a simulation study on two integrated tuned vibration absorbers designed to control the global flexural vibration of lightly damped thin structures subject to broad frequency band disturbances. Tunable Vibration and Helmholtz Absorbers are also used to control at target resonance frequencies respectively the flexural response of lightly damped distributed structures and the acoustic response of lightly damped cavities subject to broadband stochastic excitations [81]. Electromagnetic TVAs have been used to implement a time–varying shunted electro–magnetic Tunable Vibration Absorber for broad–band vibration control of thin structures. Here the mechanical fundamental natural frequency of the electromechanical absorber is continuously swept in a given broad frequency band whereas its mechanical damping is continuously adapted to maximize the vibration absorption from the hosting structure where it is mounted [82, 83]. TVAs equipped with a relative displacement and relative velocity feedback control system used to vary the characteristic stiffness and damping, have also been employed to modify the characteristic natural frequency and damping ratio of a TVA. Switching TVA have been developed to cyclically tune the TVA characteristic natural frequency and damping ratio. These devices can be effectively used to iteratively control the resonant responses due to multiple targeted flexural natural modes of a duct [84].

A well known practical application of TVAs has been implemented in the Millennium footbridge in London, which was built in 1999 and opened to people on 10th June 2000. Two days later after opening the bridge was closed because of high level vibrations due to pedestrians crossing the bridge. The bridge is exposed primarily to the walk excitation produced by people. The forcing frequency is in the range of $0.6 \div 1.1 Hz$ considering alternate footsteps. The increase in vibrations led to a synchronization of the people walk with the characteristic frequency of the fundamental flexural mode of the bridge, with a consequent increase in the forcing of the structure. The oscillations caused the pedestrians to proceed in a zigzag gait in order to increase their stability, so that also the lateral vibrational mode at 0.475 Hz was excited [85, 86]. Dallard et al. [86] described in their work the two solutions studied to solve this vibration problem of the Millennium bridge. The first considered the possibility to stiffen the structure of the bridge in such a way as to increase the lowest resonance frequency. The calculations showed that, to solve the problem, the stiffness of the bridge should have been increased by seven times with large investment request. The second solution, which was actually implemented in practice, used instead 37 viscous dampers to attenuate the lateral vibration mode of the bridge and 50 tuned mass dampers, of which 26 were used to damp the vertical modes and 24 to the lateral modes [87]. Figure 1.14 shows the millennium bridge and the installation of the passive TVAs installed on it.

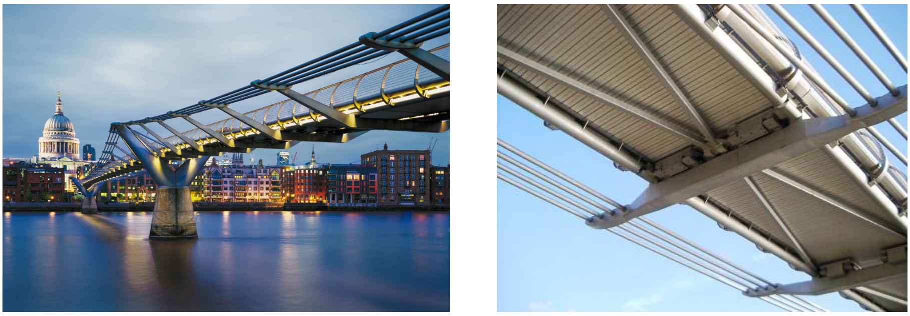

(a) **(b)**

Figure 1.14: Pictures of the Millennium bridge in London (a) and the installation of TVAs on it (b).

Semi-active TVAs have been implemented also for structural vibration control in aeronautical applications. The engines of aircraft produce relevant vibrations into the fuselage, causing an increase in noise and a consequent decrease in comfort on board. This phenomenon is amplified when the airplanes are equipped with turbo-fan engines, therefore TVAs systems have been studied and used to control the vibration and noise of the fuselage. Douglas Aircraft DC9-V is powered by two turbo-fan engines installed in the tail of the plane. These motors generate tonal excitations, which results into high vibration and noise levels into the fuselage and cabin, affecting the comfort of passengers [88, 89].

Figure 1.15 (b) shows the adaptive tuned vibration absorbers installed on the Douglas DC9 turbo-fan engines and designed by Barry Controls

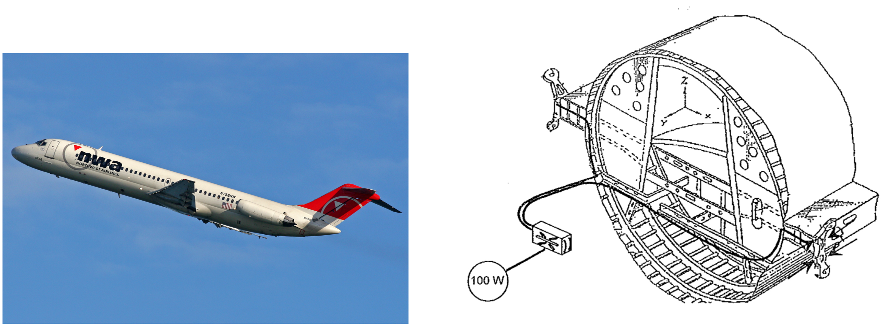

(a) (b)

Figure 1.15: Pictures of Douglas DC9 aircraft (a) and sketch of the Adaptive vibration absorber mounted on its engine yokes [89] (b).

and Hood Technology. The system is composed of two circular parallel rings connected together through a series of flexible rods in such a way as to hug the structure of the engine. An electrical motor, driven by a control system, changes the compression or tension of the rods in order to change the stiffness of the TVA and thus its natural frequency. The system was able to adapt over the rpm range of $65 \div 100\%$ with noise reduction up to 25 dB. Also passive solutions had been considered during the preliminary design phases, but the variable speed of the motor, the change in stiffness suspension due to the ageing of the material and the range of the operating temperature caused the device detune.

1.6 Objectives of the thesis

The aim of this thesis is to investigate and find solutions to attenuate vibrations in washing machines for the market of professional laundries. The objectives are to produce analytical models for the dynamic responses of these appliances and to improve their mechanical design to reduce the oscillations of the tub-drum assembly and the force transmitted to the ground via the visco-elastic mounts. More specifically the study has been focussed on two vibration control solutions: first a semi-active mount equipped with an adaptive damper and second, a tunable vibration absorber.

1.7 Contributions of the thesis

The principal contributions of the thesis can be summarised in the following points.

- *Modelling*:
  Two degrees of freedom analytical models for the dynamic response of professional washing machines have been developed. This has involved experimental characterization work considering the washed load during the extraction phase. Furthermore, analytical models of semi-active dampers and adaptive vibration absorbers have been developed to predict the oscillations of the tub-drum assembly and the force transmission to ground via the four mounts when these devices are installed on the appliance.

- *Prototyping*:
  Design and manufacturing of semi-active isolator and tunable vibration absorber demonstrators for professional washing machines, which have been used to a) validate the models and b) to investigate their vibration control features. More specifically a semi-active friction damper with a quick release damping system based on a drum rotation speed control and cantilever tunable dynamic absorber have been investigated.

- *Validation*:
  The analytical results were validated through experimental analyses performed for all the systems considered. In particular, the spectra of the oscillations and force transmission of the tub-drum assembly equipped with either the semi-active dampers or the TVAs have been measured and evaluated.

- *Publications*:
  The work carried out on the dampers and TVAs has been presented at the *International Conference on Recent Advances in Structural Dynamics (RASD)* on 15^{th} - 17^{th} April 2019 - Valpre, Lyon, France.

  The work on water retention has been condensed in the paper *Empirical model of textile water retention in professional washing machines* submitted to *The Journal of the Textile Institute* with Publisher Taylor & Francis.

  The designs of the semi-active isolator and tunable vibration absorber have been patented with the European Applications Numbers PCT/EP2019/079221 & PCT/EP2019/079251 respectively.

1.8 Structure of the thesis

The thesis is structured in 5 chapters.

- CHAPTER 1 - INTRODUCTION
  This chapter gives an overview of professional washing machines. The purpose is to provide general informations regarding the evolution of the product and to point out the main problems related to its mechanical design. More specifically, all washing phases are described with particular attention to the extraction cycle and to the vibration isolation, focusing on the oscillations of the tub-drum assembly and on the force transmitted to the ground. Passive and semi-active vibration control solutions presented in literature have been revised in order to identify the most relevant ones to improve the dynamic response of the system and to mitigate the vibration effects. The focus was on the semi-active damper and the adaptive vibration absorber.
- CHAPTER 2 - PLANE VIBRATION MODEL OF WASHING MACHINE TUB-DRUM ASSEMBLY
  This chapter first presents model and identification of the principal mechanical components that generate relevant contributions to the dynamic response of a washing machine. The equations of motion of the modelled washing machine are initially derived in the time domain using Newton's laws. The frequency response functions that characterised the dynamic response of the machine during spinning are then analysed and commented with respect to the physical parameters of the machine. The water retention during spinning is also modelled and experimentally evaluated in order to estimate the loads applied to the system.
- CHAPTER 3 - PASSIVE AND SEMI-ACTIVE SUSPENSIONS
  This chapter defines the lumped parameter models and derives the constitutive equations both in time and frequency domains for the washing machine with the semi-active dampers. A parametric study is first presented to single out the key parameters of the machine that contribute to mitigate the amplitude of oscillations at resonance frequencies and to lower the force transmission to ground at higher frequencies. Secondly, the design of the semi-active dampers built for this study is described, focusing on the mechanical components necessary to vary the damping value of the device. The chapter closes with the analysis of the measured spec-

tra of drum oscillations and force transmission with this specific configuration.

- CHAPTER 4 - PASSIVE AND SEMI-ACTIVE TVAs
  This chapter introduces the vertical plane vibration model of the tub-drum assembly when adaptive tunable absorbers are mounted on the tub-drum assembly to improve the vibration control and isolation response of the entire washing machine. The constitutive equations are derived both in time and frequency domain for the tub-drum assembly equipped with the cantilever beam vibration absorbers. A parametric study is carried out to define the geometrical dimensions used in the design and manufacturing phase. The chapter closes with the representation and description of the experimental spectra of drum oscillations and force transmission in this configuration.

- CONCLUSIONS
  The overall conclusions of the study are presented to evaluate the results obtained in terms of conformity between analytical and experimental data. Finally, new possible solutions and developments are proposed.

- BIBLIOGRAPHY

2

Plane vibration model of washing machine tub-drum assembly

This chapter describes the model for the plane oscillations of a professional washing machine tub-drum assembly. In particular it introduces the lumped parameter model developed to predict and estimate the oscillations of the tub-drum and the force transmission to ground when the appliance is set on the extraction cycle. For this purpose the constitutive equations are described both in time and frequency domain. An experimental procedure is established to characterise the water extraction from garments during the spinning phase and to define the mathematical formulae that best describe this phenomenon. Finally the experimental validation of the plane vibration model of the tub-drum mounted on elastic mounts is performed both in terms of tub-drum oscillations and ground force transmission.

2.1 Lumped parameter vibration model

A lumped parameter model is developed to describe and predict the oscillations of the tub-drum assembly and the transmission to the floor when the washing machine operates the extraction cycle. As describe in Section 1.2, the drying phase is a critical process where high excitations levels are involved. In fact the spinning extraction phase involves a constant rise of the drum rotational velocity, which overrides the natural frequency of the system, where the drum oscillations are greatly magnified, and reaches high drum revolution speeds, which greatly increase the stress and force transmission to the floor of the machine and thus the machine noise emission and the machine walking problems. Professional washing machines have wide scalability in order to cover larger market requests. Thus the mechanical features and configurations of the machine vary despite the use of similar or equivalent components. This is the reason why a simple and general lumped parameter model is proposed in this chapter to describe the vibration characteristic phenomena of the washing machine, which can help the identification of the possible strategies to reduce the vibrations of the appliance with acceptable confidence.

The analytical model is derived using Newton's laws of motion and the constitutive laws for the elastic and dissipative effects of the mounts used to suspend the tub-drum assembly of the machine. For this reason it is important that the main mechanical components involved in the dynamic response of the machine are properly selected and the way they affect the tub oscillations, drum impacts, walking and transmissibility phenomena are clearly outlined. A professional washing machine is an assembly of several mechanical components, which can be placed and mounted in different configurations based on the dimension of the machine, its washing capacity, customer requests, performance limitations and market needs. This work considers the front load W565H professional washing machine provided by "The Research Hub by Electrolux Professional" and described in Figure 2.1 and Table 2.1.

(a) (b)

Figure 2.1: Professional washing machine W565H by Electrolux Professional on a) with external panels and b) without external panels.

The W565H machine is one of the smallest industrial appliances with 7 kg of maximum washing capacity and drum speed up to 1245 rpm. The mechanical configuration relevant for the dynamic response analysis

Table 2.1: Mechanical parameters of the W565H professional washing machine used in this study.

Main specifications	**W565H**		
Fill Factor Max	1/10		
Drum volume	65		l
Drum diameter	520		mm
Extraction speed	1245		rpm
G-factor	450		
Standard heating alternatives (electricity)	5.4/7.5		kW
Low energy heating alternatives (electricity)	2.0/3.0		kW
Consumption data Normal $60^{\circ}C$ Economy (Water temperature $15^{\circ}C$ cold water and $65^{\circ}C$ hot water)			
	Full load 7 kg	Half load 3.5 kg	
Total time	46	43	min
Water consumption (cold+hot)	43+11	20+6	l
Energy consumption (motor/heating/hot water)	0.15/0.3/0.7	0.15/0.15/0.3	kWh
Residual moisture	48	49	%
Floor requirements			
Frequency of the dynamic force	20.8		Hz
Floor load at max extraction	1.8 ÷ 0.5		kN
Sounds level			
Soundpower/pressure level at extraction (ISO 60704)	73/58		dB
Soundpower/pressure level at wash (ISO 60704)	57/43		dB

is showed in Figure 2.1 (b) where the machine is shown without the external panels. The system consists of two frames made of steel plates, one suspended and one anchored to the ground through screws. The two frames are connected together by four passive mounts consisting of friction dampers and helical steel linear springs connected in parallel. The upper frame houses the washing tub which is composed by a stator case with a rotating metallic cylinder inside. The latter houses the clothes during the washing operations and has a perforated surface to facilitate the flow of water during the extraction phase. The rotational motion is provided by an electric motor connected to the cylinder through a pulley system. The suspended frame also has seats, which host ballast weights to increase its total inertia and thus minimise its oscillations at high revolution speeds. As described in the previous chapter, the wet clothes inside the rotating cylinder unfold on the inner surface of the drum in a stochastic way. Therefore the mass distribution of the rotor is continuously modified and produces time-varying unbalance effects. When the drum speeds up, this imbalance mass behaves like a rotating load where the centrifugal force generates vibrations and mechanical stress in the structure. The positioning of the garments in the rotating drum is influenced by many factors such as the filling coefficient, the type and dimension of fabrics, the washing cycle settings, etc. Thus the mechanical components that are relevant to describe the dynamic response of washing machines are:

- tub-drum assembly geometry and its dimensions;
- dampers;
- springs;
- ballast masses.

During the spinning cycle the drum undergoes a ramp such that the angular velocity is accelerated up to the programmed spinning velocity, which depends on the type of textile (cotton, wool, polyester, etc.). This velocity is higher than that for the distribution washing phase, where the clothes get stuck on the surface of the drum since the centrifugal force equals the gravitational one. The centrifugal force F acting on a given amount of garments with surface density ρ and placed at distance r_c from the center of revolution, is:

$$F = \omega^2 \int_A \rho r_c \mathrm{d}A, \tag{2.1}$$

where ω is the angular speed of the drum and A the surface of the textile. The gravitational force F_g acting on the same amount of garments is:

$$F_g = g \int_A \rho \, \mathrm{d}A, \tag{2.2}$$

where g is the gravitational acceleration. The distance between the clothes and the center of the drum r_c is about the radius of cylinder r, so that the speed ω_d where the garments get stuck to the rotating drum is given by:

$$\omega_d = \sqrt{\frac{g}{r}}. \tag{2.3}$$

At this angular speed, the rotating drum presents a layer of clothes stochastically distributed on its internal surface, which slightly increase the total mass of the tub-drum suspended assembly and also tends to unbalance the rotor as shown in Figure 2.2.

Since dynamic unbalance effect is lower compared to that generated by the static unbalance, only the latter is taken into account and thus considered as the only source of excitation acting on the drum in this

Figure 2.2: Layer of cotton towels distribution at the end of the extraction cycle.

study. Due to the contribution due to water extracted from the layer of clothes, the centrifugal unbalance can be modelled as a time dependent lumped equivalent unbalance mass $m_u(t)$ acting on the internal surface of the drum. Therefore, considering the scheme shown in Figure 1.8, only the vertical Y and horizontal X displacements, respectively along y and x axes, are relevant for this study.

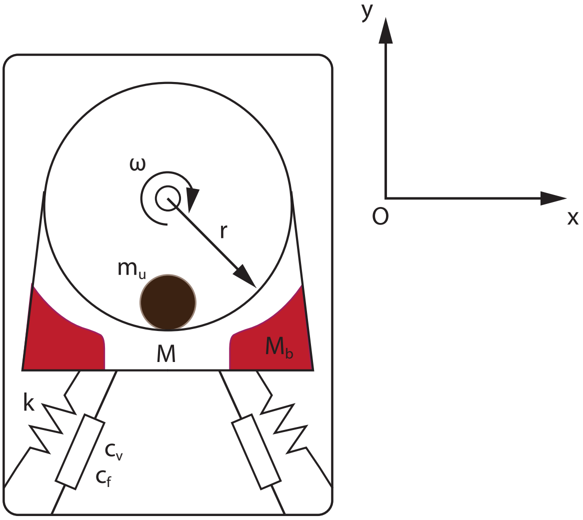

Figure 2.3: Sketch of a professional washing machine with all the mechanical components that are considered in the analysis.

Figure 2.3 shows a sketch of a professional washing machine with all the mechanical components considered for the dynamic response analyses. In this scheme M is the total suspended mass without the total ballast masses M_b and of the mass of the extracted water $M_w(t)$. Also c_v is the equivalent viscous damping contribute and c_f is the total friction damping produced by four passive suspension dampers. Finally k is the equivalent stiffness of the four helical springs.

To effectively simplify the design and cost of the suspension system, helical springs and dampers are installed in such a way as to simultaneously operate both along vertical and horizontal directions. Thus cross coupling effects between orthogonal radial directions have to be considered and incorporated into the analytical model [41]. Thus, Figure 2.4 shows the two Degrees Of Freedom (DOFs) lumped parameter dynamic model of professional washing machines considered in this study.

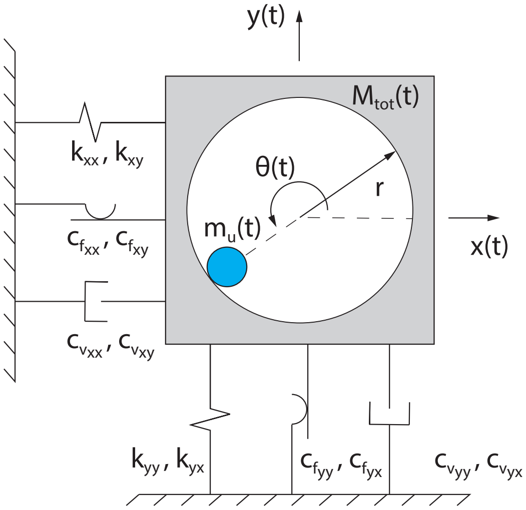

Figure 2.4: Two degrees of freedom (DOFs) lumped parameter dynamic model of the professional washing machine.

2.2 Constitutive equations

The time dependent rotating centrifugal force $\mathbf{F}_i(t)$ produced by the lumped equivalent unbalance mass along the i-th direction of motion, is described by the following formula:

$$\mathbf{F}_i(t) = m_u(t) r \omega(t)^2 \hat{\mathbf{x}}_\mathbf{i}, \tag{2.4}$$

where $\hat{\mathbf{x}}_\mathbf{i}$ is the unit position vector. This force acts on the suspended mass, which is linked to the frame of the machine through the suspension system. The suspension equivalent spring is assumed to be linear based on the assumption of small displacements, which is accepted throughout the whole spinning phase up to the maximum rotational speed for small unbalance loads.

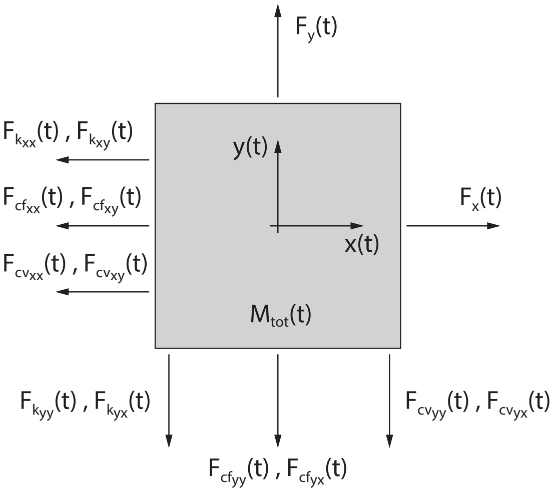

Figure 2.5: Free body diagram of the suspended tub-drum assembly for a professional washing machine.

The total suspended mass M_{tot} is defined as follow:

$$M_{tot}(t) = M + M_b + M_w(t) + m_u(t), \tag{2.5}$$

where M is the mass of the tub-drum assembly without the ballast masses M_b, $M_w(t)$ is the mass of water in the tub and $m_u(t)$ is equivalent lumped unbalance mass. As shown in Figure 2.5, the tub-drum assembly is exposed to the centrifugal, damping and elastic forces along the horizontal and vertical directions. Newton's law of motion in vector form is thus given by:

$$M_{tot}(t)\ddot{\mathbf{x}} = \mathbf{F}(t) - \mathbf{F}_\mathbf{k}(t) - \mathbf{F}_{\mathbf{c_f}}(t) - \mathbf{F}_{\mathbf{c_v}}(t), \tag{2.6}$$

where $\ddot{\mathbf{x}}(\mathbf{t})$ is the second time derivative of the position vector $\mathbf{x}(t)$, $\mathbf{F}(t)$ the centrifugal force, $\mathbf{F_k}(t)$ the spring force, $\mathbf{F_{c_f}}(t)$ the damping friction force and $\mathbf{F_{c_v}}(t)$ the damping viscous force.

Under the hypothesis of small displacements, the elastic, damping and friction forces in the suspension system are described by the following constitutive equations:

$$\mathbf{F_k}(t) = \mathbf{k}\mathbf{x}(t), \tag{2.7}$$

$$\mathbf{F_{c_v}}(t) = \mathbf{c_v}\dot{\mathbf{x}}(t), \tag{2.8}$$

$$\mathbf{F_{c_f}}(t) = \mathbf{c_f}\hat{\mathbf{x}}(t), \tag{2.9}$$

where $\mathbf{k}$, $\mathbf{c_v}$ and $\mathbf{c_f}$ are respectively the fully populated matrices of the stiffness, viscous damping and friction damping contributes.

Thus, substituting Equations (2.7), (2.8) and (2.9) into Equation (2.6) gives:

$$M_{tot}(t)\ddot{\mathbf{x}} = m_u(t)r\omega(t)^2\hat{\mathbf{x}} - k\mathbf{x}(t) - c_v\dot{\mathbf{x}}(t) - c_f\hat{\mathbf{x}}(t). \tag{2.10}$$

This equation can be broken into the following two scalar differential equations for the oscillations in x and y directions:

$$\begin{cases} M_{tot}(t)\ddot{x}(t) = m_u(t)r\omega(t)^2\cos\theta - k_{xx}x(t) - c_{v_{xx}}\dot{x}(t) \\ \qquad - c_{f_{xx}}sgn\left(x(t)\right) - k_{xy}y(t), -c_{v_{xy}}\dot{y}(t) - c_{f_{xy}}sgn\left(y(t)\right), \\ \\ M_{tot}(t)\ddot{y}(t) = m_u(t)r\omega(t)^2\sin\theta - k_{yy}y(t) - c_{v_{yy}}\dot{y}(t) \\ \qquad - c_{f_{yy}}sgn\left(y(t)\right) - k_{yx}x(t) - c_{v_{yx}}\dot{x}(t) - c_{f_{yx}}sgn\left(x(t)\right). \end{cases} \tag{2.11}$$

The spinning law for the angular speed ω of the drum is defined by the spinning phase of the washing cycle while the time dependence of unbalance mass is described in the following Section 2.5.

The design of the suspension system is of fundamental importance to minimise high vibrations of the tub-drum assembly and high force transmission to ground, which has to reduce the walking phenomenon, the noise radiation and the structural stress of the machine frame. In order to evaluate the force transmitted to the ground through the four feet of the appliance, only the vertical component R is taken into account. The horizontal component of the force transmission is tangential to the floor and responsible of the sliding of the machine. Therefore it is not considered in this study. The vertical component of the transmitted force is given by the following relation:

$$R(t) = c_{v_{yx}}\dot{x}(t) + c_{v_{yy}}\dot{y}(t) + c_{f_{yx}} sgn\left(x(t)\right) + c_{f_{yy}} sgn\left(y(t)\right) \\ + k_{yx}x(t) + k_{yy}y(t). \quad (2.12)$$

2.3 Frequency Response Functions

The Frequency Response Functions (FRFs) that characterise the vibration response of the machine are derived from the time domain equations of motion using the *Laplace* transformation and then considering the link between this domain and the frequency domain through the well known relation $s = j\omega$ [90].

The *Laplace* transform of friction damping force does not include the amplitude of oscillation dependence, in fact $\mathcal{L}\left[sgn(x(t))\right] = \frac{2}{s}$, so an alternative model has to be taken into account. Under the hypothesis of stationary conditions for the dynamic load, it is possible to determine a viscous damping coefficient equivalent to the that for the Coulomb friction damping. The idea is to equate the energy dissipated by the two types of damping over an oscillation cycle. Assuming a generic harmonic forcing:

$$F(t) = F_0 \sin(\omega t), \quad (2.13)$$

the steady state response is of the type:

$$u(t) = A\sin(\omega t + \phi), \quad (2.14)$$

$$\dot{u}(t) = \omega A\cos(\omega t + \phi), \quad (2.15)$$

where A is the amplitude of oscillation of the friction damper subjected to the force $F(t)$. In a period of oscillation T, the friction damper undergoes a total displacement given by:

$$u(T) = A\sin(\omega T + \phi) = 4A. \quad (2.16)$$

Therefore the work done by the Coulomb friction force L_{c_f} in a period T is:

$$L_{c_f} = 4AF_{att} \quad (2.17)$$

where F_{att} is the Coulomb friction force provided by the friction dampers. In a period T, the same amount of energy L_{visc} can be dissipated by an equivalent viscous damper that generates a force F_{visc} with an equivalent damping contribute c_{eq}, given by the following formula:

$$L_{visc} = \oint F_{Visc} du = \oint c_{eq} \dot{u} du. \tag{2.18}$$

Assuming a variable substitution $du = \dot{u}dt$, the work of the equivalent viscous force can be derived as:

$$L_{visc} = \oint c_{eq} \dot{u}^2 dt = c_{eq}\, \omega^2 A^2 \int_0^{\frac{2\pi}{\omega}} \cos^2(\omega t + \phi) dt = \pi c_{eq}\, \omega A^2. \tag{2.19}$$

In order to have the same energy dissipation, the two work expressions given in Equations (2.17) and (2.19) are set to be equal. As a result, the equivalent viscous damping coefficient results:

$$c_{eq} = \frac{4F_{att}}{\pi A \omega}, \tag{2.20}$$

where the damping constant depends on the frequency of excitation ω, on the Coulomb friction force and on the amplitude of oscillation of the tub-drum assembly. Thus the damping ratio ξ that characterised the damping effect on the harmonic oscillations of the suspended tub-drum assembly is given by:

$$\xi = \frac{c_{eq}}{c_c} = \frac{2F_{att}}{\pi A \omega m \omega_n}, \tag{2.21}$$

where c_c is the critical damping [91].

The response of a standard second order mechanical system [40] can be expressed in the following canonical form:

$$U(j\omega) = \frac{1}{1 - \left(\dfrac{\omega}{\omega_n}\right)^2 + j2\xi \dfrac{\omega}{\omega_n}} \frac{F_0(j\omega)}{k}. \tag{2.22}$$

Substituting Equation (2.21) into Equation (2.22) and considering that $U(j\omega) \equiv A(j\omega)$, the complex amplitude of the response of the second order system with friction damping results:

$$A(j\omega) = \frac{\dfrac{F_0(j\omega)}{k} - j\dfrac{4F_{att}}{\pi m \omega_n^2}}{1 - \left(\dfrac{\omega}{\omega_n}\right)^2}. \tag{2.23}$$

The real part of the function $\mathcal{R}\{A(j\omega)\}$ exists only when:

$$\frac{F_a tt}{F_0} < \frac{\pi}{4}. \tag{2.24}$$

In a professional washing machine the condition of Equation (2.24) is satisfied for most of the spinning velocities.

Considering the lumped 2DOFs model shown in Figure 2.4, the equivalent viscous damping model for the Coulomb friction and the time domain equations of motion described in Equations (2.11) and (2.12), the frequency-dependent complex amplitude for the oscillations of the tub-drum assembly and for the force transmitted are given by:

$$X(j\omega) = \frac{m_u r\omega^2 - j\frac{4}{\pi}\left[F_{cf_{xx}} + F_{cf_{xy}}\right] - \left[c_{v_{xy}} j\omega + k_{xy}\right] Y(j\omega)}{-M_{tot}\omega^2 + j\omega c_{v_{xx}} + k_{xx}}, \tag{2.25}$$

$$Y(j\omega) = \frac{m_u r\omega^2 - j\frac{4}{\pi}\left[F_{cf_{yy}} + F_{cf_{yx}}\right] - \left[c_{v_{yx}} j\omega + k_{yx}\right] X(j\omega)}{-M_{tot}\omega^2 + j\omega c_{v_{yy}} + k_{yy}}, \tag{2.26}$$

$$\begin{aligned} R(j\omega) = j\frac{4}{\pi}\left[F_{cf_{yy}} + F_{cf_{yx}}\right] + \left[c_{v_{yx}} j\omega + k_{yx}\right] X(j\omega) \\ + \left[j\omega c_{v_{yy}} + k_{yy}\right] Y(j\omega). \end{aligned} \tag{2.27}$$

Therefore the FRFs for the harmonic oscillations of the tub-drum assembly in x and y directions and the force transmitted to ground via the four spring-dampers result:

$$G_x(j\omega) = \frac{X(j\omega)}{F(j\omega)}, \tag{2.28}$$

$$G_y(j\omega) = \frac{Y(j\omega)}{F(j\omega)}, \tag{2.29}$$

$$T(j\omega) = \frac{R(j\omega)}{F(j\omega)}. \tag{2.30}$$

2.3.1 Friction and viscous damping contributes

In order to better understand the contributes of the two types of damping, a parametric analysis is performed by comparing the spectra of the suspended tub-drum assembly oscillations and the ground force transmission with respect to a realistic range of values of friction force for the tested professional washing machine, which are reported in Table 2.2.

Table 2.2: List of friction forces used in the friction damping model for the parametric study.

	$F_{cf_{xx}}$	$F_{cf_{xy}}$	$F_{cf_{yx}}$	$F_{cf_{yy}}$	
Case 1	50	30	30	50	N
Case 2	100	60	60	100	N
Case 3	150	100	100	150	N

Figures 2.6 and 2.7 show respectively the simulated spectra of the tub-drum assembly oscillations and force transmission for low (blue solid line), medium (red dotted line) and high (black dashed line) friction damping levels. From this graph it is possible to appreciate how increasing the Coulomb damping enhances the tub-drum assembly vibration response and force transmission at low frequencies. In particular at low frequencies the system presents higher oscillations of the drum, which are due to the large forces necessary to evince the threshold force necessary to generate sliding friction. Therefore, large friction damping levels stiffen the suspension system at low angular speeds, preventing the compression of the springs and thus slightly lowering the fundamental natural frequencies of the tub-drum assembly. Thus the force transmission gets bigger. The only relevant contribute to attenuate the peaks oscillation at resonance frequencies, is given by the viscous damping, which is proportional to the factors c_v. At higher frequencies, the friction force does not influence the oscillations of the tub-drum assembly while the force transmission increases proportionally to the equivalent damping coefficient for the Coulomb friction damping. Therefore, the benefits of real friction dampers are given by the low manufacturing and maintenance costs and the viscous damping side effects they produce.

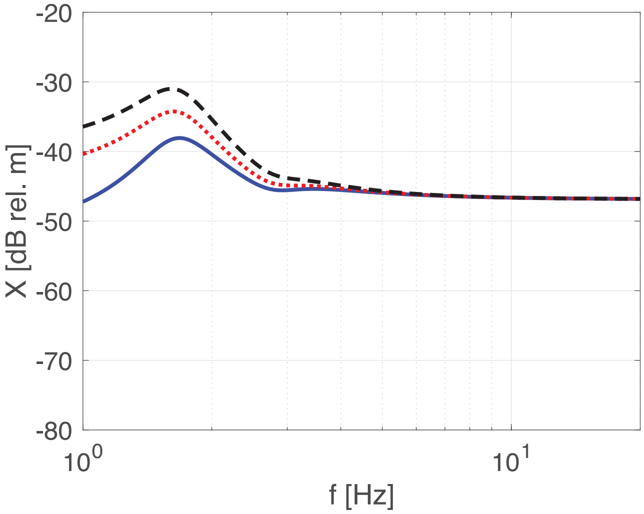

(a)

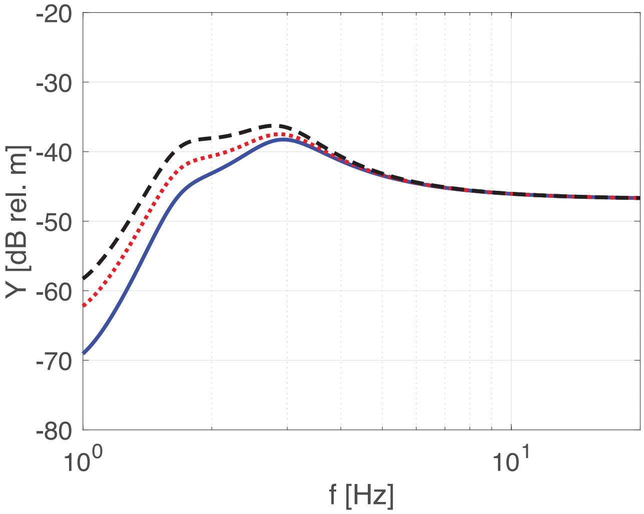

(b)

Figure 2.6: Analytical spectra of the tub-drum assembly oscillations along horizontal (a) and vertical (b) directions by varying the friction force of the passive damper: *Case 1* (blue solid line), *Case 2* (red dotted line), *Case 3* (black dashed line) of Table 2.2.

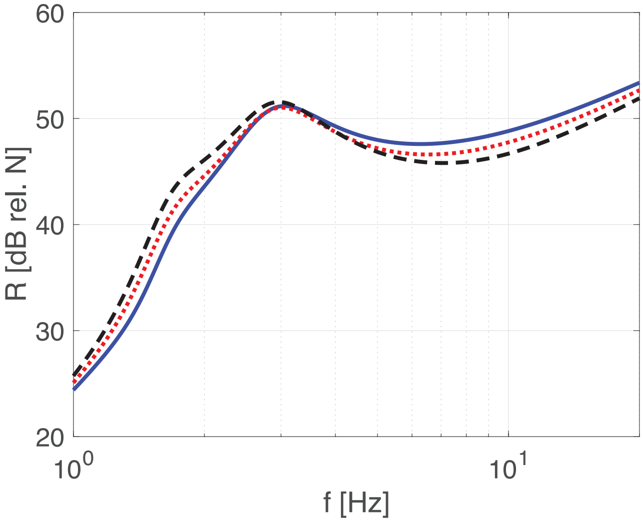

Figure 2.7: Analytical spectra of ground force transmission by varying the friction force of the passive damper: *Case 1* (blue solid line), *Case 2* (red dotted line), *Case 3* (black dashed line) of Table 2.2.

Figure 2.8 and 2.9 show respectively the simulated spectra of drum oscillations and force transmission for low (blue solid line), medium (red dotted line) and higher (black dashed line) viscous damping levels as reported in Table 2.3.

Table 2.3: List of viscous damping contributes used for the parametric study.

	$c_{v_{xx}}$	$c_{v_{xy}}$	$c_{v_{yx}}$	$c_{v_{yy}}$	
Case 1	200	40	40	400	N
Case 2	350	80	60	650	N
Case 3	500	120	80	900	N

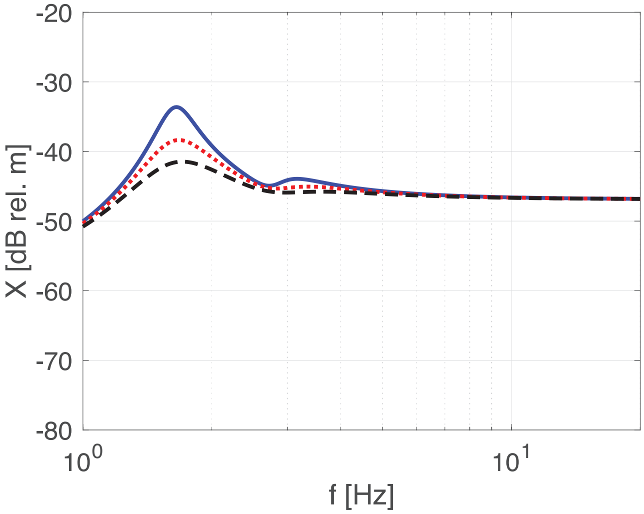

(a)

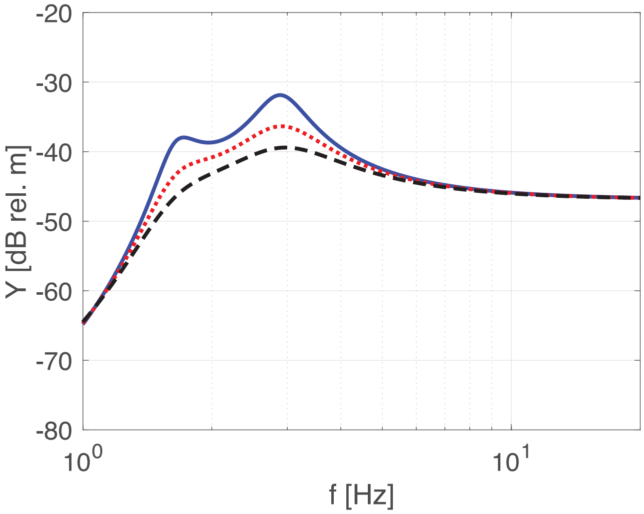

(b)

Figure 2.8: Analytical spectra of the tub-drum assembly oscillations along horizontal (a) and vertical (b) directions by varying the viscous damping component of the passive damper: *Case 1* (blue solid line), *Case 2* (red dotted line), *Case 3* (black dashed line) of Table 2.3.

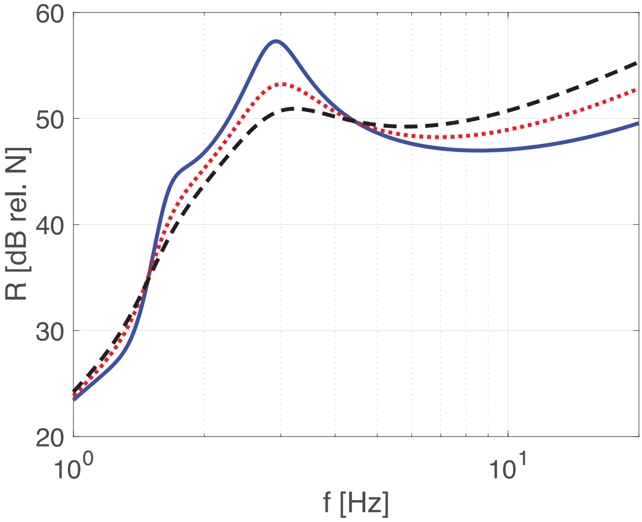

Figure 2.9: Analytical spectra of ground force transmission by varying the viscous damping component of the passive damper: *Case 1* (blue solid line), *Case 2* (red dotted line), *Case 3* (black dashed line) of Table 2.3.

The viscous damping effect produced by the damper is a key factor to attenuate the resonant response of the tub-drum oscillations and the force transmitted to the ground at resonance frequency. Although at low frequencies there are no relevant variations of the spectra by changing the viscous damping contribute, at higher frequencies the mechanical impedance of the damper increases proportionally to frequency and so does the force transmission. Instead, the oscillations of the drum result damping independent at frequencies higher than the fundamental natural frequency.

2.4 Experimental validation of the model

This section compares the simulated and measured FRFs that characterise the drum oscillations in x and y directions and the force transmitted to the floor by the professional washing machine. First of all, the main mechanical parameters have to be identified in order to provide the right input data necessary to validate the model. In general, the input parameters were collected from direct measurements on the components of the washing machine (geometry, weights), from mechanical and electrical static measurements and from datasheets of the components. Moreover some data were identified from the measured FRFs X/F, Y/F and R/F. For this purpose, initially the dampers were removed from the machine in such a way as to obtain the low-damped configuration, with the aim to reduce non linear effects into the system and estimate the stiffness of the suspension system along the horizontal and vertical directions. Figure 2.10 shows a picture of the experimental setup used to produce the experimental validation tests. The washing machine was located on top of a base framework structure specifically built for these tests (the CAD drawings are collected in Appendix A), which was equipped with strain gauge load cells (*Flintec ZLS Planar Beam*) to measure the vertical components of the force transmission via the four feet of the machine. As shown in sketch of Figure 2.11, the drum was equipped with two *PCB Piezotronics* accelerometers positioned on top and on the flank of the drum in such a way as to measure the vertical and horizontal accelerations. The excitation was generated first in horizontal direction and later in vertical direction, by using an anchored *Tira Vib S51140* shaker connected to the drum via a stinger. The excitation was electronically controlled in such a way as to perform a frequency sweep within the operation frequency range of the appliance. The main mechanical features of the W565H machine by Electrolux Professional considered in this study are reported in Table 2.4.

Figure 2.10: Picture of the setup used to experimental validate the dynamic model along the vertical direction.

Table 2.4: Mechanical parameters of the W565H professional washing machine used for small displacement validation.

Parameter	Value	
M	69	kg
M_b	17	kg
r	0.26	m
k_{xx}	5305	N/m
k_{xy}	50	N/m
k_{yx}	100	N/m
k_{yy}	19350	N/m
c_{xx}	120	Ns/m
c_{xy}	20	Ns/m
c_{yx}	30	Ns/m
c_{yy}	140	Ns/m
n	$0 \div 1245$	rpm

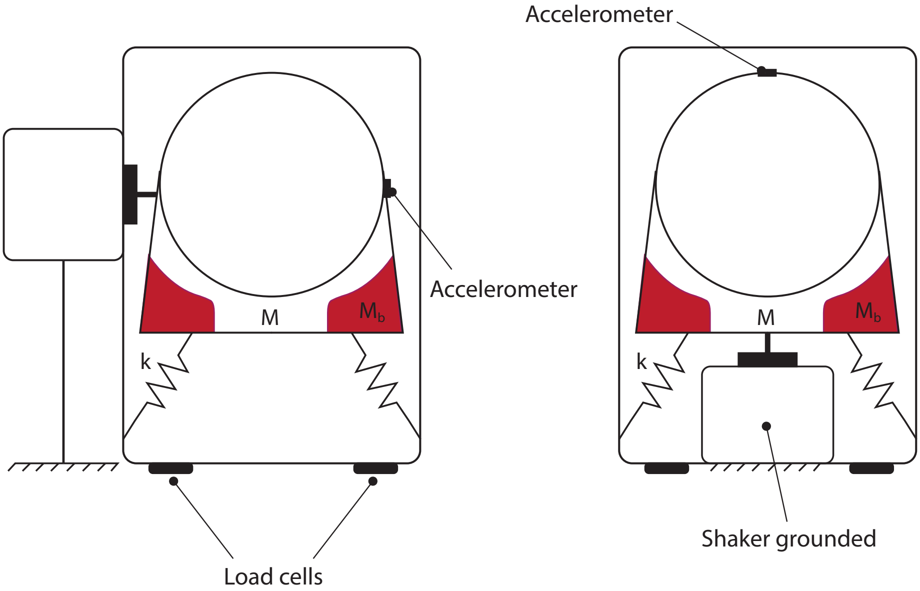

Figure 2.11: Sketch of the setup used to experimentally validate the dynamic model with the low-damped configuration along the horizontal (left hand side) and vertical (right hand side) directions.

2.4.1 Validation of the lightly damped suspension configuration

The FRFs spectra for the amplitude of the drum oscillations along horizontal (Plot a) and vertical (Plot b) directions are shown in Figure 2.12.

The black solid lines show the experimental spectra that present resonance peaks in correspondence of the fundamental natural frequencies for the horizontal and vertical oscillations of the tub-drum assembly mounted on the lightly damped springs. The horizontal mode presents a resonance frequency at $\omega_{r_x} = 1.2Hz$ while the vertical one at about $\omega_{r_y} = 2.3Hz$, which are within the common range of professional appliances. The coupling of the horizontal and vertical natural modes is visible in both the X/F and Y/F FRF spectra, in correspondence of $\omega = \omega_{r_x}$ and $\omega = \omega_{r_y}$ respectively. At higher frequencies, above the fundamental natural frequencies, the response is characterised by a mass law with a 40 dB per decade down slope. The red dashed lines show the simulated results when the parameters of Table 2.4 are used in the model presented in Section 2.3. The simulated FRFs agree well with the measured ones in the entire frequency range of operation of the professional washing machine, except for a small feature at about 6 Hz which is probably related to another higher order vibration mode. The coupling effects are predicted with a small frequency shift with respect to the measured FRFs.

Figure 2.13 shows the transmissibility FRFs when the shaker excites the drum vertically. The amplitude spectrum presents two resonance peaks in correspondence of the natural frequency for the horizontal and vertical natural modes of the system. Then it falls down at a 40 dB per decade rate. At the fundamental natural frequency of the vertical mode there is the maximum transfer of the vertical component of force from the machine to the hosting structure, therefore the damping contribute must be accurately designed in order to mitigate this effect that produces noise and vibration of the floor. The simulated and measured FRFs agree less well at low frequency where the measured FRFs is about 2 dB higher. At frequencies higher than 6 Hz, the measure shows some features, which are not predicted by the model and can be related to the dynamic of the base framework used to clamp the washing machine.

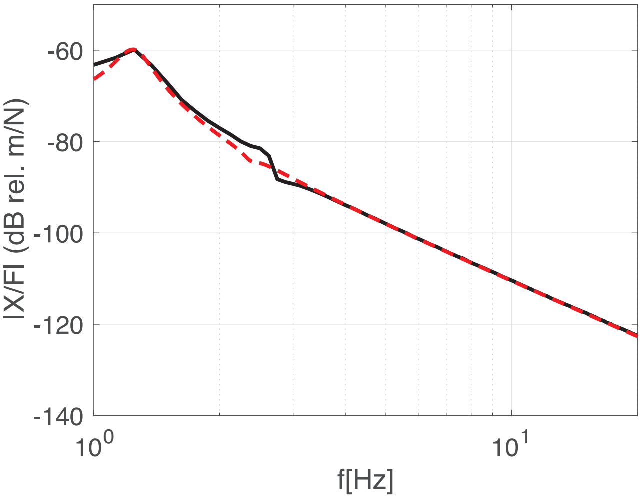

(a)

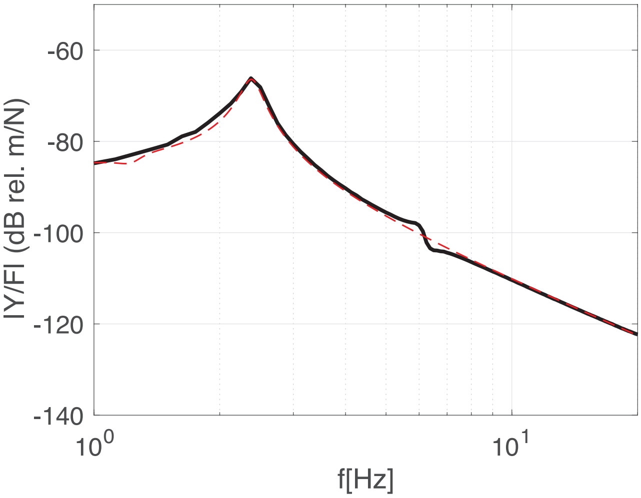

(b)

Figure 2.12: Comparison between the simulated (red dashed line) and the measured (black line) FRFs relative to the amplitude of the tub-drum assembly oscillations along horizontal (a) and vertical (b) directions for the low-damped configuration.

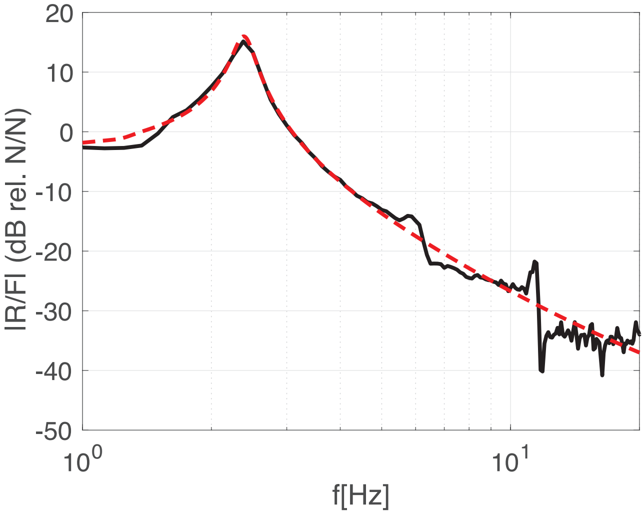

Figure 2.13: Comparison between the simulated (red dashed line) and the measured (black line) FRFs relative to the amplitude of the transmissibility for the low-damped configuration.

2.4.2 Validation of the heavily damped suspension configuration

The simulated and the measured FRFs spectra for the amplitude of the drum oscillations in horizontal and vertical directions and for the force transmitted to the ground, shown respectively in Figures 2.15 and 2.16, have also been compared for the heavily damped suspension system configuration in order to estimate the accuracy of the model for a real machine. For this purpose the suspension system of the machine was equipped with the helical linear springs and four standard passive friction dampers connected in parallel. The experimental setup was arranged on of the same professional washing machine considered in the previous section, located on top of the base framework structure equipped with four strain gauge load cells (*Flintec ZLS Planar Beam*) to measure the vertical component of force transmission through the four feet of the machine. The drum was equipped with two accelerometers, one at its top and one at its flank, in such a way as to measure simultaneously both vertical and horizontal accelerations. A lumped mass was clamped inside the drum in order to generate the static unbalance, which, for given rotation speed, produces a centrifugal force, that is, a combination of harmonic forces in quadrature, oriented in vertical and horizontal directions respectively. The centrifugal force was therefore identified from the drum angular speed, measured with an incremental encoder (*Lika rotapuls IT65*) and from the weight of unbalance placed inside the rotor. The washing machine normally performs a frequency sweep accelerating from the distribution speed ω_d to the extraction speed established according to the type of washed load. Since it was not possible to directly control the electric motor to impose a specific acceleration law of the drum, the latter was accelerated up to the highest speed and then let it slows down until it stopped in order to cover the entire frequency spectrum. Figure 2.14 shows the sketch of the experimental rig setup to validate the model on real operative conditions. Table 2.5 provides the mechanical parameters of the appliance which have been used in the simulation.

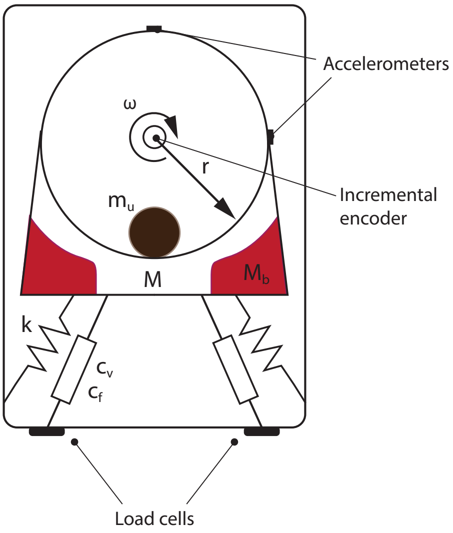

Figure 2.14: Sketch of the experimental setup used to validate the two DOFs lumped parameter model on real operative conditions.

Table 2.5: Mechanical parameters of the two DOFs model for the W565H professional washing machine.

Parameter	Value	
M	69	kg
M_b	17	kg
r	0.26	m
m_u	1.5	kg
k_{xx}	9810	N/m
k_{xy}	1150	N/m
k_{yx}	6500	N/m
k_{yy}	27555	N/m
$c_{v_{xx}}$	380	Ns/m
$c_{v_{xy}}$	120	Ns/m
$c_{v_{yx}}$	80	Ns/m
$c_{v_{yy}}$	720	Ns/m
$F_{cf_{xx}}$	120	N
$F_{cf_{xy}}$	20	N
$F_{cf_{yx}}$	30	N
$F_{cf_{yy}}$	120	N
n	$0 \div 1245$	rpm

Figure 2.15 shows the comparison between measured (black solid line) and simulated (red-dashed line) spectra of the amplitude of oscillation of the drum in horizontal (Plot a) and vertical (Plot b) directions.

The model does reliably predict the response of the system at low frequencies with respect to the amplitude of oscillation in vertical direction while along the x axis the simulation overestimate the tub-drum assembly oscillations up to 20 dB. The differences between analytical and measured FRFs may be due to a lack of accuracy of the mathematical model to reproduce the contributes of friction passive damping. Nevertheless, at lowest frequencies the experimental data have lower signal coherence, probably due to the measurement frequency range of the accelerometers. Experimental spectra show two resonance peaks, the first is primarily due to the horizontal natural mode while the second is primarily due to the vertical natural mode of the tub-drum assembly on the four spring-damper mounts. This is due to the fact that the centrifugal force excites the tub-drum assembly which is mounted on helical linear springs and dampers oriented at 12° with respect to the vertical axis, which coupled the two natural modes and thus produce resonant responses both in horizontal and vertical directions. Despite the analytical model includes the coupling of the two fundamental natural vibrational modes, small differences up to 2 dB can be observed among simulated and measured trends, in terms of amplitude of oscillations, close to the fundamental natural frequencies of the horizontal and vertical natural modes. Moreover, the measured spectrum of the amplitude of oscillation along the horizontal direction shows a slightly shift in frequency of the coupled vibrational vertical mode. Nevertheless, the simulation well approximates the response of the system at frequencies higher than the resonance frequency, which are actually of greater importance for the vibration control and force transmission isolation. It is observed that the resonance peaks are slightly shifted towards higher frequencies because the four passive dampers increase the stiffness of the suspensions. In particular up to 1.7 Hz for the horizontal mode and up to 3.0 Hz for the vertical one. This is justified by the design of the dampers, which are characterized by a spongy material that rubs against a metal rod and introduces stiffness effects. Since the unbalance mass varies the center of mass of the rotating drum, at high frequencies the system responds with a constant oscillation level that tends to the eccentricity factor d. The amplitude can be derived from the equation of motion for the drum body, so that:

$$d(\omega \gg \omega_n) = \frac{m_u\, r}{M_{tot}}. \tag{2.31}$$

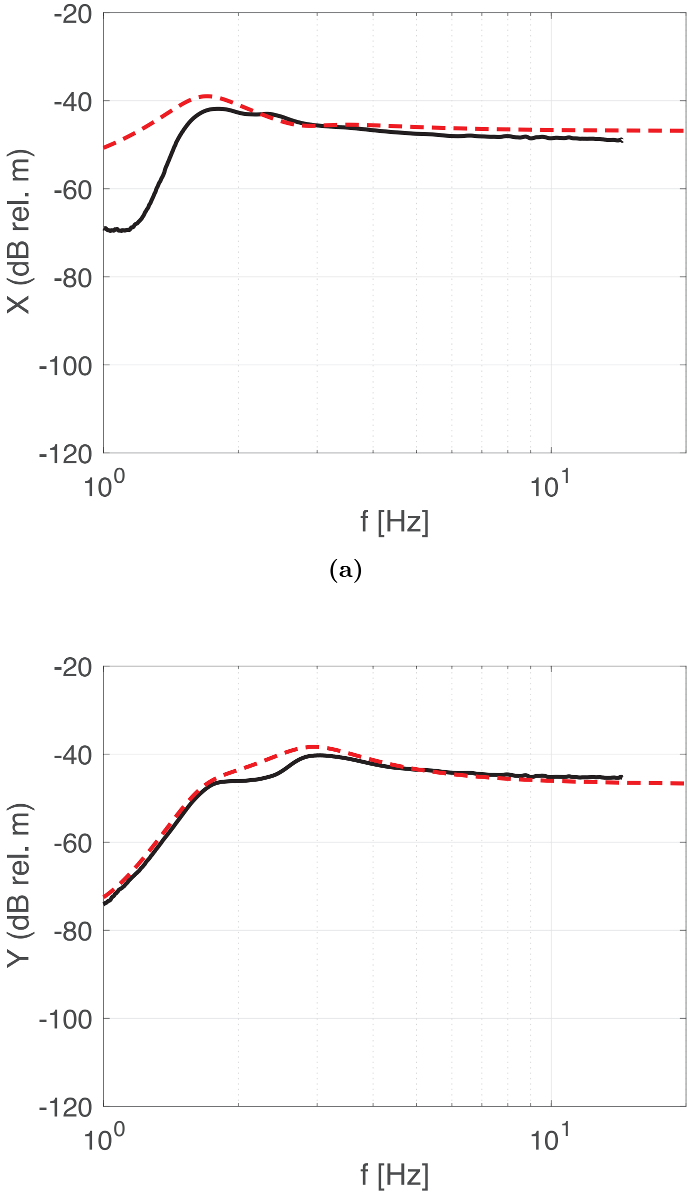

(a)

(b)

Figure 2.15: Comparison between the simulated (red dashed line) and the measured (black line) spectra relative to the tub-drum assembly oscillations along horizontal (a) and vertical (b) directions for the standard passive damped configuration.

This expression shows that, at high rotation speeds, the amplitude of the oscillation solely depends on the ratio between the unbalance mass and tub-drum-ballast mass, i.e. m_u/M_{tot}. Therefore, to guarantee low oscillations at higher frequencies a large ballast mass should be used.

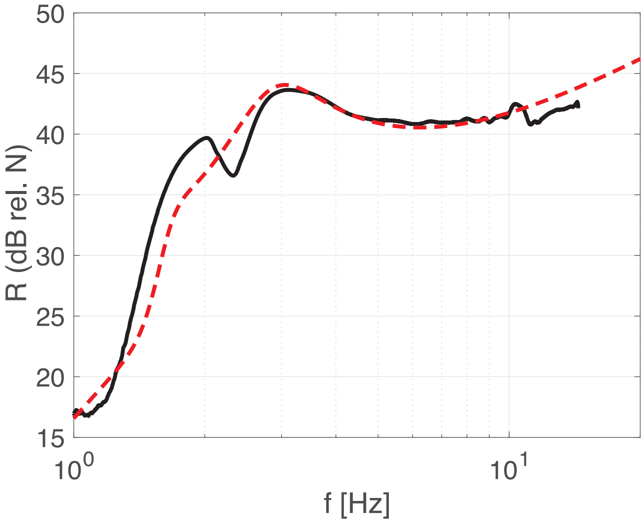

Figure 2.16: Comparison between the simulated (red dashed line) and the measured (black line) spectra relative to ground force transmission for the standard passive damped configuration.

The comparison of measured and simulated force transmission FRFs is shown in Figure 2.16. The simulation overestimates the force transmission at the lowest frequencies, where the same considerations taken for oscillations spectra seen above hold. The measured response (black solid line) presents two well attenuated resonance peaks in correspondence of the horizontal and vertical fundamental natural modes. The model well approximates the resonance frequencies of the vibrational modes, but underestimate the amplitude of the force transmission close to the natural frequency of the horizontal natural mode of the system. At high spinning speed, the simulated FRF agrees with the experimental FRF showing a constant increment of the force transmitted except at about 10 Hz where dynamics, probably related to the base framework, can be observed. In this case, for angular speeds greater than the fundamental natural frequencies, the transmitted force is given by the modulus of the suspension complex stiffness multiplied by the amplitude of the oscillation derived in Equation (2.31), so that:

$$R(\omega \gg \omega_n) = \frac{m_u\, r}{M_{tot}} \left[\left(c^2_{v_{yx}} + c^2_{v_{yy}} + c^2_{eq_{yx}} + c^2_{eq_{yy}} \right) \omega^2 + k^2_{yx} + k^2_{yy} \right]^{1/2} . \quad (2.32)$$

Therefore, the dampers transmit a force proportional to frequency, which indeed is the cause of the constant rise in the spectrum above the fundamental resonance frequencies.

To verify that the vibrational modes of the drum are each other dependent, the relative displacement of two known dots markers attached on the door of the drum were measured by using a camera system as shown in Figure 2.17.

Figure 2.17: Positions of the markers in the drum.

The experimental time history results, relative to two tonal excitations at the resonance frequencies of the machine, are shown in Figure 2.18. As noticed above, the amplitude of oscillation at the horizontal natural frequency are lower compare to those at the vertical natural mode. Despite the markers are placed on the same rigid body, the points have different tracks over time so that the translational components are not independent from each other. This is due to the fact that the excitation generates slight rotational oscillations of the drum around the z axis of Figure 1.8.

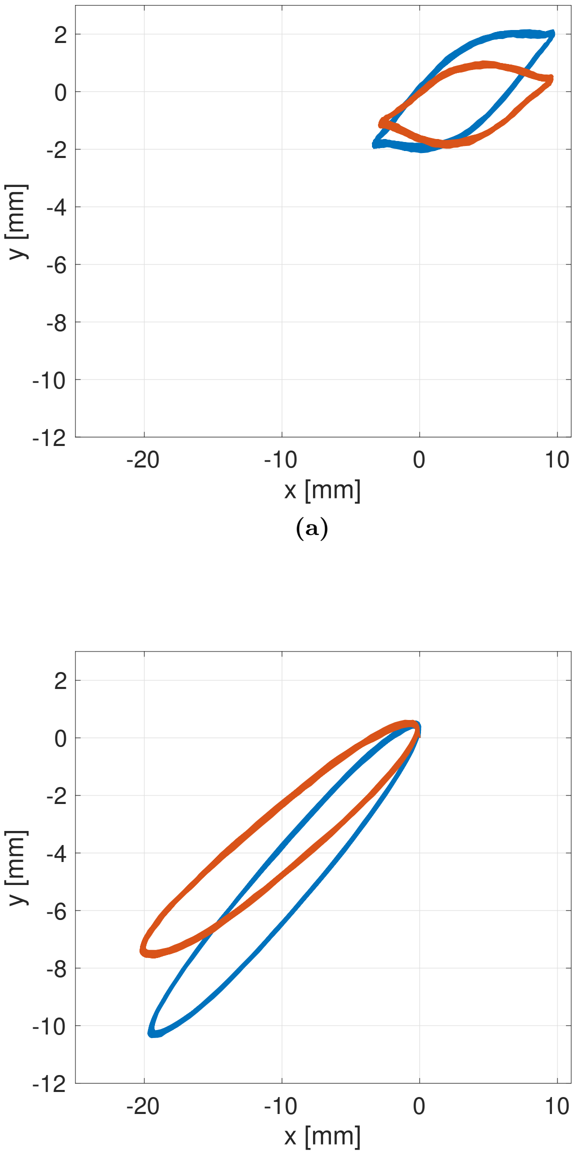

(a)

(b)

Figure 2.18: Relative time history of the positions of two markers stuck on the door of the drum excited at tonal frequencies: (a) 1.7 Hz and (b) 3.0 Hz. The blue line is relative to the left hand side sticker and the red line to the right hand side one.

2.5 Load characterisation

The spinning cycle aims at removing the water content from cloths thanks to the centrifugal force. This phenomenon is called dewatering.

As described in the previous sections, during the spinning phase, the load in the rotating drum is a time dependent variable because the amount of unbalance and the speed of the drum change during the extraction cycle. While the acceleration law of the drum is defined and controlled by the washing cycle, the variation of the unbalance is related to the dewatering process. In fact, the water extracted modifies the local weight of the garments and thus affects the inertia distribution and the centrifugal force. Many aspects may affect the dewatering process, like the properties of the textile (ageing, materials, density, etc.), the filling factor, the water temperature, the distribution of the cloths in the inner surface of drum and the usage of detergent or softener. In general, the literature lacks models of water retention of clothes in washing machines, which represent a key factor for the dynamic characterization of the load. These models are also useful for manufacturers to optimize washing cycles and save time and costs for the end users. Due to the complexity of the dewatering phenomenon and the amount of parameters that could affect the water extraction, an experimental analysis was carried out in order to define the equations that best describe the drying process of the clothes in a washing machine under the spinning cycle.

The aim of this section is to develop an empirical model to predict water retention in cotton towels with reference to time and spinning acceleration of professional washing machines. An approximated law is derived from a large set of water extraction data taken on a number of washing machines operated with typical spinning programmes. Normally, when washing machines are used to certificate water Retention (R_t) performances, textile samples are exposed to specific centrifugal forces, water temperatures and spinning cycles. Also, the experimental apparatus for the measurements is defined in all its details by standard guidelines [11]. The International Standard IEC 60456 defines R_t as:

$$R_t = \frac{m_{wet} - m_{cd}}{m_{cd}} 100, \tag{2.33}$$

where m_{wet} is the total mass of the wet garments and m_{cd} is the mass of the garments when they are conditioned into a standard environment at the temperature of $(20 \pm 2)°C$ and relative humidity of $(65 \pm 5)\%$ for sufficient time. The condition-dry mass differs from the bone-dry mass m_{bd} which is the mass of the textile where the remaining moisture content has been reduced to a lower level at which the mass variation must be less than 1% or 20g compared to the previous measurement taken after a specific drying cycle.

The centrifugal force dF acting on an infinitesimal mass dm_{wet} of wet cloths is given by:

$$dF = dm_{wet}\omega^2 r, \tag{2.34}$$

where ω is the angular speed of the drum and r is its radius. To compare the performance of the spinning cycle independently from the type of washing machine, the dimensionless acceleration G is used, which is defined as follows:

$$G = \frac{\omega^2 r}{g}. \tag{2.35}$$

Thus, the dimensionless acceleration G is given by the ratio between the centrifugal acceleration ($a_c = \omega^2 r$) to which the washing load is subject and the gravitational acceleration g. With this parameter the spinning cycle can be characterized only in terms of machine features (speed and radius). During the water extraction cycle, the garments placed inside the drum tends to form a layer with no uniform thickness on the internal surface of the tub. To take into account this aspect, the Fill Factor (FF) parameter is commonly used, which describes the quantity of textile in relation with the washing capacity of the machine:

$$FF = \frac{m_{cd}}{V}, \tag{2.36}$$

where V is the drum volume.

2.5.1 Experimental test: setup and method

Three professional washing machines of different washing capacity (6.5 kg, 7.5 kg and 13 kg) were tested to investigate their water retention performances during the spinning phase. Figure 2.19 shows a sketch and a picture of the experimental setup used to produce the measures presented in this paper. The machines were tested separately making sure the same conditions of use and washing cycles were implemented. More specifically, the same spinning sequences were implemented to guarantee equal normalised accelerations G in all experiments. During this phase the water ejected from the drainage pipe of the appliance was gathered into a basin, which laid on two load beam cells equipped with *Tedea th-huntleigh 3410* sensors, in order to measure the mass of the liquid discharged in time. The drum temperature and speed time history were recorded using respectively a thermocouple type K and a tachometer dynamo by *Servo-Tek SB-757A-2*. All the signals were logged by an *Ahlborn Almemo 2590-9 V5* data acquisition system (DAQ) connected to a Windows PC.

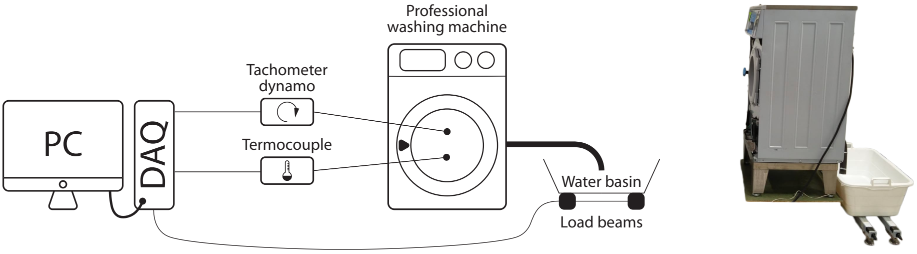

(a) (b)

Figure 2.19: Sketch (a) and picture (b) of the experimental setup used to evaluate dewatering performances of professional washing machines.

A dedicated sample load composed of a controlled amount of new standard cotton towels was prepared for each test in accordance with the International Standard [11]. Table 2.6 reports the properties of the cotton towels used for the experiments. All the samples had to be conditioned before proceeding with the tests in order to establish the dry conditioned mass which is representative of the dry levels of the garments. Thus all the cotton towels were placed in a controlled climatic chamber at imposed temperature and humidity. The masses m_{cd}, m_{wet}, and m_{bd} were measured with a digital scale of Carl Liden DIGI DI-10. At the end of each spinning test every group of samples were dried with a professional tumble dryer.

Table 2.6: Features of the samples used to evaluate dewatering performances of professional washing machines.

Material	Terry
Quality	100% cotton
Colour	White
Dimension (cm)	70 x 140
Density (g/m2)	460

Many conditions may affect water retention measurement in a washing machine. In order to obtain repeatable tests an own standard procedure was defined following the normative [11] recommendations in such a way as to compare the water retention history and washing machine performances. Figure 2.21 and Figure 2.22 show the procedure followed for each of the three different cotton loads prepared for the appliances. The results of this thesis were obtained at specific water temperature, Fill Factor (FF) and in absence of detergent. All three clusters of cotton towels were conditioned and selected in such a way as to respect the filling coefficient. In order to realise the correct weight of condition dry towels, stabilisation washing cycles were initially performed using another washing machine of large capacity. These pre-treatments were done for a larger amount of towels with reference to the amount requested by the Fill Factor. Starting from a selection of new towels, during the stabilisation phase, all the samples were washed five times using a reference detergent and a standard $60°C$ cotton program, without intermediate drying. This pre-treatment was followed by a normalization phase in which the towels were washed without detergent using a standard $60°C$ cotton program and then dried up to bone dry condition. The loads were later hung to a drying rack and placed in a conditioning chamber under controlled temperature of $(20 \pm 2)°C$ and relative humidity of $(65 \pm 5)\%$ for at least 15 hours. This procedure was done to moisten the towels in such a way as to obtain the conditioned mass. The right quantity of samples was then selected to ensure the correct total conditioned mass m_{cd} with respect to the fill factor chosen for the experiments. To avoid a performance decay due to extreme ageing, the sample load was used up to a maximum of 80 tests.

The series of tests implemented to measure the dewatering performances of the machines started by drying the cotton load up to the fixed textile bone-dry mass m_{bd}. Experience has shown that the way in which a washing machine is loaded could slightly influence the measurement results. The following loading sequence was therefore specified to guarantee a correct repeatability of the tests: first grasp the towels in the centre, shake it to hang loosely, fold it twice to a third of its total size and then place them in the drum.

Starting from a real washing program, a customised washing cycle was designed to perform the planned tests. As shown in Figure 2.20, the chosen cycle is composed of four parts: water filling, clockwise (CW) and counter-clockwise (CCW) washing, drain and final long spinning. The numerical limit of the customised washing cycle are not here reported

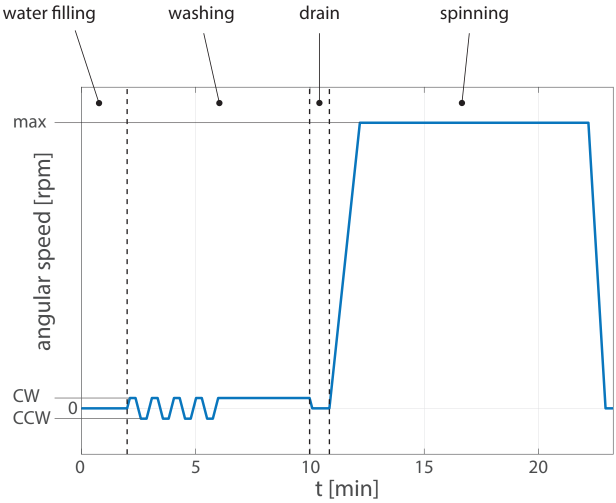

Figure 2.20: Customised washing cycle used to perform water retention tests.

due to Non Disclosure Agreement (NDA) with the company.

Extraction is the most important phase for the tests presented in this study, which therefore was reached in the shortest time possible by setting the same maximum drum acceleration for all the appliances considered. The spinning cycle was set to last 10 minutes. During this phase, the angular speed of the drum was maintained constant within the unavoidable variations due to the load dynamic unbalance effects. In order to analyse the influence of the G parameter, the test series was performed for different values of extraction speed for each appliance. At the end of the procedure, the wet mass of the sample, m_{wet}, was recorded as a reference value for further analysis. Water extraction performance was expressed as the amount of remaining moisture content in the load at the end of the program relative to the conditioned mass after the final spinning operation.

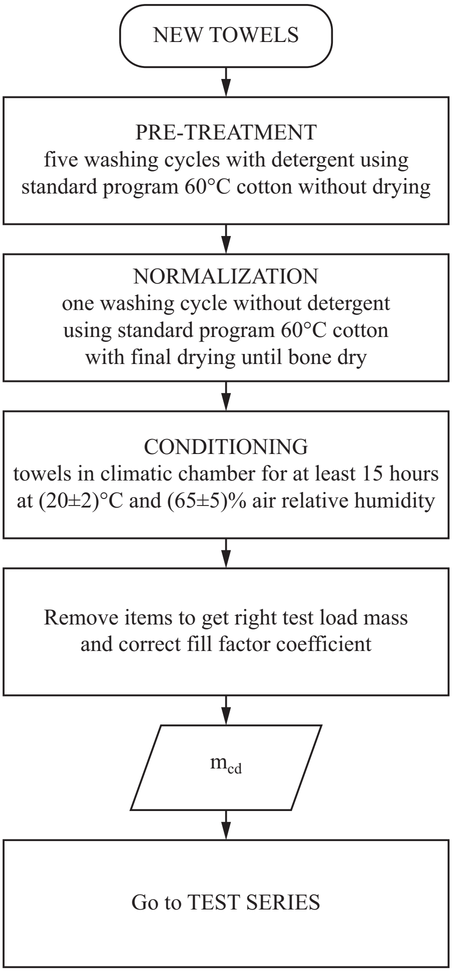

Figure 2.21: Flow chart to prepare the load before the test series through a stabilization, normalization, conditioning and weight process.

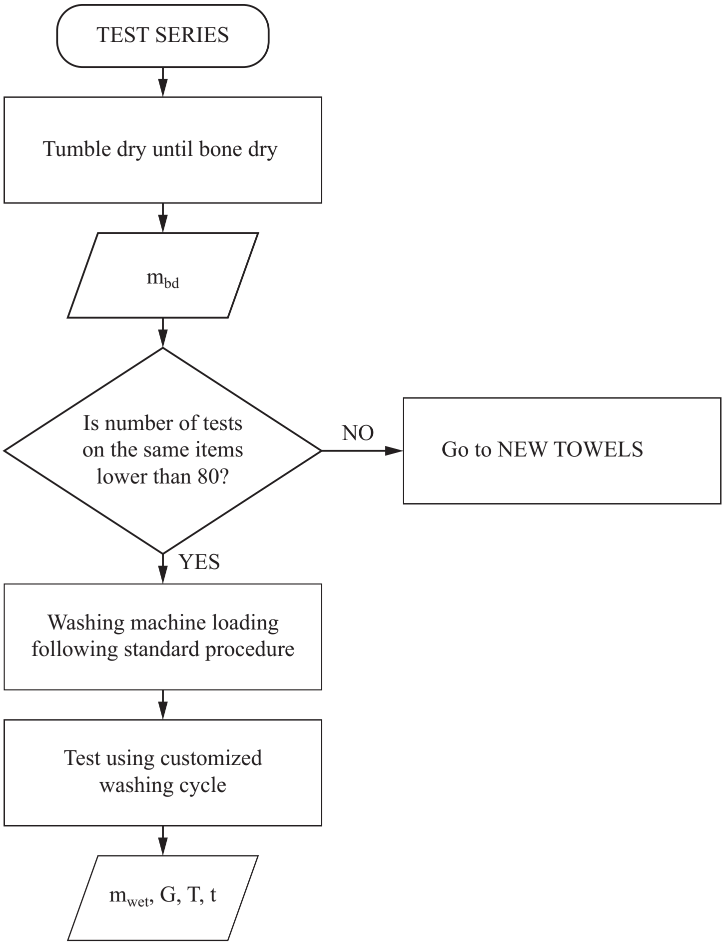

Figure 2.22: Flow chart describing the test procedure followed to test the dewatering performances of washing machines.

2.5.2 Dewatering model

Time-analysis repeatability

To derive the retention value defined in Equation (2.33), the measured data acquired had to be processed. In fact, the water extracted during the spinning $m_{w,ext}$ and weighted by the load cells, does not appear explicitly in the definition of R_t, which instead, according to Equation (2.33) refers to the total amount of water in the textiles. For this reason, the numerator of Equation (2.33) was rewritten as:

$$m_{wet}(t) - m_{cd} = m_{H_2O}(t), \tag{2.37}$$

where m_{H_2O} is the residual mass of water in the towels at specific time. Assuming water mass conservation, the sum of the water ejected during the spinning and the residual water in the textile must be equal to a constant C, that is:

$$m_{w,ext}(t) + m_{H_2O}(t) = C. \tag{2.38}$$

The constant C is calculated considering the masses at the end of the cycle such that:

$$C = m_{wet}(t = t_{fin}) - m_{cd} + m_{w,ext}(t = t_{fin}), \tag{2.39}$$

where $m_{wet}(t = t_{fin})$ is the entire wet cotton load weighted at the end of the tests. Substituting the above expressions into Equation (2.33), the percentage of residual moisture content with reference to time can be derived with the following expression:

$$R_t(t) = \frac{m_{wet}(t = t_{fin}) - m_{cd} + m_{w,ext}(t = t_{fin}) - m_{w,ext}(t)}{m_{cd}} 100. \tag{2.40}$$

Figure 2.23 shows the water retention time history of the cotton towels during a spinning phase at fixed speed, temperature and fill factor in a professional appliance. As found by studies on hydrology and soil retention, the residual moisture decreases rapidly during the beginning of the extraction cycle that starts at saturation condition. As the fabric samples continues to drain water, the capillary force tends to equal the centrifugal force on the water molecules reducing the extraction performance as shown on the right-hand side of the graph.

To verify the validity of the methodology described above, a number of tests were repeated at three different speeds in order to cover low, medium and high revolution frequency ranges, for all the washing machines

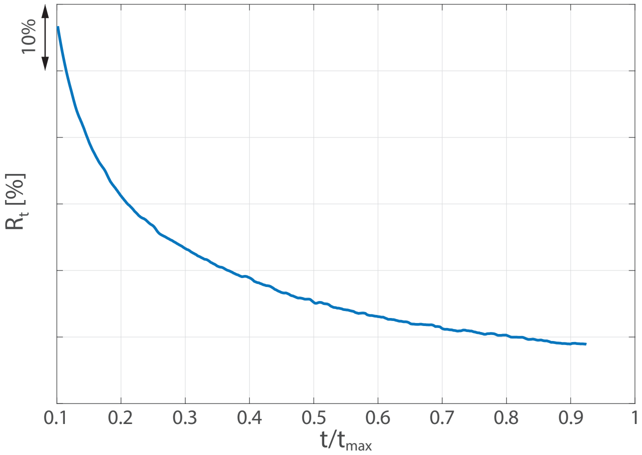

Figure 2.23: Water retention time history of the towels inside the drum during a spinning cycle of $t_{max} = 10\ min$, considering a specified extraction speed, fill factor coefficient and drum dimension and shape. The limits of the retention time dependence are covered by NDA.

considered. In this respect, Figure 2.24 shows an example of the repeatability tests performed at controlled drum speed for one of the three washing machine tested. The solid blue, red dashed and black dotted lines show the water retention time history for the same load composition and normalised acceleration G for different tests. The curves overlap reasonably well in the whole time range except at the very beginning of the extractions where variations of moisture content up to 5% can be noticed. Here the clothes distribution and the acceleration law of the drum can effectively influence the dewatering process. Nevertheless, these results confirm the validity of the proposed methodology and show that the clothes distribution does not influence the washing machine dewatering time history with respect to the filling factor considered in the tests for longer time. The maximum differences between the final residual moisture values $\Delta R(t_{max})\%$, measured at the end of each tests, are collected in Table 2.7 for all the machines with reference to the considered extraction speeds. The final water content in the towels differs less than 1.6% after the spinning cycle and the variation gets lower as the revolution speed gets higher. Indeed, at maximum $450G$, the difference on the final water content is lower than 0.3% regardless of the washing machine used to perform the test series.

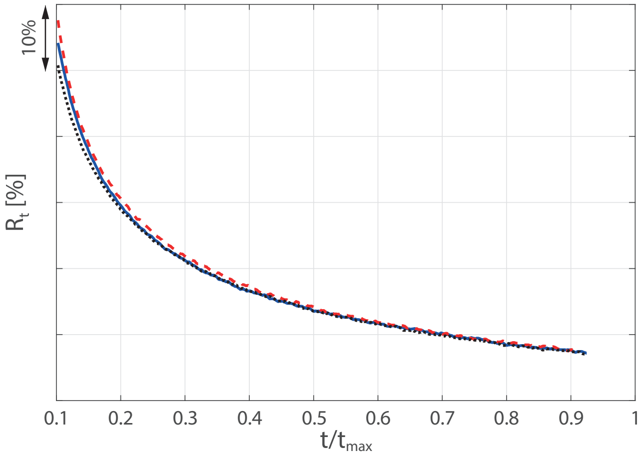

Figure 2.24: Repeatability of water retention tests at fixed spinning speed and washing machine. The blue line is the repeatability test number 1, the dashed red line represents test number 2 and the black dotted line the number 3. The limits of the retention time dependence are covered by NDA.

Table 2.7: Comparison of water retention repeatability results at three different speeds for all the washing machines (WMs) considered.

		$\Delta R(t_{max})\%$		
		WM 1	WM 2	WM 3
Low speed	50G	1.6%	1.2%	0.4 %
Medium speed	250G	0.8%	0.8%	0.3%
High speed	450G	0.3%	0.3%	0.2%

Proposed empirical dewatering model

The experiments presented in the previous section are time consuming and referred to specific and constant G-acceleration values. In order to extend the study to the whole possible working range of the machine an empirical function is fitted to the measured data with reference to constant temperature ($20°C$), textile type (Cotton Towels as in Table 2.6), fill factor ($1/10\,kg/l$) and no use of detergent. In this way, it is therefore possible to predict the residual moisture content of 100% cotton at the time and speed desired. Literature lacks mathematical models that describe retention phenomena using washing machines, so the challenge is to define a general equation able to fit, with a good accuracy, all the experimental data. For this purpose, the water retention time history analysis described before was performed for a set of 11 G-acceleration factors for each of the three washing machines. The G value chosen in this activity are: 50, 90, 130, 170, 210, 250, 290, 330, 370, 410, 450 in such a way as to distribute the data overall the common working frequency range of professional washing machines. As reported in the introduction, the experimental results are best described by polynomial equations. The best approximation carried out with the data available consists in the following fifth order polynomial expression:

$$R_t\%(t,G) = \sum_{i=0}^{5}\sum_{j=0}^{5-i} a_{ij} t^i G^j, \tag{2.41}$$

where a_{ij} are the coefficients of the polynomial reported in Table 2.8, while Figure 2.25 shows the water retention fitting surface with respect to t and G given in Equation (2.41) using the test data presented in this study.

High water residual content occurs for low value of G because the mechanical action is too weak to evince the flow resistances inside the textile even for long spinning time. Moreover, a significant amount of water content appears for short extraction cycles even if the revolution speed increases up to the maximum value. A fast dewatering effect can be observed when both parameters are low, whereas a flattening behaviour occurs when they become higher. Best dewatering performances are reached for highest values of G and t, where the moisture content decreases more than 100% compared to the initial point. The surface shows that G has a greater impact on water extraction compared to time. This is because the water extraction limit is reached faster and the capillary force on the fabrics equals the centrifugal force.

Table 2.8: Values of the coefficients of fifth order fitting polynomial expression use to model dewatering phenomenon on professional washing machines

Coefficient	Value	Coefficient	Value
a_{00}	55.75	a_{20}	0.96
a_{01}	-9.60	a_{21}	-0.23
a_{02}	0.93	a_{22}	-0.08
a_{03}	-3.04	a_{23}	-0.03
a_{04}	3.55	a_{30}	-0.13
a_{05}	-0.70	a_{31}	0.03
a_{10}	-6.11	a_{32}	0.04
a_{11}	0.90	a_{40}	1.33
a_{12}	0.79	a_{41}	0.01
a_{13}	0.14	a_{50}	-0.67
a_{14}	-0.39		

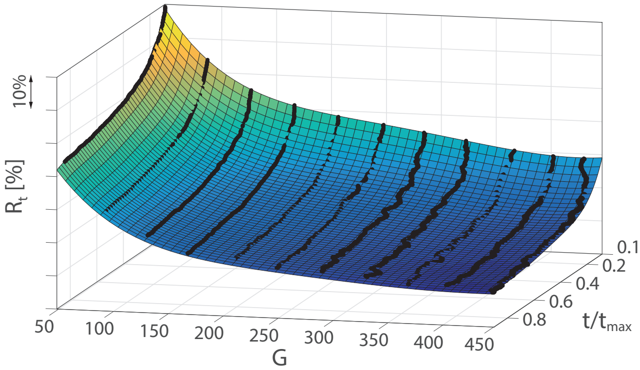

Figure 2.25: Water retention surface fitted on experimental data by a fifth order polynomial equation for a professional washing machine. The limits of the retention $R\%$ are covered by NDA.

To evaluate the accuracy of the proposed function, the difference between the measured data and the values estimated with the proposed polynomial function were estimated and plotted in Figure 2.26. The plot shows that when the extraction time is higher than $t/t_{max} = 0.2$

the variations are comprised between ±2% and reaches 10% for spinning time lower than $t/t_{max} = 0.1$ (1 minute). These larger differences are due to the fact that short extraction time could be affected by different ramp up behaviours of the machine due to dissimilar unbalance excitations.

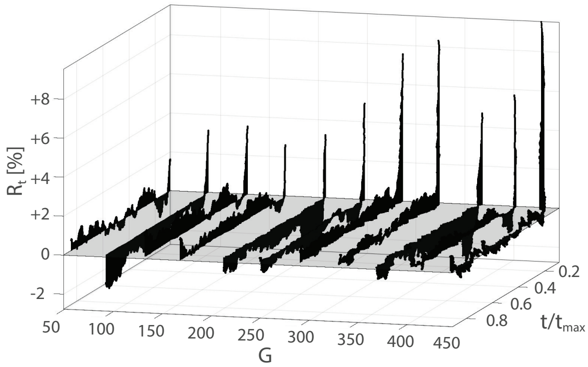

Figure 2.26: Data residual of the fitting polynomial equation with respect to the experimental data for a professional washing machine.

The study described above was repeated for all the three professional washing machines considered using the same fitting equation. Additional parameters were considered to compare the model reliability and accuracy. A summary of R-square and Root Mean Square Error ($RMSE$) is reported in Table 2.9. For each of the three machines, the R^2 parameters are close to one, indicating that the proposed retention function replicates well the observed data. The RMSEs indicate that the washing machine with the biggest washing capacity (WM_3) is best approximated by the proposed function. In any case, the RMSE values are similar for all the appliances and low enough to guarantee the validity of the proposed model.

Table 2.9: Statistical parameters to evaluate the accuracy of the model for the three washing machines.

	WM_1	WM_2	WM_3
R-square	0.9991	0.9991	0.9992
RMSE	0.7359	0.6692	0.6080

Model scaling

The washing machines used in this study have different drum dimensions and washing capacity. An investigation to identify the impact of the tub shape geometry on water retention performances was thus carried out. All the experiments were performed under the hypothesis of the same Fill Factor FF coefficient $(1/10\,kg/l)$ to guarantee a constant relation between the amounts of cloths and drum volume. This FF value guarantees a distribution of the garments over the entire internal surface of the tub such that empty regions are practically missing. Nevertheless different geometries imply different thickness of the cloth layers during spinning, with possible consequences on the dewatering process. A study of the effects caused by the different thickness is therefore needed. Indeed, as described by Equation (2.36), under the hypothesis of constant and full filled distribution of textiles along the longitudinal axis of the drum, the fill factor coefficient can be rewritten as:

$$FF = \rho_t \left[1 - \frac{(r-s)^2}{r^2} \right], \tag{2.42}$$

where ρ_t is the towels volume density, r is the drum radius and s is the average thickness of the textile layer stuck on the drum during the extraction. These are reasonable hypothesis, since as the speed of the rotating drum rise up, the garments tend to evenly distribute on its internal cylindrical surface along the circumference and the depth of the tub.

Therefore, considering Equation (2.42), it can be noticed that, provided they are loaded with the same fill factor $FF_1 = FF_2$, two different washing machines have different average thickness of the washed layer:

$$\frac{s_1}{s_2} = \frac{r_1}{r_2}. \tag{2.43}$$

Here subscript 1 and 2 indicate two washing machines with dissimilar shape of the drum. For this reason an experimental scaling analysis was performed to examine the impact of the different dimensions of the drum and thickness of cloth layer on dewatering performances.

To classify the drum shape of the three different washing machines considered, the shape factor S_f, defined as the ratio between the drum depth d and its diameter D, was considered:

$$S_f = \frac{d}{D}. \tag{2.44}$$

Table 2.10 contains the shape factor classification of all the machines considered. Two appliances have the same shape factor but different washing capacity, while the third one differs by 16.7% compared to the others. This range is representative of the professional washing machines portfolio available on the market.

Table 2.10: Shape factor coefficients of the washing machine considered.

	WM_1	WM_2	WM_3
S_f	0.6	0.6	0.7

To evaluate the impact of the shape factor on dewatering performances, the absolute difference in terms of residual moisture ΔR_t was derived for all the possible pairings of washing machines considered and then represented in Figure 2.27. The content of water is shown as a function of G-acceleration at $t/t_{max} = 0.1$ (a) and at $t/t_{max} = 0.8$ (b).

Taking into account the washing machines number i and j, the variation in residual moisture content ΔR_t was calculated with the following formula:

$$\Delta R_{t_{ij}} = |R_{t_i} - R_{t_j}| \tag{2.45}$$

where R_{t_i} and R_{t_j} are the residual moisture contents respectively of the i-th and j-th washing machine at specific time and G-acceleration.

At the beginning of the extraction phase, the variation of water retention among the machines fluctuates up to 6% overall the G range studied without any visible influence related to the drum shape. For longer extraction time there is a great variation of dewatering performances that reaches a ΔR_t of $10 \div 12\%$ at low speeds when appliances of different shape factor are compared. Over $100G$, the results get closer to each other with a maximum 2% of residual moisture content variation. Therefore, it can be concluded that the shape factor impacts the dewatering performance only at low G-acceleration factors while no relevant correlation can be observed for extraction cycles shorter than two minutes. Low values of G generate lower centrifugal forces that mitigate the dewatering performances and make the thickness of the layer of cloths and their distribution inside the drum, relevant for the process as shown in Figure 2.27 (b). A standard spinning cycle for cotton garments is typically set at high angular speed for long period; for this reason the

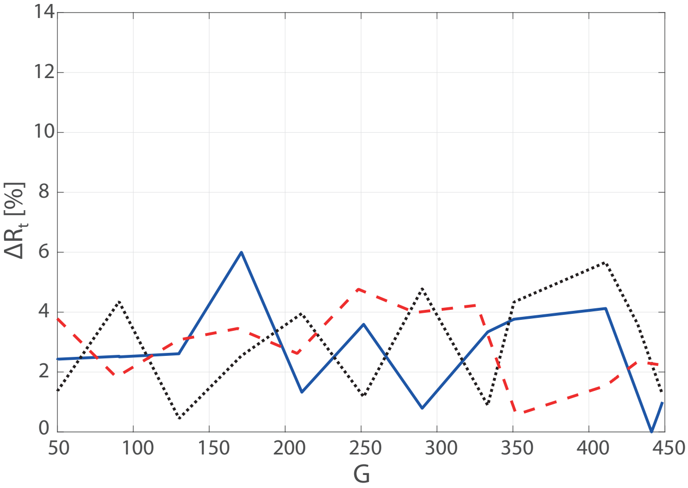

(a)

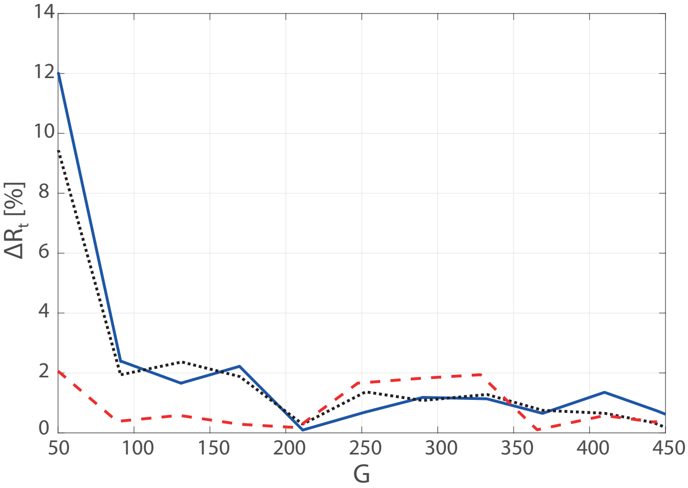

(b)

Figure 2.27: Comparison of water retention variation among the machines as a function of G-acceleration at $t/t_{max} = 0.1$ (a) and at $t/t_{max} = 0.8$ (b) of spinning time. Each line denotes the absolute difference of water retention between two washing machines. The blue line shows the absolute variation between WM_1 and WM_3, the black dotted line between WM_2 and WM_3, and the red dashed line between WM_1 and WM_2.

influence of shape factor on professional laundry is not relevant under the hypothesis of this study. Indeed a unique polynomial model to predict water retention performances is valid for the professional washing machine within an accuracy lower than 2%.

3

Passive and semi-active suspensions

This chapter investigates the vibration of the tub-drum assembly and the force transmission to the floor of the washing machine equipped with semi-active dampers. The aim is to develop a semi-active damper, which can both attenuate the oscillations of the tub-drum assembly and mitigate the force transmission to the floor via the four mounts. For this purpose specific in-house semi-active dampers have been designed and manufactured. The model and equations of motion presented in Section 2.2 are thus revised in such a way as to take into account the effects of semi-active dampers whose damping effect can be tuned to both reduce the tub-drum oscillation and the force transmission to the floor. The study first revises the mechanical features of the proposed semi-active damper. Then, it presents a comprehensive design study of a practical semi-active damper and a detailed report on the fabrication of a prototype device.

3.1 Lumped parameter model

As described in Section 2.4 the elastically suspended tub-drum assembly is characterised by two resonances in the working range of angular speeds, i.e. frequencies, which are due to the fundamental natural modes in horizontal and vertical directions of the elastically suspended tub-drum assembly. The classical passive dampers play a fundamental role in mitigating the resonant response of the system by dissipating its vibration energy at low frequencies. However they do not produce benefits at higher frequencies. Actually, as was discussed in Subsection 2.4.2, when the dampers are set with large damping factors to effectively minimise the tub-drum oscillations and the ground force transmission at the two fundamental resonance frequencies, the force transmission actually increases at higher frequencies where the machine spins. Indeed, at frequencies close to the two resonances the oscillations of the drum are characterised by large values which depend on damping, whereas, as described by Equation (2.31), they tend to the eccentricity of the rotor at higher frequencies. The ground force transmission is instead damping dependent at frequencies close to resonance and at higher frequencies. However, high damping effects reduce the force transmission at the two resonance frequencies only. Instead, low damping effects are needed to reduce the force transmission at higher frequencies. Thus, to ensure tub-drum vibration control and isolation of force transmission to ground in the whole frequency range of operation of the washing machine, the suspension holding the tub-drum assembly should be equipped with tunable dampers, which are set to produce high damping at low frequencies close to the fundamental resonance frequencies and low damping at high frequencies, where the machine is normally set to spinning. The classical suspension elements used to hold the tub-drum components of washing machines are composed of helical springs connected in parallel with high damping components, which link the case of the appliance with the suspended assembly. To provide experimental ground to these observations, initial tests were carried out for two configurations of the suspension system in the washing machine:

- only lightly damped helical springs

- helical springs and heavy dampers connected in parallel

Figure 3.1 shows the measured spectra for the horizontal (a) and vertical (b) tub-drum oscillations, normalised with respect to the resonance frequency of the fundamental heave natural mode in vertical direction, for the lightly damped (blue solid line) and heavily damped (red dashed line) configurations of the suspension.

From these plots it is possible to appreciate how the suspension damping effectively contributes to attenuate the resonance peaks at low frequencies. In fact the peak response of the fundamental natural mode in horizontal direction is reduced by 33 dB while the peak response of the fundamental natural mode in vertical direction is attenuated by 56 dB. At higher frequencies, above these two resonance frequencies, the oscillations in vertical and horizontal directions converge to a constant value, which is given by the eccentricity, for both the lightly damped and heavily damped configurations of the suspensions. In this frequency range only an increment of the total mass, by adding ballast to the tub-rotor system, can effectively lower the eccentricity factor, as described by Equation (2.31), and thus the amplitude of the vibrations.

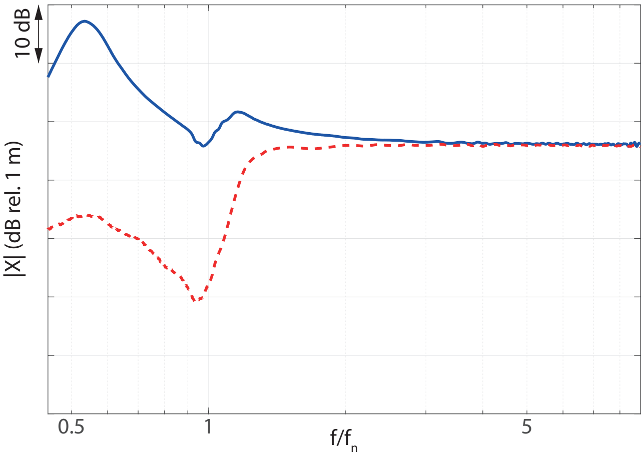

(a)

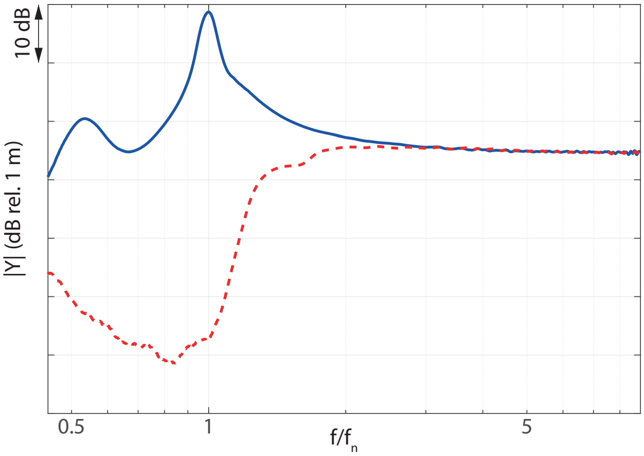

(b)

Figure 3.1: Comparison of the experimental spectra of the tub-drum assembly oscillations along horizontal (a) and vertical (b) directions with two different configurations of the suspension system: lightly passive damped (solid blue line) and heavily passive damped (red-dashed line) suspension system. The limits of the amplitude are covered by NDA.

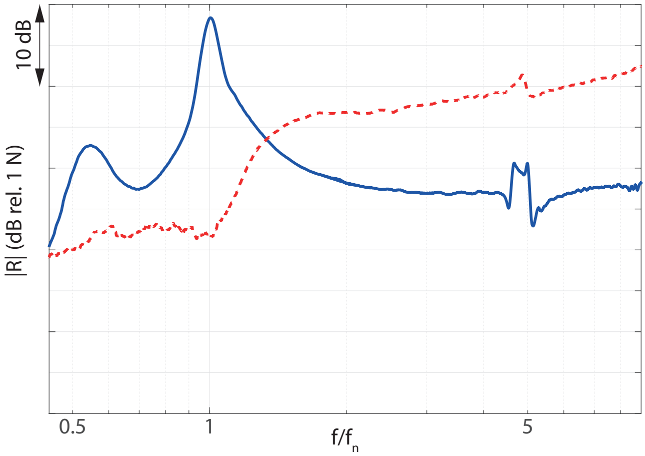

Figure 3.2: Comparison of the experimental spectra of force transmission with two different configurations of the suspension system: lightly passive damped (solid blue line) and heavily passive damped (red-dashed line) suspension system. The limits of the amplitude are covered by NDA.

The normalised spectra of the amplitude of the force transmission for both the lightly damped helical springs suspension and heavily damped helical springs and shock absorbers suspension are shown in Figure 3.2 respectively with the solid and dashed lines. The passive friction dampers reduce the amplitude of the resonance peaks by 11 dB for the horizontal fundamental natural mode and by 27 dB for the vertical one, which is responsible for the maximum transfer of force from the machine to the ground. At higher frequencies, above the resonance frequencies of the two fundamental natural modes due to the vertical and horizontal oscillations of the suspended tub-drum assembly, as described by Equation (2.32), the force transmission increases with the square of the angular speed of the drum and proportionally to the damping coefficient of the suspension. This increases the force transmitted to the floor with consequent problems of noise, vibration and machine walking. At full angular speed of the drum (20 Hz), the force transmitted by the lightly damped suspension is about 11 dB lower than that transmitted by the heavily damped suspension.

In summary, the frequency behaviour of the washing machine can be divided in two regions. First, low frequencies, where high damping level is needed to mitigate the dynamic response of the machine. Second, the higher frequencies where low damping effects can effectively reduce the force transmission to ground without affecting the amplitude of the oscillations of the drum. Therefore, the implementation of a suspension system formed by lightly damped helical springs and a dampers, where the damping coefficient can be switched from high values at low frequencies to low values at high frequencies, has been studied. Semi-active dampers are considered, which provide different damping contributes based on the frequency of excitation of the system (that is the angular speed of the drum).

Figure 3.3 shows the new configuration of the two DOFs lumped parameter model of professional washing machines equipped with semi-active dampers in place of passive shock absorbers.

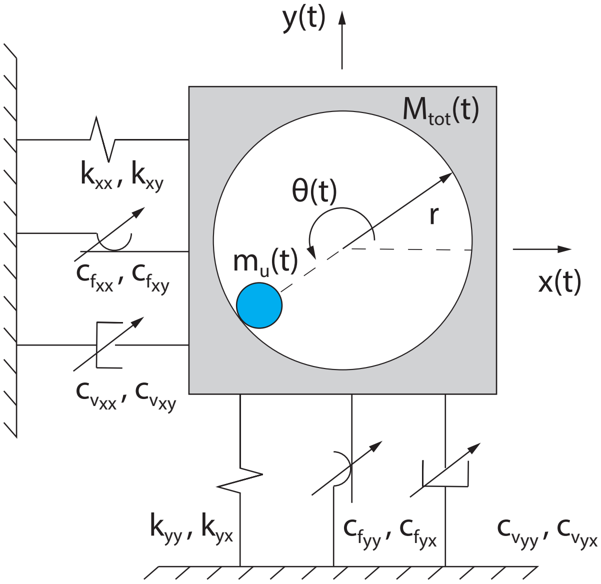

Figure 3.3: Two degrees of freedom (DOFs) lumped parameter dynamic model of the professional washing machine when semi-active dampers substitute passive shock absorbers.

3.2 Constitutive equations

Based on the discussion presented in the previous section, semi-active dampers with only two levels of damping are considered: a high damping level set to minimise the drum oscillations and force transmission at low frequencies where the response of the machine is controlled by the fundamental natural modes of the elastically suspended tub-drum assembly; a low damping level set to reduce the force transmission at higher frequencies above the resonance frequencies of the fundamental natural modes. This solution helps to simplify the mechanical design of the devices and keeps the manufacturing and life cost sustainable. Considering Equations (2.11) and (2.12) the equations of motion for the machine equipped with the semi-active dampers can be rewritten in terms of the following equations:

$$\begin{cases} M_{tot}(t)\ddot{x}(t) = m_u(t)r\omega(t)^2\cos\theta - k_{xx}x(t) - \hat{c_{v_{xx}}}\dot{x}(t) \\ \qquad - \hat{c_{f_{xx}}}sgn\left(x(t)\right) - k_{xy}y(t), -\hat{c_{v_{xy}}}\dot{y}(t) - \hat{c_{f_{xy}}}sgn\left(y(t)\right), \\ \\ M_{tot}(t)\ddot{y}(t) = m_u(t)r\omega(t)^2\sin\theta - k_{yy}y(t) - \hat{c_{v_{yy}}}\dot{y}(t) \\ \qquad - \hat{c_{f_{yy}}}sgn\left(y(t)\right) - k_{yx}x(t) - \hat{c_{v_{yx}}}\dot{x}(t) - \hat{c_{f_{yx}}}sgn\left(x(t)\right). \end{cases} \tag{3.1}$$

The vertical force is now given by:

$$R(t) = \hat{c_{v_{yx}}}\dot{x}(t) + \hat{c_{v_{yy}}}\dot{y}(t) + \hat{c_{f_{yx}}}sgn\left(x(t)\right) + \hat{c_{f_{yy}}}sgn\left(y(t)\right) + k_{yx}x(t) + k_{yy}y(t). \tag{3.2}$$

Here $\hat{c_{v_{xx}}}$, $\hat{c_{v_{xy}}}$, $\hat{c_{v_{yx}}}$, $\hat{c_{v_{yy}}}$, $\hat{c_{f_{xx}}}$, $\hat{c_{f_{xy}}}$, $\hat{c_{f_{yx}}}$ and $\hat{c_{f_{yy}}}$ are the self and cross viscous and friction damping contributes generated by the linear dampers mounted at a 12° with respect to the vertical axis. These factors are time dependent, more specifically they change between two limiting values based on the angular speed of the drum which is generated by the electrical motor controlled electronically. The damping laws for the ij-th damping contribute can be assumed equal to:

$$\hat{c_{v_{ij}}} = \begin{cases} c_{v_{ij}} & if \quad \omega(t) < \omega_s(t), \\ \approx 0 & if \quad \omega(t) > \omega_s(t), \end{cases} \tag{3.3}$$

$$\hat{c_{f_{ij}}} = \begin{cases} c_{f_{ij}} & if \quad \omega(t) < \omega_s(t), \\ \approx 0 & if \quad \omega(t) > \omega_s(t), \end{cases} \tag{3.4}$$

where ω_s is the switching frequency at which the damping coefficients are changed.

3.3 Frequency Response Functions

The Frequency Response Functions (FRFs) when this particular configuration of semi-active dampers is used to control the dynamic response of professional wahing machine is described below with respect to the FRFs derived in Equations (2.25), (2.26) and (2.27):

$$X(j\omega) = \frac{m_u r\omega^2 - j\frac{4}{\pi}\left[F_{c\hat{f_{xx}}} + F_{c\hat{f_{xy}}}\right] - \left[c_{\hat{v_{xy}}} j\omega + k_{xy}\right] Y(j\omega)}{-M_{tot}\omega^2 + j\omega c_{\hat{v_{xx}}} + k_{xx}}, \quad (3.5)$$

$$Y(j\omega) = \frac{m_u r\omega^2 - j\frac{4}{\pi}\left[F_{c\hat{f_{yy}}} + F_{c\hat{f_{yx}}}\right] - \left[c_{\hat{v_{yx}}} j\omega + k_{yx}\right] X(j\omega)}{-M_{tot}\omega^2 + j\omega c_{\hat{v_{yy}}} + k_{yy}}, \quad (3.6)$$

$$\begin{aligned} R(j\omega) = j\frac{4}{\pi}\left[F_{c\hat{f_{yy}}} + F_{c\hat{f_{yx}}}\right] + \left[c_{\hat{v_{yx}}} j\omega + k_{yx}\right] X(j\omega) \\ + \left[j\omega c_{\hat{v_{yy}}} + k_{yy}\right] Y(j\omega), \quad (3.7) \end{aligned}$$

where:

$$c_{\hat{v_{ij}}} = \begin{cases} c_{v_{ij}} & if \quad \omega < \omega_s, \\ \approx 0 & if \quad \omega > \omega_s, \end{cases} \quad (3.8)$$

$$F_{c\hat{f_{ij}}} = \begin{cases} F_{c_{f_{ij}}} & if \quad \omega < \omega_s, \\ \approx 0 & if \quad \omega > \omega_s. \end{cases} \quad (3.9)$$

Therefore the FRFs for the harmonic oscillations of the tub-drum assembly in x and y directions and the force transmitted to ground via the four spring-dampers result:

$$G_x(j\omega) = \frac{X(j\omega)}{F(j\omega)}, \quad (3.10)$$

$$G_y(j\omega) = \frac{Y(j\omega)}{F(j\omega)}, \quad (3.11)$$

$$T(j\omega) = \frac{R(j\omega)}{F(j\omega)}. \quad (3.12)$$

The switching frequency ω_s depends on the mechanism used to generate friction between the inner piston and the outer cylinder of the absorber, which is prone to variations based on use, temperature, lubricants, etc. However, considering real working conditions, these changes are small and of the order of 0.5 Hz at most, so that ω_s can be estimated in first approximation by neglecting the Coulomb damping contribute. The practical realization of the semi-active dampers will probably require a feedback control loop to vary damping level based on the angular speed of the drum. However, for smooth spinning transitions, the switching frequency can be set with an open loop architecture such that the high to low damping configuration is simply switched when the drum velocity crosses a critical spinning frequency as shown in Figure 3.4. Since it is not possible to identify a unique and unequivocal point at which the amplitude of the transmissibility spectrum does not depend on damping, the switching frequency ω_s is numerically estimated such that the magnitude of transmissibility is equal to 1. Therefore, is this the switching frequency that has been used in this study to move the isolator from high to low damping configurations.

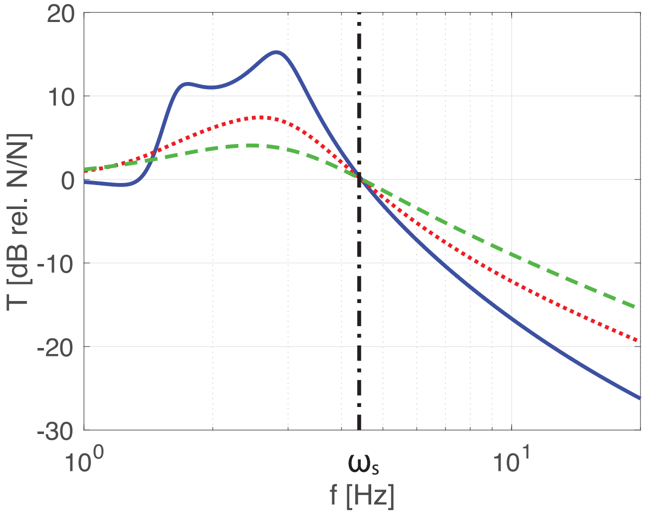

Figure 3.4: Comparison of simulated transmissibility for three different configurations of viscous damping and neglected Coulomb friction. Solid blue line refers to lightly damped suspension, red dotted line to normally damped and green dashed to heavily damped configuration.

The switching frequency is therefore given by the following expression:

$$|T(j\omega_s)| = 1. \tag{3.13}$$

Figures 3.5 and 3.6 show simulated spectra respectively for the oscillations of the tub-drum assembly and for the force transmission with three different configurations of the suspension system: lightly passive damped (red dotted line), heavily passive damped (black dashed line) and in-house semi-active damped (blue solid line) suspension system. The semi-active solution switches from high damping to null damping at the frequency ω_s and vice versa. All the resonance peaks at low speeds of the drum are reduced thanks to the heavy damping generated by the semi-active damper. Also the amplitude of the transmitted force has constant level at high speed of the drum thanks to the low damping generated by the semi-active damper.

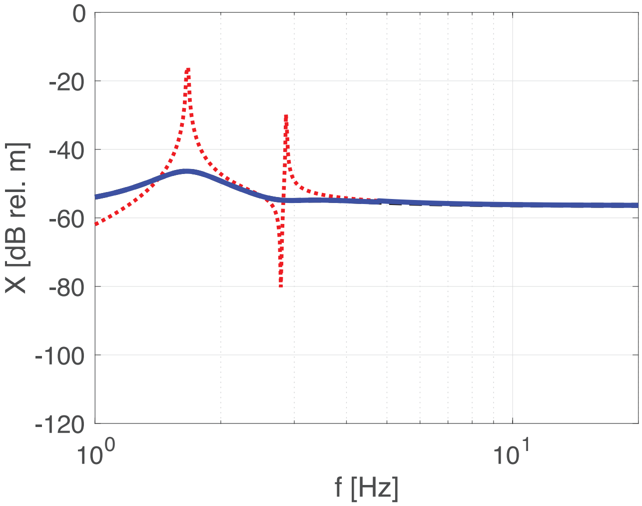

(a)

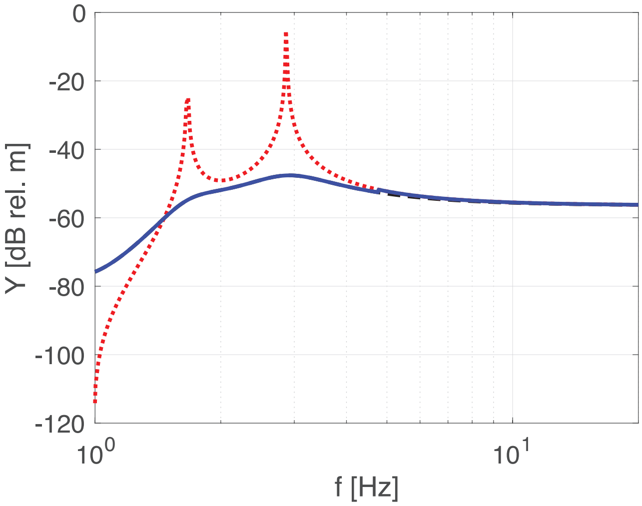

(b)

Figure 3.5: Comparison of the analytical spectra of the tub-drum assembly oscillations along horizontal (a) and vertical (b) directions with three different configurations of the suspension system: lightly passive damped (red dotted line), heavily passive damped (black dashed line) and in-house semi-active damped (blue solid line) suspension system.

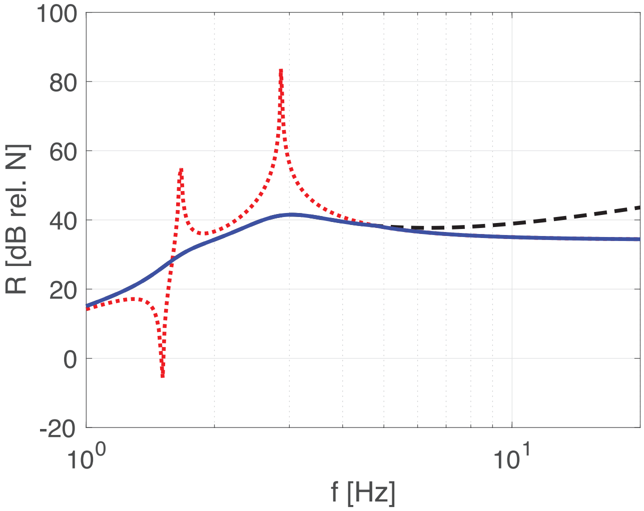

Figure 3.6: Comparison of the analytical spectra of force transmission with three different configurations of the suspension system: lightly passive damped (red dotted line), heavily passive damped (black dashed line) and in-house semi-active damped (blue solid line) suspension system.

3.4 Design and implementation

Following the considerations made in the previous sections, a semi-active damper with two levels of damping has been designed and manufactured, which can be used to lower the ground force transmission at high spinning velocities and preserve the low drum vibration and force transmission levels at low frequencies, where the dynamic response of the washing machine is controlled by the resonant responses of the fundamental natural modes of the elastically suspended tub-drum assembly in horizontal and vertical directions. The proposed system employs a switch on/off pincers clumping device, where the damping effect is controlled by an electromagnetic transducer, which, based on the angular speed of the drum, releases or stops the clamping pincers. Figure 3.7 shows the sketch of the open control loop system.

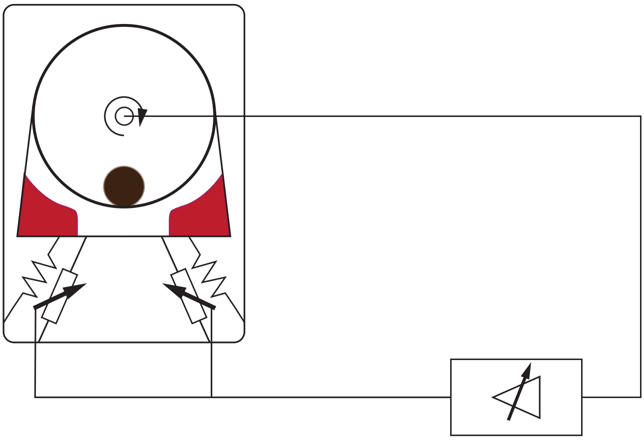

Figure 3.7: Sketch of the angular speed control loop used to switch the damping levels of semi-active dampers.

Figures 3.8 and 3.9 show respectively the front and back views of the in-house assembled damper specifically designed and manufactured for the control of the dynamic response of professional washing machines. The system is characterised by a hollow cylindrical shell made with 3D printed plastic. The tip of the cylindrical part (A) has two flat surfaces that house a silent block bushing made of rubber, which generates the connection to the ground frame of the washing machine, allowing small rotational vibration of the tub-drum assembly. A second 3D printed

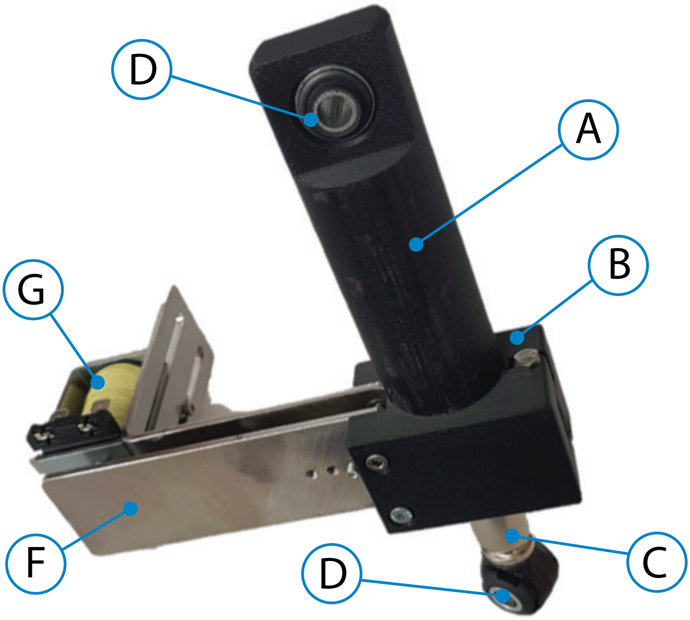

Figure 3.8: Front view picture of the mechanical design of the semi-active damper.

element (B) is linked to the previous by a pivot rod, which allows the relative rotation of the components A and B, which form a brake shoe system. As shown in Figure 3.11, the internal surfaces of the brake shoe encompass two circular cavities designed to house replaceable half-moon braking pads (E) of polymeric or plastic-based materials used to dissipate vibration energy by friction. A metallic rod (C) with silent block bushing at its extremity (D) is used to connect this component to the frame of the suspended tub-drum assembly of the machine through a through-all hole. The bushing contributes to attenuate the rotational vibration modes of the tub-drum assembly. The rod is inserted into the cylindrical shell of the semi-active damper in such a way as it slides within the calibrated rail generated by the half-moon friction inserts without being in contact with the inner surface of the cylindrical case. The relative movements between the piston and the brake shoe assembly dissipate the vibration energy of the suspended components by rubbing the beam against the inserts. Figure 3.10 shows the CAD drawing of the semi-active damper components using CATIA V5 software.

Since the total friction force is proportional to the clamping force that acts on the half-moon inserts, the damping ratio can be adjusted by varying the clamping force of the brake shoe system. Thus a simple mechanism is built to tune the two levels of damping ratio from light to heavy damping. The brake shoe elements present holes at the opposite sides of the pivot, where two metal brackets (F) are screwed. One of them is completely flat, while the other is 90° bent in such a way as to house the electromagnetic actuator (G) at its end, as shown in Figure 3.13.

Figure 3.12 shows the tuning screw (H), which is placed in the proximity of the brake shoes in such a way as to pre-load a hard spring that forces the brackets together. The clamping force and consequently the damping level of the shock absorber can be tuned by adjusting the screwing. Overall, this configuration leads to a friction damper that generates high and low damping levels.

A linear solenoid transducer is fixed at the free ends of the brackets in such a way as, when it is powered, it opposes the compression force of the regulating spring. In this way the two brake shoe components are moved apart from each other by their rotation around the pivot and the normal force that pushes the friction inserts against the metallic rod falls down. This configuration provides the lowest damping level into the system. Unfortunately residual friction damping can be generated by the rubbing of the tip of the rod against the inner surface of the cylindrical shell due to misalignment of the semi-active damper ends. For this reason the tip of the piston rod has been properly rounded and the internal diameter of the cylindrical shell enlarged as much as possible in order to lower the contact surface between the parts and decrease hanging risks.

This design of the semi-active damper guarantees passive damping behaviour in case of brake down of the actuator or electrical failure, so that all the resonant oscillations of the tub-drum assembly and force transmission are attenuated in any case. Moreover the length of the brackets can be chosen based on available space and force/cost ratio of the solenoid actuator.

Appendix B contains the CAD drawings of the components designed to assemble the semi-active damper proposed.

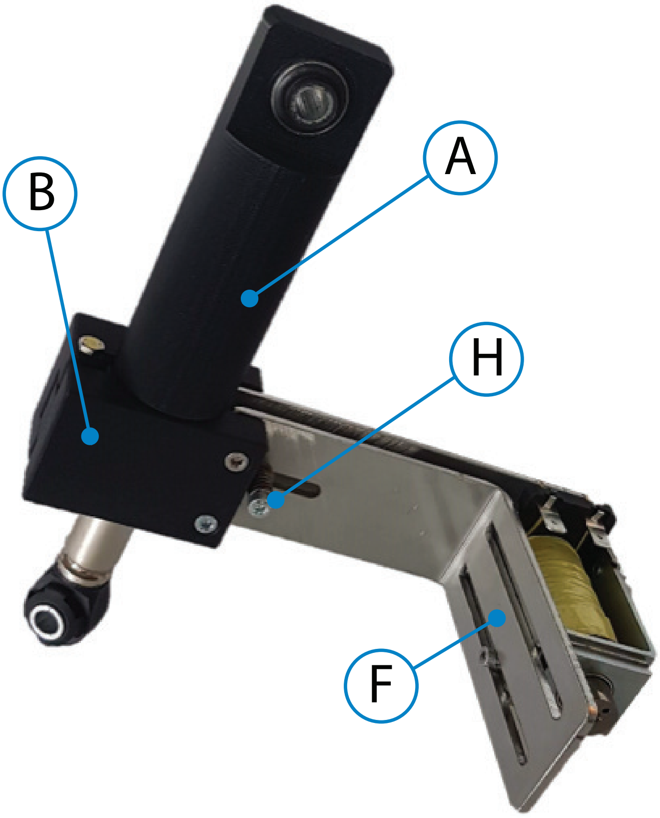

Figure 3.9: Back view picture of the mechanical design of the semi-active damper.

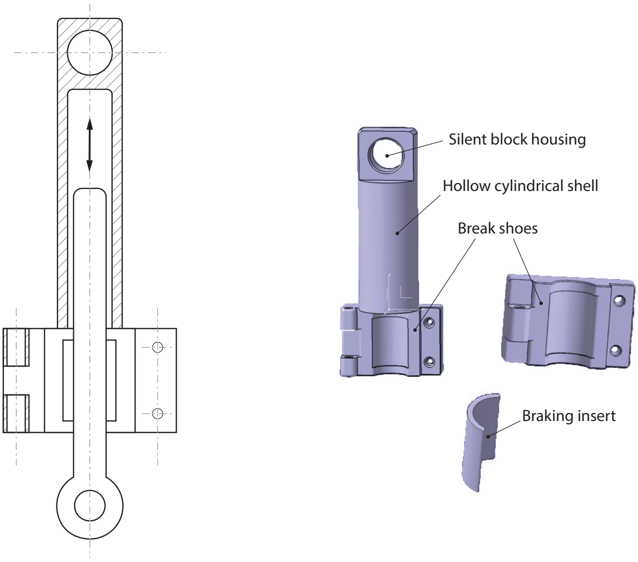

Figure 3.10: CAD sketch of the components designed for the semi-active damper.

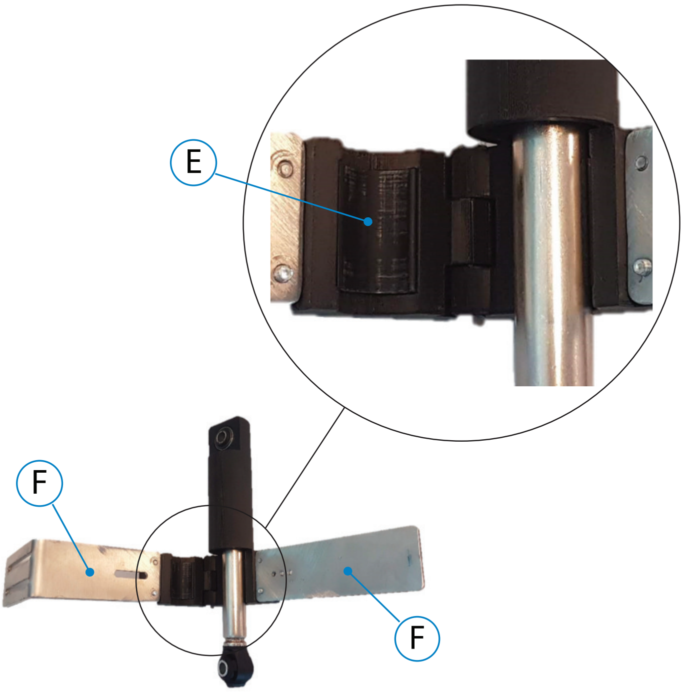

Figure 3.11: Details view of the brake shoe elements for the semi-active damper.

Figure 3.12: Details view of the tuning screw used to calibrate the maximum damping level for semi-active damper.

Figure 3.13: Details view of the actuator used to control the damping level for the semi-active damper.

3.5 Experimental results

Figure 3.14 shows the experimental setup used to produce the measurements presented in this chapter. The washing machine was located on top of the same base framework structure considered in Sections 2.4, which was equipped with strain gauge load cells (*Flintec ZLS Planar Beam*) to measure the force transmission through the four feet of the machine. As shown in sketch (b), the drum was equipped with two *PCB Piezotronics* accelerometers positioned on top and on the flank of the drum in such a way as to measure the vertical and horizontal accelerations. A lumped mass was clamped inside the drum in order to generate a static unbalance, which, for a given speed of rotation, produces a centrifugal force, given by a combination of harmonic forces in quadrature, oriented in vertical and horizontal directions respectively. The centrifugal force was therefore identified from the drum angular speed, measured with an incremental encoder (*Lika rotapuls IT65*).

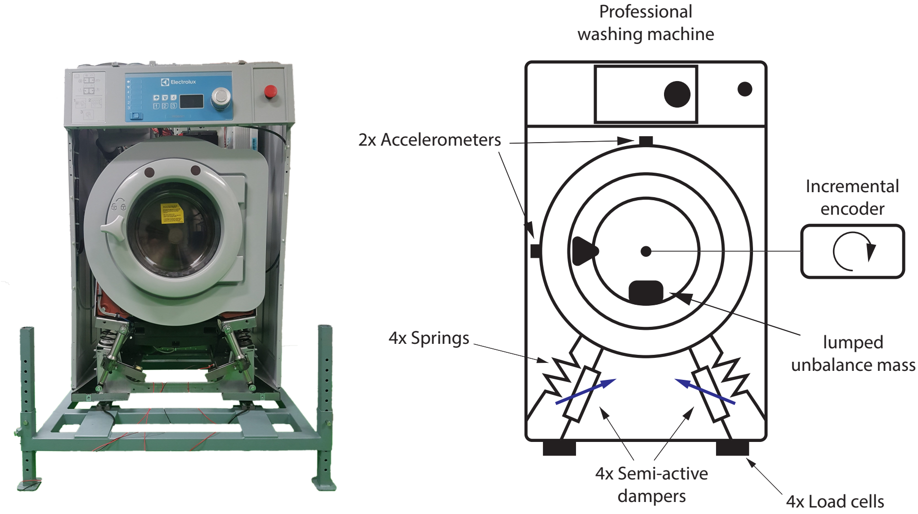

(a) **(b)**

Figure 3.14: Picture (a) and sketch (b) of the experimental setup used to perform semi-active damper validation.

The drum suspension system was composed by four helical linear springs connected in parallel with either the standard passive dampers or the in-house manufactured semi-active friction-based dampers. The two passive dampers were chosen in such a way as to implement a large damping and a very light damping. The in-house manufactured semi-active dampers were designed with the disengaging mechanism described in Section 3.4 to switch the damping levels.

Experimental measurements are first presented for the spectra of the drum displacements in horizontal and vertical directions and then for the spectrum of force transmission to the ground. The measurements consider three configurations of the passive and semi-active dampers: a) fixed low damping level, b) fixed high damping level, c) switching low to high and high to low damping levels. The switching operation mode was set in such a way as the higher damping level is implemented for low angular speeds up to the switching speed ω_s described by Equation (3.13).

Figure 3.15 shows the spectra of the amplitude of the drum oscillations in horizontal (Plot a) and vertical (Plot b) directions produced by 0.5 kg of unbalanced load placed inside the drum. The solid blue line shows the measured spectra when the dampers implement constant low-damping levels. The spectra of the oscillations are characterised by two resonance peaks at low frequencies followed by a constant level, which is about 25 dB lower than that of the higher resonance peak. The constant amplitude level was derived in Equation (2.31) and it is equal to the eccentricity factor. Equation (2.31) shows that, at high rotation speeds, the amplitude of the oscillation solely depends on the ratio between the unbalance mass and drum-ballast mass, i.e. m_u/M_{tot}. Therefore, to guarantee low oscillations at higher frequencies a large ballast mass should be used. The two resonance peaks are due to the transversal and horizontal fundamental natural modes, which are characterised respectively by dominant horizontal and vertical oscillations of the elastically suspended drum. As one would expect, the spectrum of the horizontal displacement (Plot a) shows a much higher resonance peak for the horizontal natural mode whereas the spectrum of the vertical displacement (Plot b) shows a much higher resonance peak for the transversal natural mode. The dashed red line shows the measured spectra when the dampers implement the high-damping fixed levels. Large reductions of the drum oscillations, comprised between 20 to 55 dB, are produced for low drum angular speeds up to ω_s. No reductions are instead obtained for higher angular speeds of the drum, since, as discussed above, at these speeds the drum oscillation solely depends on the ratio between the unbalance mass and drum-ballast mass, i.e. m_u/M_{tot}. The dotted black line shows the measured spectra when the semi-active dampers implement the high damping levels for angular speeds below ω_s and low damping levels for angular speeds above ω_s. Once more, large reductions of the drum oscillations comprised between 20 and 45 dB are generated for drum angular speeds lower than ω_s. Moreover, no reductions are produced for angular speeds higher than ω_s.

Figure 3.16 shows the spectrum of the total force transmitted to the ground via the four feet of the washing machine. The solid blue line shows the measured spectrum when the dampers implement the low-damping fixed levels. Also in this case, the spectrum is characterised by two resonance peaks at low frequencies followed by a somewhat constant level, except for some dynamics at 5 times the fundamental natural frequency of the vertical vibrational mode. In this case, for angular speeds greater than the fundamental natural frequencies, the transmitted force is given by the modulus of the suspension complex stiffness multiplied by the amplitude of the oscillation as derived in Equation (2.32). Thus, indeed for very small levels of damping the total transmitted force for angular speeds greater than ω_s can be assumed constant and equal to the following expression:

$$R(\omega \gg \omega_s) = \frac{m_u r}{M_{tot}} \sqrt{k_{yx}^2 + k_{yy}^2}. \tag{3.14}$$

However, when large damping levels are implemented in the four suspensions, as shown by the red dashed line, large reductions are obtained for the force transmitted at low frequencies. More specifically, the transmitted force at the resonance frequencies of the fundamental oscillation modes are brought down by 10 dB and 25 dB. Nevertheless, as Equation (2.32) suggests, with large damping factors the total force transmitted at higher frequencies tends to rise proportionally to frequency such that the force transmission becomes up to 11 dB larger at the maximum spinning frequency. Indeed for angular speeds greater than ω_s Equation (2.32) can be approximated with the following expression:

$$R(\omega \gg \omega_s) = \frac{m_u r}{M_{tot}} \omega \sqrt{c_{v_{yx}}^2 + c_{v_{yy}}^2 + c_{eq_{yx}}^2 + c_{eq_{yy}}^2}. \tag{3.15}$$

The dotted black line shows the spectrum of the transmitted force when the semi-active dampers implement the high damping levels for angular speeds below ω_s and low damping levels for angular speeds above ω_s. The combination of low-frequency high-damping and high-frequency low damping produces the better compromise in terms of force transmission. Indeed, compared to the suspension with light damping, at

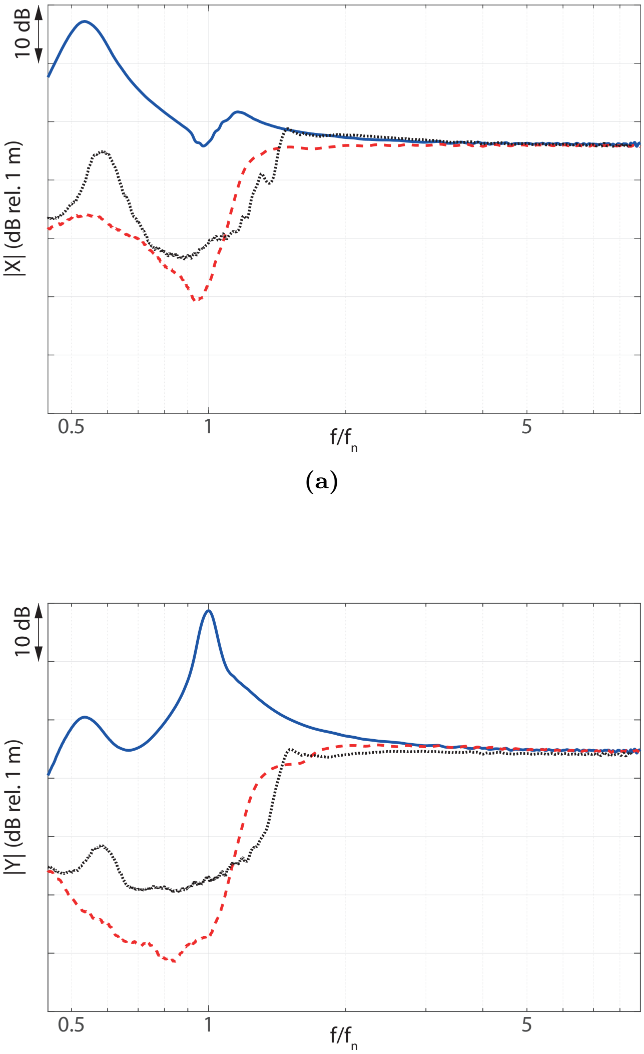

(a)

(b)

Figure 3.15: Spectra of the measured horizontal and vertical drum oscillations using a lightly damped suspension (solid blue line), a heavily damped suspension (red dashed line) and, a semi-active suspension that switches from high to low damping levels (dotted black line). The limits are covered by NDA.

low frequencies below ω_s, the force transmission is greatly mitigated. In particular, when the angular speed equals the two fundamental natural frequencies, the transmitted force is brought down by about 30 and 20 dB respectively. Also, at higher frequencies above ω_s, compared to the suspension with light damping, the force transmission is about 2 to 4 dB higher, but still at rather low levels that can be accepted in practice. Moreover, design and manufacturing improvements of the semi-active damper might further reduce the residual damping and effectively lower the force transmitted to the ground.

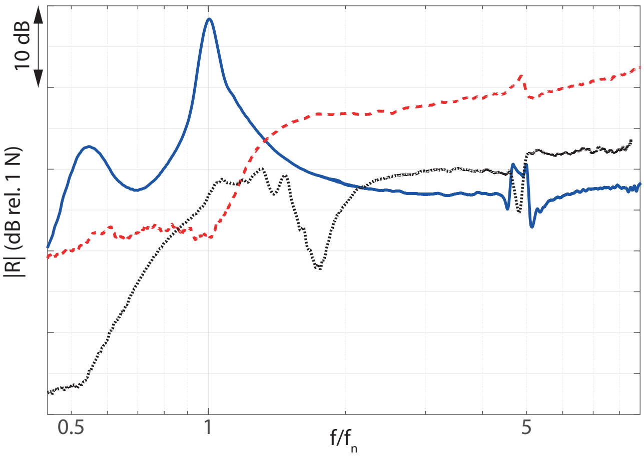

Figure 3.16: Spectra of the measured force transmitted to the ground using a lightly damped suspension (solid blue line), a heavily damped suspension (red dashed line) and, a semi-active suspension that switches from high to low damping levels (dotted black line). The limits are covered by NDA.

4

Passive and semi-active TVAs

This chapter investigates the vibration of the tub-drum assembly and force transmission to the floor of the washing machine equipped with semi-active Tunable Vibration Absorber. As suggested by Equation (2.31) for the tub-drum oscillations at higher frequencies, ballast masses are installed on the tub-drum frame to reduce the eccentricity factor. To obtain low factors, big amount of ballasts are required; therefore this solution has practical limitations in terms of implementability and final cost. In this chapter an alternative solution is investigated, where the ballast masses are replaced by tunable vibration absorbers. The idea is to have time varying vibration absorbers whose tuning frequency is modulated to the spinning of the drum. In this way, both drum oscillations and force transmission to ground can be effectively lowered at the drum spinning velocity. For this purpose the ballast masses are substituted by in-house made TVAs, which are formed by a cantilever beam with a block mass whose position can be moved along the beam such that the fundamental resonance frequency of the system can be varied. First of all, the cantilever beam TVA is presented and its equations of motion are derived both in time and frequency domains. Then, a two DOFs lumped parameter model is developed to predict both the amplitude of the drum oscillations along horizontal and vertical directions and the amplitude of ground force transmission for a professional washing machine equipped with cantilever beam TVAs. A parametric study is then presented to describe the effects produced by the TVAs. Finally the design and implementation of the TVA prototype is presented. The experimental validation of the proposed TVA solution closes the chapter with the analysis of the measured spectra obtained on the washing machine equipped with the TVAs.

4.1 Cantilever beam model

The vibrational absorber considered in this study is composed of a cantilever beam with a tip mass. Figure 4.1 shows a sketch of the device, which is characterised by a beam, fixed on an external support built in the tub-drum frame and a calibrated tip mass located at its end.

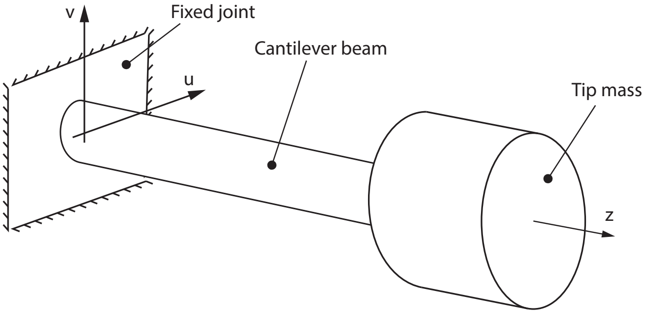

Figure 4.1: Sketch of the cantilever beam with tip mass TVA.

The oscillations of the tub, along the vertical (v) and horizontal (u) axes, excite the base of the cantilever beam, which in turn is affected by the inertial load generated by the tip masses via the elastic deflection of the beam. The differential equations, for the flexural response of the cantilever beam and block mass, are derived with respect to the non-inertial system of reference shown in Figure 4.1. The formulation is derived only for the flexural vibration in the vertical plane. The resulting equations are rearranged into a lumped parameter formulation, which is combined with the lumped element formulation for the oscillations of the tub-drum assembly in vertical direction. To this end, as shown in Figure 4.2, the model of the cantilever beam system with tip mass in the non-inertial system of reference is used. Therefore the flexural equations of motion derived with respect to the non-inertial system of reference are rearranged with respect to the inertial system of reference.

Equilibrium equations, with reference to the rotation and translation of an infinitesimal element of beam are given by [92,93] under the hypothesis of the uniform Euler–Bernoulli beam model. Considering the motion shown in Figure 4.3 the following equations are derived:

$$\frac{\partial T(z,t)}{\partial z} = -f(z,t), \tag{4.1}$$

Figure 4.2: Model of the cantilever beam system with tip mass with respect to the non-inertial reference system.

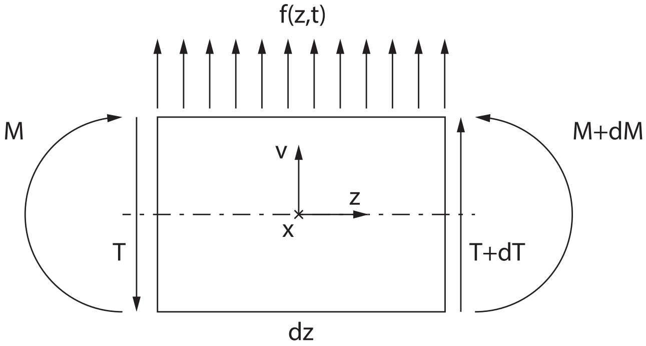

Figure 4.3: Free body diagram of the infinitesimal element of the beam.

$$\frac{\partial M(z,t)}{\partial z} = -T(z,t), \tag{4.2}$$

where T and M are respectively the shear force and the internal bending moment at a cross-section of the beam, while $f(z)$ is the distributed force per unit length of the beam. Combination of Equations (4.1) and (4.2) gives:

$$\frac{\partial^2 M(z,t)}{\partial z^2} = f(z,t). \tag{4.3}$$

The internal bending moment at any cross section is related to the rotational displacement of the beam as follows:

$$M(z,t) = EI\frac{\partial^2 v(z,t)}{\partial^2 z}. \tag{4.4}$$

Here E is the Young's module of elasticity of the material and I is the cross sectional area moment of inertia, estimated with respect to the neutral axis of the beam section. Substituting Equation (4.4) into (4.3), gives:

$$EI\frac{\partial^4 v(z,t)}{\partial z^4} = f(z,t) \tag{4.5}$$

To obtain the equation of the motion with respect to the non-inertial system of reference, the inertia to flexural displacements of the beam has to be taken into account. This inertia effect results as an external distributed force acting on the beam, so that:

$$f_1(z,t) = -\rho A\frac{\partial^2 v(z,t)}{\partial t^2}, \tag{4.6}$$

where ρ is the density per unit of length of the material and A the cross sectional surface area, which is uniform along the beam. The external force is due to the inertial contribution of the tip mass, which has been modelled as a lumped parameter. Hence:

$$f_2(z,t) = -F_{m_t}(t)\delta\left(z-L\right) - \frac{\partial}{\partial z}\left[M_{m_t}(t)\delta\left(z-L\right)\right] \tag{4.7}$$

where F_{m_t} is the lumped inertial force of the tip mass, M_{m_t} is the lumped inertial moment produced by the mass and calculated with respect to the axis of symmetry and δ is the Delta Dirac function. The total force $f(z,t)$ acting on the infinitesimal element of the beam is given by:

$$f(z,t) = f_1(z,t) + f_2(z,t) \tag{4.8}$$

Combining Equations (4.5), (4.6), (4.7) and (4.8) in one expression gives the following differential equation for the flexural vibrations of the cantilever beam with tip mass:

$$\begin{aligned}\rho A\frac{\partial^2 v(z,t)}{\partial t^2} + EI\frac{\partial^4 v(z,t)}{\partial z^4} &= -F_{m_t}(t)\delta(z-L)+\\ &\quad -\frac{\partial}{\partial z}\left[M_{m_t}(t)\delta(z-L)\right].\end{aligned} \tag{4.9}$$

To find the natural frequencies of the beam and tip mass, the homogeneous equation that derives from Equation (4.9) is considered:

$$\rho A\frac{\partial^2 v(z,t)}{\partial t^2} + EI\frac{\partial^4 v(z,t)}{\partial z^4} = 0. \tag{4.10}$$

The method of variables separation is used to solve this linear homogeneous partial differential equation [94]. Thus the vertical displacement is written as:

$$v(z,t) = \Phi(z)q(t), \tag{4.11}$$

where $\Phi(z)$ is function of z only while $q(t)$ is function of t only.

The response of a linear system excited by an harmonic function is of the type:

$$v(z,t) = \Phi(z) cos(\omega t + \phi). \tag{4.12}$$

Substituting Equation (4.12) into Equation (4.10), and neglecting the time dependence, gives:

$$\frac{\partial^4 \Phi(z)}{\partial z^4} - \left(\frac{b}{L}\right) \Phi(z) = 0, \tag{4.13}$$

in which L is the length of the beam and b is a parameter defined as follows:

$$b = \sqrt[4]{\frac{\rho A \omega^2}{EI}} L. \tag{4.14}$$

The solutions of Equation (4.13) can be sought in terms of a $e^{\lambda z}$ function, so that the following characteristic equation for the homogeneous Equation (4.13) is obtained:

$$e^{\lambda z} \left[\lambda^4 - \left(\frac{b}{L}\right)^4 \right] = 0, \tag{4.15}$$

where λ_i are the eigenvalues. The linear combinations of non-trivial solutions of Equation (4.15) can be casted in the following expression::

$$\begin{aligned} \Phi(z) = C_1 \sinh\left(\frac{bz}{L}\right) + C_2 \cosh\left(\frac{bz}{L}\right) + \\ + C_3 \sin\left(\frac{bz}{L}\right) + C_4 \cos\left(\frac{bz}{L}\right). \end{aligned} \tag{4.16}$$

where Φ_i are the eigenfunctions. The solutions must satisfy the boundary conditions of the cantilever beam with tip mass. Considering Figure 4.2, the left hand side of the cantilever beam is fixed in such a way as to avoid translational and rotational displacements. This leads to the following boundary conditions:

$$v(z)\Big|_{z=0} = 0, \tag{4.17}$$

$$\frac{\partial v(z)}{\partial z}\Big|_{z=0} = 0. \tag{4.18}$$

On the right hand side, the tip mass imposes the shear and bending stresses to balance respectively the mass translational and rotational inertia. These stresses are described by the following relations:

$$F_{m_t}(t)\delta\left(z-L\right)\Big|_{z=L} = m_t\frac{\partial^2 v(z,t)}{\partial t^2}\Big|_{z=L}, \tag{4.19}$$

$$M_{m_t}(t)\delta\left(z-L\right)\Big|_{z=L} = I_{m_t}\frac{\partial^2}{\partial t^2}\left[\frac{\partial v(z,t)}{\partial z}\right]\Big|_{z=L}, \tag{4.20}$$

where m_t is the tip mass and I_{m_t} is the moment of inertia with respect to the transverse axis of the tip mass. Considering Equations (4.2), (4.4), (4.19) and (4.20), the right hand side boundary conditions can thus be written as follows:

$$-EI\frac{\partial^3 v(z,t)}{\partial z^3}\Big|_{z=L} = -m_t\frac{\partial^2 v(z,t)}{\partial t^2}\Big|_{z=L}, \tag{4.21}$$

$$EI\frac{\partial^2 v(z,t)}{\partial z^2}\Big|_{z=L} = -I_{m_t}\frac{\partial^3 v(z,t)}{\partial t^2\partial z}\Big|_{z=L}. \tag{4.22}$$

Considering the separation of variables given in Equation (4.11), the four boundary conditions can be rewritten as follows:

$$\Phi(z)\Big|_{z=0} = 0, \tag{4.23}$$

$$\frac{\partial\Phi(z)}{\partial z}\Big|_{z=0} = 0, \tag{4.24}$$

$$EI\frac{\partial^2\Phi(z)}{\partial z^2}\Big|_{z=L} + I_{m_t}\omega^2\frac{\partial\Phi(z)}{\partial z}\Big|_{z=L} = 0, \tag{4.25}$$

$$EI\frac{\partial^3\Phi(z)}{\partial z^3}\Big|_{z=L} - m_t\omega^2\Phi(z)\Big|_{z=L} = 0. \tag{4.26}$$

Since Equation (4.13) is of fourth order, its general solution, described in Equation (4.16), contains four spatial constants of integration. In order to operate a modal decomposition of the equations of motion, the fundamental natural frequencies of the cantilever beam with tip-mass have to be calculated, thus b is an unknown parameter with respect to Equation (4.14). In conclusion a total of five unknowns coefficients have to be derived. Since there are only four spatial boundary conditions, it is not possible to evaluate all the unknowns uniquely, thus only the shape of $\Phi(z)$ can be derived, but not its amplitude.

Imposing Equations (4.23) and (4.24) in Equation (4.16), gives:

$$C_3 = -C_1, \tag{4.27}$$

$$C_4 = -C_2. \tag{4.28}$$

Having set the boundary conditions given in Equations (4.23), (4.24), (4.25) and (4.26) and taking into account the solutions of Equations (4.27) and (4.28), the following system of equations has to be satisfied:

$$\mathbf{DC} = \mathbf{0}, \tag{4.29}$$

where $\mathbf{C} = \begin{bmatrix} C_1 \\ C_2 \end{bmatrix}$ is the vector of unknown constants and $\mathbf{D}$ is the matrix defined as follows:

$$\mathbf{D} = \begin{bmatrix} d_{11} & d_{12} \\ d_{21} & d_{22} \end{bmatrix}, \tag{4.30}$$

where

$$\begin{aligned}
d_{11} &= \sinh(b) + \sin(b) - \frac{I_{m_t}}{\rho A}\left(\frac{b}{L}\right)^3 \left[\cosh(b) - \cos(b)\right], \\
d_{12} &= \cosh(b) + \cos(b) - \frac{I_{m_t}}{\rho A}\left(\frac{b}{L}\right)^3 \left[\sinh(b) + \sin(b)\right], \\
d_{21} &= \cosh(b) + \cos(b) + \frac{m_t}{\rho A}\frac{b}{L} \left[\sinh(b) - \sin(b)\right], \\
d_{22} &= \sinh(b) - \sin(b) + \frac{m_t}{\rho A}\frac{b}{L} \left[\cosh(b) - \cos(b)\right].
\end{aligned} \tag{4.31}$$

The non-trivial solutions of the algebraic system of Equation (4.29) can be calculated numerically by imposing the determinant of the matrix of Equation (4.30) equal to zero.

$$\det(\mathbf{D}) = 0. \tag{4.32}$$

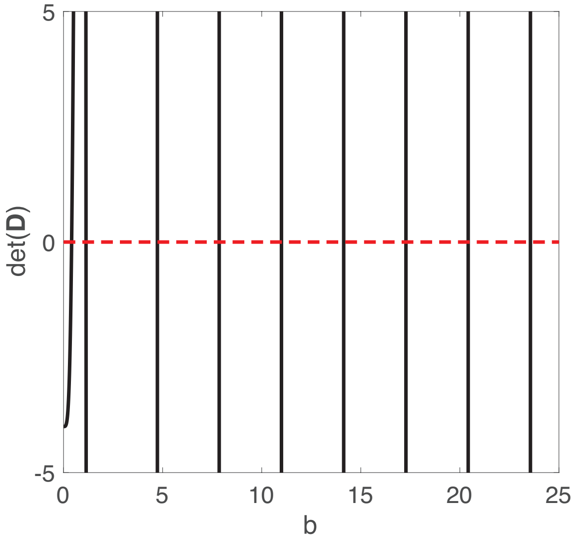

Figure 4.4: Graphical solution of non linear algebraic equation obtained by imposing the determinant of matrix **D** equal to zero.

Figure 4.4 shows the graph of det($\mathbf{D}$) with respect to the parameter b. The graph indicates there is a sequence of crossing points to the horizontal axis, that is a sequence of values of b for which $\det(\mathbf{D}) = 0$ is verified. The values provide the fundamental natural frequencies ω_{n_i} for the cantilever beam with tip mass system. Thus, rearranging Equation (4.14), follows:

$$\omega_{n_i} = \sqrt{\frac{b_i^4 EI}{L^4 \rho A}}. \tag{4.33}$$

At this point the eigenfunctions $\Phi_i(z)$, i.e. the shape function of the natural modes, can be derived from Equation (4.16).

Under the assumptions of Section 4.1, the i-th natural mode of the cantilever beam with tip-mass system corresponding to the ω_{n_i} natural frequency results:

$$\Phi_i(z) = C_1\Big[\sinh\left(\frac{b_i z}{L}\right) - \sin\left(\frac{b_i z}{L}\right) \\ + \alpha\left[\cosh\left(\frac{b_i z}{L}\right) - \cos\left(\frac{b_i z}{L}\right)\right]\Big], \quad (4.34)$$

where α is defined as:

$$\alpha = -\frac{\cosh(b_i) + \cos(b_i) + \dfrac{m_t}{\rho A}\dfrac{b_i}{L}\left[\sinh(b_i) - \sin(b_i)\right]}{\sinh(b_i) - \sin(b_i) + \dfrac{m_t}{\rho A}\dfrac{b_i}{L}\left[\cosh(b_i) - \cos(b_i)\right]}. \quad (4.35)$$

All eigenfunctions are orthogonal [94] and hence, by definition, independent to each other. So for a constrained beam the state of displacements can be expressed as a series of eigenfunctions $\Phi_i(z)$ multiplied by the relative time dependent harmonic functions $\hat{q}_i(t)$:

$$v(z,t) = \sum_{i=1}^{\infty} \Phi_i(z)\hat{q}_i(t). \quad (4.36)$$

Same conclusions can be derived for the beam displacements in horizontal direction:

$$u(z,t) = \sum_{n=1}^{\infty} \Psi_n(z)\hat{p}_n(t), \quad (4.37)$$

where $\Psi_n(z)$ is the n-th eigenfunctions relative to the n-th vibration mode of the beam and $p_n(t)$ the relative time dependent harmonic functions.

4.2 Constitutive equations

The equations for the flexural vibrations of the beam and tip mass have been derived above with respect to the non-inertial system of reference positioned at the joint of the beam with the tub-drum frame. Therefore they should now be reworked with reference to the inertial reference system in order to derive the equations of motion of the tub-drum assembly equipped with the cantilever beam TVAs. In first approximation, the vibration modes of the TVAs system are considered uncoupled. Figure 4.5 shows the resulting two DOFs lumped parameter model of the professional washing machine equipped with cantilever beam vibration absorbers.

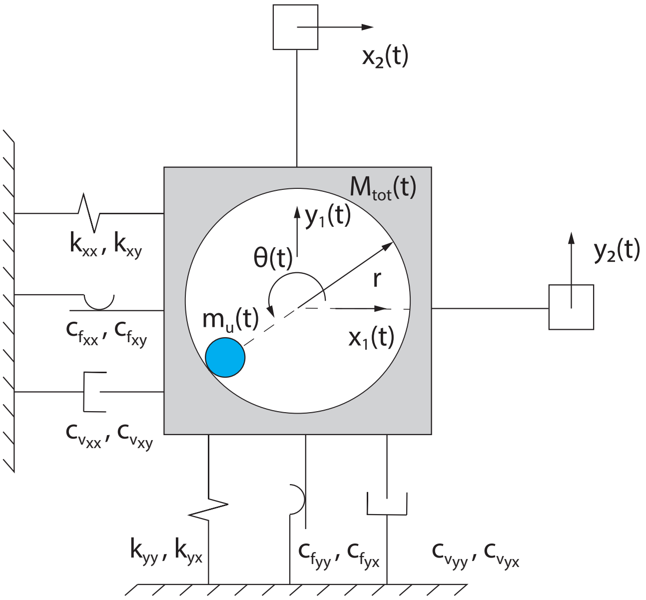

Figure 4.5: Two DOFs lumped parameter model of professional washing machine equipped with cantilever beam TVAs system.

Considering the inertial system of reference, the displacement of the beam can be written as the linear combination of the relative and the joint base displacements. Considering the vertical direction, the displacement with respect to the inertial system of reference is expressed as follows:

$$y_2(z,t) = y_1(t) + v(z,t), \tag{4.38}$$

where $y_2(z,t)$ is the vertical displacement of the infinitesimal element of the beam and $y_1(t)$ is the vertical displacement of the tub-drum assembly.

Equation (4.38) can be rewritten with respect to the relative displacement of the beam, so that:

$$v(z,t) = y_2(z,t) - y_1(t). \tag{4.39}$$

Substituting Equations (4.19), (4.20) and (4.39) into Equation (4.9), the equation of motion of the cantilever beam TVA system with respect to the inertial system of reference becomes:

$$\rho A\left[\frac{\partial^2 y_2(z,t)}{\partial t^2}-\frac{\partial^2 y_1(t)}{\partial t^2}\right]+EI\frac{\partial^4 y_2(z,t)}{\partial z^4}=-I_{m_t}\frac{\partial^3 y_2(z,t)}{\partial t^2\partial z}\delta(z-L)$$

$$-m_t(t)\left[\frac{\partial^2 y_2(z,t)}{\partial t^2}-\frac{\partial^2 y_1(t)}{\partial t^2}\right]\delta(z-L). \quad (4.40)$$

Since the eigenfunctions and eigenvalues, i.e. modes and natural frequencies, relative to the flexural vibration of the cantilever beam are independent from the considered reference system, the displacements can be expressed as a series of the eigenfunctions $\Phi_i(z)$ multiplied by the relative time dependent harmonic functions $q_i(t)$ as follows:

$$y_2(z,t)=\sum_{i=1}^{\infty}\Phi_i(z)q_i(t). \quad (4.41)$$

The homogeneous equation of motion of the cantilever beam with tip-mass TVA derived with respect to the non-inertial system of reference results:

$$\left[\rho A+m_t\delta(z-L)\right]\frac{\partial^2 y_2(z,t)}{\partial t^2}+EI\frac{\partial^4 y_2(z,t)}{\partial z^4}=0. \quad (4.42)$$

Since the eigenfunctions $\Phi_i(z)$ satisfy this homogeneous equation and considering that, for harmonic excitation, the response of a linear system is a series of harmonic functions, the following relation can be derived:

$$\sum_{i=1}^{\infty}EI\frac{\partial^4\Phi_i(z)}{\partial z^4}=\sum_{i=1}^{\infty}\left[\rho A+m_t\delta(z-L)\right]\Phi_i(z)\omega_i^2. \quad (4.43)$$

As a result, the equation of motion Equation (4.40) can be rewritten by considering the linear combination of flexural modes as follows:

$$\sum_{i=1}^{\infty}\Phi_i(z)\frac{\partial^2 q_i(t)}{\partial t^2}\left[\rho A+m_t\delta(z-L)\right]+$$

$$\sum_{i=1}^{\infty}\left[\rho A+m_t\delta(z-L)\right]\Phi_i(z)\omega_i^2 q_i(t)=\frac{\partial^2 y_1(t)}{\partial t^2}\left[\rho A+m_t\delta(z-L)\right]$$

$$-\sum_{i=1}^{\infty}I_{m_t}\left.\frac{\partial\Phi_i(z)}{\partial z}\right|_{z=L}\frac{\partial^2 q_i(t)}{\partial t^2}. \quad (4.44)$$

The TVA effectively absorbs the vibration energy of the tub-drum assembly at its fundamental natural frequency. In order to expand the operation frequency range, the TVA has to be continuously tuned in such a way as to synchronise its fundamental natural frequency to the frequency of the unbalance harmonic excitation acting on the tub-drum assembly. In practice, this can be effectively implemented by sliding the position of the mass along the beam of the TVA such that the fundamental natural frequency of the TVA is varied. Therefore the formulation will take into account only the response due to the first fundamental flexural mode of the beam and tip mode. Consequently the displacement of the cantilever beam with tip mass is approximated as follows:

$$y_2(z,t) \approx \Phi_1(z) q_1(t). \tag{4.45}$$

Substituting Equation (4.45) into Equation (4.44), the equation of motion for the flexural vibrations of the cantilever beam results:

$$\begin{aligned} &\Phi_1(z) \frac{\partial^2 q_1(t)}{\partial t^2} \left[\rho A + m_t \delta(z-L)\right] + \left[\rho A + m_t \delta(z-L)\right] \Phi_1(z) \omega_1^2 q_1(t) \\ &\quad = \frac{\partial^2 y_1(t)}{\partial t^2} \left[\rho A + m_t \delta(z-L)\right] - I_{m_t} \frac{\partial \Phi_1(z)}{\partial z}\bigg|_{z=L} \frac{\partial^2 q_1(t)}{\partial t^2}. \end{aligned} \tag{4.46}$$

As previously derived in Equation (4.34), the i-th eigenfunction $\Phi_i(z)$ relative to the i-th eigenvalue λ_i, is defined to within an arbitrary constant C_1. In order to uniquely obtain the amplitude of the vibrational mode, the constant is derived through a normalization procedure, such that the resulting natural modes are referred to as normal modes. In particular, taking advantage of the orthogonal properties of the eigenfunctions, the mass normalization is considered in this study by setting:

$$\int_0^L \Phi_1^2(z) \left[\rho A + m_t \delta(z-L)\right] = 1. \tag{4.47}$$

Combing Equation (4.47) with Equation (4.46), the normalized equation of motion of the cantilever beam TVA, approximated to the first vibration mode, with respect to the inertial system of reference, becomes:

$$\frac{\partial^2 q_1(t)}{\partial t^2} + \omega_1^2 q_1(t) = \frac{\partial^2 y_1(t)}{\partial t^2} \int_0^L \Phi_1(z) \left[\rho A + m_t \delta(z-L)\right] dz$$

$$- I_{m_t} \left.\frac{\partial \Phi_1(z)}{\partial z}\right|_{z=L} \int_0^L \Phi_1(z) dz \frac{\partial^2 q_1(t)}{\partial t^2}. \quad (4.48)$$

This equation is now enriched with a modal viscous damping contribute which is expressed in terms of damping ratio ξ. Thus the normalized equation of motion of the cantilever beam is rearranged as follows:

$$\frac{\partial^2 q_1(t)}{\partial t^2} + 2\xi_{1_y} \frac{\partial q_1}{\partial t} + \omega_1^2 q_1(t) = \frac{\partial^2 y_1(t)}{\partial t^2} \int_0^L \Phi_1(z) \left[\rho A + m_t \delta(z-L)\right] dz$$

$$- I_{m_t} \left.\frac{\partial \Phi_1(z)}{\partial z}\right|_{z=L} \int_0^L \Phi_1(z) dz \frac{\partial^2 q_1(t)}{\partial t^2}. \quad (4.49)$$

Once the cantilever beam with tip mass is installed in the tub-drum frame of the professional washing machine, an exchange of dynamic forces are generated in the region of the joint. In particular, the cantilever beam and tip mass system transfers a shear stress to the tub-drum assembly structure. The shear force $T(z,t)$ is defined as follows [95]:

$$T(z,t) = -EI \frac{\partial^3 v(z,t)}{\partial z^3}. \quad (4.50)$$

Thus, considering Equation (4.39) the following equation is derived:

$$\frac{\partial^3 v(z,t)}{\partial z^3} \equiv \frac{\partial^3 y_2(z,t)}{\partial z^3}, \quad (4.51)$$

Equation (4.50) can be rewritten with respect to the inertial system of reference:

$$T(z,t) = -EI \frac{\partial^3 y_2(z,t)}{\partial z^3}. \quad (4.52)$$

Figure 4.6 shows the free body diagram of the professional washing machine characterised by the elastically suspended tub-drum assembly and the cantilever beam TVAs system installed on it.

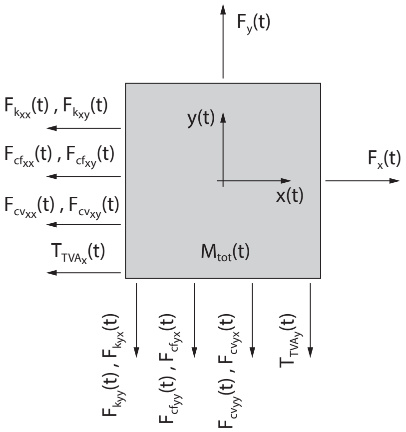

Figure 4.6: Free body diagram of the professional washing machine suspended tub-drum assembly mass with cantilever beam TVAs system.

The equations of motion for the vibration in vertical direction are summarised below:

$$\begin{aligned}M_{tot}(t)\ddot{y}_1(t) &= m_u(t)r\omega(t)^2\sin\theta - k_{yy}y_1(t)\\&- c_{v_{yy}}\dot{y}_1(t) - c_{f_{yy}}sgn\left(y_1(t)\right) - k_{yx}x_1(t) - c_{v_{yx}}\dot{x}_1(t)\\&- c_{f_{yx}}sgn\left(x_1(t)\right) + EI\left.\frac{\partial^3 y_2(z,t)}{\partial z^3}\right|_{z=0},\end{aligned} \tag{4.53}$$

$$y_2(z,t) \approx \Phi_1(z)q_1(t), \tag{4.54}$$

$$\begin{aligned}\frac{\partial^2 q_1(t)}{\partial t^2} + 2\xi_{1_y}\frac{\partial q_1}{\partial t} + \omega_1^2 q_1(t) &= \frac{\partial^2 y_1(t)}{\partial t^2}\int_0^L \Phi_1(z)\left[\rho A + m_t\delta(z-L)\right]dz\\&- I_{m_t}\left.\frac{\partial \Phi_1(z)}{\partial z}\right|_{z=L}\int_0^L \Phi_1(z)dz\frac{\partial^2 q_1(t)}{\partial t^2}.\end{aligned} \tag{4.55}$$

By analogy it is possible to derive the same equations of motion for the horizontal direction as follows:

$$\begin{aligned} M_{tot}(t)\ddot{x}_1(t) &= m_u(t)r\omega(t)^2\cos\theta - k_{xx}x_1(t) \\ &\quad - c_{v_{xx}}\dot{x}_1(t) - c_{f_{xx}}sgn\left(x_1(t)\right) - k_{xy}y_1(t), -c_{v_{xy}}\dot{y}_1(t) \\ &\quad - c_{f_{xy}}sgn\left(y_1(t)\right), +EI\left.\frac{\partial^3 x_2(z,t)}{\partial z^3}\right|_{z=0}, \end{aligned} \tag{4.56}$$

$$x_2(z,t) \approx \Psi_1(z)p_1(t). \tag{4.57}$$

$$\begin{aligned} \frac{\partial^2 p_1(t)}{\partial t^2} + 2\xi_{1_x}\frac{\partial p_1}{\partial t} + \omega_1^2 p_1(t) &= \frac{\partial^2 x_1(t)}{\partial t^2}\int_0^L \Psi_1(z)\left[\rho A + m_t\delta(z-L)\right]dz \\ &\quad - I_{m_t}\left.\frac{\partial \Psi_1(z)}{\partial z}\right|_{z=L}\int_0^L \Psi_1(z)dz\frac{\partial^2 p_1(t)}{\partial t^2}. \end{aligned} \tag{4.58}$$

The vertical component of the force transmitted through the passive suspension system is derived as:

$$\begin{aligned} R(t) &= c_{v_{yx}}\dot{x}_1(t) + c_{v_{yy}}\dot{y}_1(t) + c_{f_{yx}}sgn\left(x_1(t)\right) + c_{f_{yy}}sgn\left(y_1(t)\right) \\ &\quad + k_{yx}x_1(t) + k_{yy}y_1(t). \end{aligned} \tag{4.59}$$

4.3 Frequency Response Functions

Considering the lumped parameter model shown in Figure 4.5, Frequency Response Functions are derived in this section for the oscillations of tub-drum assembly and the force transmitted to ground via the visco-elastic mounts with reference to the unbalance harmonic excitation. Based on the sketch of Figure 4.5, the equations of motion of the two DOFs lumped parameter model, described in Section 2.3, are coupled to the equations of motion for the cantilever beam TVAs, derived in the previous sections. As done above, the equations of motion for the oscillations in vertical direction are discussed in detail, whereas the equations of motion for the oscillations in the horizontal direction are derived by analogy. The FRFs that characterise the vibration of the machine are derived from the time domain equations of motion using the Laplace transformation and then considering $s = j\omega$ [90]. The vertical displacement of the cantilever beam in the frequency domain $Y_2(z, j\omega)$ can thus be written as follows:

$$Y_2(z, j\omega) \approx \Phi_1(z) Q_1(j\omega), \tag{4.60}$$

where $Q_1(j\omega)$ is the first frequency dependent harmonic function relative to the shape function $\Phi_1(z)$.

The Fourier transform of the shear force function in Equation (4.52) is given by:

$$T(z, j\omega) = -EI \frac{\partial^3 Y_2(z, j\omega)}{\partial z^3}. \tag{4.61}$$

It is now necessary to express Equation (4.49) in the frequency domain in order to derive a formulation that uniquely describes the harmonic function $Q_1(j\omega)$. This relationship is then used to derive the FRFs of the tub-drum oscillations and ground force transmission, with reference to physical coordinates. Therefore the harmonic function $Q_1(j\omega)$ can be written as:

$$Q_1(j\omega) = H_1(j\omega) Y_1(j\omega), \tag{4.62}$$

where $H_1(j\omega)$ is the FRF function defined as:

$$\begin{aligned} H_1(j\omega) &= \frac{Q_1(j\omega)}{Y_1(j\omega)} \\ &= \frac{-\omega^2 \int_0^L \Phi_1(z) \left[\rho A + m_t \delta(z - L)\right] dz}{-\omega^2 + 2\xi_{1_y} j\omega + \omega_1^2 - I_{m_t} \omega^2 \left.\frac{\partial \Phi_1(z)}{\partial z}\right|_{z=L} \int_0^L \Phi_1(z) dz}. \end{aligned} \tag{4.63}$$

Equation (4.60) can be rewritten as follows:

$$Y_2(z, j\omega) \approx \Phi_1(z) H_1(j\omega) Y_1(j\omega). \tag{4.64}$$

Combining Equations (4.60), (4.61) and (4.63) the shear force can be written in the frequency domain as follows:

$$T(z, j\omega) = -EI \frac{\partial^3 \Phi_1(z)}{\partial z^3} H_1(j\omega) Y_1(j\omega). \tag{4.65}$$

With reference to the free body diagram shown in Figure 4.6, the force T_{TVA_y} exchanged between the cantilever beam and the tub-drum frame is equal to the value of the shear force at the rigid joint. Therefore it can be derived as:

$$T_{TVA_y}(z,j\omega) = -EI\frac{\partial^3\Phi_1(z)}{\partial z^3}\bigg|_{z=0} H_1(j\omega)Y_1(j\omega). \tag{4.66}$$

Introducing Equation (4.66) into the Equations (2.25), (2.26) and (2.27), the equation of motion in frequency domain, relative to the free body diagram of Figures 4.6, becomes:

$$Y_1(j\omega) = \frac{m_u r\omega^2 - j\frac{4}{\pi}\left[F_{cf_{yy}} + F_{cf_{yx}}\right] - \left[c_{v_{yx}}j\omega + k_{yx}\right]X_1(j\omega)}{-M_{tot}\omega^2 + j\omega c_{v_{yy}} + k_{yy} - EI\frac{\partial^3\Phi_1(z)}{\partial z^3}\bigg|_{z=0} H_1(j\omega)}. \tag{4.67}$$

Similar considerations are drawn for the FRFs relative to the tub-drum harmonic vibrations and force transmission for horizontal direction. Therefore the displacement of the drum $X_1(j\omega)$ is described by the following equation:

$$X_1(j\omega) = \frac{m_u r\omega^2 - j\frac{4}{\pi}\left[F_{cf_{xx}} + F_{cf_{xy}}\right] - \left[c_{v_{xy}}j\omega + k_{xy}\right]Y_1(j\omega)}{-M_{tot}\omega^2 + j\omega c_{v_{xx}} + k_{xx} - EI\frac{\partial^3\Psi_1(z)}{\partial z^3}\bigg|_{z=0} N_1(j\omega)}, \tag{4.68}$$

where $N_1(j\omega)$ is the FRF function defined as:

$$\begin{aligned} N_1(j\omega) &= \frac{P_1(j\omega)}{X_1(j\omega)} \\ &= \frac{-\omega^2\int_0^L \Psi_1(z)\left[\rho A + m_t\delta(z-L)\right]dz}{-\omega^2 + 2\xi_{1_x}j\omega + \omega_1^2 - I_{m_t}\omega^2\frac{\partial\Psi_1(z)}{\partial z}\bigg|_{z=L}\int_0^L \Psi_1(z)dz}, \end{aligned} \tag{4.69}$$

and $P_1(j\omega)$ is the first frequency dependent harmonic function relative to the eigenfunction $\Psi_1(z)$.

The displacement of the cantilever beam TVA is estimated as follows:

$$X_2(z,j\omega) \approx \Psi_1(z)N_1(j\omega)X_1(j\omega). \tag{4.70}$$

The vertical component of the ground force transmission is:

$$\begin{aligned} R(j\omega) = j\frac{4}{\pi}\left[F_{cf_{yy}} + F_{cf_{yx}}\right] + \left[c_{v_{yx}}j\omega + k_{yx}\right]X_1(j\omega) \\ + \left[j\omega c_{v_{yy}} + k_{yy}\right]Y_1(j\omega). \end{aligned} \tag{4.71}$$

Therefore the FRFs for the harmonic oscillations of the tub-drum assembly in x and y directions and the force transmitted to the ground via the suspension system, result:

$$G_{1_x}(j\omega) = \frac{X_1(j\omega)}{F(j\omega)}, \tag{4.72}$$

$$G_{1_y}(j\omega) = \frac{Y_1(j\omega)}{F(j\omega)}, \tag{4.73}$$

$$G_{2_x}(j\omega) = \frac{X_2(j\omega)}{F(j\omega)}, \tag{4.74}$$

$$G_{2_y}(j\omega) = \frac{Y_2(j\omega)}{F(j\omega)}, \tag{4.75}$$

$$T(j\omega) = \frac{R(j\omega)}{F(j\omega)}. \tag{4.76}$$

As explained above, only the first flexural mode of the cantilever beam and tip mass is taken into consideration while the coupling effect of the TVAs has bean neglected. It is therefore important to guarantee the same fundamental natural frequency relative to the first vibration mode of the absorber, along the horizontal and vertical directions. For this purpose an annular cross section of the beam was chosen in order to obtain a symmetrical behaviour of the device in the two orthogonal directions. This consideration allows the derivation of cross sectional moment of inertia I with respect to the neutral axis of the beam and its cross sectional area A:

$$I = \pi\frac{d_e^4 - d_i^4}{64}, \tag{4.77}$$

$$A = \pi\frac{d_e^2 - d_i^2}{4}. \tag{4.78}$$

Figure 4.7 shows the simulated spectra relative to the amplitude of drum oscillations along horizontal (Plot a) and vertical (Plot b) directions derived considering the mechanical input parameters summarised in Table 4.1, which tune the TVA at about $10Hz$ for instance.

The red dashed lines show the amplitude of oscillations in the vertical and horizontal directions of the tub-drum assembly for the standard configuration, already discussed in Section 2.4, while the blue solid lines show the responses of the tub-drum assembly with the cantilever beams TVAs. The two configurations are characterised by comparable oscillations amplitudes at low frequencies along both horizontal and vertical directions.

Table 4.1: Mechanical parameters of the two DOFs model of W565H professional washing machine with cantilever beam TVA systems.

Parameter	Value	
M	69	kg
M_b	17	kg
m_u	0.5	kg
r	0.26	m
k_{xx}	9810	N/m
k_{xy}	1150	N/m
k_{yx}	6500	N/m
k_{yy}	27555	N/m
c_{xx}	380	Ns/m
c_{xy}	120	Ns/m
c_{yx}	80	Ns/m
c_{yy}	720	Ns/m
$F_{cf_{xx}}$	120	N
$F_{cf_{xy}}$	20	N
$F_{cf_{yx}}$	30	N
$F_{cf_{yy}}$	120	N
n	$0 \div 1245$	rpm
ξ_{1_y}	0.01	
ξ_{1_x}	0.01	
w_1	10	Hz
m_t	12	kg
I_{m_t}	0.23	$kg\,m^2$

At higher frequencies than the fundamental natural frequency of the tub-drum assembly, the amplitudes of the oscillations for the standard configuration tends to an asymptotic value described by Equation (2.31). The new setup presents an antiresonance and a resonance in rapid succession around $10Hz$, which is the imposed fundamental natural frequency of the cantilever beam TVA. At that frequency the beam-mass first natural mode is effectively excited and the kinetic energy of the tub-drum assembly is efficiently transferred to the vibration absorbers.

Figure 4.8 shows the spectra for the amplitude of oscillation of the tip mass of the cantilever beam system. In correspondence of the horizontal

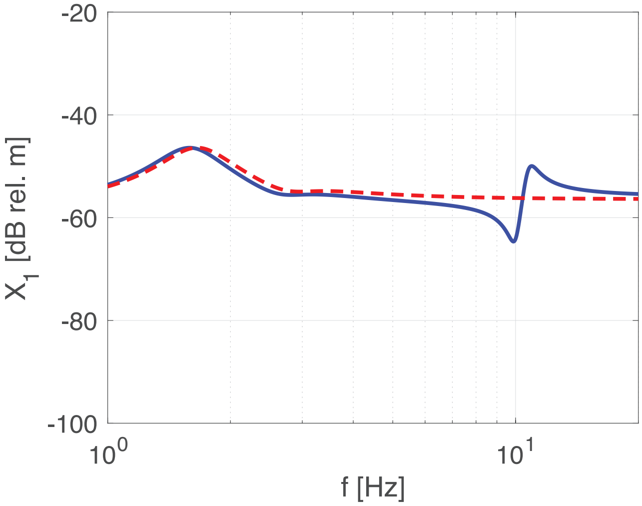

(a)

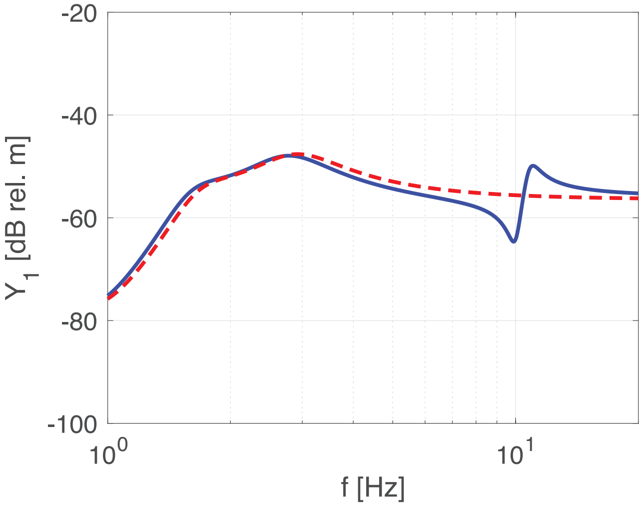

(b)

Figure 4.7: Comparison of the simulated spectra relative to the tub-drum assembly oscillations for standard (red dashed line) configuration and with TVA system (blue solid line) along horizontal (a) and vertical (b) directions.

and vertical fundamental natural frequency of the tub-drum assembly, the tip mass moves together whit the drum to then increase the relative displacements up to the maximum value at the fundamental natural frequency relative to the first vibration mode of the beam and tip mass.

Similar considerations can be derived for the spectrum of force transmitted shown in Figure 4.9. The two configurations show similar responses in the low frequencies range. At frequencies higher than the fundamental natural frequency of the tub-drum assembly, the TVA influences on the force transmitted. The force transmitted to ground is the lowest in correspondence of the first fundamental natural frequency of the TVA cantilever beam.

The TVA solution would become convenient when the TVA tuning is continously adapted to work at the angular speed of the drum. Therefore it is necessary develop a semi-active system which tracks on the angular speed of the drum in such a way as to generate an antiresonance at the frequency of excitation. The control loop has to avoid any possible miss-tune of the device that could actually produce an increment of the response and thus bring to failure the machine or seriously damage the structure.

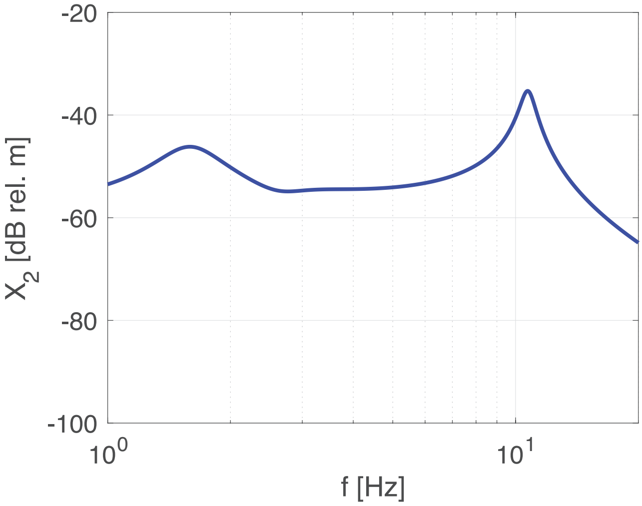

(a)

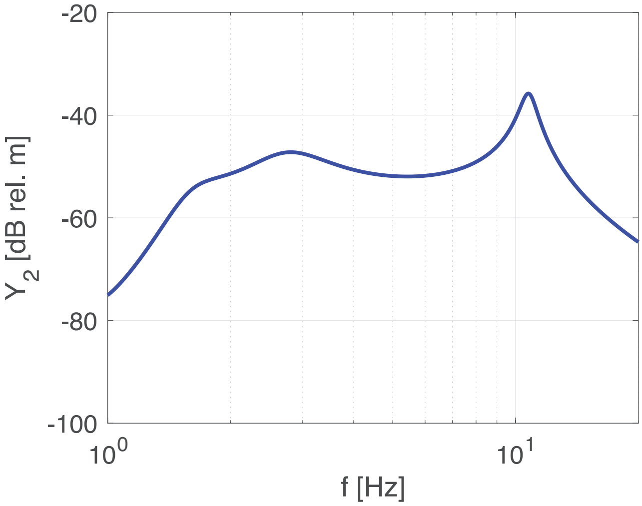

(b)

Figure 4.8: Simulated spectra relative to tip mass oscillations of the TVA system.

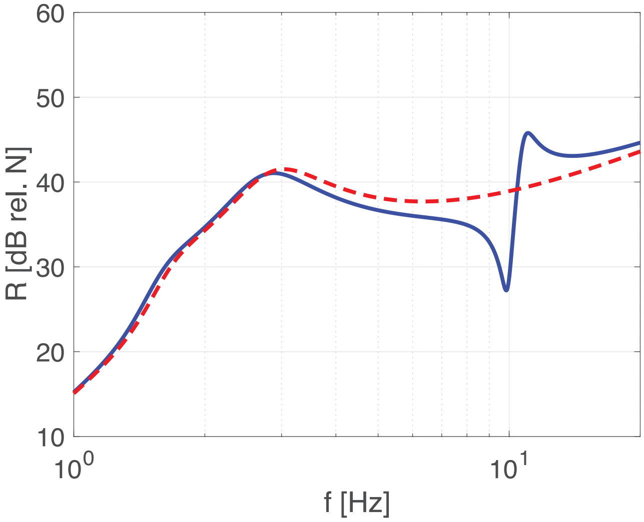

Figure 4.9: Comparison of the simulated spectra relative to force transmission for standard (red dashed line) configuration and with TVA system (blue solid line).

4.4 Parametric study

This section presents a parametric study, which is performed to evaluate the influence of the mechanical parameters of the components of the TVA on the spectra for the amplitude of the oscillations and ground force transmission of the tub-drum assembly. The TVA gives the possibility to lower the oscillations of the drum and consequently the force transmission to ground. Thus large ballasts are not required any more to increase the inertial load of the tub-drum assembly in order to lower the eccentricity factor of Equation (2.31) and thus the tub-drum oscillations and force transmission. This leads to new designs of the washing machines characterised by much lower ballast masses so that the total weight and cost of the appliances can also be sensibly reduced. In fact, a portion of the ballast masses is used for the TVA devices while the rest is removed from the machine. Thus the effects of the total mass M_{tva} of the cantilever beam with tip mass is considered into the dimensionless mass ratio factor μ defined as follows:

$$\mu = \frac{M_{tva}}{M + M_b + M_w(t) + m_u(t)}. \tag{4.79}$$

Neglecting the amount of unbalance $m_u(t)$ and the water content $M_w(t)$, which are small during the extraction cycle, mass ratio factor of the system can be expressed by the following relation:

$$\mu = \frac{M_{tva}}{M + M_b}. \tag{4.80}$$

With a view on cost saving and cost efficiency, it is important to lower the total weight of the appliance, without increasing the amplitude of oscillations of the tub-drum assembly and the force transmitted to the ground. Therefore a parametric study is performed by removing all the ballast masses, which are substituted by TVA devices. Since part of the ballast is used as TVA, Equation (4.80) can be rewritten as follows:

$$\mu = \frac{\beta M_b}{M}, \tag{4.81}$$

where β is the portion of ballast mass used as TVA. For the W565H professional washing machine, the range of mass ratio considered in this study is $0 \leq \mu \leq 0.24$.

Table 4.2: Range of mass ratio μ used for spectra comparison.

μ	M_{tot}	M_{tva}
0.05	69 kg	3.4 kg
0.12	69 kg	8.5 kg
0.24	69 kg	17 kg

Figure 4.10 shows the simulated FRF spectra for the amplitude of oscillations of the tub-drum assembly for the mass ratios μ listed in Table 4.2. Normally high values of μ involve the use of great quantity of ballast masses as TVA system. This solution tends to maintain constant the total static weight of machine. Since the fundamental natural frequency of the tub-drum assembly depends on its total mass and the mass of the TVA, higher values of μ would lower the horizontal and vertical fundamental natural frequencies of the drum. Heavy TVAs amplify both the amplitude and the band of the antiresonance and resonance peaks in correspondence of the first fundamental natural frequency of the tunable mass damper. In fact, the TVA absorbs more kinetic energy because of their higher inertial load produced by the tip mass. Therefore increasing the mass of the vibration absorber can help to lower the amplitude of oscillations of the drum even for lightweight tub-drum assembly.

Similar consideration can be derived for the simulated spectrum for the amplitude of force transmission of Figure 4.11.

A damping effect is normally introduced into the cantilever beam to attenuate the resonance peaks and lower the amplitude of oscillations of the tip mass at the fundamental natural frequency of the absorber. The damping is chosen in such a way as to obtain large reductions of drum oscillations and acceptable maximum amplitude of oscillation of the tip mass.

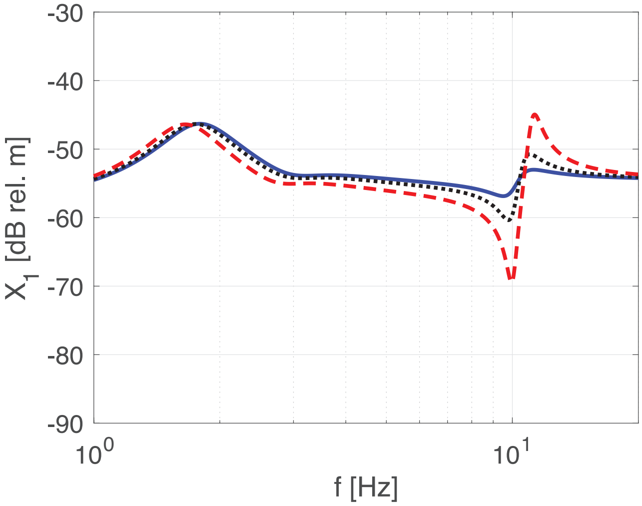

(a)

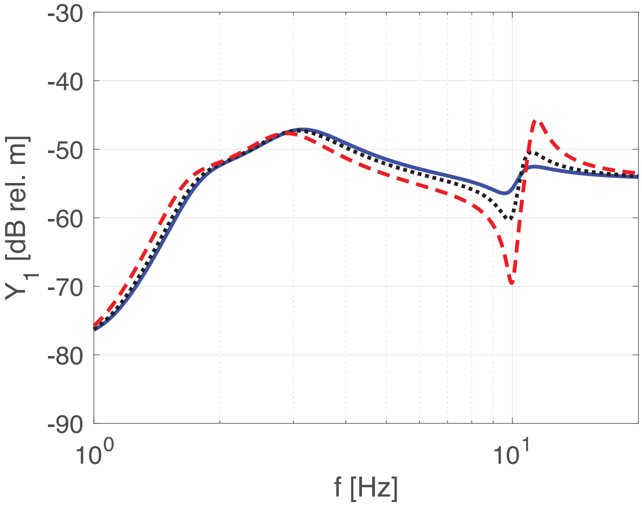

(b)

Figure 4.10: Comparison of the simulated spectra relative to the tub-drum assembly oscillations for washing machine equipped with TVAs system for different mass ratio μ along horizontal (a) and vertical (b) directions. The solid blue line shows the response for $\mu = 0.05$, the black dotted line for $\mu = 0.12$ and the red dashed line for $\mu = 0.24$.

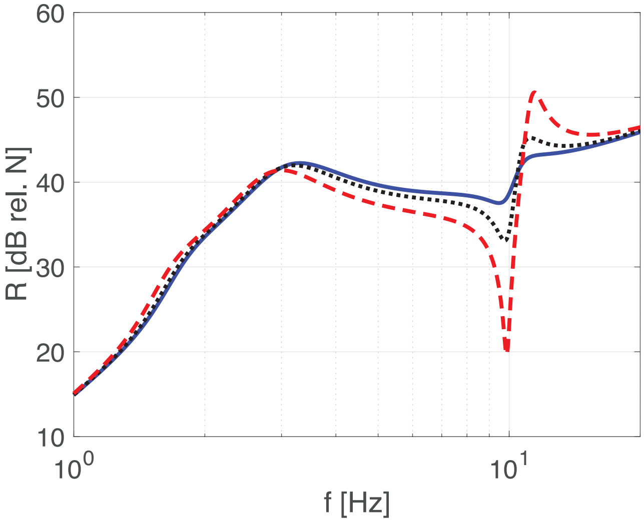

Figure 4.11: Comparison of the simulated spectra relative to force transmission for washing machine equipped with TVAs system with different mass ratio μ along horizontal (a) and vertical (b) directions. The solid blue line shows the response for $\mu = 0.05$, the black dotted line for $\mu = 0.12$ and the red dashed line for $\mu = 0.24$.

In practice, the cantilever beam-tip mass TVA is tuned by sliding the tip mass along the beam in order to vary the eigenfunctions and the relative eigenvalues, which are the fundamental natural modes and the fundamental natural frequencies of the dynamic vibration absorber in accordance with Equations (4.33) and (4.16). When the tip mass is moved, the portion of beam at the free end is neglected in the model since it is characterised by much lower inertia with respect to the tip mass. The position of the tip mass has to be derived by an iterative procedure involving the numerical solution of the eigenfunctions in such a way as to tune its fundamental natural frequency relative to the first vibrational mode of the beam. Figure 4.12 shows the length of the cantilever beam as function of its first fundamental natural frequency for different value of tip mass. Table 4.3 provides the mechanical parameters of the beam that have been used to perform the simulations.

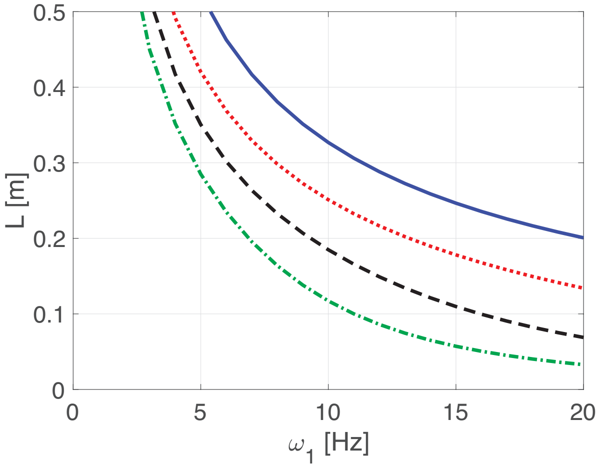

Figure 4.12: Length of the cantilever beam as function of the first fundamental natural frequency for different value of tip mass. Solid blue line refers to $m_t = 5kg$, red dotted line to $m_t = 9kg$, black dashed line to $m_t = 13kg$ and green dashed-dotted line to $m_t = 17kg$.

Table 4.3: Mechanical parameters of the beam.

Parameter	Value	
material	brass	
d_e	20	mm
d_i	18	mm
E	9.0 e+10	N/m^2
ρ	8500	kg/m^3

4.5 Design and implementation

The solution proposed in this thesis consists in substituting the ballast masses of the washing machine with cantilever beam TVAs in such a way as to lower tub-drum oscillations, ground force transmission and the total weight of the appliance.

As shown in Figure 1.10, ballasts of different weights are normally placed on the four corners of the tub-drum frame, with the aim to increase the total mass of the stator and thus to lower the eccentricity factor and to statically balance the system.

Figure 4.13 shows the CAD drawing of one of the four cantilever beam TVAs designed for this study. Also Figure 4.14 shows their installation on the tub-drum frame of the appliance in place of the ballast masses.

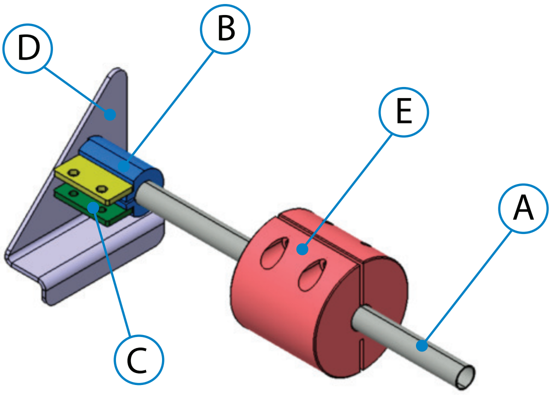

Figure 4.13: CAD sketch of the assembly of the cantilever beam TVA.

As discussed above, the ballasts were substituted by dynamic absorbers in the attempt to guarantee the same static balance along the three rotational degrees of freedom of the tub-drum. The dynamic absorbers were manufactured in-house. Two TVAs were installed in the front and two in the back of the tub-drum frame and they differed for dimensions. Since the four TVAs are tuned to work at the same frequency, in first approximation, their overall effects can be modelled in terms of an equivalent mass-spring-damper TVAs as done above in Section 4.2.

The TVAs are composed by three components: the beam (A), the joint connection (B,C,D) and the tip mass (E). A circular cross sec-

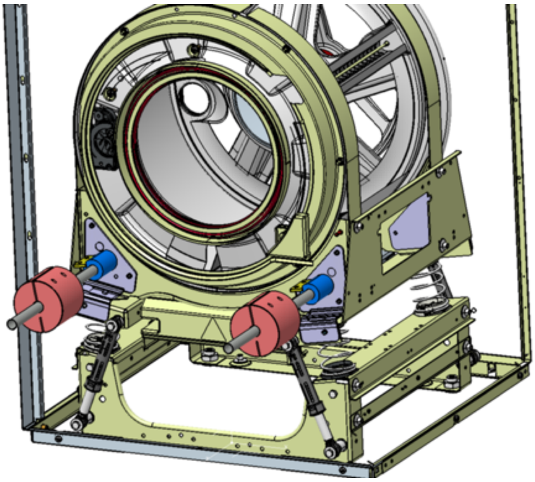

Figure 4.14: CAD sketch of the installation of cantilever beam TVAs.

tional geometry of the beams and weights was chosen in order to obtain symmetric vibrational absorbers along the horizontal and vertical directions of motion. In this way similar vibrational modes and fundamental natural frequencies are obtained for horizontal and vertical oscillations. Moreover, the coupling effect of the TVAs during the operation is minimised. Polymeric hollow cylinders were pressed into the beams near the fixing points to the tub-drum assembly in order to increase the damping factor of the TVAs. The beams were inserted into bushing supports (B) which were fixed to the tub-drum frame via flat metallic plates (D). The bushings present a milling along their longitudinal directions where two small plates are welded in order to locate the tightening screws. On the opposite side, a longitudinal cut is provided to decrease the mechanical strength of the material. The tightening of the screws cause the yielding of the material so that the beam can be clamped by friction.

The four plate supports (D) have been fixed to the tub-drum frame at the pre-existing holes used to fix the ballasts.

The tip masses (E) are made by a cylindrical piece of steel with a through-all longitudinal hole. The cylinder is characterised by two longitudinal cuts, which locally lowered the mechanical strength of the material. Two screws are placed crosswise the first cut in such a way as to yield the opposite slice of material when tightened. This increases the friction between the pipe and the internal surface of the tip mass,

Table 4.4: Mechanical features of the components used to build the front and back TVAs.

Parameter	Nomenclature	Value	
material of the front beam	brass		
Young's module of brass	E_{br}	9.0 e+10	N/m^2
Density of brass	ρ_{br}	8500	kg/m^3
material of the back beam	alluminum		
Young's module of aluminium	E_{all}	7.0 e+10	N/m^2
Density of aluminium	ρ_{all}	2700	kg/m^3
External diameter of the front beams	d_{e_f}	20	mm
Internal diameter of the front beams	d_{i_f}	18	mm
External diameter of the back beams	d_{e_b}	14	mm
Internal diameter of the back beams	d_{i_b}	12	mm
Front tip masses	m_{t_f}	5	kg
Back tip masses	m_{t_b}	1.5	kg

avoiding relative sliding during working conditions.

The TVAs are manually tuned by sliding the tip masses along the beams as shown in Figure 4.12. This solution aims to replicate a tuning system which can be eventually used to obtain electro-mechanically driven semi-active mass dampers.

Table 4.4 provides the mechanical features of the cantilever beams used in this study. They are divided in front and back respectively and identified by subscripts "f" and "b".

The tip masses are designed in order to maintain the static balance of the drum. The proposed configuration allows to lower the total weight of the machine by 25% of the weight of the ballast. In this way the initial requirements of obtain lightweight machine is satisfied.

Figure 4.15 shows the picture of the professional washing machine equipped with the cantilever beam mass dampers, while Figure 4.16 shows the detailed views of the cantilever beam mass damper built in-house.

Appendix C contains the CAD drawings of the components designed to assemble the semi-active cantilever beam TVAs.

Figure 4.15: Picture of the professional washing machine equipped with cantilever beam mass dampers.

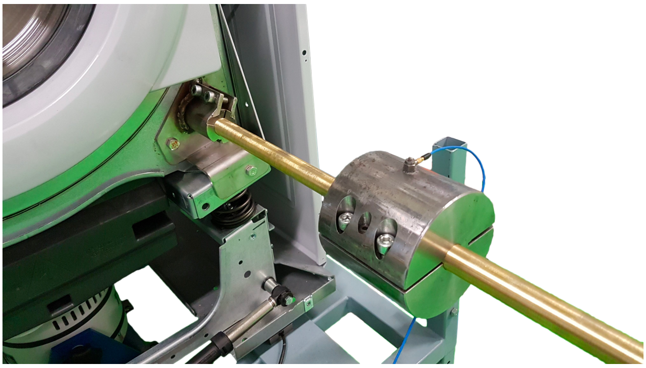

Figure 4.16: Detail view of the front side cantilever beam mass damper.

4.6 Experimental results

Figure 4.15 shows the experimental setup used to perform the measures presented in this chapter. The four tunable mass dampers, described in Section 4.5, are installed in the four corners of the drum-frame in place of the ballasts masses. The professional washing machine was located on the same base frame structure used to perform the experimental tests presented in Sections 2.4 and 3.5. The base frame was equipped with four strain gauge load cells (*Flintec ZLS Planar Beam*) to measure the total vertical component of force transmission through the feet of the appliance.

Two types of external excitations were used to perform the experimental analysis when the machine was equipped with the TVAs on either the lightly damped and the heavily damped suspension configurations. As shown in sketch (a) of Figure 4.17, for the lightly damped suspension configuration, the excitation was generated only in vertical direction by using a *Tira Vib S51140* shaker connected to the drum via a stinger. The excitation was controlled in such a way as to perform a frequency sweep within the operation frequency range of the appliance. The drum was equipped with a *PCB Piezotronics* accelerometers positioned on top of the drum in such a way as to measure the vertical accelerations. For the heavily damped suspension configuration of sketch (b) in Figure 4.17, the excitation was instead generated by an unbalance mass placed in the drum set to rotate with a ramp time-varying velocity. The lumped mass was clamped inside the drum in order to generate a static unbalance, which, for a given speed of rotation, produces a centrifugal force, that is, a combination of harmonic forces in quadrature, oriented in vertical and horizontal directions respectively. The centrifugal force was therefore identified from the drum angular speed, measured with an incremental encoder (*Lika rotapuls IT65*). In this case the drum was equipped with two *PCB Piezotronics* accelerometers positioned on top and on the side of the drum in such a way as to measure the vertical and horizontal accelerations.

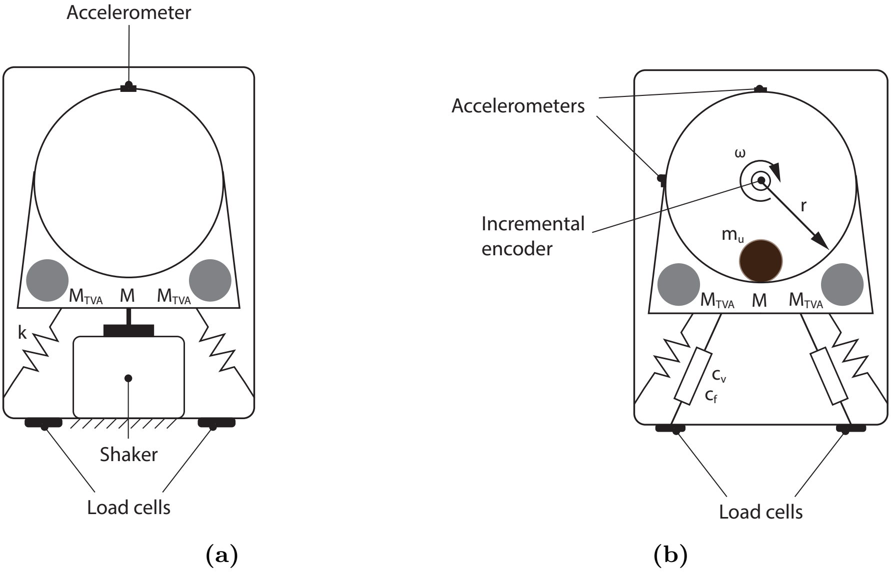

Figure 4.17: Sketches of the experimental setups used to perform the experimental spectra of the dynamic response of a professional washing machine equipped with cantilever beam TVAs. Sketch (a) refers to the experimental setup used with the lightly damped suspension configuration and sketch (b) refers to the heavily damped suspension configuration.

4.6.1 Measured FRFs spectra of the professional washing machine equipped with TVA and the light damped suspension configuration

The red dashed line in Figure 4.18 shows the simulated FRF spectrum for the amplitude of the drum oscillations along vertical direction for the washing machine equipped with four TVAs and the lightly damped suspension configuration.

The fundamental natural frequency of the flexural vibrational mode of the cantilever beam with tip mass system has been set to 15.5 Hz. The solid lines show the measured amplitude of oscillations of the tub-drum assembly mounted on the lightly damped springs. The first resonance peak at $2.4Hz$ is due to the fundamental natural frequency for the vertical

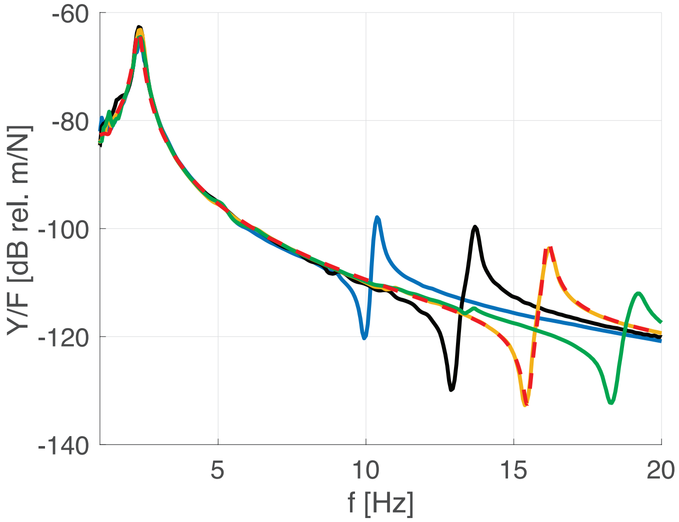

Figure 4.18: Comparison between the simulated (red dashed line) and measured (solid lines) FRFs relative to drum oscillations along vertical direction for the washing machine equipped with four cantilever beam with tip mass TVAs. The solid lines refers to the measured spectra with all the TVAs tuned at different fundamental resonance frequencies: $10Hz$ (solid blue), $13Hz$ (solid black), $15.5Hz$ (solid yellow) and $18Hz$ (solid green).

vibrational mode of the tub-drum assembly. At higher frequencies, above the fundamental natural frequency, the amplitude of oscillation of the system falls down at a 40 dB per decade rate up to the first fundamental natural frequencies of the TVAs. Here the kinetic energy of the tub-drum is transferred to the tuned mass dampers. This causes a narrow band reduction of the drum oscillations along the vertical direction as highlighted by the antiresonances shown in the spectra. The amplitude of oscillation of the drum along vertical direction is reduced up to -17 dB at 15.5 Hz. Sliding the tip masses along the beams, varies the first fundamental natural frequency of the cantilever beam absorbers and thus shifts the frequency of the antiresonances of the tub-drum assembly. As predicted with the simulations, secondary resonance peaks arise at frequencies just above the resonance frequency of the vibration absorbers. At higher frequencies the amplitude of oscillation of the tub-drum system decreases with a 40 dB down slope per decade. in the frequency range of interest, the simulated FRFs agree well with the respective measured FRFs.

Figure 4.19 shows the transmissibility FRFs spectra when the shaker excites the drum vertically. The amplitude spectra present resonance peaks in correspondence of the fundamental natural frequency for the vertical natural mode of the drum. Then, the force falls down at a 40 dB per decade rate up to the fundamental natural frequency for the vertical oscillation of the cantilever beam TVAs, where reductions of transmissibility up to -15 dB are observed compared to standard configuration. The force transmission per unit excitation is also characterised by a response peak at frequencies just above the fundamental resonance frequency of the TVA. With respect to the case with the TVA tuned at 15.5 Hz (yellow solid line), the simulated and measured FRF agrees quite well over the range of frequencies of interest, except for some dynamic in the range of $10 \div 12\,Hz$ that is not predicted.

These spectra show the possibility to cut down the oscillations of the tub-drum system and the ground force transmission by properly tuning the TVAs system. It is important the fundamental natural frequency of the TVAs are carefully adapted to the angular speed of the drum in such a way as to avoid the TVA would actually magnify the oscillations and force transmission of the drum as highlighted by the resonance peaks at frequencies slightly higher than the angular speed of the drum. Thus the tip masses of the TVAs have to be sided in such a way as the antiresonance frequency in the spectra of the tub-drum assembly oscillations and of the force transmission, coincides with the angular speed of the drum.

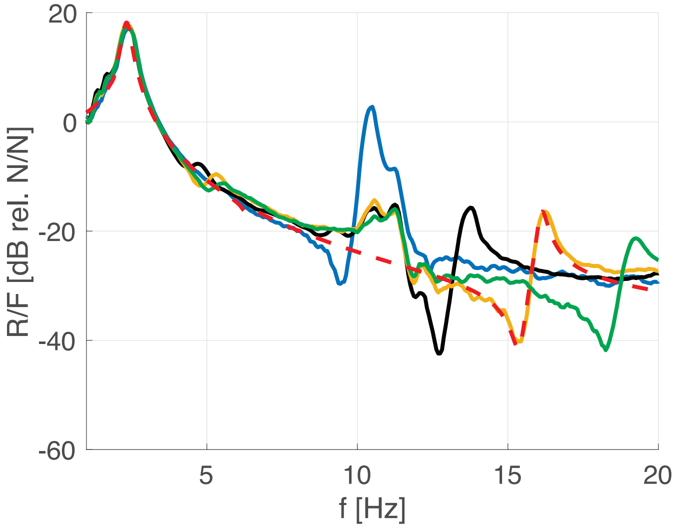

Figure 4.19: Comparison between the simulated (red dashed line) and measured (solid lines) FRFs relative to force transmission for the washing machine equipped with four cantilever beam with tip mass TVAs. The solid lines refers to the measured spectra with all the TVAs tuned at different fundamental resonance frequencies: $10Hz$ (solid blue), $13Hz$ (solid black), $15.5Hz$ (solid yellow) and $18Hz$ (solid green).

4.6.2 Measured FRFs spectra of the professional washing machine equipped with TVA and heavily damped suspension configuration

Figure 4.20 shows the simulated (red dashed lines) and measured (blue solid lines) FRFs spectra for the amplitude of the drum oscillations in horizontal (Plot a) and vertical (Plot b) directions for the washing machine equipped with four TVAs absorbers and the heavily damped suspension configuration. Table 4.5 provides the mechanical parameters of the appliance which have been used to simulate the FRFs spectra for drum oscillations in horizontal and vertical directions and the force transmitted to ground. The mechanical features of the cantilever beam TVAs are reported in Table 4.4.

The FRFs spectra were measured by spinning the drum with lumped unbalance mass on it up to the desired speed and then let it slow down until it stopped, as done for the validation tests presented in Section 2.4.2.

Table 4.5: Mechanical parameters of the appliance equipped with TVAs which have been used in the simulation of the FRFs of drum oscillations for horizontal and vertical directions and for the force transmitted to the ground.

Parameter	Value	
M	69	kg
M_b	0	kg
r	0.26	m
m_u	0.394	kg
k_{xx}	11700	N/m
k_{xy}	2180	N/m
k_{yx}	7450	N/m
k_{yy}	31515	N/m
$c_{v_{xx}}$	1320	Ns/m
$c_{v_{xy}}$	120	Ns/m
$c_{v_{yx}}$	80	Ns/m
$c_{v_{yy}}$	1520	Ns/m
$F_{cf_{xx}}$	140	N
$F_{cf_{xy}}$	30	N
$F_{cf_{yx}}$	40	N
$F_{cf_{yy}}$	140	N

The experimental tests were performed using $0.394kg$ of unbalance mass placed inside the rotating drum.

The measured spectra of the amplitude of oscillations of the tub-drum assembly show large attenuations of the peak responses at the fundamental natural frequencies of the vertical and horizontal vibrational modes. The low amplitude oscillations, due to small amount of unbalance, changes the contributions of the passive heavily damped suspension system. Furthermore, the fundamental natural frequencies for the horizontal and vertical oscillations of the drum are slightly shifted to higher frequencies. These are justified by two different phenomena. The total mass of the tub-drum assembly has been lowered in favour of the TVAs system while the suspension system is stiffened and damped due to the lower amplitude of oscillations. This is because the inner parts of the standard passive heavily damped shock absorbers are composed

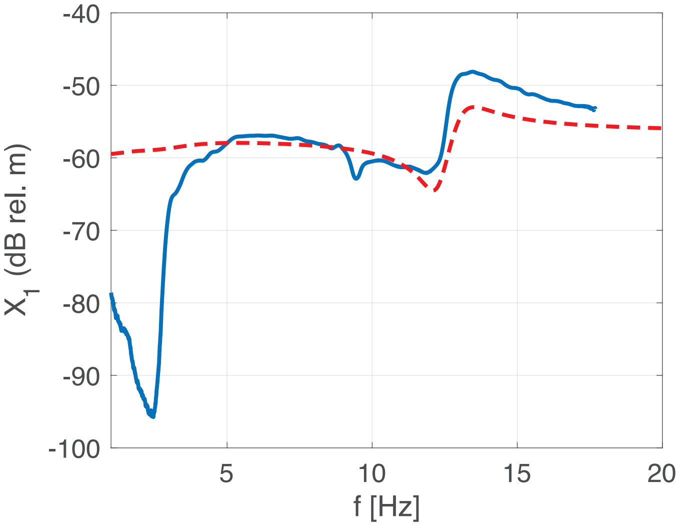

(a)

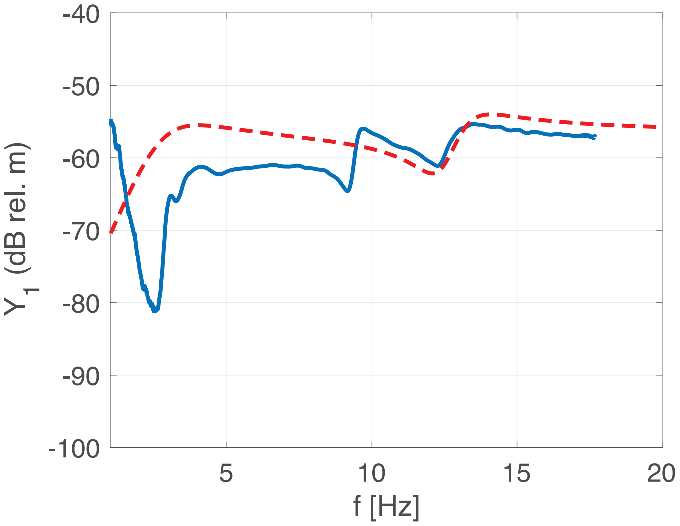

(b)

Figure 4.20: Comparison between the simulated (red dashed line) and measured (black solid line) FRFs relative to drum oscillations along horizontal and vertical direction for the washing machine equipped with four cantilever beam with tip mass TVAs. The solid lines refers to the measured spectra with all the TVAs tuned at the fundamental resonance frequencies of $12.3Hz$ in vertical direction.

of spongy material drenched with oily and greasy viscous fluid that increases the total stiffness and damping of the suspension for small displacements and generate a non linear dynamic response of the dampers. The superposition of these contributes increases the fundamental natural frequencies for the horizontal and vertical oscillations of the drum and smooth the resonance peaks. The measured spectra show antiresonances at $11.9Hz$ and at $12.3Hz$ respectively for the horizontal and vertical vibrational modes. Since the TVA beams have annular cross section, the fundamental natural frequencies of the cantilever beams with tip masses for horizontal and vertical oscillations, are slightly different. This means that the in-house TVAs assemblies are not orthogonally symmetric. At frequencies above the first fundamental natural frequency of the vibration absorbers, the responses are characterised by the dynamics of the TVA system. The simulated FRFs do not agree well with the measured ones, in particular for the spectra along the y axis. The model predicts the amplitude of oscillation of the tub-drum equipped with TVA devices by considering only the first fundamental natural frequency for horizontal and vertical directions of the mass-cantilever beams TVA, thus the dynamic effects relative to higher vibrational modes is not predicted. Furthermore the TVAs were tuned by sliding the tip masses along the beams. This solution modifies the length of the beam and in particular the static bending moment applied at the joint connections. As a result, the tub-drum assembly slightly rotates up to the new configuration of equilibrium. This changes the orientation of the accelerometers and affects the measures. Better agreement was observed for the horizontal direction of oscillation, where the tuning of the TVAs do not modify the static bending moment at the frame of the tub-drum system. Moreover, the model does not include non linearity effects and the coupling of the TVAs systems.

Figure 4.21 shows the simulated (red dashed line) and the measured (solid blue line) FRF spectra of the ground force transmission. The resonance peaks, relative to the fundamental horizontal and vertical natural vibrational modes of the tub-drum assembly, are significantly attenuated. This is due to the increased damping contribute caused by the lower amplitude oscillations of the system. The antiresonance frequency is slightly shifted with respect to the fundamental natural frequency of the TVAs. However the use of the vibrational absorbers reduces the force transferred to the ground down to 31 dB with a reduction of 7 dB. At higher frequencies the measured FRFs spectra of the force increase proportionally with the damping contribute as predicted by the model. The simulated spectrum does not agree well with the measured one because it underestimates the amplitude of force transmitted below the fundamental natural frequency of the cantilever beams and overestimates this value at higher frequencies. Furthermore the antiresonance is shifted in frequency.

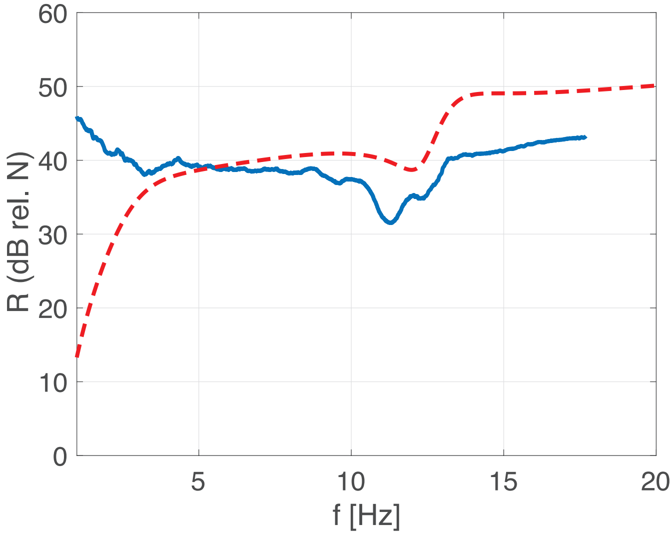

Figure 4.21: Comparison between the simulated (red dashed line) and measured (black solid line) FRFs relative to ground force transmission for the washing machine equipped with four cantilever beam with tip mass TVAs. The solid lines refers to the measured spectra with all the TVAs tuned at the fundamental resonance frequencies of $12.3Hz$ in vertical direction.

5

Summary, conclusions and future works

This thesis has presented analytical, simulation and experimental work on two vibration control systems for professional washing machines, which are characterised by a tub-drum-ballast masses assembly suspended on four helical springs and friction dampers connected in parallel. The study was focussed on the control of the tub-drum oscillations along the vertical and horizontal directions and on the control of the tub-drum normal force transmitted to ground via the four spring-damper elements during a customised extraction cycle. The study considered the vibration control effects produced by two semi-active devices. Firstly, a semi-active damper, which enhances the vibration isolation effect offered by the suspension system that holds the tub-drum assembly. Secondly, a semi-active Tuned Vibration Absorber, which replaces the ballast masses to absorb the vibration energy of the tub-drum assembly at the spinning frequency.

Mechanical lumped parameter models were developed to predict the time-history and frequency response functions of the displacements of the tub-drum assembly along vertical and horizontal directions and the normal force transmitted to the ground via the isolation system, with reference to the harmonic excitation produced by the unbalanced spinning drum and considering three configurations of the washing machine. Firstly, the standard isolation configuration, where the tub-drum assembly is suspended on four helical springs and friction dampers connected in parallel. Secondly, a semi-active isolation configuration, where the tub-drum assembly is suspended on four helical springs connected in parallel with tunable friction dampers, which switch the damping level from a very high value at low spinning velocities to a very low value at high spinning velocities. Thirdly, a semi-active vibration absorption configuration, where the tub-drum assembly is suspended on four helical springs and friction dampers connected in parallel and the ballast masses are replaced by tunable vibration absorbers, which are manually adapted to absorb vibration energy at the spinning velocity of the drum.

The study provided also an empirical model of the time and frequency dependent residual moisture content in clothes, which can be used to predict the variation of the amount of unbalance load during the spinning cycle. Constant garments composition, constant temperature, constant filling coefficient and no use of detergent were assumed. Furthermore, the empirical model was validated for the typical range of shape factors of the drum available in professional markets.

Chapter 2 presented and validated experimentally the lumped parameter model for the coupled horizontal and vertical oscillations of the tub-drum assembly mounted on four helical springs and friction dampers connected in parallel and for the normal force transmission to the ground via the four suspensions. Simulated and experimental FRFs spectra for the amplitude of oscillation in horizontal and vertical directions and for the normal force transmitted to ground were found in good agreement with the respective measured FRFs. The simulated and measured FRFs spectra for the oscillations in horizontal and vertical directions are characterised by two resonance peaks at 1.2 Hz and 2.3 Hz, which are due to the horizontal and vertical vibration natural modes of the visco-elastically suspended tub-drum assembly. At higher frequencies, the spectra for the amplitude of drum oscillations in horizontal and vertical directions level to a constant value, which is independent on the stiffness and damping levels of the suspensions and, instead, depend on the eccentricity factor of the unbalanced drum. The simulated and measured FRFs spectra of the force transmitted are also characterised by the two resonance peaks at 1.2 Hz and 2.3 Hz, which are due to the horizontal and vertical vibration natural modes of the visco-elastically suspended tub-drum assembly. However, at higher frequencies, the transmitted force monotonically rises proportionally to frequency. The measured FRFs spectra with the heavily damped suspensions did not perfectly overlap the simulated FRFs. The measured resonance frequencies were slightly shifted up to 1.7 Hz and 3.0 Hz respectively for the horizontal and vertical modes. This was due to stiffening effects produced by the dampers. At higher frequencies the FRFs were characterised by a constant value, which is proportional to the eccentricity factor and does not depend on the damping of the suspensions. The measured and simulated force transmission matched quite well at higher frequencies but not in the proximity of the resonance frequency of the horizontal vibrational mode. This was due to the non perfect identification and repeatability of the damping effect produced by the suspensions.

The second chapter also defined a measurement methodology and provided an experimental model to predict dewatering from the washed load during the spinning cycle of professional washing machines. The study was focussed on the residual moisture content, which is the parameter commonly used to evaluate performances of washing machines and thus is used to design the extraction cycle and drying phase. Because of the complexity of the washing process in domestic and professional appliances, an experimental approach was chosen to derive an empirical model for the dewatering phenomenon during extraction cycle. The model was derived under the hypothesis of constant garments' composition, constant temperature, constant filling coefficient and no use of detergent. An experimental set up was designed and built in accordance with the international standards for this type of measurements. Repeatability analysis demonstrated the general validity of the procedure on the entire spinning speed and washing capacity range. In fact, the maximum variation in terms of measured residual moisture content was lower than 0.3% at high speed. Water retention time histories for different G-acceleration factors were used to define a polynomial function, which can be used to predict dewatering performances as a function of time and G-acceleration, regardless of drum geometry. Best performances occur at high values of time and G-acceleration, where the water retention value decreases up to 120% with respect to the initial water content. The G-acceleration factor showed the greatest impact on residual moisture content compared to time. The accuracy of the proposed empirical model equation was evaluated calculating the data residuals, which were lower than ±2% for all the appliances, when the extraction cycle is longer than 2 minutes. Finally a scaling analysis showed no considerable influence of the drum shape and capacity on water retention performances over 100-G. Therefore, for the shape factor range and the G-acceleration typically adopted on professional washing machines, one-dimensional polynomial function was used to predict dewatering performances.

Chapter 3 presented and validated experimentally the lumped parameter model for the coupled horizontal and vertical oscillations of the tub-drum assembly mounted on four helical springs and semi-active friction dampers connected in parallel and for the normal force transmission to ground via the four suspensions. The semi-active friction based damper was specifically designed for a professional washing machine. It was operated in such a way as to implement high damping levels at low frequencies, where the dynamic response of the drum was controlled by the fundamental natural modes for vertical and transverse oscillations of the tub-drum assembly mounted on four helical springs and semi-active dampers, and low damping levels at higher frequencies, where the normal force transmission to ground is proportional to frequency and the friction damping level in the suspension. The experimental results produced in this study have shown that the semi-active damper effectively brings down the tub-drum oscillations in vertical and horizontal direction in the low frequency region characterised by the resonance peaks due to the two fundamental natural modes. In particular, when the washing machine spins at the two fundamental resonance frequencies, the drum oscillations are reduced by 20 and 55 dB respectively. The amplitude of the oscillations did not vary at higher frequencies since it solely depends on the ratio between the unbalance mass and drum. The proposed semi-active damper effectively brought down also the normal force transmitted to ground for low angular speeds of the drum. Indeed the amplitude of the force transmitted when the drum angular velocity coincided with the two fundamental resonance frequencies of the drum-springs system was reduced by about 30 and 20 dB respectively. More importantly, the force transmission at higher frequencies remained constant rather than rising as found for the machine equipped with the passive damper. As a result, at full spinning angular speed the force transmitted to ground was reduced by 7 dB compared to that found with the passive damper configuration. This is a very important result, which shows how the proposed semi-active damper can be effectively used to mitigate both the high oscillations and force transmission at low spinning velocity of the drum in correspondence to the fundamental resonance frequencies as well as the force transmission at the highest spinning velocity of the drum.

Chapter 4 presented and validated experimentally the lumped parameter model for the partially coupled horizontal and vertical oscillations of the tub-drum-TVA assembly mounted on four helical springs and friction dampers connected in parallel and for the normal force transmission to ground via the four suspensions. A prototype TVA was designed and tested. The TVA was formed by a cantilever beam with annular cross section and a cylindrical mass with a circular hole having the same dimension as the external diameter of the clamped beam. The cylindrical mass was inserted in the beam such that it can slide along its length. In this way the natural frequency of the fundamental bending modes in the horizontal and vertical planes could be varied over a wide frequency range comprised between the fundamental resonance frequencies that characterise the response of the machine and higher spinning frequency of the washing machine. Simulation and experimental results have shown that the proposed TVAs can be effectively used to absorb vibration kinetic energy of the tub-drum assembly at the tuning frequency. Therefore, both the tub-drum oscillations in vertical and horizontal direction and the normal force transmission to ground could be effectively reduced, both in correspondence to the low frequency resonances and at higher frequencies. However this requires a fine tuning of the TVA, otherwise the dynamics of the TVA could even enhance the oscillations and force transmission to the ground. Therefore a fine tracking system is required to continuously adapt the tuning of the TVA to the spinning velocity of the drum. Nevertheless, the experimental results presented in this chapter have shown that the vertical vibrational mode of the drum and force transmitted were reduced of -17 dB and -15 dB respectively with the lightly damped springs suspension configuration.

The lumped parameter model predicted roughly the measured FRFs spectra over the entire frequency range. The TVA had little effect on lower the tub-drum assembly oscillations when it was mounted in heavily damped spring-dampers suspension. Small differences in the fundamental natural frequencies of the first vibrational mode of the absorbers were produced by asymmetric dynamics of the four dampers.

Future work

The study presented in this thesis has brought up few topics that would be interesting to further investigate in future studies as listed below:

- Integrate the dewatering model in the lumped parameter model for the vibrations and force transmission of the tub-drum assembly.
- Extend the validity of the proposed model by taking into consideration the coupling effects of different cantilever beam and tip mass vibration absorbers.
- Study and investigate non-linearities in the mechanical model.
- Improve the design of the semi-active dampers so that they can really operate in a professional machine for all the life cycle of the appliance.
- Develop a compact self-tuning vibration absorber such that its first fundamental resonance frequency is automatically adapted to the revolution speed of the drum.

- Develop a “Digital Twin” model able to predict the oscillations of the tub-drum assembly and the force transmitted, to suggest real time solutions and to implement remote control.

Bibliography

[1] J. Fox, "Why It Took the Washing Machine So Long to Catch On," 2017.

[2] D. F. McKenzie, D. McKenzie, and M. Bell, *A Chronology and Calendar of Documents Relating to the London Book Trade 1641-1700: Volume III: 1686-1700; Indexes*, vol. 3. Oxford University Press, 2005.

[3] Yale University, "Beetham's royal patent washing mill No. 27 Fleet Street, London," 2011.

[4] A. J. Fisher, "Drive mechanism for washing machines," 1910.

[5] A. J. Fisher, "Yielding shaft-coupling," 1919.

[6] Electrolux AB, "Electrolux Annual Report 2018," tech. rep., 2018.

[7] Coin Laundry Association, "Coin Laundry Association Industry Overview."

[8] I. Rüdenauer, C.-O. Gensch, M. Blepp, E. Brommer, G. Kathrin, S. Mudgal, R. Cervantes, T. Faninger, L. Lyons, and D. Seifried, "Preparatory Studies for Eco-design Requirements of Energy-using Products Lot 24: Professional Washing Machines, Dryers and Dishwashers," Tech. Rep. 0, 2011.

[9] K. Ellmer, M. Fuchs, U. Bauer, T. Schneider, P. U. Thamsen, T. Morgenthal, J. Villwock, and A. Hanau, "Research project simulation wäschepflege–recommendations for improving resource efficiency in the laundry process in households in germany," *Journal of Cleaner Production*, vol. 153, pp. 539–547, 2017.

[10] D. Carter and D. Shah, "The role of surface tension on the residual water content of fabrics," *Journal of surfactants and detergents*, vol. 8, no. 1, pp. 91–94, 2005.

[11] IEC Central Office, *International Standard IEC 60456.* Geneva: International Electrotecnical Commission, 5.0 ed., 2010.

[12] R. H. Brooks and A. T. Corey, "Properties of porous media affecting fluid flow," *Journal of the irrigation and drainage division*, vol. 92, no. 2, pp. 61–90, 1966.

[13] A. Cheng and M. Gulliksson, *Finite difference methods for saturated-unsaturated flow in porous media.* Mitthögskolan, FSCN, 2003.

[14] A. T. Corey, "Measurement of water and air permeability in unsaturated soil 1," *Soil Science Society of America Journal*, vol. 21, no. 1, pp. 7–10, 1957.

[15] L. A. Richards, "Capillary conduction of liquids through porous mediums," *Physics*, vol. 1, no. 5, pp. 318–333, 1931.

[16] C. Brasquet and P. Le Cloirec, "Pressure drop through textile fabrics-experimental data modelling using classical models and neural networks," *Chemical Engineering Science*, vol. 55, no. 15, pp. 2767–2778, 2000.

[17] L. Loeb, "Water retention by cotton fabric under compressional loading," *Textile Research Journal*, vol. 35, no. 7, pp. 621–625, 1965.

[18] A. Salehi Rad, S. Hosseini Varkiyani, and M. Haghighat Kish, "Water retention in hollow fibres nonwoven mat," *Journal of The Textile Institute*, vol. 104, no. 9, pp. 994–1002, 2013.

[19] C. E. Mongan, "Validity of darcy's law under transient conditions," tech. rep., 1985.

[20] E. Ghane, N. R. Fausey, and L. C. Brown, "Non-darcy flow of water through woodchip media," *Journal of hydrology*, vol. 519, pp. 3400–3409, 2014.

[21] C. T. Beckett and C. E. Augarde, "Prediction of soil water retention properties using pore-size distribution and porosity," *Canadian Geotechnical Journal*, vol. 50, no. 4, pp. 435–450, 2013.

[22] M. Castellini, S. Di Prima, and M. Iovino, "An assessment of the best procedure to estimate the soil water retention curve: A comparison with the evaporation method," *Geoderma*, vol. 320, pp. 82–94, 2018.

[23] S. Maggi, "Estimating water retention characteristic parameters using differential evolution," *Computers and Geotechnics*, vol. 86, pp. 163–172, 2017.

[24] E. Ebrahimi, H. Bayat, M. R. Neyshaburi, and H. Zare Abyaneh, “Prediction capability of different soil water retention curve models using artificial neural networks,” *Archives of Agronomy and Soil Science*, vol. 60, no. 6, pp. 859–879, 2014.

[25] R. Moosavizadeh-Mojarrad and A. R. Sepaskhah, “Predicting soil water retention curve by artificial neural networks,” *Archives of Agronomy and Soil Science*, vol. 57, no. 1, pp. 3–13, 2011.

[26] J. Zheng, “The new direction of computational fluid dynamics and its application in industry,” *Journal of Physics: Conference Series*, vol. 1064, p. 012060, 07 2018.

[27] S. Rief, E. Glatt, E. Laourine, D. Aibibu, C. Cherif, and A. Wiegmann, “Modeling and cfd-simulation of woven textiles to determine permeability and retention properties,” *AUTEX Research Journal*, vol. 11, no. 3, pp. 78–83, 2011.

[28] A. Szymkiewicz, *Modelling water flow in unsaturated porous media: accounting for nonlinear permeability and material heterogeneity.* Springer Science & Business Media, 2012.

[29] T. Narasimhan and P. Witherspoon, “An integrated finite difference method for analyzing fluid flow in porous media,” *Water Resources Research*, vol. 12, no. 1, pp. 57–64, 1976.

[30] A. Reatto, E. M. da Silva, A. Bruand, E. S. Martins, and J. E. F. W. Lima, “Validity of the centrifuge method for determining the water retention properties of tropical soils,” *Soil Science Society of America Journal*, vol. 72, no. 6, pp. 1547–1553, 2008.

[31] “Determination of soil-water retention curve for a young residual soil using a small centrifuge,” *18th International Conference on Soil Mechanics and Geotechnical Engineering*, no. 1937, pp. 1175–1178, 2013.

[32] M. C. Caputo and J. R. Nimmo, “Quasi-steady centrifuge method for unsaturated hydraulic properties,” *Water resources research*, vol. 41, no. 11, 2005.

[33] M. Z. Chen, C. Papageorgiou, F. Scheibe, F.-C. Wang, and M. C. Smith, “The missing mechanical circuit element,” *IEEE Circuits and Systems Magazine*, vol. 9, no. 1, pp. 10–26, 2009.

[34] S. Petrulyte and R. Baltakyte, "Investigation into the wetting phenomenon of terry fabrics," *Fibres & Textiles in Eastern Europe*, vol. 16, no. 4, pp. 62–66, 2008.

[35] S. Petrulyte and R. Baltakyte, "Static water absorption in fabrics of different pile height," *Fibres & Textiles in Eastern Europe*, vol. 17, no. 3, pp. 60–65, 2009.

[36] T. Nygårds, *Washing machine design optimization based on dynamics modeling.* PhD thesis, 2011.

[37] S. Bae, J. Lee, Y. Kang, J. Kang, and J. Yun, "Dynamic analysis of an automatic washing machine with a hydraulic balancer," *Journal of Sound and vibration*, vol. 257, no. 1, pp. 3–18, 2002.

[38] "Consumers Union of USA: Stopping Vibration Washing Machines," 2011.

[39] D. Conrad and W. Soedel, "On the problem of oscillatory walk of automatic washing machines," *Journal of Sound and Vibration*, vol. 188, no. 3, pp. 301–314, 1995.

[40] J. P. Den Hartog, *Mechanical vibrations.* Courier Corporation, 1985.

[41] M. Adams, *Rotating Machinery Vibration: From Analysis to Troubleshooting.* EBSCO ebook academic collection, Taylor & Francis, 2000.

[42] "Electrolux Professional internal properties," tech. rep., Electrolux Professional Laundry System Sweden AB, 2017.

[43] A. Preumont, *Vibration control of active structures: an introduction*, vol. 246. Springer, 2018.

[44] "Suspa Inc.."

[45] "Sanhua Aweco Appliance System."

[46] Q. Nguyen, S.-B. Choi, and J. Woo, "Optimal design of magnetorheological fluid-based dampers for front-loaded washing machines," *Proceedings of the Institution of Mechanical Engineers, Part C: Journal of Mechanical Engineering Science*, vol. 228, no. 2, pp. 294–306, 2014.

[47] B. C. Yalçın and H. Erol, "Semiactive vibration control for horizontal axis washing machine," *Shock and Vibration*, vol. 2015, 2015.

[48] J. D. Carlson, “Magnetorheological Fluids,” in *Smart Materials* (CRC Press, ed.), ch. Magnetorheological Fluids, Taylor & Francis, 1 ed., 2009.

[49] A. Grunwald and A.-G. Olabi, “Design of magneto-rheological (mr) valve,” *Sensors and Actuators A: Physical*, vol. 148, no. 1, pp. 211–223, 2008.

[50] F. D. Goncalves and J. D. Carlson, “Investigating the time dependence of the mr effect,” *International Journal of Modern Physics B*, vol. 21, no. 28n29, pp. 4832–4840, 2007.

[51] F. D. Goncalves, M. Ahmadian, and J. Carlson, “Investigating the magnetorheological effect at high flow velocities,” *Smart Materials and Structures*, vol. 15, no. 1, p. 75, 2005.

[52] J. C. Poynor, “Innovative designs for magneto-rheological dampers,” 2001.

[53] J. D. Carlson and M. J. Chrzan, “Magnetorheological fluid dampers,” Jan. 11 1994. US Patent 5277281.

[54] B. Ebrahimi, *Development of hybrid electromagnetic dampers for vehicle suspension systems.* PhD thesis, 2009.

[55] B. A. Reichert, *Application of magnetorheological dampers for vehicle seat.* PhD thesis, Virginia Polytechnic Institute and State University, Blacksburg, 1997.

[56] H.-W. Chen and Q. Zhang, “Design of horizontal axis washing machine with ball balancer and mr dampers,” *International Journal of Precision Engineering and Manufacturing*, vol. 18, no. 12, pp. 1783–1793, 2017.

[57] C. Spelta, F. Previdi, S. M. Savaresi, G. Fraternale, and N. Gaudiano, “Control of magnetorheological dampers for vibration reduction in a washing machine,” *Mechatronics*, vol. 19, no. 3, pp. 410–421, 2009.

[58] M. J. Chrzan and J. D. Carlson, “Mr fluid sponge devices and their use in vibration control of washing machines,” in *Smart Structures and Materials 2001: Damping and Isolation*, vol. 4331, pp. 370–378, International Society for Optics and Photonics, 2001.

[59] J. Buśkiewicz and G. Pittner, “Reduction in vibration of a washing machine by means of a disengaging damper,” *Mechatronics*, vol. 33, pp. 121–135, 2016.

[60] G. R. Park, S. M. Jeon, S. C. Park, J. H. Kim, C. S. Jun, and S. Y. Oh, “Washer damper thereof, and control method thereof,” Aug. 19 2008. US Patent 7,412,852.

[61] P. Gardonio and S. Elliott, “Passive and active isolation of structural vibration transmission between two plates connected by a set of mounts,” *Journal of Sound and Vibration*, vol. 237, no. 3, pp. 483–511, 2000.

[62] P. Gardonio, S. Elliott, and R. Pinnington, “Active isolation of structural vibration on a multiple-degree-of-freedom system, part ii: effectiveness of active control strategies,” *Journal of Sound and Vibration*, vol. 207, no. 1, pp. 95–121, 1997.

[63] P. Gardonio and S. J. Elliott, “A Study of Control Strategies for the Reduction of Structural Vibration Transmission,” *Journal of Vibration and Acoustics*, vol. 121, no. 4, pp. 482–487, 1999.

[64] M. Zilletti, *Self-tuning vibration absorbers.* PhD thesis, University of Southampton, 2001.

[65] M. Brennan and J. Dayou, “Global control of vibration using a tunable vibration neutraliser,” *Noise & Vibration Worldwide*, vol. 32, no. 5, pp. 16–23, 2001.

[66] H. Frahm, “Device for damping vibrations of bodies,” 1911.

[67] J. Ormondroyd, “The theory of the dynamic vibration absorber,” *Trans., ASME, Applied Mechanics*, vol. 50, pp. 9–22, 1928.

[68] M. Brennan and J. Dayou, “Global control of vibration using a tunable vibration neutralizer,” *Journal of Sound and Vibration*, vol. 232, no. 3, pp. 585–600, 2000.

[69] M. Brennan, “Characteristics of a wideband vibration neutralizer,” *Noise Control Engineering Journal*, vol. 45, no. 5, pp. 201–207, 1997.

[70] P. L. Walsh and J. Lamancusa, “A variable stiffness vibration absorber for minimization of transient vibrations,” *Journal of sound and vibration*, vol. 158, no. 2, pp. 195–211, 1992.

[71] L. Virgin and R. Davis, “Vibration isolation using buckled struts,” *Journal of Sound Vibration*, vol. 260, pp. 965–973, 2003.

[72] J. C. Clemens, “Platelike dynamic vibration absorbers—comparison of measurement and theory,” *The Journal of the Acoustical Society of America*, vol. 75, no. 2, pp. 638–638, 1984.

[73] T. Asami, O. Nishihara, and A. M. Baz, “Analytical solutions to h_∞ and h_2 optimization of dynamic vibration absorbers attached to damped linear systems,” *J. Vib. Acoust.*, vol. 124, no. 2, pp. 284–295, 2002.

[74] E. Rustighi, M. Brennan, and B. Mace, “A shape memory alloy adaptive tuned vibration absorber: design and implementation,” *Smart Materials and Structures*, vol. 14, no. 1, p. 19, 2004.

[75] T.-H. Huang, J.-Y. Kuan, and H.-P. Huang, “Design of a new variable stiffness actuator and application for assistive exercise control,” in *2011 IEEE/RSJ International Conference on Intelligent Robots and Systems*, pp. 372–377, IEEE, 2011.

[76] A. Jafari, N. G. Tsagarakis, and D. G. Caldwell, “Awas-ii: A new actuator with adjustable stiffness based on the novel principle of adaptable pivot point and variable lever ratio,” pp. 4638–4643, 2011.

[77] A. H. Von Flotow and T. S. Mixon, “Adaptively tuned vibration absorber,” Dec. 9 1997. US Patent 5,695,027.

[78] M. Blaszkiewicz, R. Newnham, and Q. Xu, “Tunable transducers as smart materials,” in *TRANSDUCERS’91: 1991 International Conference on Solid-State Sensors and Actuators. Digest of Technical Papers*, pp. 899–903, IEEE, 1991.

[79] A. D. Dimarogonas, “A smart electrorhelogical fluid dynamic vibration absorber,” *ASME, DE-58, Intelligent Structures, Materials and Vibrations*, pp. 7–15, 1993.

[80] P. Gardonio and M. Zilletti, “Integrated tuned vibration absorbers: a theoretical study,” *The Journal of the Acoustical Society of America*, vol. 134, no. 5, pp. 3631–3644, 2013.

[81] P. Gardonio and E. Turco, “Tuning of vibration absorbers and helmholtz resonators based on modal density/overlap parameters of distributed mechanical and acoustic systems,” *Journal of Sound and Vibration*, vol. 451, pp. 32–70, 2019.

[82] E. Turco and P. Gardonio, "Sweeping shunted electro-magnetic tuneable vibration absorber: Design and implementation," *Journal of Sound and Vibration*, vol. 407, pp. 82–105, 2017.

[83] D. E. Casagrande, P. Gardonio, and M. Zilletti, "Sweeping piezoelectric patch vibration absorbers," in *Journal of Physics: Conference Series*, pp. 1–12, 2016.

[84] M. Zilletti and P. Gardonio, "Experimental implementation of switching and sweeping tuneable vibration absorbers for broadband vibration control," *Journal of Sound and Vibration*, vol. 334, pp. 164–177, 2015.

[85] S. Živanović, A. Pavic, and P. Reynolds, "Vibration serviceability of footbridges under human-induced excitation: a literature review," *Journal of sound and vibration*, vol. 279, no. 1-2, pp. 1–74, 2005.

[86] P. Dallard, T. Fitzpatrick, A. Flint, A. Low, R. R. Smith, M. Willford, and M. Roche, "London millennium bridge: pedestrian-induced lateral vibration," *Journal of Bridge Engineering*, vol. 6, no. 6, pp. 412–417, 2001.

[87] P. Dallard, A. Fitzpatrick, A. Flint, S. Le Bourva, A. Low, R. Ridsdill Smith, and M. Willford, "The london millennium footbridge," *Structural Engineer*, vol. 79, no. 22, pp. 17–21, 2001.

[88] P. Gardonio, "Review of active techniques for aerospace vibro-acoustic control," *Journal of Aircraft*, vol. 39, no. 2, pp. 206–214, 2002.

[89] A. H. Von Flotow, M. Mercadal, K. B. Scribner, T. Mixon, and C. Roeseler, "Adaptively tuned vibration absorber for reduction of aircraft cabin noise," Feb. 23 1999. US Patent 5,873,559.

[90] K. Shin and J. Hammond, *Fundamentals of signal processing for sound and vibration engineers.* John Wiley & Sons, 2008.

[91] J. Brar and R. Bansal, *A Text Book of Theory of Machines.* Firewall Media, 2004.

[92] P. Hagedorn and A. DasGupta, *Vibrations and waves in continuous mechanical systems.* Wiley Online Library, 2007.

[93] S. Timoshenko, *Vibration Problems in Engineering.* Creative Media Partners, LLC, 2018.

[94] G. Cain and G. H. Meyer, *Separation of variables for partial differential equations: an eigenfunction approach.* Chapman and Hall/CRC, 2005.

[95] *Theory of elasticity.* Engineering societies monographs, McGraw-Hill, 1987.

Appendix A

This appendix includes the technical drawings of the elements which have been designed and manufactured to assemble the base-framework.

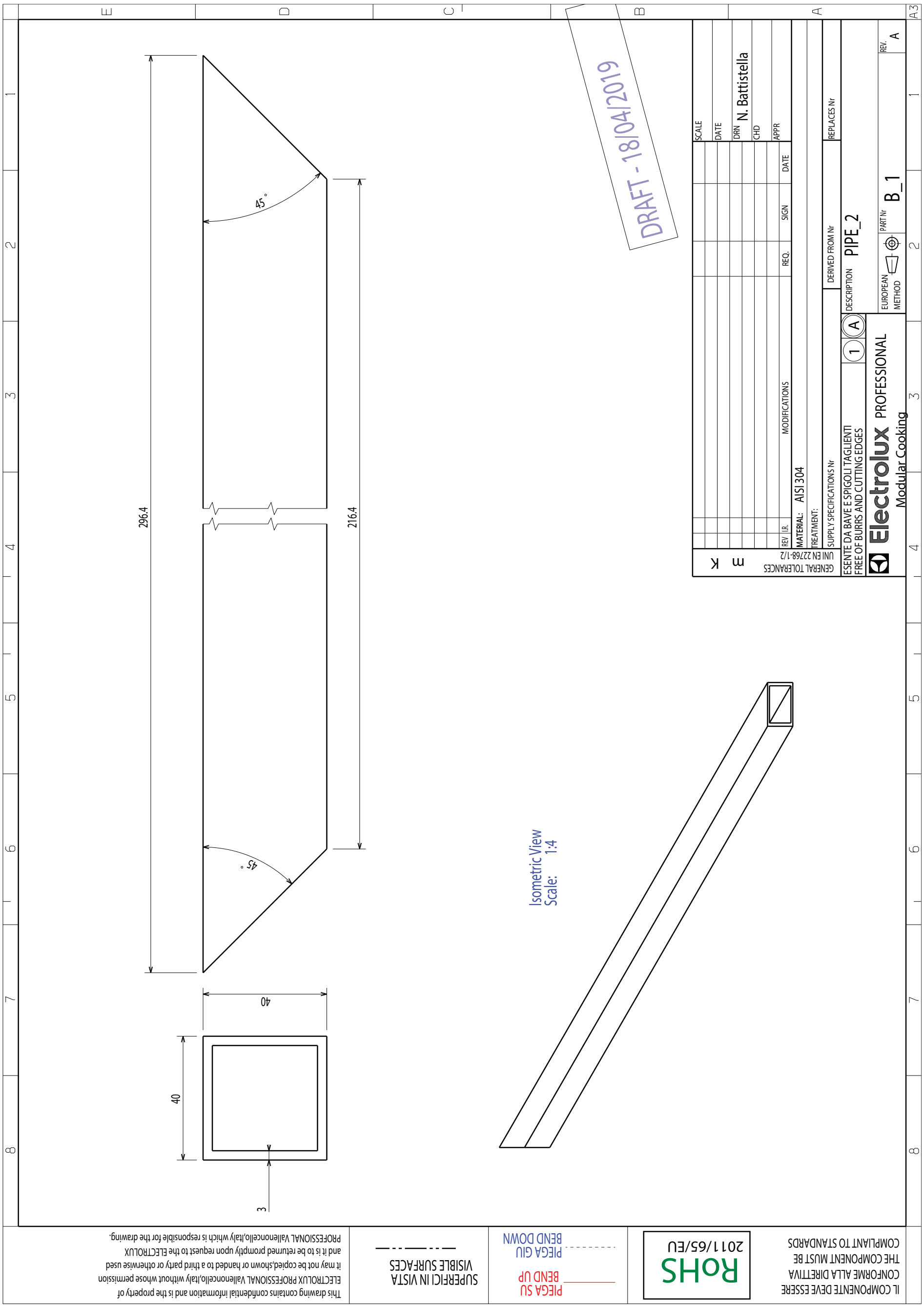

DRAFT - 18/04/2019
296.4
216.4
45°
45°
40
40
3
Isometric View
Scale: 1:4
SCALE
DATE
DRN N. Battistella
CHD
APPR
REPLACES Nr
DERIVED FROM Nr
DESCRIPTION PIPE_2
PART Nr B_1
REV. A
EUROPEAN METHOD
MODIFICATIONS
REQ.
SIGN
DATE
REV
I.R.
MATERIAL: AISI 304
TREATMENT:
SUPPLY SPECIFICATIONS Nr
GENERAL TOLERANCES UNI EN 22768-1/2
m
K
ESENTE DA BAVE E SPIGOLI TAGLIENTI
FREE OF BURRS AND CUTTING EDGES
1
A
Electrolux PROFESSIONAL
Modular Cooking
A3
IL COMPONENTE DEVE ESSERE CONFORME ALLA DIRETTIVA
THE COMPONENT MUST BE COMPLIANT TO STANDARDS
RoHS
2011/65/EU
PIEGA SU
BEND UP
PIEGA GIU
BEND DOWN
SUPERFICI IN VISTA
VISIBLE SURFACES
This drawing contains confidential information and is the property of ELECTROLUX PROFESSIONAL Vallenoncello,Italy without whose permission it may not be copied,shown or handed to a third party or otherwise used and it is to be returned promptly upon request to the ELECTROLUX PROFESSIONAL Vallenoncello,Italy which is responsible for the drawing.
A
B
C
D
E
1
2
3
4
5
6
7
8

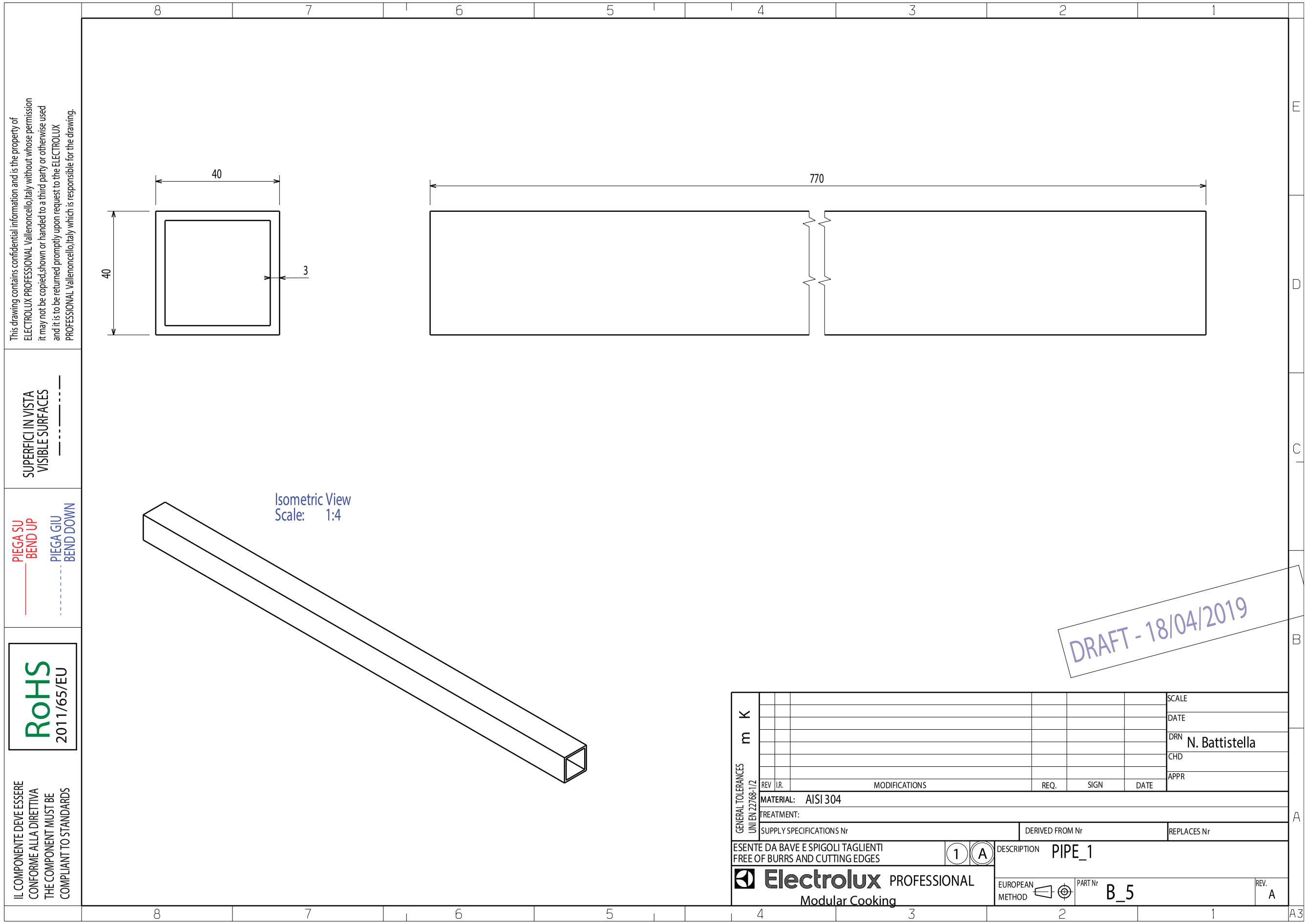
40
40
3
770
Isometric View
Scale: 1:4
DRAFT - 18/04/2019
This drawing contains confidential information and is the property of ELECTROLUX PROFESSIONAL Vallenoncello,Italy without whose permission it may not be copied,shown or handed to a third party or otherwise used and it is to be returned promptly upon request to the ELECTROLUX PROFESSIONAL Vallenoncello,Italy which is responsible for the drawing.
SUPERFICI IN VISTA
VISIBLE SURFACES
PIEGA SU
BEND UP
PIEGA GIU
BEND DOWN
RoHS
2011/65/EU
IL COMPONENTE DEVE ESSERE CONFORME ALLA DIRETTIVA
THE COMPONENT MUST BE COMPLIANT TO STANDARDS
GENERAL TOLERANCES
UNI EN 22768-1/2
m K
REV
I.R.
MODIFICATIONS
REQ.
SIGN
DATE
SCALE
DATE
DRN N. Battistella
CHD
APPR
MATERIAL: AISI 304
TREATMENT:
SUPPLY SPECIFICATIONS Nr
DERIVED FROM Nr
REPLACES Nr
ESENTE DA BAVE E SPIGOLI TAGLIENTI
FREE OF BURRS AND CUTTING EDGES
1
A
DESCRIPTION PIPE_1
Electrolux PROFESSIONAL
Modular Cooking
EUROPEAN METHOD
PART Nr B_5
REV. A
A3

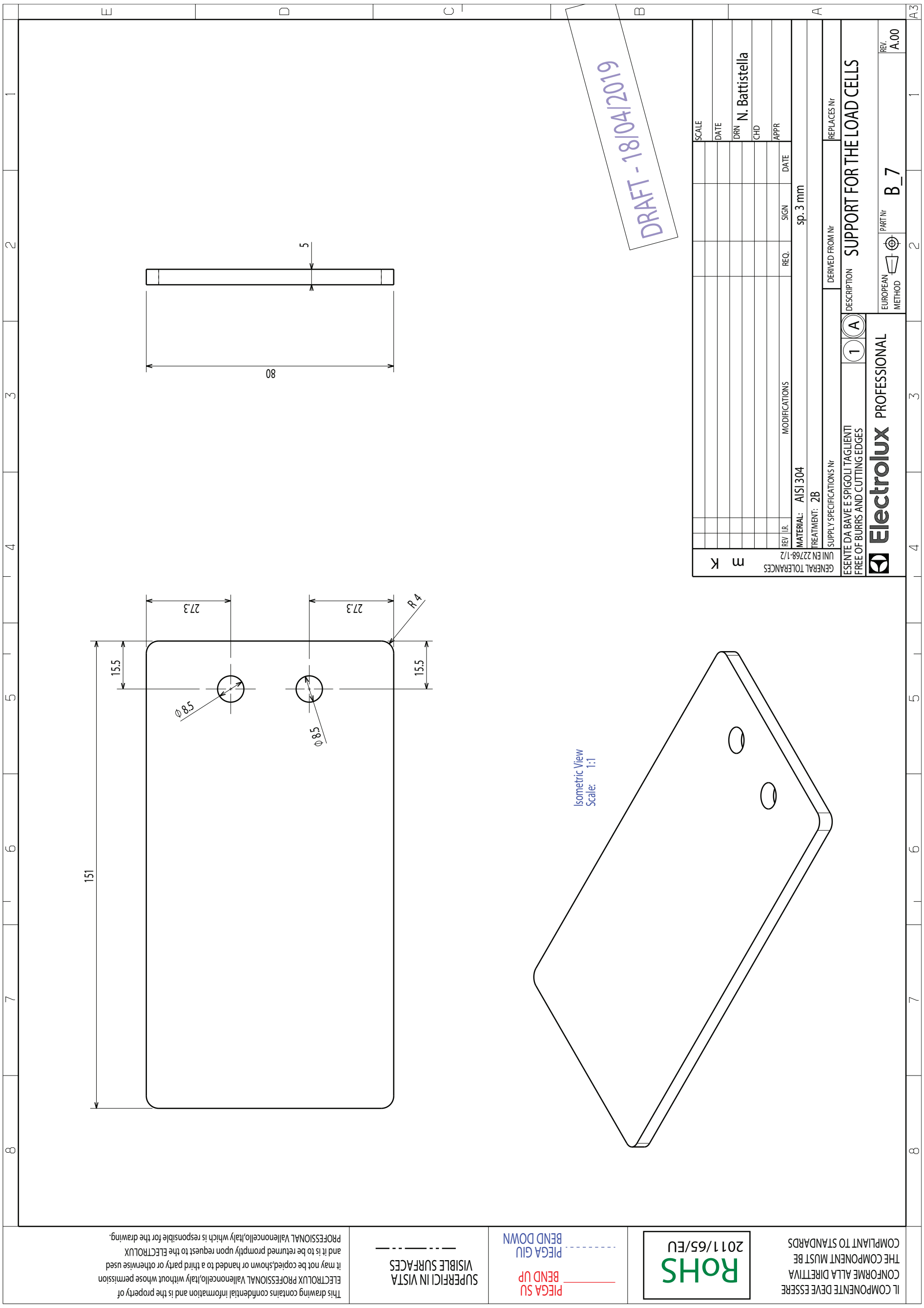
DRAFT - 18/04/2019
SCALE
DATE
DRN N. Battistella
CHD
APPR
REPLACES Nr
SUPPORT FOR THE LOAD CELLS
REV. A.00
PART Nr B_7
EUROPEAN METHOD
DESCRIPTION
DERIVED FROM Nr
DATE
SIGN
REQ.
sp. 3 mm
MODIFICATIONS
REV. I.R.
MATERIAL: AISI 304
TREATMENT: 2B
SUPPLY SPECIFICATIONS Nr
GENERAL TOLERANCES
UNI EN 22768-1/2
m K
ESENTE DA BAVE E SPIGOLI TAGLIENTI
FREE OF BURRS AND CUTTING EDGES
Electrolux PROFESSIONAL
5
80
27.3
27.3
R 4
15.5
15.5
ϕ 8.5
ϕ 8.5
151
Isometric View
Scale: 1:1
IL COMPONENTE DEVE ESSERE CONFORME ALLA DIRETTIVA
THE COMPONENT MUST BE COMPLIANT TO STANDARDS
RoHS 2011/65/EU
PIEGA SU BEND UP
PIEGA GIU BEND DOWN
SUPERFICI IN VISTA VISIBLE SURFACES
This drawing contains confidential information and is the property of ELECTROLUX PROFESSIONAL Vallenoncello,Italy whose permission it may not be copied,shown or handed to a third party or otherwise used and it is to be returned promptly upon request to the ELECTROLUX PROFESSIONAL Vallenoncello,Italy which is responsible for the drawing.
A B C D E
1 2 3 4 5 6 7 8
A3

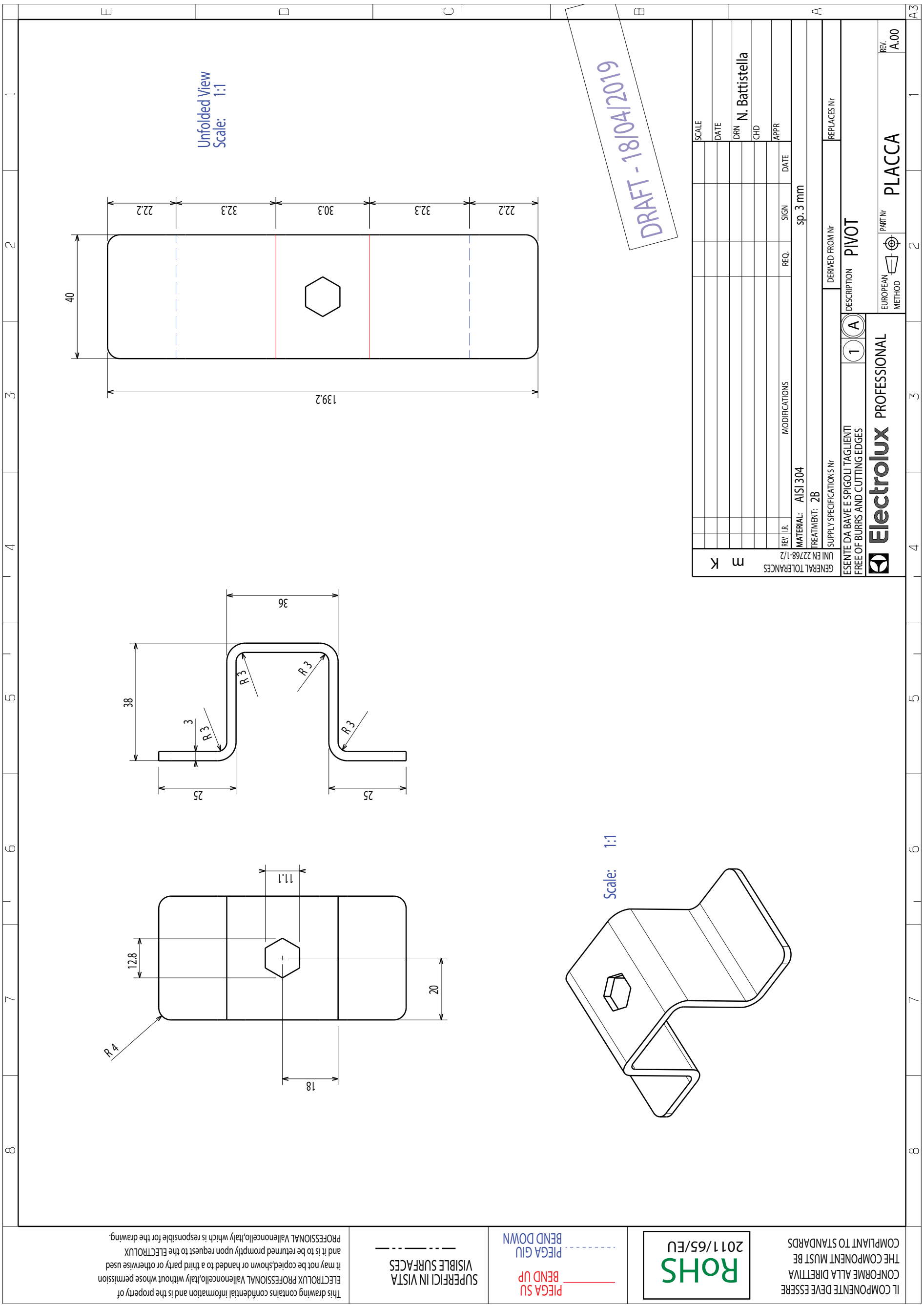
DRAFT - 18/04/2019
Unfolded View
Scale: 1:1
22.2
32.3
30.3
32.3
22.2
40
139,2
36
38
R 3
R 3
R 3
R 3
3
25
25
11.1
12.8
20
18
R 4
Scale: 1:1
SCALE
DATE
DRN N. Battistella
CHD
APPR
REV.
I.R.
MODIFICATIONS
REQ.
SIGN
DATE
sp. 3 mm
MATERIAL: AISI 304
TREATMENT: 2B
SUPPLY SPECIFICATIONS Nr
DERIVED FROM Nr
REPLACES Nr
DESCRIPTION PIVOT
PART Nr PLACCA
REV. A.00
EUROPEAN METHOD
1 A
Electrolux PROFESSIONAL
ESENTE DA BAVE E SPIGOLI TAGLIENTI
FREE OF BURRS AND CUTTING EDGES
GENERAL TOLERANCES
UNI EN 22768-1/2
m K
A3
IL COMPONENTE DEVE ESSERE CONFORME ALLA DIRETTIVA
THE COMPONENT MUST BE COMPLIANT TO STANDARDS
RoHS
2011/65/EU
PIEGA SU
BEND UP
PIEGA GIU
BEND DOWN
SUPERFICI IN VISTA
VISIBLE SURFACES
This drawing contains confidential information and is the property of ELECTROLUX PROFESSIONAL Vallenoncello,Italy without whose permission it may not be copied,shown or handed to a third party or otherwise used and it is to be returned promptly upon request to the ELECTROLUX PROFESSIONAL Vallenoncello,Italy which is responsible for the drawing.
A B C D E
1 2 3 4 5 6 7 8

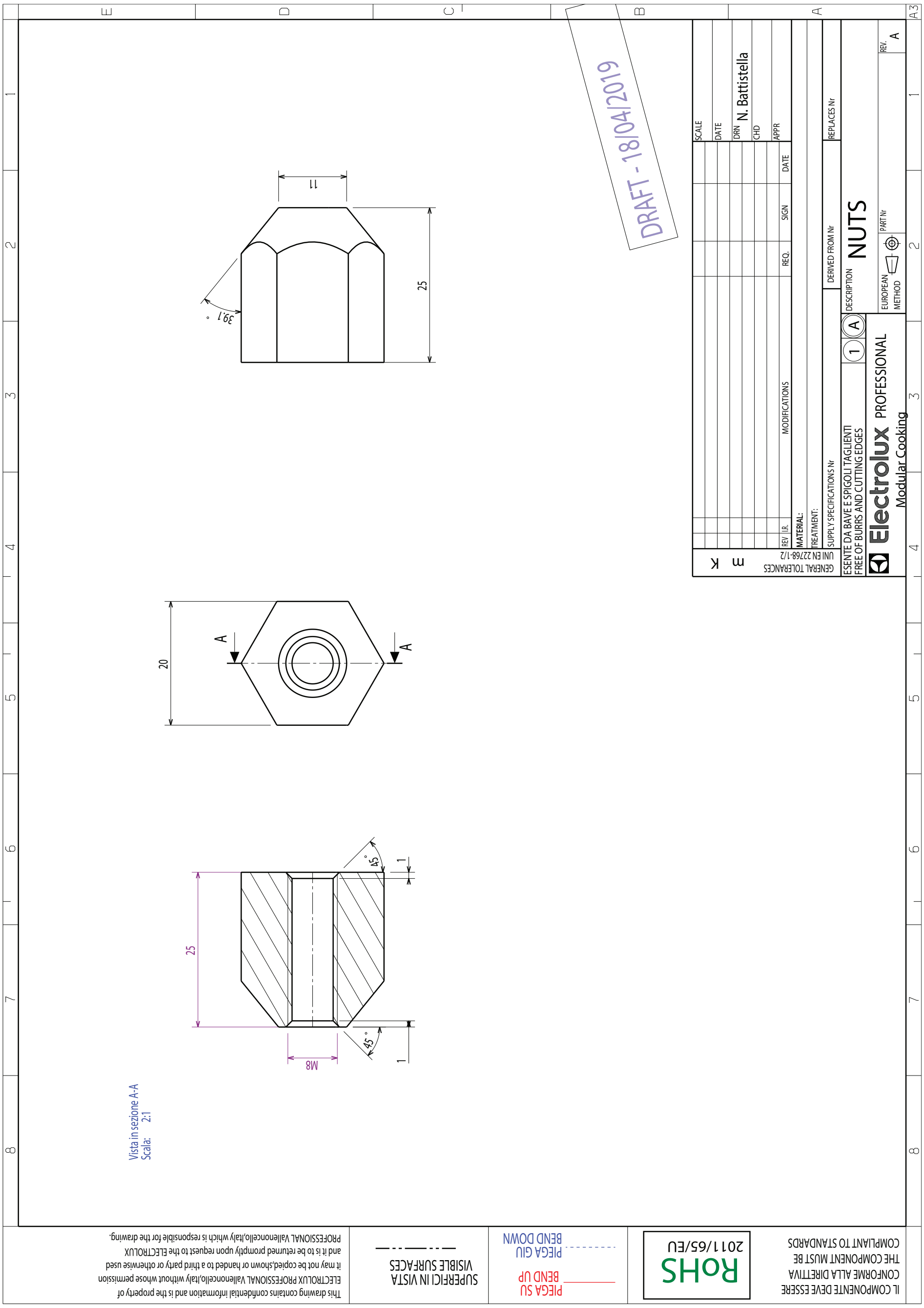
NUTS
N. Battistella
DRAFT - 18/04/2019
11
25
39,1 °
20
A
A
45 °
45 °
1
1
25
M8
Vista in sezione A-A
Scala: 2:1
SCALE
DATE
DRN
CHD
APPR
REPLACES Nr
DERIVED FROM Nr
DESCRIPTION
REV.
A
PART Nr
EUROPEAN METHOD
REV
I.R.
MODIFICATIONS
REQ.
SIGN
DATE
MATERIAL:
TREATMENT:
SUPPLY SPECIFICATIONS Nr
GENERAL TOLERANCES
UNI EN 22768-1/2
m
K
ESENTE DA BAVE E SPIGOLI TAGLIENTI
FREE OF BURRS AND CUTTING EDGES
1
A
Electrolux PROFESSIONAL
Modular Cooking
IL COMPONENTE DEVE ESSERE CONFORME ALLA DIRETTIVA
THE COMPONENT MUST BE COMPLIANT TO STANDARDS
RoHS
2011/65/EU
PIEGA SU
BEND UP
PIEGA GIU
BEND DOWN
SUPERFICI IN VISTA
VISIBLE SURFACES
This drawing contains confidential information and is the property of ELECTROLUX PROFESSIONAL Vallenoncello,Italy without whose permission it may not be copied,shown or handed to a third party or otherwise used and it is to be returned promptly upon request to the ELECTROLUX PROFESSIONAL Vallenoncello,Italy which is responsible for the drawing.
A3
A
B
C
D
E
1
2
3
4
5
6
7
8

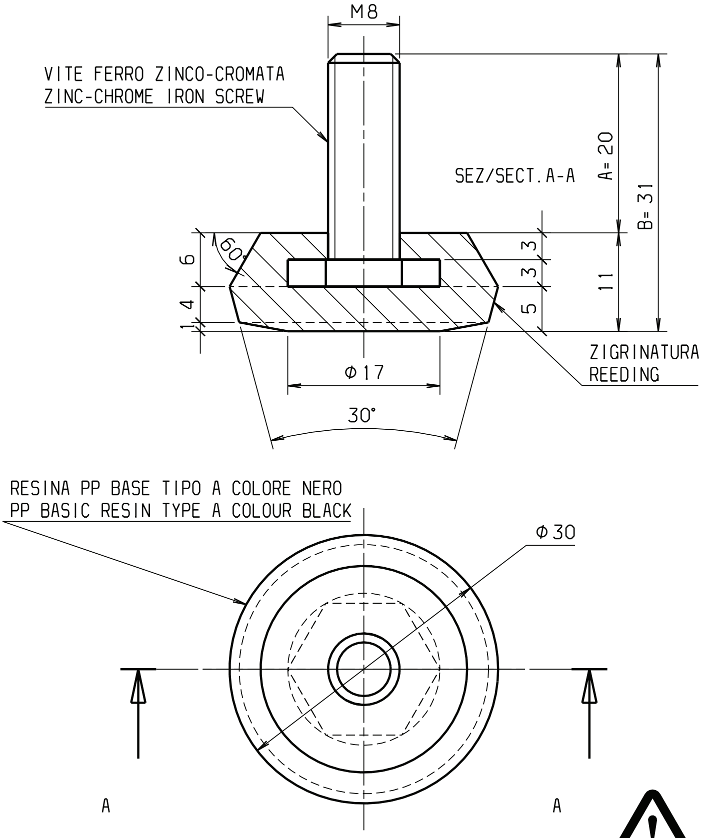

COPPIA MINIMA DI SCALETTAMENTO ALLA BASE 1Nm
MINIMUM TORQUE TO BREAK SCREW SOCKET 1Nm

[2] Critical dimensions which must be under capability

SAFETY REQUIREMENT

—— Visible surfaces.

Draft angles (not shown):

CHANGES FROM THE BASE NUMBER: A=28mm B=39mm
MODEL: LS
VARIANT NUMBER: 8306 013 00

REF.	MODIFICATIONS	SIGNATURE	REQUEST	DATE
	ESEGUITO DISEGNO A CAD	PICCO	GE.MA.	25.11.2002

MATERIAL
MODEL LB
SCALE 2:1
EUROPEAN METHOD
DESIGN USERS
REPLACES No
TREATMENT
WEIGHT
DERIVED FROM No
SUPPLY SPECIFICATIONS No -
DESIGN OWNER ITC_D
DRN ZUPPICHIN
CHD
APPR
DATE 20.03.1997

TITLE PIEDINO LIVELLATORE
ADJUSTABLE FOOT

Electrolux
Electrolux Professional SpA

CI000245
NUMBER 8306 262 00

THEORETICAL FLAT AREA
DEVELOPED FLAT AREA
GENERAL TOLERANCES
ANGLES ±0°30'
LENGTHS AND DIAMETERS
< 18 mm
18-80 mm ±1/2 IT14
> 80 mm

A4

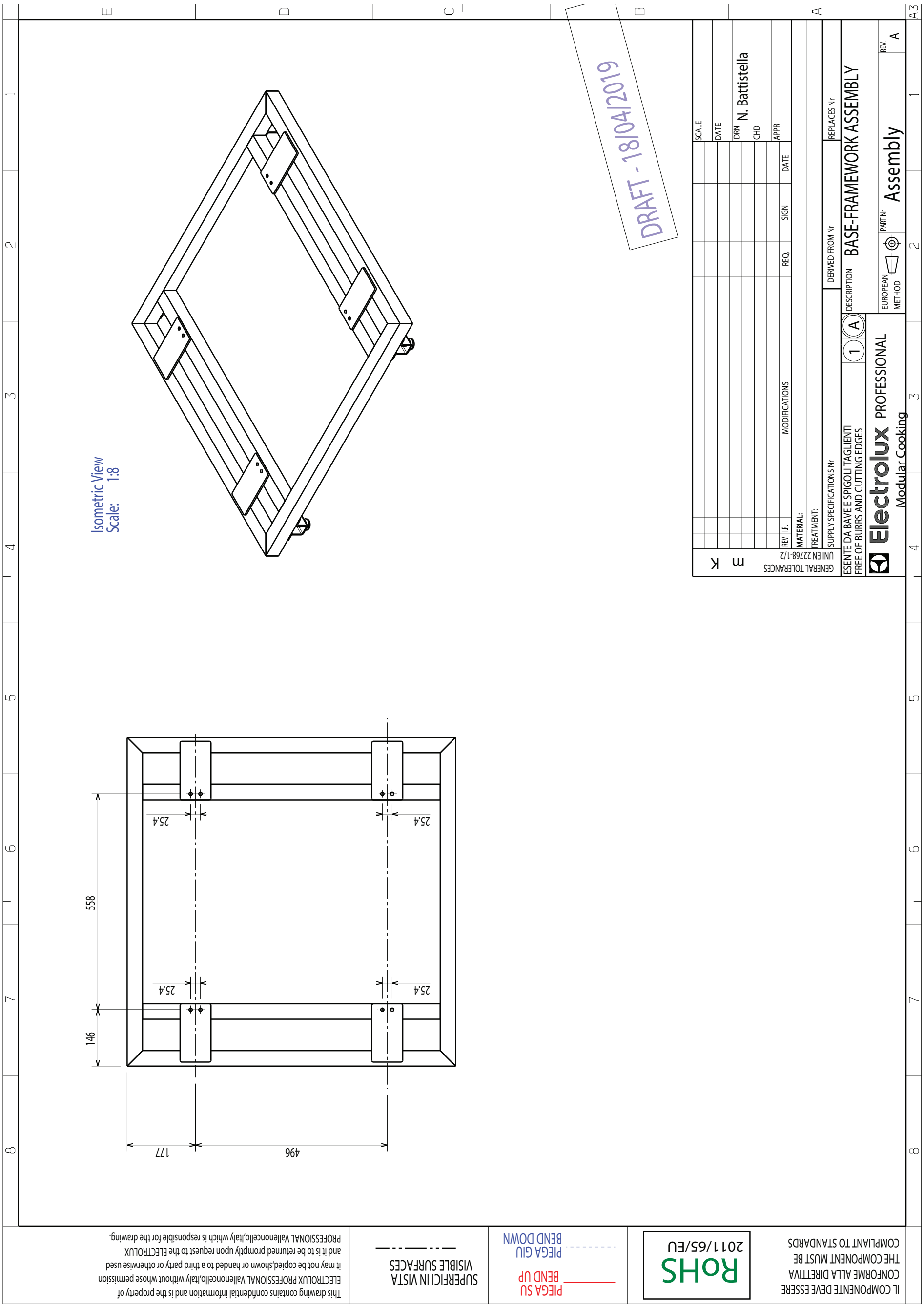
Isometric View
Scale: 1:8
DRAFT - 18/04/2019
558
146
177
496
25,4
25,4
25,4
25,4
SCALE
DATE
DRN N. Battistella
CHD
APPR
REPLACES Nr
BASE-FRAMEWORK ASSEMBLY
DESCRIPTION
DERIVED FROM Nr
REV. A
PART Nr Assembly
EUROPEAN METHOD
Electrolux PROFESSIONAL
Modular Cooking
1 A
ESENTE DA BAVE E SPIGOLI TAGLIENTI
FREE OF BURRS AND CUTTING EDGES
SUPPLY SPECIFICATIONS Nr
TREATMENT:
MATERIAL:
REV. I.R.
REQ.
SIGN
DATE
MODIFICATIONS
GENERAL TOLERANCES
UNI EN 22768-1/2
m K
A3
IL COMPONENTE DEVE ESSERE CONFORME ALLA DIRETTIVA
THE COMPONENT MUST BE COMPLIANT TO STANDARDS
RoHS
2011/65/EU
PIEGA SU
BEND UP
PIEGA GIU
BEND DOWN
SUPERFICI IN VISTA
VISIBLE SURFACES
This drawing contains confidential information and is the property of ELECTROLUX PROFESSIONAL Vallenoncello,Italy without whose permission it may not be copied,shown or handed to a third party or otherwise used and it is to be returned promptly upon request to the ELECTROLUX PROFESSIONAL Vallenoncello,Italy which is responsible for the drawing.
A B C D E
1 2 3 4 5 6 7 8

Appendix B

This appendix includes the technical drawings of the elements which have been designed and manufactured to assemble the semi-active damper.

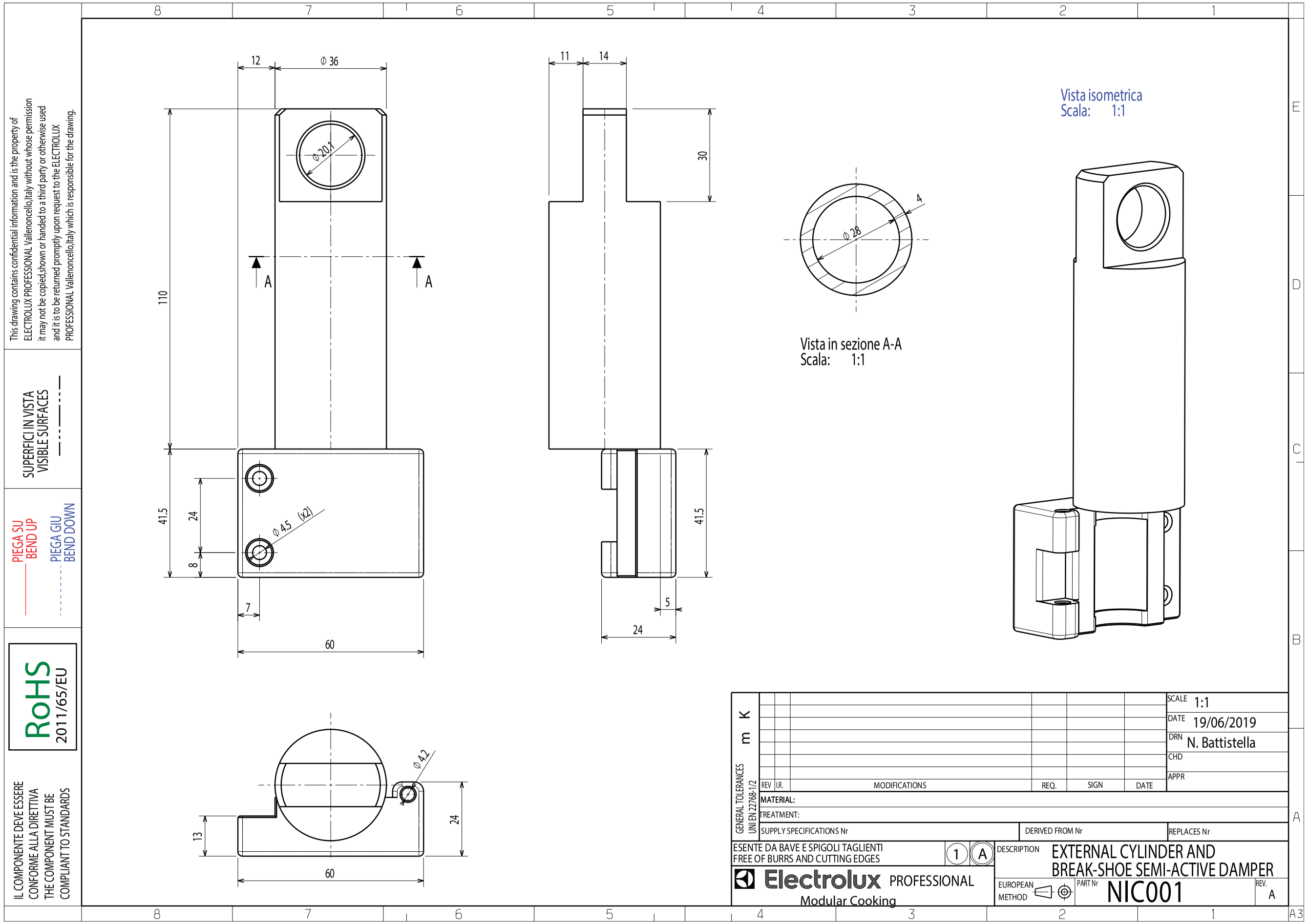
Vista isometrica
Scala: 1:1
Vista in sezione A-A
Scala: 1:1
ϕ 28
4
12
ϕ 36
ϕ 20.1
110
A
A
41.5
24
8
7
60
ϕ 4.5 (x2)
11
14
30
41.5
5
24
ϕ 4.2
13
24
60
This drawing contains confidential information and is the property of ELECTROLUX PROFESSIONAL Vallenoncello,Italy without whose permission it may not be copied,shown or handed to a third party or otherwise used and it is to be returned promptly upon request to the ELECTROLUX PROFESSIONAL Vallenoncello,Italy which is responsible for the drawing.
SUPERFICI IN VISTA
VISIBLE SURFACES
PIEGA SU
BEND UP
PIEGA GIU
BEND DOWN
RoHS
2011/65/EU
IL COMPONENTE DEVE ESSERE CONFORME ALLA DIRETTIVA
THE COMPONENT MUST BE COMPLIANT TO STANDARDS
SCALE 1:1
DATE 19/06/2019
DRN N. Battistella
CHD
APPR
m K
GENERAL TOLERANCES UNI EN 22768-1/2
REV I.R. MODIFICATIONS REQ. SIGN DATE
MATERIAL:
TREATMENT:
SUPPLY SPECIFICATIONS Nr
DERIVED FROM Nr
REPLACES Nr
ESENTE DA BAVE E SPIGOLI TAGLIENTI
FREE OF BURRS AND CUTTING EDGES
1 A
DESCRIPTION EXTERNAL CYLINDER AND BREAK-SHOE SEMI-ACTIVE DAMPER
Electrolux PROFESSIONAL
Modular Cooking
EUROPEAN METHOD
PART Nr NIC001
REV. A
A3
8 7 6 5 4 3 2 1
E D C B A

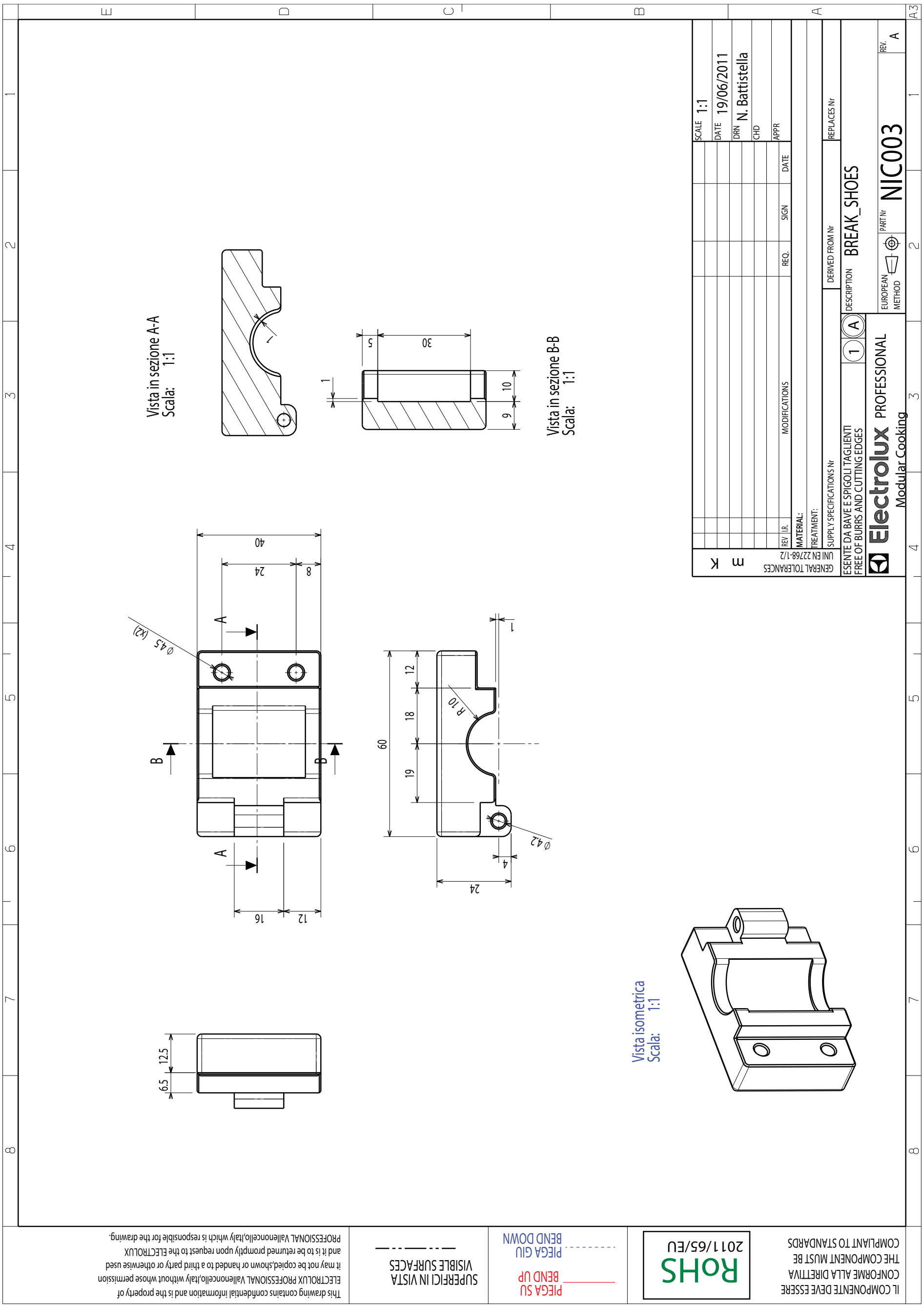
Vista in sezione A-A
Scala: 1:1
Vista in sezione B-B
Scala: 1:1
Vista isometrica
Scala: 1:1
40
24
8
Ø 4.5 (X2)
A
A
B
B
60
12
18
19
R 10
Ø 4.2
4
24
1
16
12
6.5
12.5
5
30
1
10
9
SCALE 1:1
DATE 19/06/2011
DRN N. Battistella
CHD
APPR
REV.
I.R.
MODIFICATIONS
REQ.
SIGN
DATE
MATERIAL:
TREATMENT:
SUPPLY SPECIFICATIONS Nr
DERIVED FROM Nr
REPLACES Nr
ESENTE DA BAVE E SPIGOLI TAGLIENTI
FREE OF BURRS AND CUTTING EDGES
1
A
DESCRIPTION
BREAK_SHOES
Electrolux PROFESSIONAL
Modular Cooking
EUROPEAN METHOD
PART Nr
NIC003
REV.
A
GENERAL TOLERANCES
UNI EN 22768-1/2
m K
A3
E
D
C
B
A
1
2
3
4
5
6
7
8
IL COMPONENTE DEVE ESSERE CONFORME ALLA DIRETTIVA
THE COMPONENT MUST BE COMPLIANT TO STANDARDS
RoHS
2011/65/EU
PIEGA SU
BEND UP
PIEGA GIU
BEND DOWN
SUPERFICI IN VISTA
VISIBLE SURFACES
This drawing contains confidential information and is the property of ELECTROLUX PROFESSIONAL Vallenoncello,Italy without whose permission it may not be copied,shown or handed to a third party or otherwise used and it is to be returned promptly upon request to the ELECTROLUX PROFESSIONAL Vallenoncello,Italy which is responsible for the drawing.

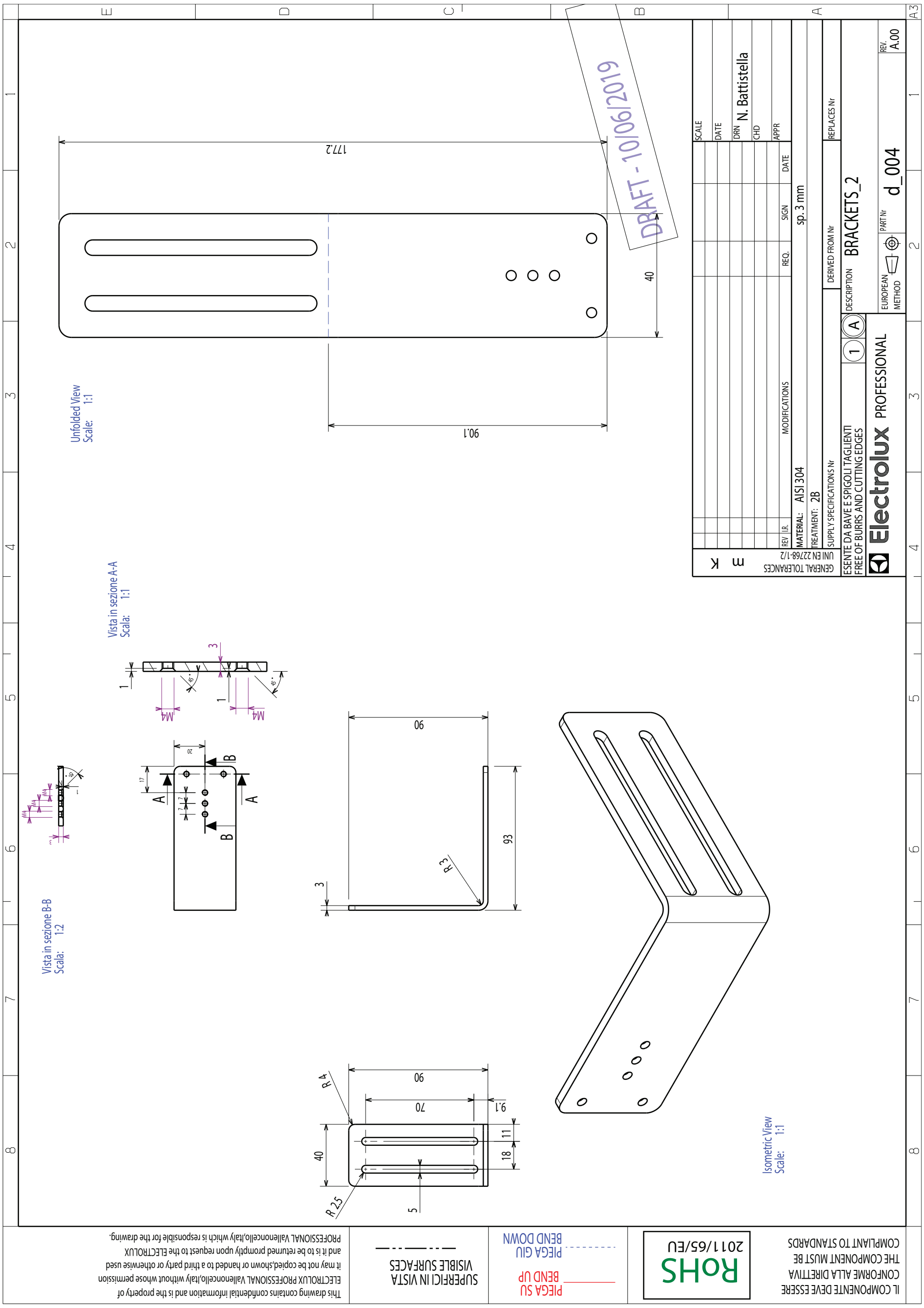
Unfolded View
Scale: 1:1
177.2
40
90.1
DRAFT - 10/06/2019
Vista in sezione A-A
Scala: 1:1
Vista in sezione B-B
Scala: 1:2
M4
3
1
A
B
90
93
R 3
3
70
9.1
40
11
18
R 4
R 2.5
5
Isometric View
Scale: 1:1
SCALE
DATE
DRN N. Battistella
CHD
APPR
REV. I.R.
MODIFICATIONS
REQ.
SIGN
DATE
MATERIAL: AISI 304
TREATMENT: 2B
sp. 3 mm
SUPPLY SPECIFICATIONS Nr
DERIVED FROM Nr
REPLACES Nr
DESCRIPTION BRACKETS_2
PART Nr d_004
REV. A.00
EUROPEAN METHOD
Electrolux PROFESSIONAL
ESENTE DA BAVE E SPIGOLI TAGLIENTI
FREE OF BURRS AND CUTTING EDGES
GENERAL TOLERANCES UNI EN 22768-1/2
m K
A3
IL COMPONENTE DEVE ESSERE CONFORME ALLA DIRETTIVA
THE COMPONENT MUST BE COMPLIANT TO STANDARDS
RoHS
2011/65/EU
PIEGA SU BEND UP
PIEGA GIU BEND DOWN
SUPERFICI IN VISTA VISIBLE SURFACES
This drawing contains confidential information and is the property of ELECTROLUX PROFESSIONAL Vallenoncello,Italy without whose permission it may not be copied,shown or handed to a third party or otherwise used and it is to be returned promptly upon request to the ELECTROLUX PROFESSIONAL Vallenoncello,Italy which is responsible for the drawing.

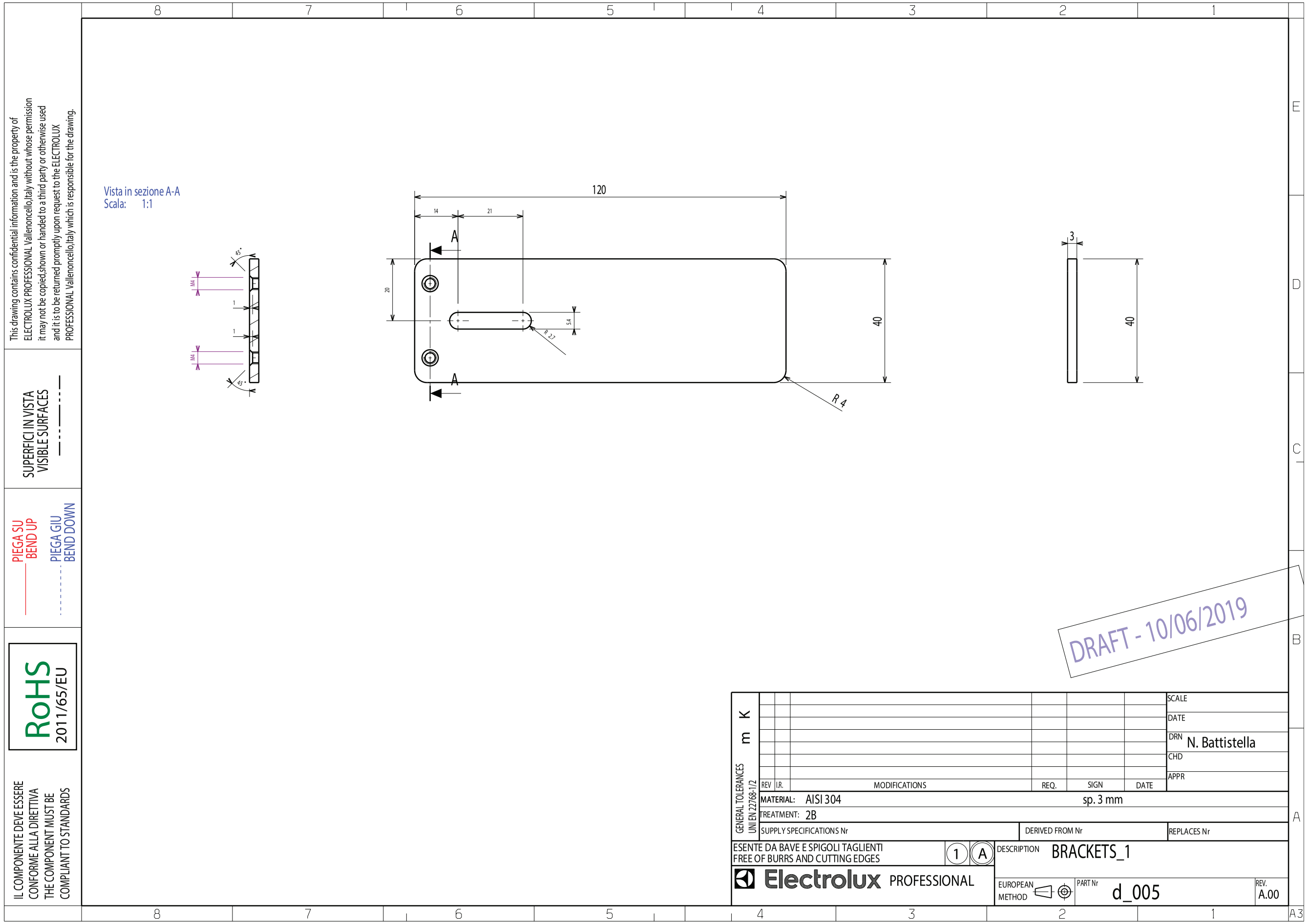

This drawing contains confidential information and is the property of ELECTROLUX PROFESSIONAL Vallenoncello,Italy without whose permission it may not be copied,shown or handed to a third party or otherwise used and it is to be returned promptly upon request to the ELECTROLUX PROFESSIONAL Vallenoncello,Italy which is responsible for the drawing.

SUPERFICI IN VISTA
VISIBLE SURFACES

PIEGA SU
BEND UP

PIEGA GIU
BEND DOWN

RoHS
2011/65/EU

IL COMPONENTE DEVE ESSERE
CONFORME ALLA DIRETTIVA
THE COMPONENT MUST BE
COMPLIANT TO STANDARDS

GENERAL TOLERANCES
UNI EN 22768-1/2
m K

REV	I.R.	MODIFICATIONS	REQ.	SIGN	DATE

SCALE
DATE
DRN N. Battistella
CHD
APPR

MATERIAL: AISI 304 sp. 3 mm
TREATMENT: 2B
SUPPLY SPECIFICATIONS Nr
DERIVED FROM Nr
REPLACES Nr

ESENTE DA BAVE E SPIGOLI TAGLIENTI
FREE OF BURRS AND CUTTING EDGES
① Ⓐ

DESCRIPTION BRACKETS_1

Electrolux PROFESSIONAL

EUROPEAN METHOD
PART Nr d_005
REV. A.00

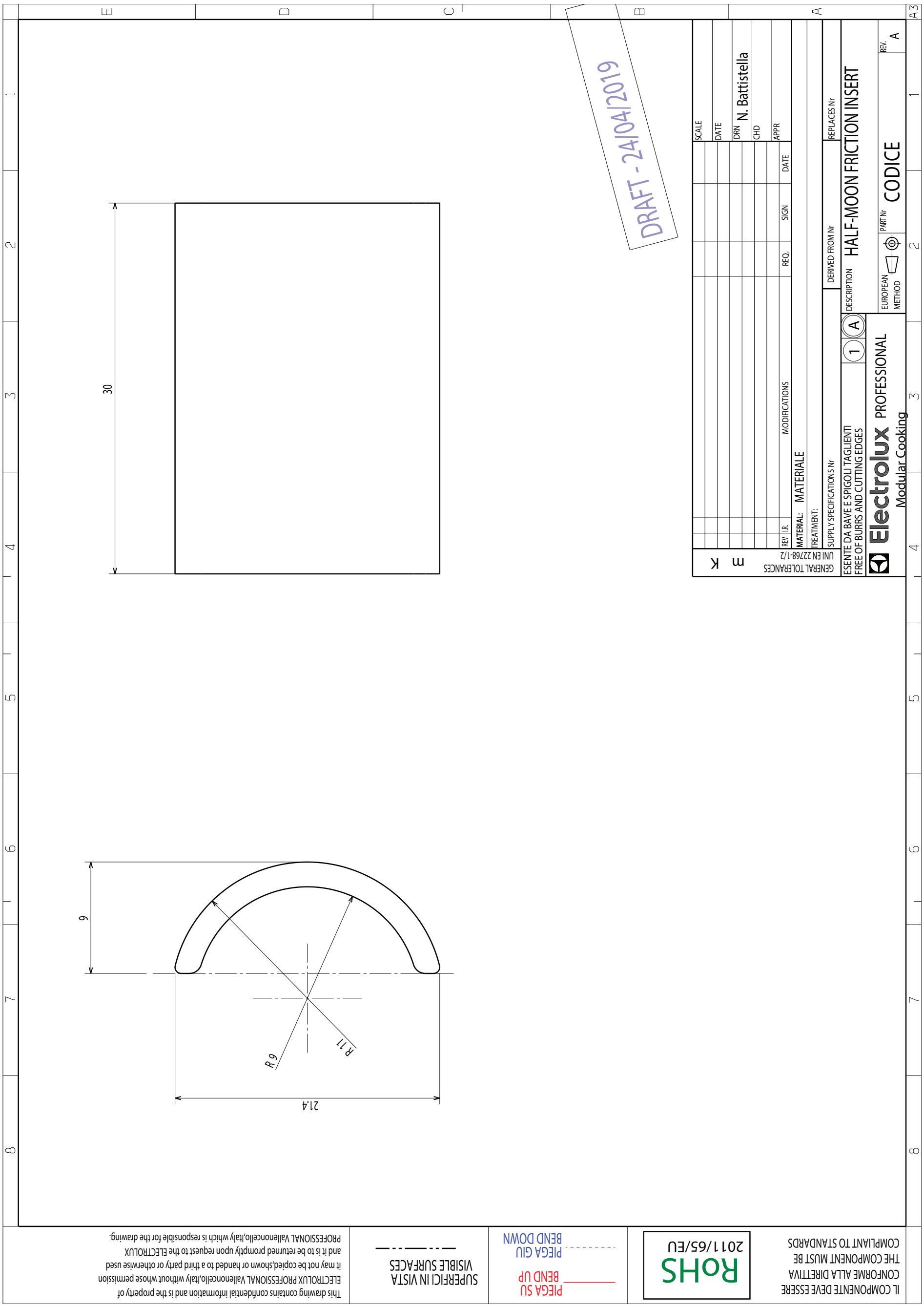
DRAFT - 24/04/2019
30
9
R 9
R 11
21.4
SCALE
DATE
DRN N. Battistella
CHD
APPR
REV I.R. MODIFICATIONS REQ. SIGN DATE
MATERIAL: MATERIALE
TREATMENT:
SUPPLY SPECIFICATIONS Nr
DERIVED FROM Nr
REPLACES Nr
GENERAL TOLERANCES UNI EN 22768-1/2
m K
ESENTE DA BAVE E SPIGOLI TAGLIENTI
FREE OF BURRS AND CUTTING EDGES
1 A
DESCRIPTION HALF-MOON FRICTION INSERT
Electrolux PROFESSIONAL
Modular Cooking
EUROPEAN METHOD
PART Nr CODICE
REV. A
A3
A B C D E
1 2 3 4 5 6 7 8
IL COMPONENTE DEVE ESSERE CONFORME ALLA DIRETTIVA
THE COMPONENT MUST BE COMPLIANT TO STANDARDS
RoHS 2011/65/EU
PIEGA SU BEND UP
PIEGA GIU BEND DOWN
SUPERFICI IN VISTA VISIBLE SURFACES
This drawing contains confidential information and is the property of ELECTROLUX PROFESSIONAL Vallenoncello,Italy without whose permission it may not be copied,shown or handed to a third party or otherwise used and it is to be returned promptly upon request to the ELECTROLUX PROFESSIONAL Vallenoncello,Italy which is responsible for the drawing.

Appendix C

This appendix includes the technical drawings of the elements which have been designed and manufactured to assemble the Tunable Vibration Absorber.

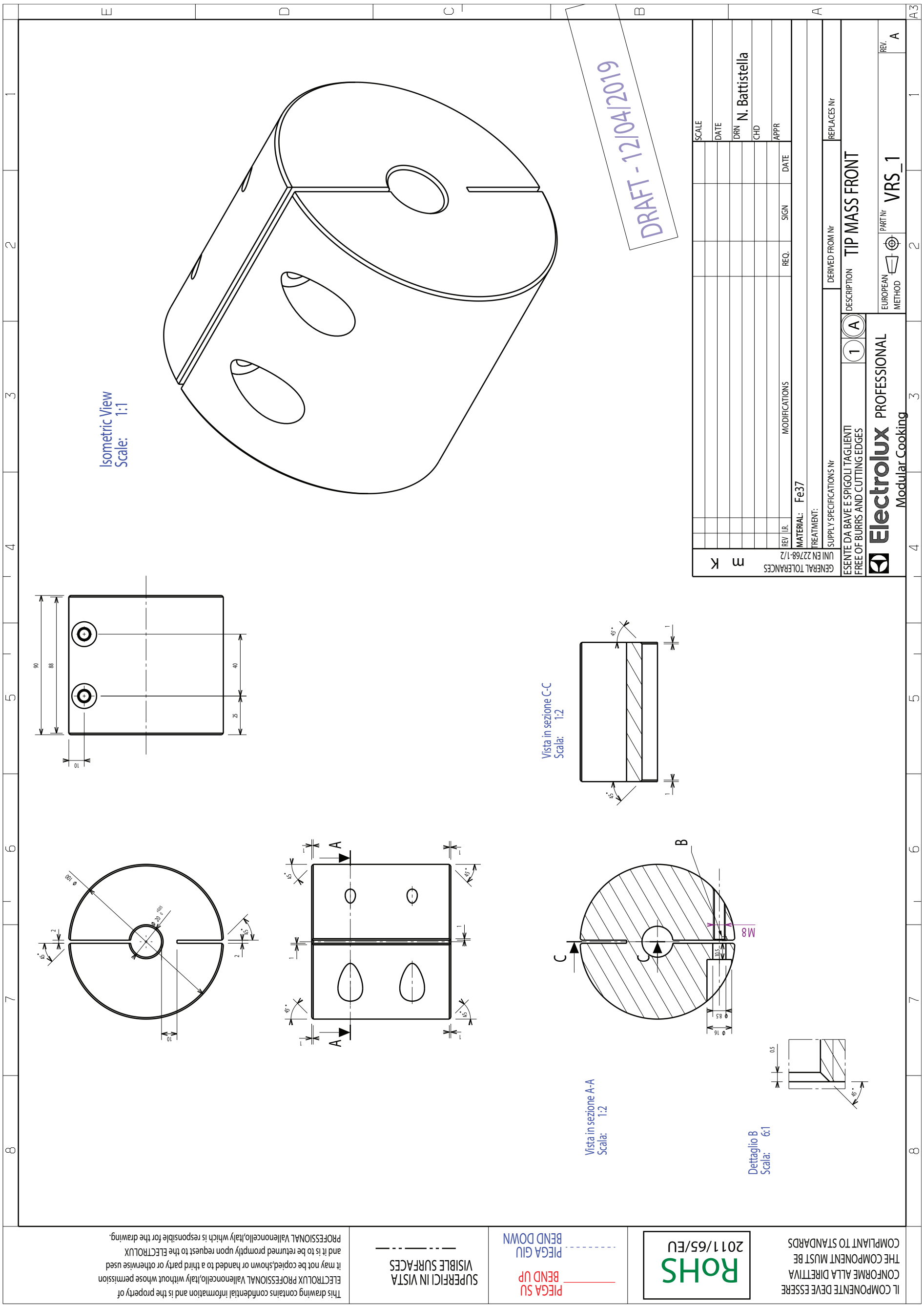
DRAFT - 12/04/2019
Isometric View
Scale: 1:1
Vista in sezione C-C
Scala: 1:2
Vista in sezione A-A
Scala: 1:2
Dettaglio B
Scala: 6:1
A
B
C
M8
90
88
40
25
10
45°
SCALE
DATE
DRN N. Battistella
CHD
APPR
REV.
I.R.
MODIFICATIONS
REQ.
SIGN
DATE
MATERIAL: Fe37
TREATMENT:
SUPPLY SPECIFICATIONS Nr
DERIVED FROM Nr
REPLACES Nr
GENERAL TOLERANCES
UNI EN 22768-1/2
m
K
ESENTE DA BAVE E SPIGOLI TAGLIENTI
FREE OF BURRS AND CUTTING EDGES
Electrolux PROFESSIONAL
Modular Cooking
DESCRIPTION TIP MASS FRONT
EUROPEAN METHOD
PART Nr VRS_1
REV. A
A3
IL COMPONENTE DEVE ESSERE CONFORME ALLA DIRETTIVA
THE COMPONENT MUST BE COMPLIANT TO STANDARDS
RoHS 2011/65/EU
PIEGA SU BEND UP
PIEGA GIU BEND DOWN
SUPERFICI IN VISTA VISIBLE SURFACES
This drawing contains confidential information and is the property of ELECTROLUX PROFESSIONAL Vallenoncello,Italy whose permission it may not be copied,shown or handed to a third party or otherwise used and it is to be returned promptly upon request to the ELECTROLUX PROFESSIONAL Vallenoncello,Italy which is responsible for the drawing.

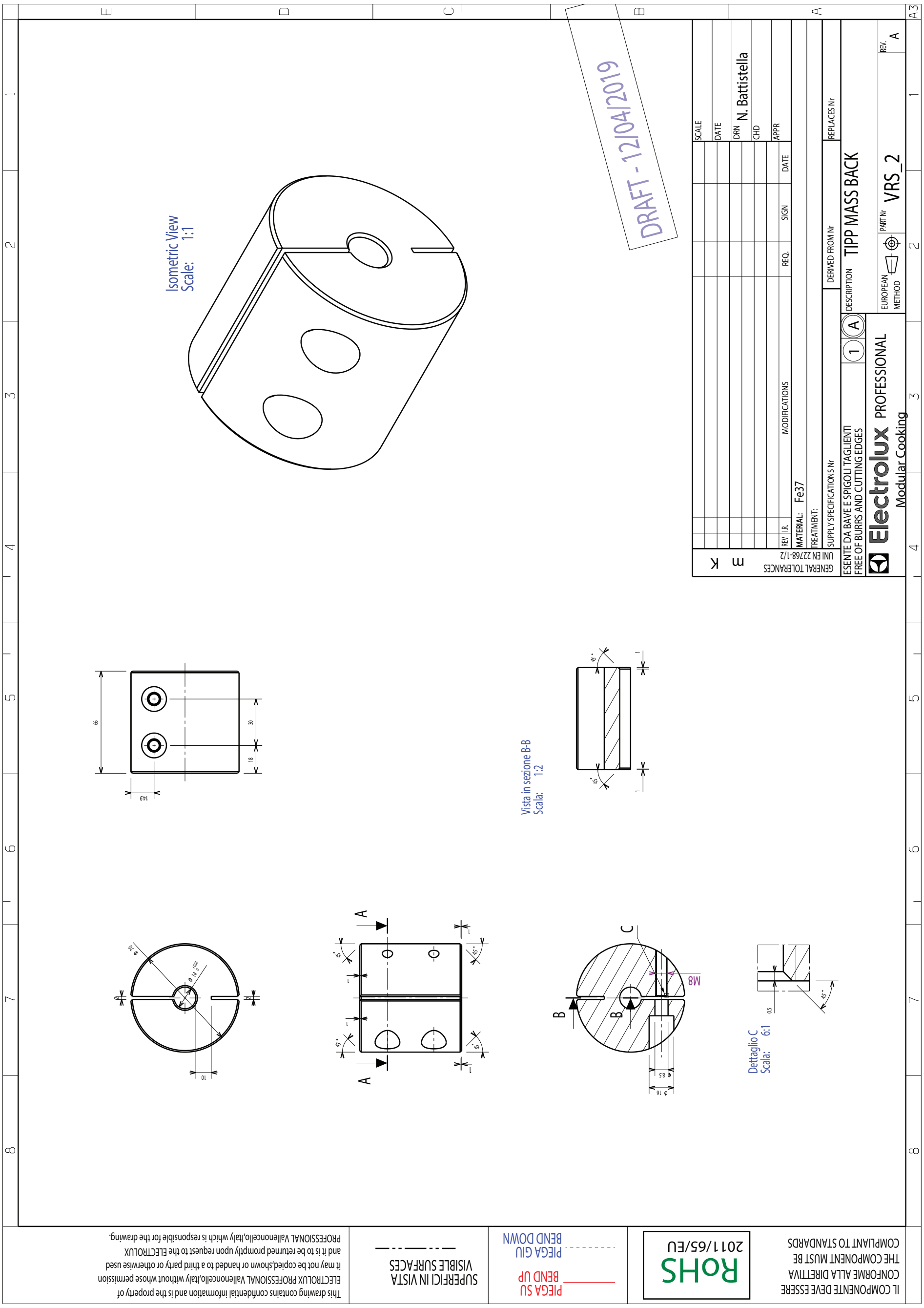
DRAFT - 12/04/2019
Isometric View
Scale: 1:1
Vista in sezione B-B
Scala: 1:2
Dettaglio C
Scala: 6:1
A
B
C
M8
66
30
18
14.9
45°
1
0.5
8.5
16
10
SCALE
DATE
DRN N. Battistella
CHD
APPR
REV
I.R.
MODIFICATIONS
REQ.
SIGN
DATE
MATERIAL: Fe37
TREATMENT:
SUPPLY SPECIFICATIONS Nr
DERIVED FROM Nr
REPLACES Nr
GENERAL TOLERANCES
UNI EN 22768-1/2
m K
ESENTE DA BAVE E SPIGOLI TAGLIENTI
FREE OF BURRS AND CUTTING EDGES
1 A
DESCRIPTION TIPP MASS BACK
Electrolux PROFESSIONAL
Modular Cooking
EUROPEAN METHOD
PART Nr VRS_2
REV. A
A3
IL COMPONENTE DEVE ESSERE CONFORME ALLA DIRETTIVA
THE COMPONENT MUST BE COMPLIANT TO STANDARDS
RoHS
2011/65/EU
PIEGA SU
BEND UP
PIEGA GIU
BEND DOWN
SUPERFICI IN VISTA
VISIBLE SURFACES
This drawing contains confidential information and is the property of ELECTROLUX PROFESSIONAL Vallenoncello,Italy without whose permission it may not be copied,shown or handed to a third party or otherwise used and it is to be returned promptly upon request to the ELECTROLUX PROFESSIONAL Vallenoncello,Italy which is responsible for the drawing.

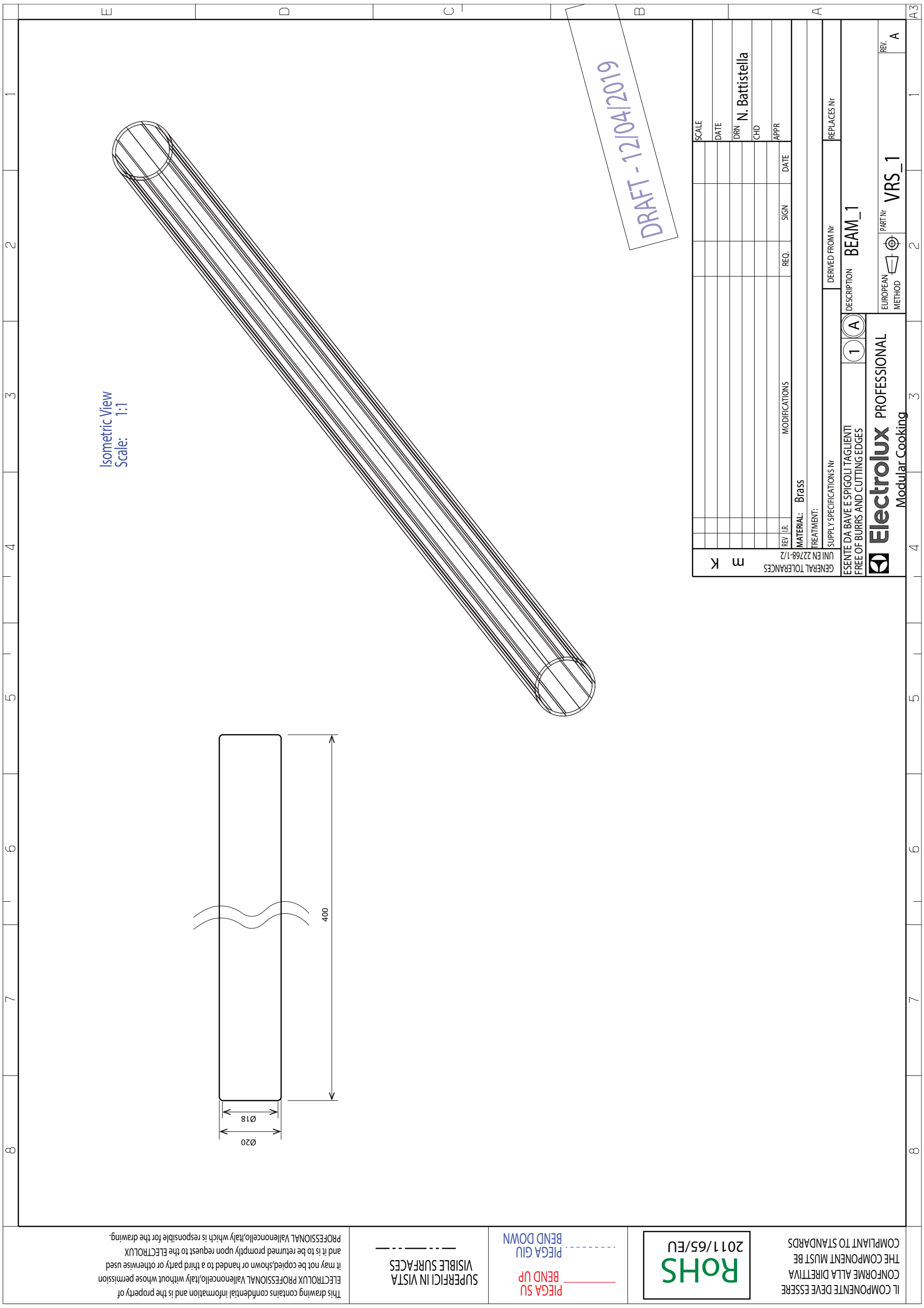
Isometric View
Scale: 1:1
DRAFT - 12/04/2019
400
Ø18
Ø20
SCALE
DATE
DRN N. Battistella
CHD
APPR
REPLACES Nr
DATE
SIGN
REQ.
MODIFICATIONS
REV
I.R.
MATERIAL: Brass
TREATMENT:
SUPPLY SPECIFICATIONS Nr
GENERAL TOLERANCES
UNI EN 22768-1/2
m
K
DERIVED FROM Nr
DESCRIPTION
BEAM_1
ESENTE DA BAVE E SPIGOLI TAGLIENTI
FREE OF BURRS AND CUTTING EDGES
1
A
Electrolux PROFESSIONAL
Modular Cooking
EUROPEAN METHOD
PART Nr
VRS_1
REV.
A
A3
IL COMPONENTE DEVE ESSERE
CONFORME ALLA DIRETTIVA
THE COMPONENT MUST BE
COMPLIANT TO STANDARDS
RoHS
2011/65/EU
PIEGA SU
BEND UP
PIEGA GIU
BEND DOWN
SUPERFICI IN VISTA
VISIBLE SURFACES
This drawing contains confidential information and is the property of
ELECTROLUX PROFESSIONAL Vallenoncello,Italy without whose permission
it may not be copied,shown or handed to a third party or otherwise used
and it is to be returned promptly upon request to the ELECTROLUX
PROFESSIONAL Vallenoncello,Italy which is responsible for the drawing.

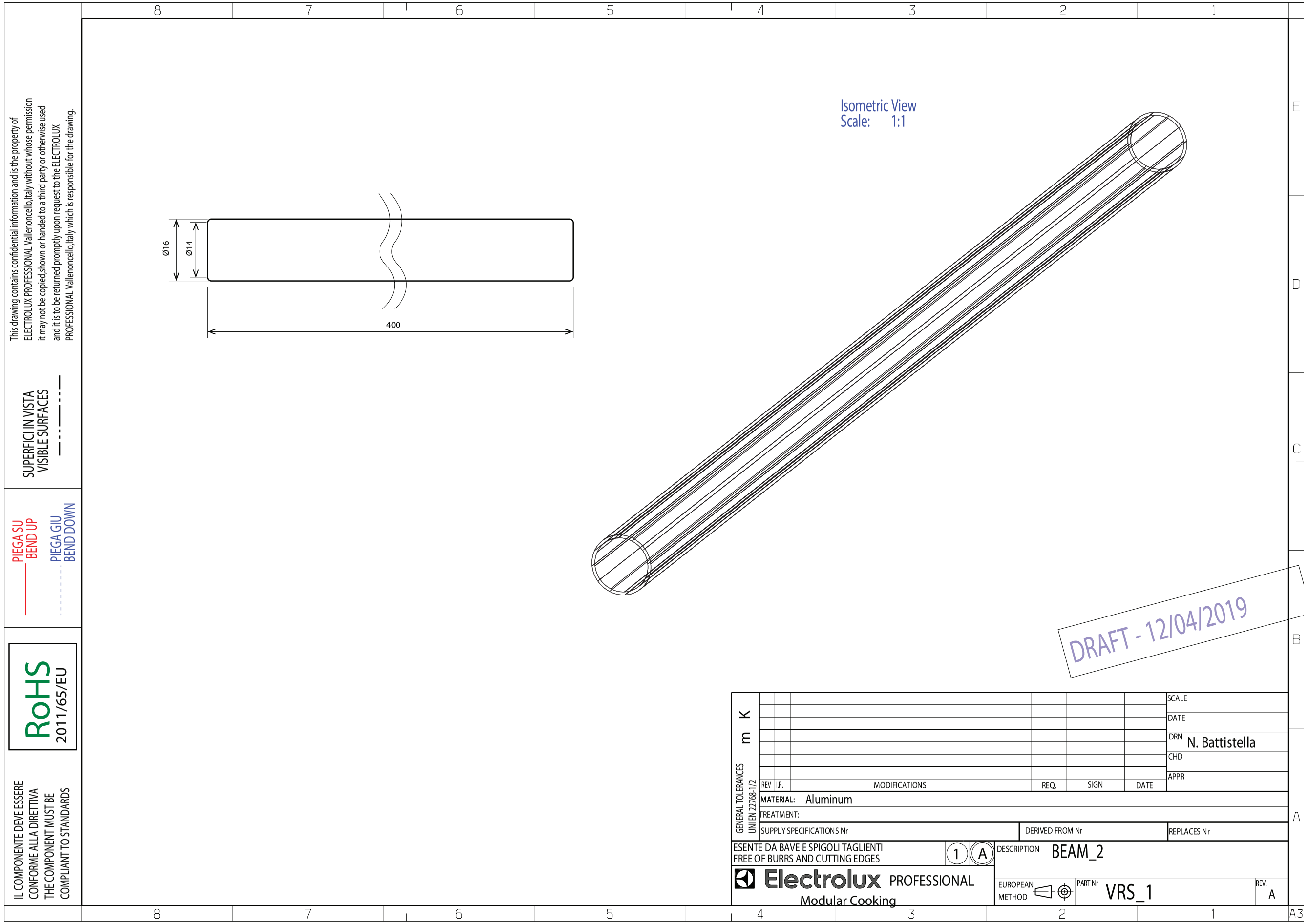

This drawing contains confidential information and is the property of ELECTROLUX PROFESSIONAL Vallenoncello,Italy without whose permission it may not be copied,shown or handed to a third party or otherwise used and it is to be returned promptly upon request to the ELECTROLUX PROFESSIONAL Vallenoncello,Italy which is responsible for the drawing.

IL COMPONENTE DEVE ESSERE CONFORME ALLA DIRETTIVA
THE COMPONENT MUST BE COMPLIANT TO STANDARDS

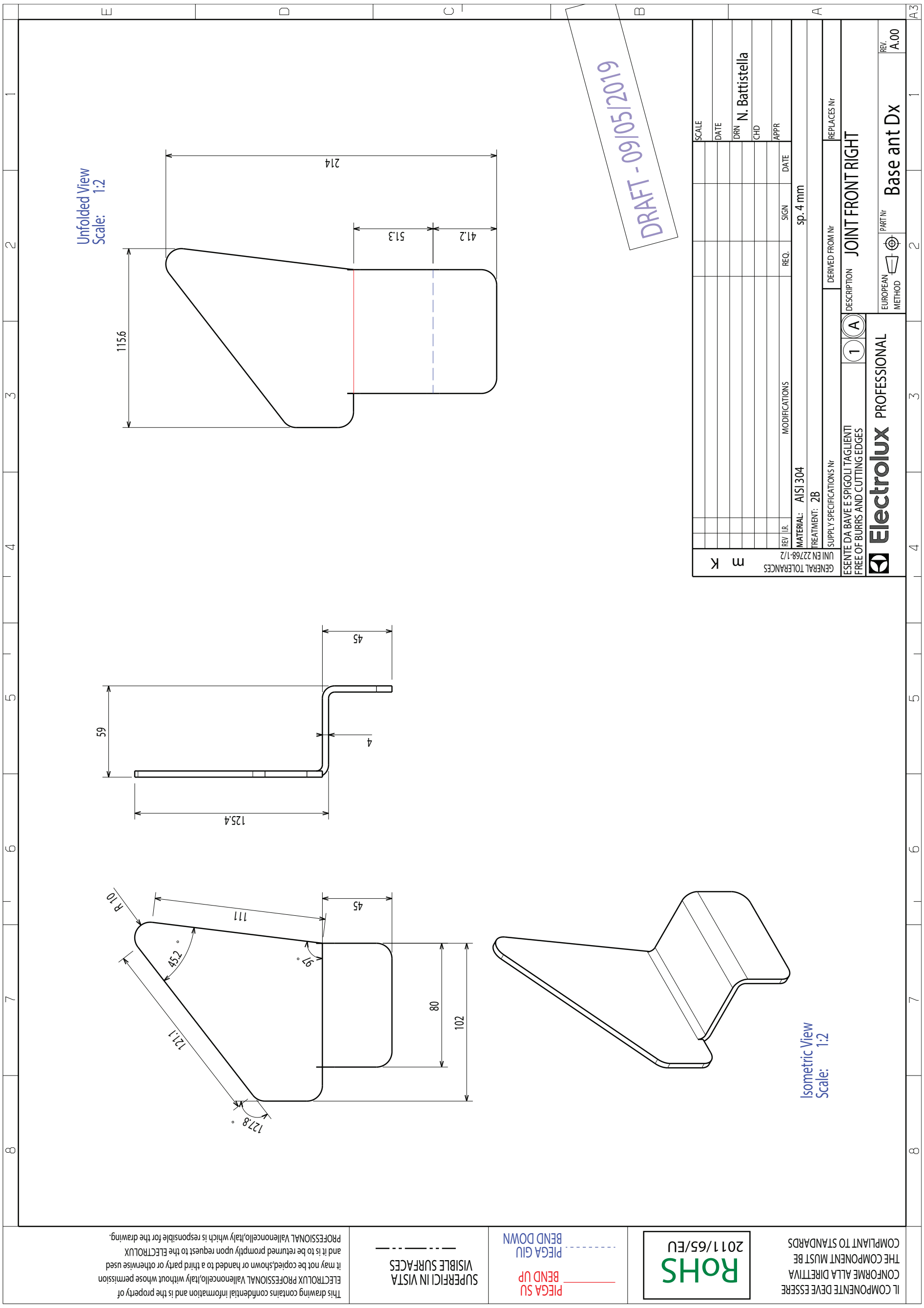
Unfolded View
Scale: 1:2
214
51.3
41.2
115.6
45
4
59
125.4
R 10
111
45.2 °
97 °
121.1
127.8 °
80
102
Isometric View
Scale: 1:2
DRAFT - 09/05/2019
SCALE
DATE
DRN N. Battistella
CHD
APPR
REV. I.R.
MODIFICATIONS
REQ.
SIGN
DATE
MATERIAL: AISI 304
TREATMENT: 2B
sp. 4 mm
SUPPLY SPECIFICATIONS Nr
DERIVED FROM Nr
REPLACES Nr
GENERAL TOLERANCES
UNI EN 22768-1/2
m K
ESENTE DA BAVE E SPIGOLI TAGLIENTI
FREE OF BURRS AND CUTTING EDGES
DESCRIPTION JOINT FRONT RIGHT
Electrolux PROFESSIONAL
EUROPEAN METHOD
PART Nr Base ant Dx
REV. A.00
A3
IL COMPONENTE DEVE ESSERE CONFORME ALLA DIRETTIVA
THE COMPONENT MUST BE COMPLIANT TO STANDARDS
RoHS 2011/65/EU
PIEGA SU BEND UP
PIEGA GIU BEND DOWN
SUPERFICI IN VISTA VISIBLE SURFACES
This drawing contains confidential information and is the property of ELECTROLUX PROFESSIONAL Vallenoncello,Italy without whose permission it may not be copied,shown or handed to a third party or otherwise used and it is to be returned promptly upon request to the ELECTROLUX PROFESSIONAL Vallenoncello,Italy which is responsible for the drawing.

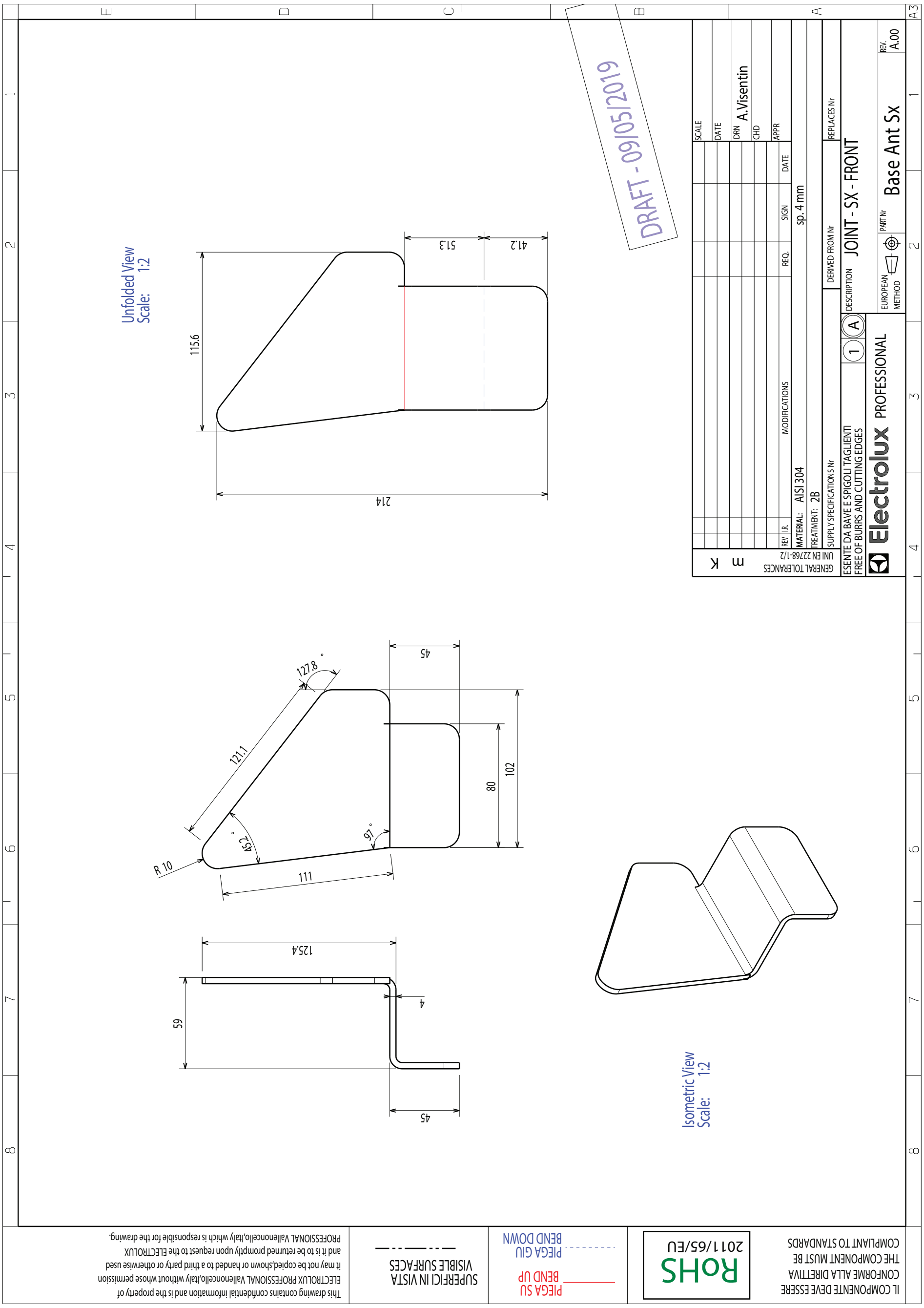
DRAFT - 09/05/2019
Unfolded View
Scale: 1:2
115.6
51.3
41.2
214
127.8 °
121.1
45
80
102
R 10
45.2 °
97 °
111
125.4
59
4
45
Isometric View
Scale: 1:2
SCALE
DATE
DRN A.Visentin
CHD
APPR
REV
I.R.
MODIFICATIONS
REQ.
SIGN
DATE
MATERIAL: AISI 304
sp. 4 mm
TREATMENT: 2B
SUPPLY SPECIFICATIONS Nr
DERIVED FROM Nr
REPLACES Nr
GENERAL TOLERANCES
UNI EN 22768-1/2
m
K
ESENTE DA BAVE E SPIGOLI TAGLIENTI
FREE OF BURRS AND CUTTING EDGES
1
A
DESCRIPTION
JOINT - SX - FRONT
Electrolux PROFESSIONAL
EUROPEAN METHOD
PART Nr
Base Ant Sx
REV.
A.00
A3
IL COMPONENTE DEVE ESSERE
CONFORME ALLA DIRETTIVA
THE COMPONENT MUST BE
COMPLIANT TO STANDARDS
RoHS
2011/65/EU
PIEGA SU
BEND UP
PIEGA GIU
BEND DOWN
SUPERFICI IN VISTA
VISIBLE SURFACES
This drawing contains confidential information and is the property of
ELECTROLUX PROFESSIONAL Vallenoncello,Italy without whose permission
it may not be copied,shown or handed to a third party or otherwise used
and it is to be returned promptly upon request to the ELECTROLUX
PROFESSIONAL Vallenoncello,Italy which is responsible for the drawing.
A
B
C
D
E
1
2
3
4
5
6
7
8

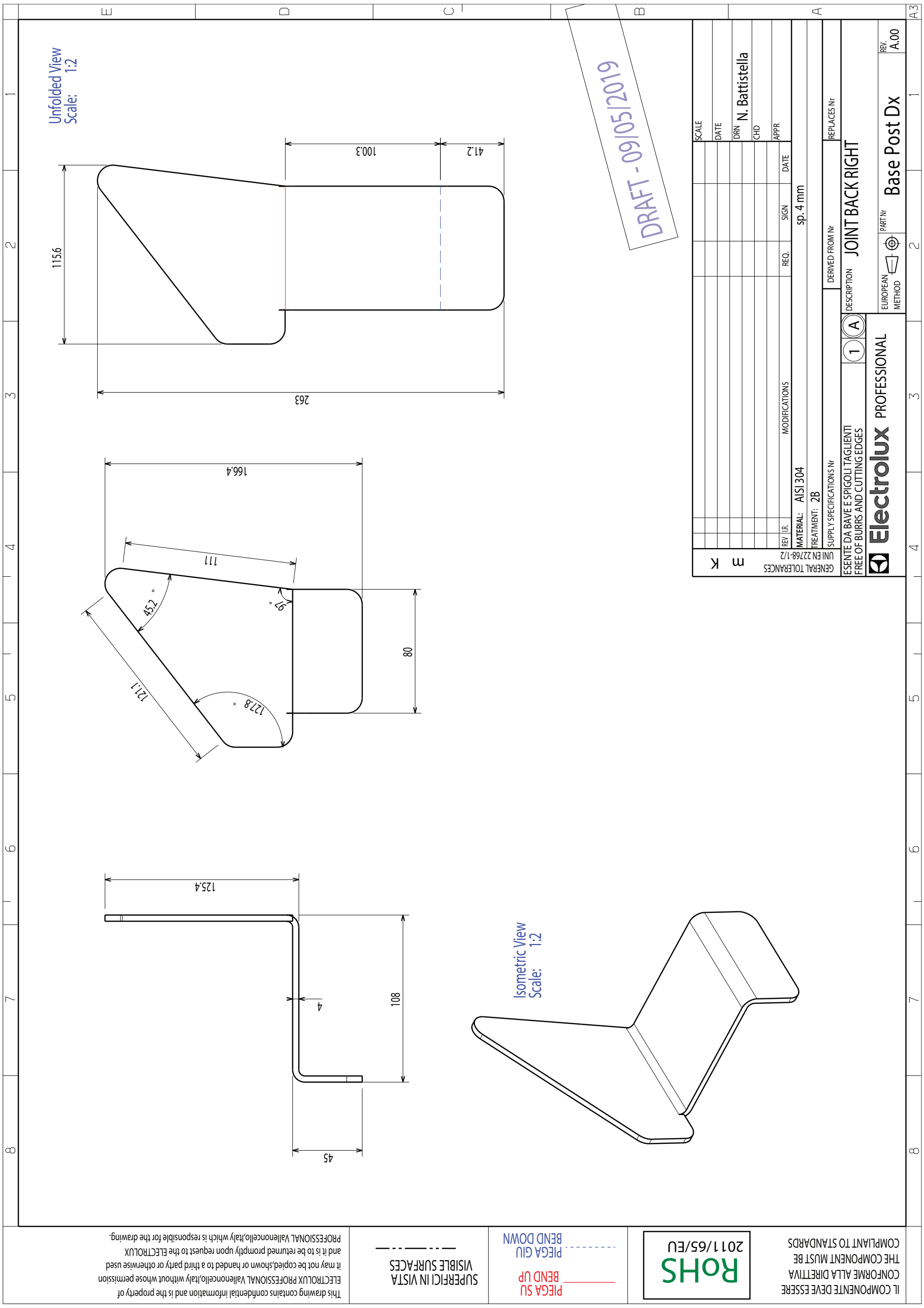
Unfolded View
Scale: 1:2
100.3
41.2
115.6
263
166.4
111
45.2 °
97 °
80
121.1
127.8 °
125.4
4
108
45
Isometric View
Scale: 1:2
DRAFT - 09/05/2019
SCALE
DATE
DRN N. Battistella
CHD
APPR
REV
I.R.
MODIFICATIONS
REQ.
SIGN
DATE
MATERIAL: AISI 304
sp. 4 mm
TREATMENT: 2B
SUPPLY SPECIFICATIONS Nr
DERIVED FROM Nr
REPLACES Nr
GENERAL TOLERANCES UNI EN 22768-1/2
m
K
ESENTE DA BAVE E SPIGOLI TAGLIENTI
FREE OF BURRS AND CUTTING EDGES
1
A
DESCRIPTION JOINT BACK RIGHT
Electrolux PROFESSIONAL
EUROPEAN METHOD
PART Nr Base Post Dx
REV. A.00
A3
A
B
C
D
E
1
2
3
4
5
6
7
8
IL COMPONENTE DEVE ESSERE CONFORME ALLA DIRETTIVA
THE COMPONENT MUST BE COMPLIANT TO STANDARDS
RoHS
2011/65/EU
PIEGA SU
BEND UP
PIEGA GIU
BEND DOWN
SUPERFICI IN VISTA
VISIBLE SURFACES
This drawing contains confidential information and is the property of ELECTROLUX PROFESSIONAL Vallenoncello,Italy without whose permission it may not be copied,shown or handed to a third party or otherwise used and it is to be returned promptly upon request to the ELECTROLUX PROFESSIONAL Vallenoncello,Italy which is responsible for the drawing.

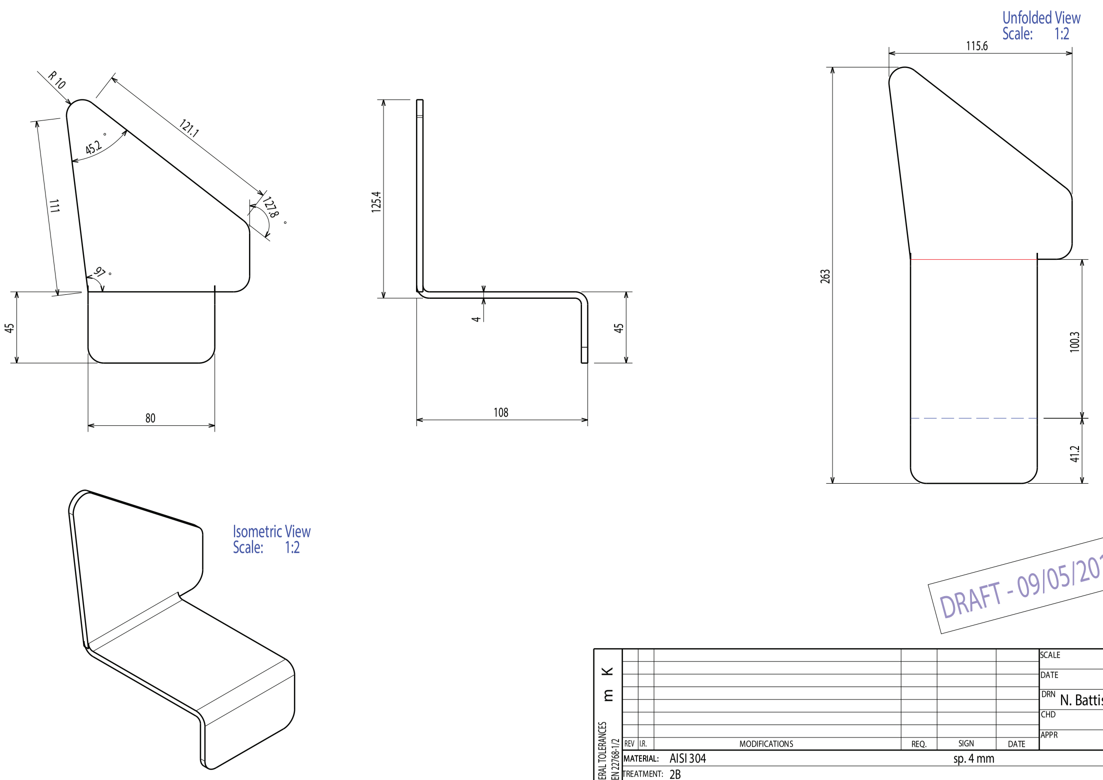

DRAFT - 09/05/2019

SUPERFICI IN VISTA
VISIBLE SURFACES

PIEGA SU
BEND UP

PIEGA GIU
BEND DOWN

RoHS
2011/65/EU

IL COMPONENTE DEVE ESSERE
CONFORME ALLA DIRETTIVA
THE COMPONENT MUST BE
COMPLIANT TO STANDARDS

GENERAL TOLERANCES
UNI EN 22768-1/2
m K

REV	I.R.	MODIFICATIONS	REQ.	SIGN	DATE

SCALE
DATE
DRN N. Battistella
CHD
APPR

MATERIAL: AISI 304
sp. 4 mm
TREATMENT: 2B
SUPPLY SPECIFICATIONS Nr
DERIVED FROM Nr
REPLACES Nr

ESENTE DA BAVE E SPIGOLI TAGLIENTI
FREE OF BURRS AND CUTTING EDGES
① Ⓐ

DESCRIPTION JOINT BACK LEFT

Electrolux PROFESSIONAL

EUROPEAN METHOD
PART Nr Base Post Sx
REV. A.00
A3

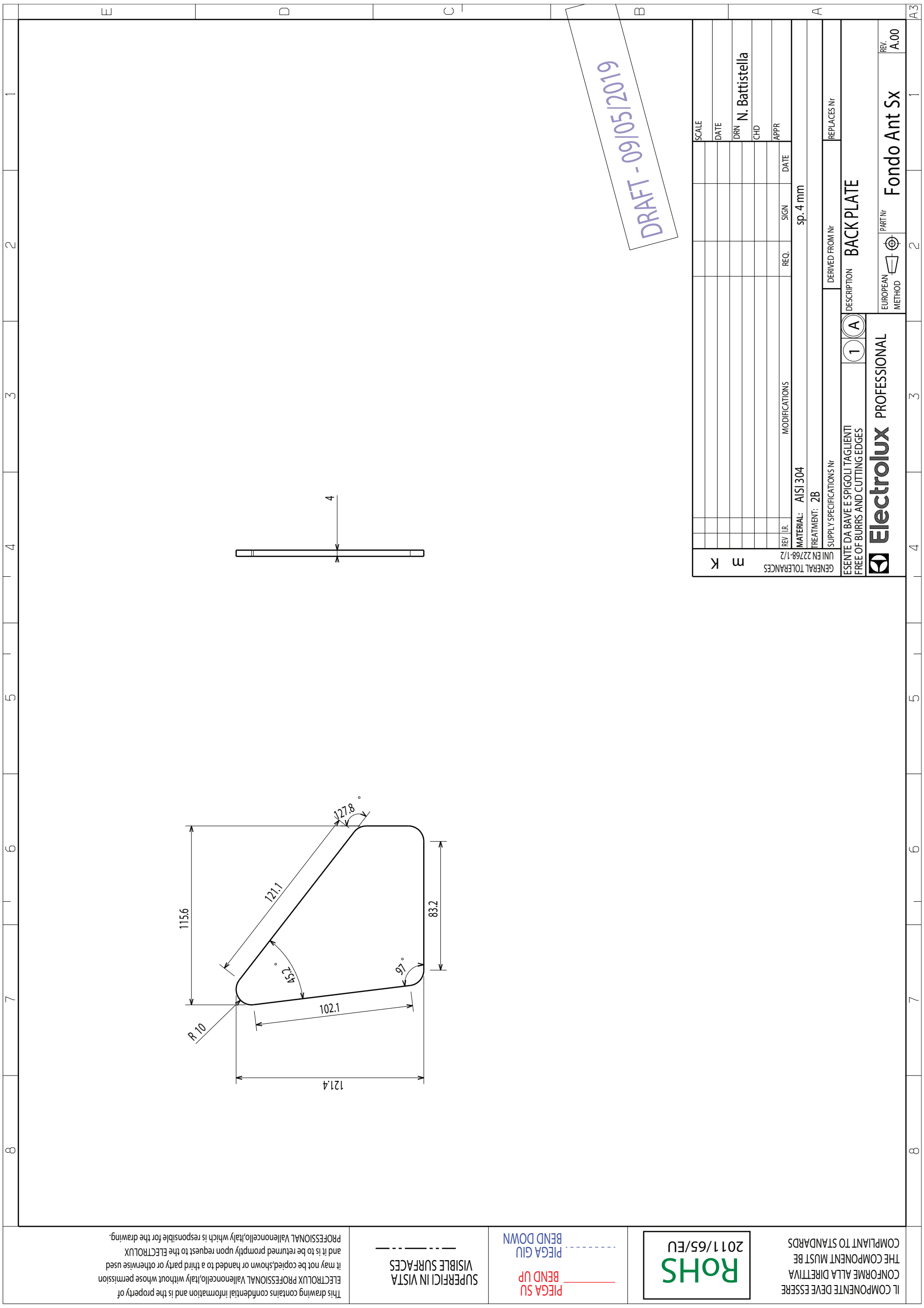
A3
E
D
C
B
A
1
2
3
4
5
6
7
8
DRAFT - 09/05/2019
4
127.8 °
121.1
115.6
83.2
45.2 °
97 °
102.1
R 10
121.4
SCALE
DATE
DRN N. Battistella
CHD
APPR
REV. I.R.
MODIFICATIONS
REQ.
SIGN
DATE
MATERIAL: AISI 304
TREATMENT: 2B
sp. 4 mm
SUPPLY SPECIFICATIONS Nr
DERIVED FROM Nr
REPLACES Nr
GENERAL TOLERANCES
UNI EN 22768-1/2
m
K
ESENTE DA BAVE E SPIGOLI TAGLIENTI
FREE OF BURRS AND CUTTING EDGES
1
A
DESCRIPTION
BACK PLATE
Electrolux PROFESSIONAL
EUROPEAN METHOD
PART Nr
Fondo Ant Sx
REV.
A.00
IL COMPONENTE DEVE ESSERE
CONFORME ALLA DIRETTIVA
THE COMPONENT MUST BE
COMPLIANT TO STANDARDS
RoHS
2011/65/EU
PIEGA SU
BEND UP
PIEGA GIU
BEND DOWN
SUPERFICI IN VISTA
VISIBLE SURFACES
This drawing contains confidential information and is the property of
ELECTROLUX PROFESSIONAL Vallenoncello,Italy without whose permission
it may not be copied,shown or handed to a third party or otherwise used
and it is to be returned promptly upon request to the ELECTROLUX
PROFESSIONAL Vallenoncello,Italy which is responsible for the drawing.

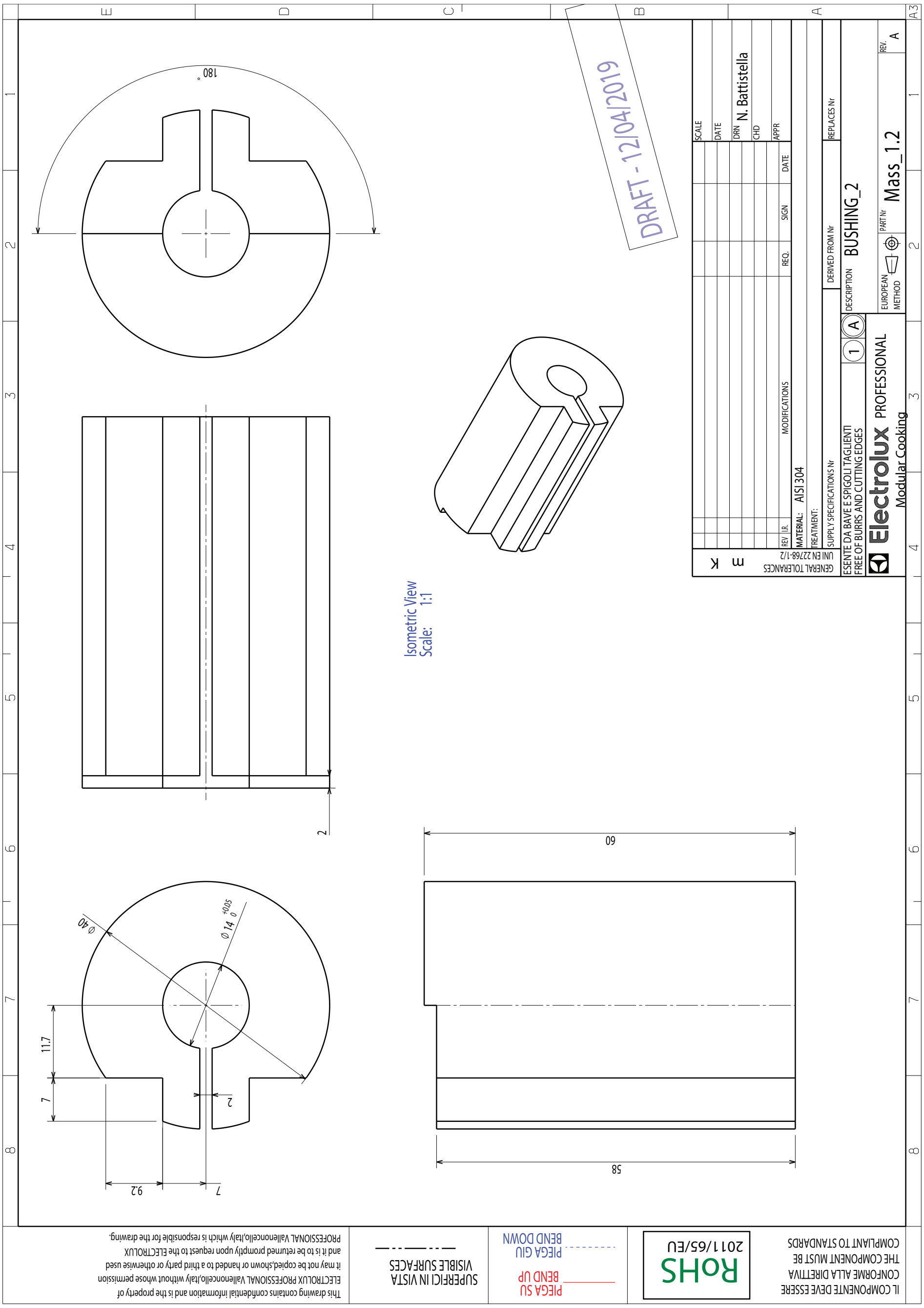
E
D
C
B
A
1
2
3
4
5
6
7
8
A3
DRAFT - 12/04/2019
180°
2
60
58
⌀ 40
⌀ 14 +0.05 0
11.7
7
2
9.2
7
Isometric View
Scale: 1:1
SCALE
DATE
DRN N. Battistella
CHD
APPR
REPLACES Nr
DERIVED FROM Nr
DESCRIPTION BUSHING_2
PART Nr Mass_1.2
REV. A
EUROPEAN METHOD
1 A
Electrolux PROFESSIONAL
Modular Cooking
ESENTE DA BAVE E SPIGOLI TAGLIENTI
FREE OF BURRS AND CUTTING EDGES
SUPPLY SPECIFICATIONS Nr
TREATMENT:
MATERIAL: AISI 304
REV
I.R.
MODIFICATIONS
REQ.
SIGN
DATE
GENERAL TOLERANCES
UNI EN 22768-1/2
m
K
IL COMPONENTE DEVE ESSERE
CONFORME ALLA DIRETTIVA
THE COMPONENT MUST BE
COMPLIANT TO STANDARDS
RoHS
2011/65/EU
PIEGA SU
BEND UP
PIEGA GIU
BEND DOWN
SUPERFICI IN VISTA
VISIBLE SURFACES

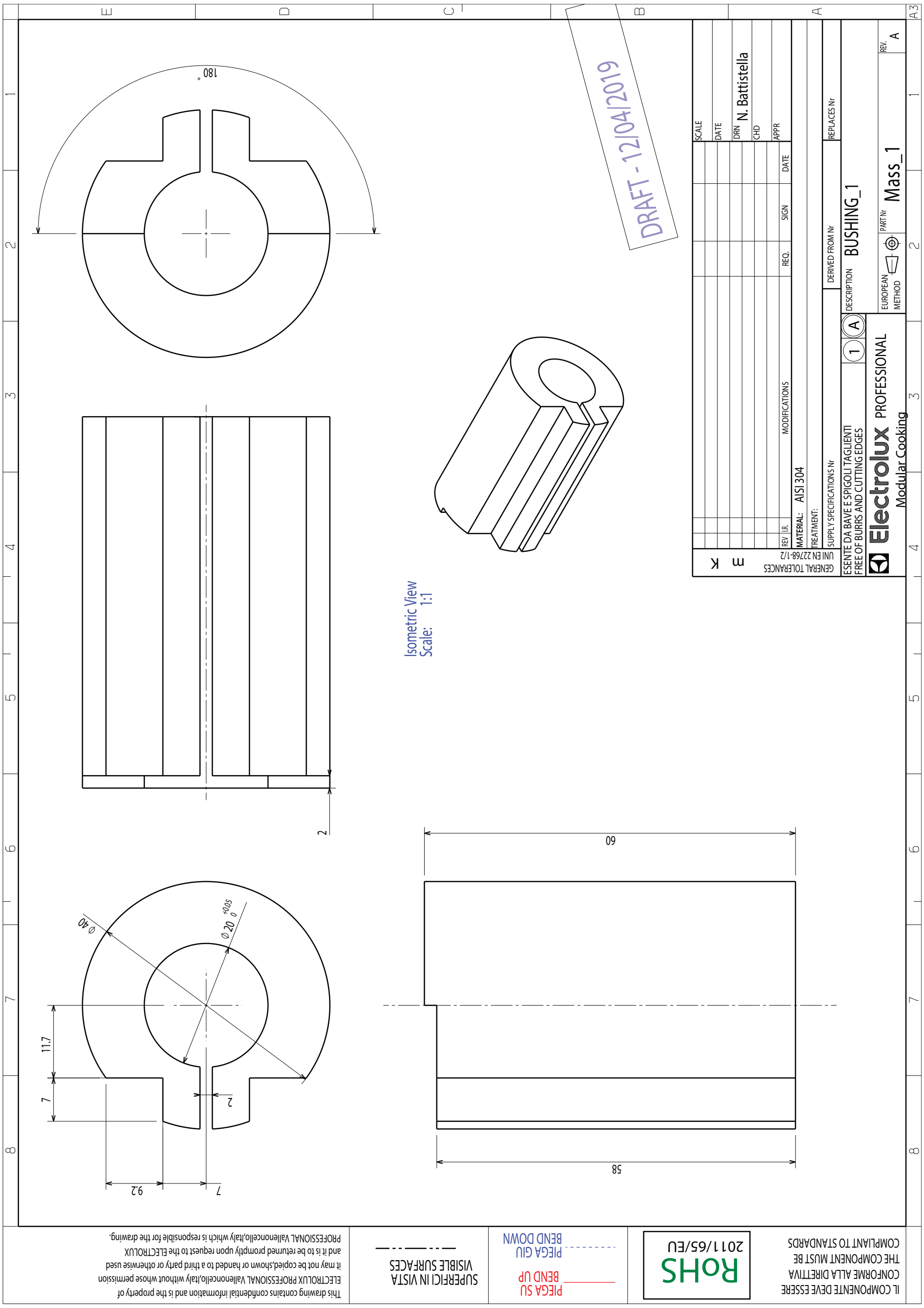
DRAFT - 12/04/2019
SCALE
DATE
DRN N. Battistella
CHD
APPR
REV.
J.R.
MODIFICATIONS
REQ.
SIGN
DATE
MATERIAL: AISI 304
TREATMENT:
SUPPLY SPECIFICATIONS Nr
DERIVED FROM Nr
REPLACES Nr
GENERAL TOLERANCES UNI EN 22768-1/2
m K
ESENTE DA BAVE E SPIGOLI TAGLIENTI
FREE OF BURRS AND CUTTING EDGES
Electrolux PROFESSIONAL
Modular Cooking
1
A
DESCRIPTION BUSHING_1
EUROPEAN METHOD
PART Nr Mass_1
REV. A
A3
Isometric View
Scale: 1:1
180°
2
60
58
Ø 40
Ø 20 +0.05 0
11.7
7
2
9.2
7
A B C D E
1 2 3 4 5 6 7 8
IL COMPONENTE DEVE ESSERE CONFORME ALLA DIRETTIVA
THE COMPONENT MUST BE COMPLIANT TO STANDARDS
RoHS
2011/65/EU
PIEGA SU
BEND UP
PIEGA GIU
BEND DOWN
SUPERFICI IN VISTA
VISIBLE SURFACES

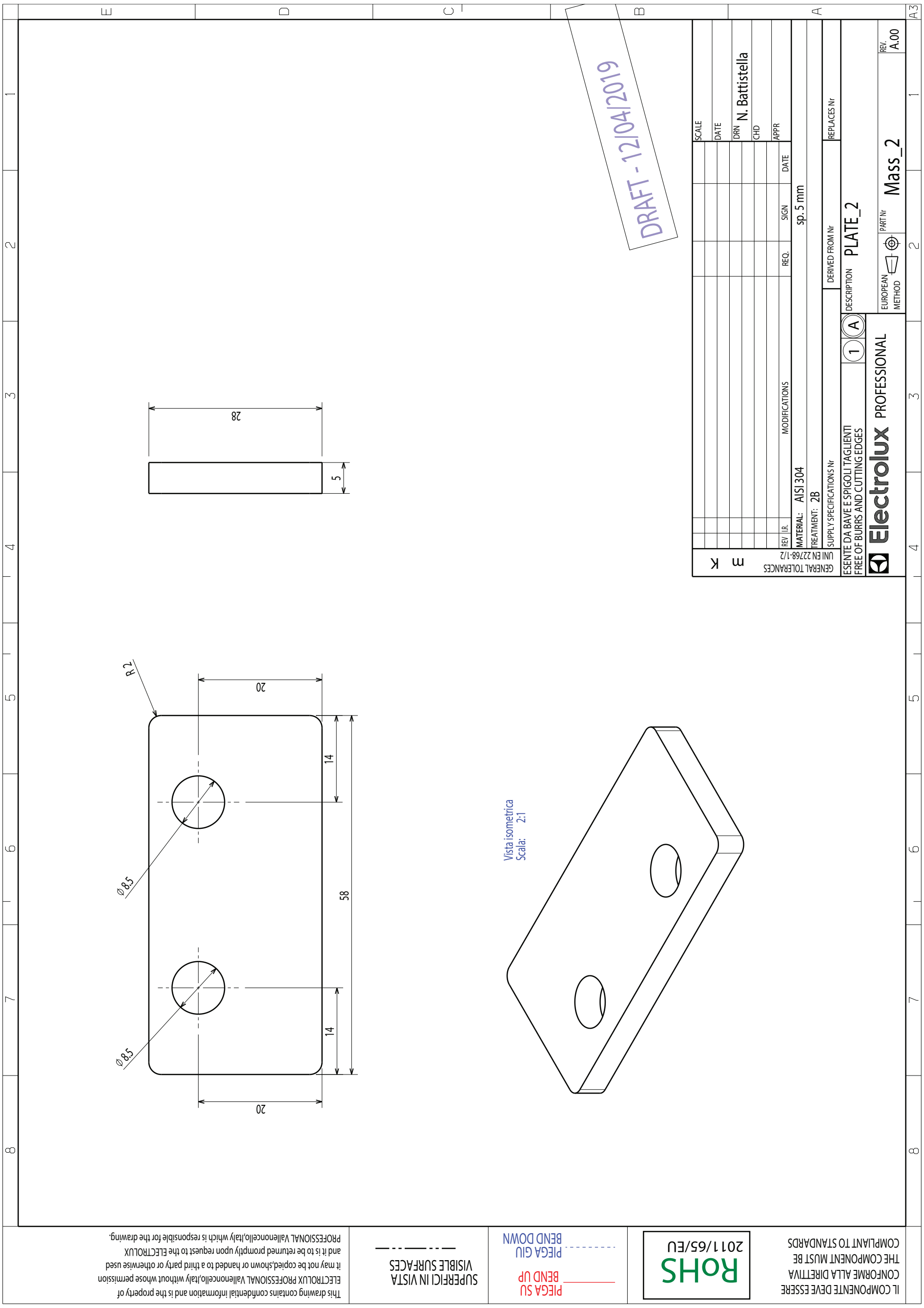
DRAFT - 12/04/2019
28
5
20
14
58
14
20
R 2
Ø 8.5
Ø 8.5
Vista isometrica
Scala: 2:1
SCALE
DATE
DRN N. Battistella
CHD
APPR
REV
I.R.
MODIFICATIONS
REQ.
SIGN
DATE
MATERIAL: AISI 304
TREATMENT: 2B
sp. 5 mm
SUPPLY SPECIFICATIONS Nr
DERIVED FROM Nr
REPLACES Nr
GENERAL TOLERANCES
UNI EN 22768-1/2
m
K
ESENTE DA BAVE E SPIGOLI TAGLIENTI
FREE OF BURRS AND CUTTING EDGES
1
A
DESCRIPTION
PLATE_2
Electrolux PROFESSIONAL
EUROPEAN METHOD
PART Nr
Mass_2
REV.
A.00
A3
IL COMPONENTE DEVE ESSERE CONFORME ALLA DIRETTIVA
THE COMPONENT MUST BE COMPLIANT TO STANDARDS
RoHS
2011/65/EU
PIEGA SU
BEND UP
PIEGA GIU
BEND DOWN
SUPERFICI IN VISTA
VISIBLE SURFACES
This drawing contains confidential information and is the property of ELECTROLUX PROFESSIONAL Vallenoncello,Italy without whose permission it may not be copied,shown or handed to a third party or otherwise used and it is to be returned promptly upon request to the ELECTROLUX PROFESSIONAL Vallenoncello,Italy which is responsible for the drawing.

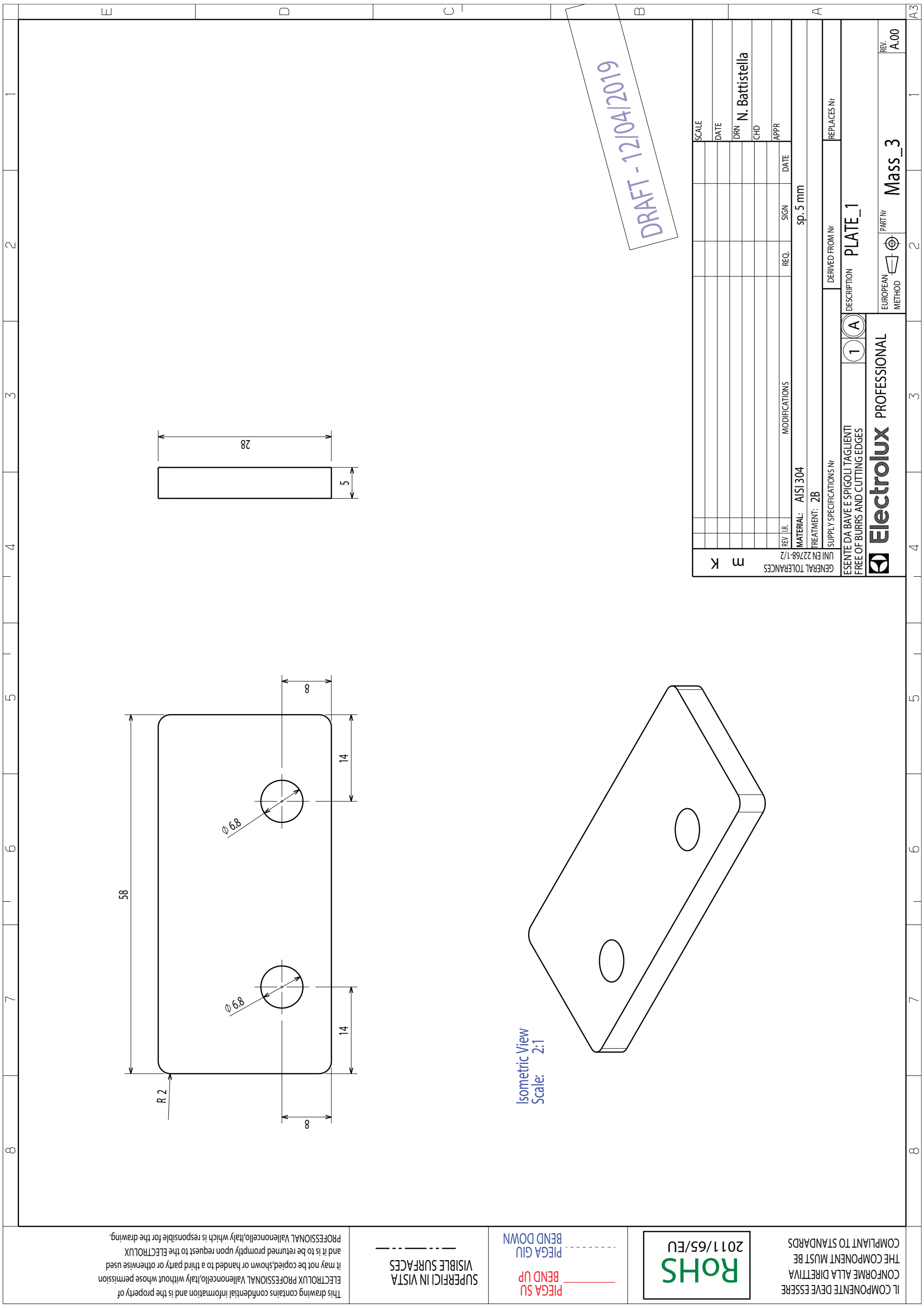
DRAFT - 12/04/2019
28
5
8
14
58
⌀ 6.8
⌀ 6.8
14
R 2
8
Isometric View
Scale: 2:1
SCALE
DATE
DRN N. Battistella
CHD
APPR
REV
I.R.
MODIFICATIONS
REQ.
SIGN
DATE
MATERIAL: AISI 304
sp. 5 mm
TREATMENT: 2B
SUPPLY SPECIFICATIONS Nr
DERIVED FROM Nr
REPLACES Nr
GENERAL TOLERANCES
UNI EN 22768-1/2
m
K
ESENTE DA BAVE E SPIGOLI TAGLIENTI
FREE OF BURRS AND CUTTING EDGES
1
A
DESCRIPTION PLATE_1
Electrolux PROFESSIONAL
EUROPEAN METHOD
PART Nr Mass_3
REV. A.00
A3
A
B
C
D
E
1
2
3
4
5
6
7
8
IL COMPONENTE DEVE ESSERE CONFORME ALLA DIRETTIVA
THE COMPONENT MUST BE COMPLIANT TO STANDARDS
RoHS 2011/65/EU
PIEGA SU
BEND UP
PIEGA GIU
BEND DOWN
SUPERFICI IN VISTA
VISIBLE SURFACES
This drawing contains confidential information and is the property of ELECTROLUX PROFESSIONAL Vallenoncello,Italy without whose permission it may not be copied,shown or handed to a third party or otherwise used and it is to be returned promptly upon request to the ELECTROLUX PROFESSIONAL Vallenoncello,Italy which is responsible for the drawing.